

AD _____

CONTRACT NUMBER DAMD17-98-1-8007

TITLE: **An Eye Oximeter for Combat Casualty Care**

PRINCIPAL INVESTIGATOR: Kurt Denninghoff, M.D.

CONTRACTING ORGANIZATION: University of Alabama at Birmingham
Birmingham, Alabama 35294-0111

REPORT DATE: December 1999

TYPE OF REPORT: Final

PREPARED FOR: U.S. Army Medical Research and Materiel Command
504 Scott Street
Fort Detrick, Maryland 21702-5012

DISTRIBUTION STATEMENT: Approved for public release; distribution unlimited

The views, opinions and/or findings contained in this report are those of the author(s) and should not be construed as an official Department of the Army position, policy or decision unless so designated by other documentation.

20010404 133

REPORT DOCUMENTATION PAGE

Form Approved
OMB No. 074-0188

Public reporting burden for this collection of information is estimated to average 1 hour per response, including the time for reviewing instructions, searching existing data sources, gathering and maintaining the data needed, and completing and reviewing this collection of information. Send comments regarding this burden estimate or any other aspect of this collection of information, including suggestions for reducing this burden to Washington Headquarters Services, Directorate for Information Operations and Reports, 1215 Jefferson Davis Highway, Suite 1204, Arlington, VA 22202-4302, and to the Office of Management and Budget, Paperwork Reduction Project (0704-0188), Washington, DC 20503

1. AGENCY USE ONLY (Leave blank)		2. REPORT DATE December 1999	3. REPORT TYPE AND DATES COVERED Final (15 Dec 97 – 30 Nov 99)	
4. TITLE AND SUBTITLE An Eye Oximeter for Combat Casualty Care			5. FUNDING NUMBERS DAMD17-98-1-8007	
6. AUTHOR(S) Kurt Denninghoff, M.D.				
7. PERFORMING ORGANIZATION NAME(S) AND ADDRESS(ES) University of Alabama at Birmingham Birmingham, Alabama 35924-0111 E-MAIL: kdenning@uabmc.edu			8. PERFORMING ORGANIZATION REPORT NUMBER	
9. SPONSORING / MONITORING AGENCY NAME(S) AND ADDRESS(ES) U.S. Army Medical Research and Materiel Command Fort Detrick, Maryland 21702-5012			10. SPONSORING / MONITORING AGENCY REPORT NUMBER	
11. SUPPLEMENTARY NOTES				
12a. DISTRIBUTION / AVAILABILITY STATEMENT Approved for public release; distribution unlimited				12b. DISTRIBUTION CODE
13. ABSTRACT (Maximum 200 Words) A noninvasive, rapidly applicable technique that provides a reliable index of oxygen delivery during shock resuscitation would be a valuable adjunct to patient management. Subject: The team at UAB and UAH is generating instrumentation and scientific data suggesting that retinal vessel oxygen saturations (both arterial and venous) may be used to identify bleeding prior to changes in vital signs and to help optimize oxygen delivery during the resuscitation of trauma victims. Purpose: The purpose of this work is to develop a noninvasive tool for measuring a hemodynamic parameter to aid in the triage and treatment of combat casualties who may be bleeding or have bled substantially. Scope: The scope of this work includes the investigation of the optical properties of the retina and developing the techniques required to accurately measure retinal large vessel oxygen saturations. As this work is being accomplished we have used models of blood loss to demonstrate the potential efficacy of this measurement in the evaluation and treatment of combat casualties. We have constructed Eye Oximeters (EOX) for measuring the oxygen saturation of blood in retinal veins and arteries. We have found that absolute calibration of the measurement in yorkshire swine is problematic secondary to back reflections and pigment variations in the retina. In order to demonstrate the correlation between retinal venous oxygen saturation, cardiac output and mixed venous oxygen saturation, we have identified a subspecies of swine, the sinclair swine, which has no pigmentation in the retina. The EOX has been used in Sinclair swine studies to demonstrate proof of concept. Retinal venous oxygen saturation correlates with cardiac output and mixed venous oxygen saturation during profound blood loss and subsequent resuscitation.				
14. SUBJECT TERMS Combat Casualty Care			15. NUMBER OF PAGES 287	
			16. PRICE CODE	
17. SECURITY CLASSIFICATION OF REPORT Unclassified	18. SECURITY CLASSIFICATION OF THIS PAGE Unclassified	19. SECURITY CLASSIFICATION OF ABSTRACT Unclassified	20. LIMITATION OF ABSTRACT Unlimited	

NSN 7540-01-280-5500

Standard Form 298 (Rev. 2-89)
Prescribed by ANSI Std. Z39-18
298-102

FOREWORD

Opinions, interpretations, conclusions and recommendations are those of the author and are not necessarily endorsed by the U.S. Army.

✓

Where copyrighted material is quoted, permission has been obtained to use such material.

✓

Where material from documents designated for limited distribution is quoted, permission has been obtained to use the material.

✓

Citations of commercial organizations and trade names in this report do not constitute an official Department of the Army endorsement or approval of the products or services of these organizations.

✓

In conducting research using animals, the investigator(s) adhered to the "Guide for the Care and Use of Laboratory Animals," prepared by the Committee on Care and Use of Laboratory Animals of the Institute of Laboratory Animal Resources, National Research Council (NIH Publication No. 86-23, revised 1985).

✓

For the protection of human subjects, the investigator(s) have adhered to the policies of applicable Federal Law 45 CFR 46.

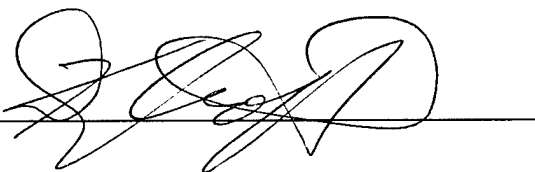
N/A

In conducting research utilizing recombinant DNA, the investigator(s) adhered to NIH Guidelines for Research Involving Recombinant DNA Molecules.

N/A

In the conduct of research involving hazardous organisms, the investigator(s) adhered to the CDC-NIH Guide for Bio-safety in Microbiological and Biomedical Laboratories.

P.I. Signature:



Date:

1/14/00

Table of Contents

<u>Section</u>	<u>Page number</u>
SF 298	2
Foreword	3
Table of Contents.....	4
Introduction.....	5
Body of Report	
EOX Prototype Modification.....	6
Model Eye Calibration Experiments.....	9
Four Wavelength Data Reduction.....	22
Optimum Wavelength Combinations	29
Multipass Transmission in Oximetry.....	34
Construct and Test EOX-2.....	39
Light Scattering by Blood in a Retinal Vessel.....	48
Four-Wavelength Saturation Measurements on Human Subjects.....	57
Swine Four-Wavelength Studies.....	62
Key Research Accomplishments.....	73
Reportable Outcomes.....	74
Conclusion.....	77
References.....	78
Appendices	
Journal Articles and Abstracts.....	
C.V.s.....	
Patents.....	
Bibliography and Paid Personnel.....	

Introduction

The need for a method to identify ongoing occult blood loss in combat casualties with a noninvasive device which is fast, accurate and simple to use is apparent.⁵ The basic principle of shock resuscitation is to ensure that the delivery of oxygen to peripheral tissues is sufficient to maintain aerobic metabolic functions. During shock, therapeutic maneuvers attempt to improve oxygen delivery by optimizing cardiac performance and/or improving the oxygen carrying capacity of blood.^{4,5} Several outcome studies have shown central venous oxygen saturation ($S_{cv}O_2$) to be a reliable index of oxygen delivery, enabling the assessment of the response to specific therapeutic maneuvers during shock.^{8,9,13-15} Unfortunately, obtaining $S_{cv}O_2$ requires invasive monitoring which is time consuming,⁵ costly¹⁶ and has associated complications.^{4,8,12} Consequently, a noninvasive, rapidly applicable technique that provides a reliable index of oxygen delivery during shock resuscitation would be a valuable adjunct to patient management.^{5,8,9,13}

Subject: *The team at UAB and UAH is generating instrumentation and scientific data suggesting that retinal vessel oxygen saturations (both arterial and venous) may be used to identify bleeding prior to changes in vital signs and to help optimize oxygen delivery during the resuscitation of trauma victims.* **Purpose:** *The purpose of this work is to develop a noninvasive tool for measuring a hemodynamic parameter to aid in the triage and treatment of combat casualties who may be bleeding or have bled substantially.* **Scope:** *The scope of this work includes the investigation of the optical properties of the retina and developing the techniques required to accurately measure retinal large vessel oxygen saturations. As this work is being accomplished we have used models of blood loss to demonstrate the potential efficacy of this measurement in the evaluation and treatment of combat casualties.* We have constructed Eye Oximeters (EOX) for measuring the oxygen saturation of blood in retinal veins and arteries. This measurement is obtained by scanning low-power laser beams into the eye and across the vessels of the optic nerve head. The light that scatters back out of the eye is collected and analyzed. From these signals, the oxygen saturation of blood within a vessel is determined by measuring the color change between oxygenated hemoglobin (HbO_2) and reduced hemoglobin (Hb). We have found that absolute calibration of the measurement is problematic secondary to back reflections and pigment variations in the retina. In order to demonstrate the correlation between retinal venous oxygen saturation, cardiac output and mixed venous oxygen saturation, we have identified a subspecies of swine, the sinclair swine, which has no pigmentation in the retina. The EOX has been used in sinclair swine studies discussed later in this report to demonstrate proof of concept. Retinal venous oxygen saturation correlates with cardiac output and mixed venous oxygen saturation during profound blood loss and subsequent resuscitation.

EOX Prototype Modifications

The Eye Oximeter prototype (EOX) includes many of the changes in the breadboard instrument²¹ which we proposed in this contract. We attempted to improve the breadboard instrument by increasing the number of laser wavelengths from two to four (629, 678, 821, and 899 nm), increasing the scan width, improving the quality of the cross polarized glint reduction system, and adding an R-wave trigger. The scan length is approximately 1 mm long, allowing an artery-vein pair to be scanned if desired. The design of this instrument is described in a manuscript that is being prepared for submission to *The Journal of Biomedical Optics*.

At the start of this grant, this device was not fully ready for use and a portion of the first year was used to complete the modifications and testing of the EOX. The addition of a r-wave trigger was performed during this contract. This trigger lets the EOX begin a scan at the r-wave of the EKG. This modification should eliminate variations in the calculated oxygen saturation that are secondary to changes across the cardiac cycle, and will eventually allow us to study changes in oxygen saturation and vessel diameter as a function of the cardiac cycle. The primary modifications to the EOX made over the last year were in the software that controls the instrument and the software that analyzes the raw scans collected by the instrument.

The instrument control software is written in Visual Basic 4.0 in the Windows 95 operating system. A screen capture of the control program is shown in Fig. 2. The data acquisition card used to control the EOX is a Microstar Laboratories DAP 1200/a. This card has an onboard i486 processor and 2 MB for RAM that allows it to run in realtime without concern

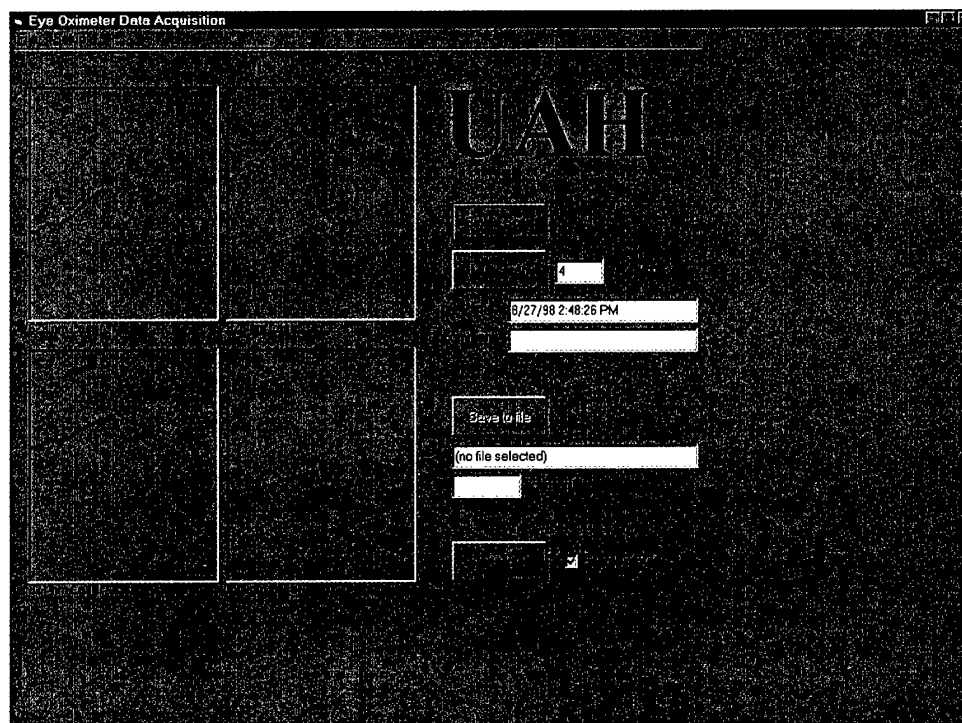


Figure 2. Screen capture of the EOX instrument control software. An artery-vein pair was scanned (artery on the right, vein on the left).

of interrupts across the PC bus. The card is programmed in the DAPL programming language that is provided by Microstar Laboratories.

The acquisition software allows the user to collect single or multiple scans and display them to the screen. If the intended vessels have been successfully scanned, then the user can save the raw scan data to a file. There is also a "movie mode" that acquires and displays scans continuously at a rate of about 3 per second. This mode is particularly useful when aligning the instrument to the head of an anesthetized swine or when fine-tuning the laser focus. However, due to laser safety considerations, this mode is not used in humans. Future versions of the software may perform the "movie mode" using only one infrared laser. This would allow active focusing of the lasers in a human subject's eye at safe laser power levels.

We have also made significant improvements in the EOX scan analysis software. Currently, the EOX data is post-processed via a separate program. A screen capture of this software is shown in Fig. 3. The software includes pattern matching routines (based on a convolution in the Fourier plane to an assumed vessel profile) that can accurately identify single vessels with high accuracy (>95% for the infrared lasers). However, these routines have not yet been updated to account for multiple vessels in a single scan. The operator is able to override the software's vessel selection through a series of mouse clicks on the vessel displays. The software then fits curves to the vessel profile to calculate the perceived transmittance of the vessel at each of the four wavelengths.²¹ The software also calculates the diameter of the vessel at each

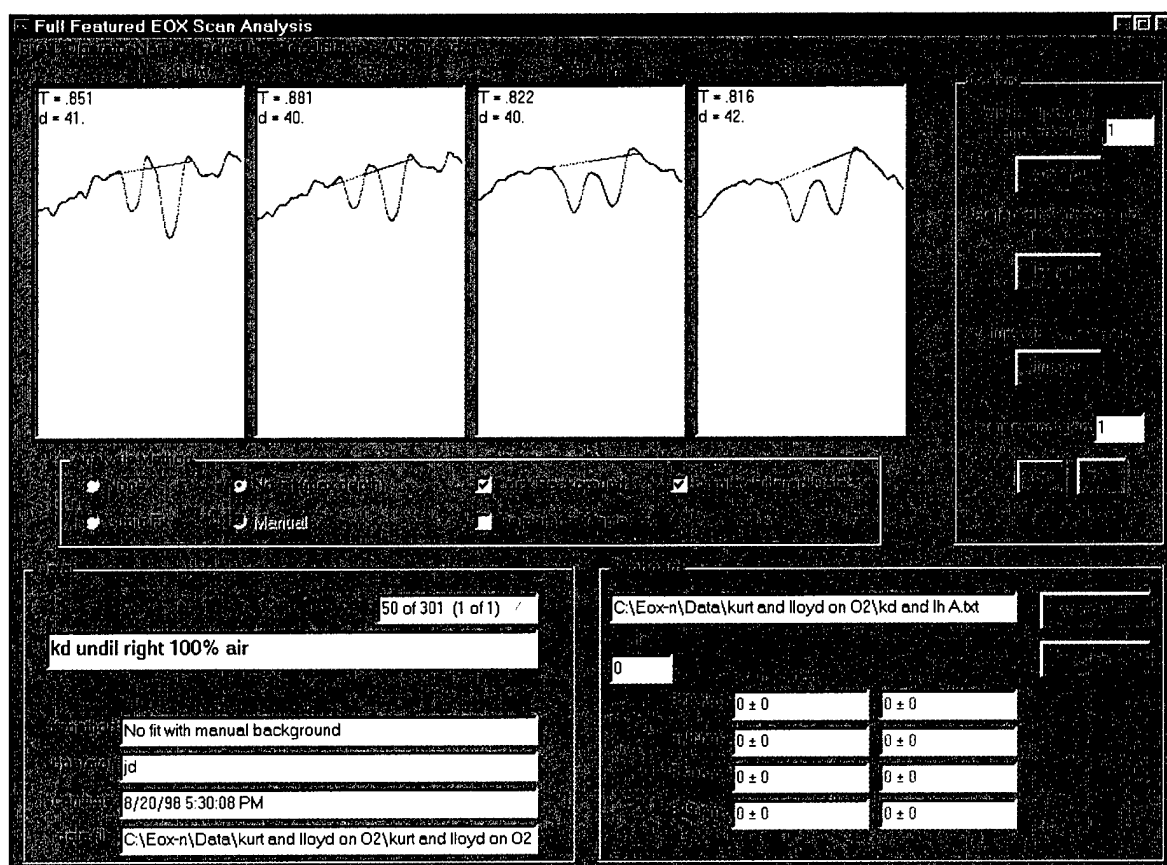


Figure 3. Screen capture of the EOX scan analysis software.

wavelength. The diameter is estimated by measuring the width (in pixels) of the scan profiles. No attempt is made to calibrate these diameters to actual retinal distances, although such a calibration could be possible if the subject's refractive error and eyeball chamber length were accurately known.

At this time, the scan analysis is still guided by a trained operator. The most challenging aspect of scan analysis is the placement of the background line (see the red lines in Fig 3). This is the line that estimates what the intensity of the retinal background would have been in the absence of the vessel. Correct placement of this line is imperative if accurate vessel transmittance values are to be obtained. Our current algorithms choose this line quite well for the 821 and 899 nm lasers, however the operator frequently has to override the automatic selection for the red (629 and 678 nm) lasers due to increased spatial variability of the fundus.

Summary

The EOX allowed us to test several of our original questions including, "do these measurements depend on vessel diameter?", "how many optical wavelengths are required to make these measurements?", and "do these measurements depend on hematocrit (or hemoglobin concentration)?" In the following sections of this report, we will refer to this prototype as the EOX.

An Optical Model of the Blood in Large Retinal Vessels

Introduction:

Several optical techniques that investigate the arteries and veins of the retina are either commercially available or are under development. These techniques include retinal Doppler flowmetry[1], large retinal vessel spectroscopic blood oximetry[2-6] and dynamic measurements of blood vessel pulsations[7]. The optical accessibility of the retina facilitates these techniques, however getting light into and out of the eye presents several interesting problems. Some of these challenges include pigment variability in the retina, lens cataracts, vessel shape, vessel proximity, and large choroidal vessels.

We present an inexpensive mechanical model that simulates the optical geometry of the eye, the blood flowing in a retinal vessel, and the diffuse reflectance properties of the ocular fundus. We also describe an apparatus used to set the hemoglobin concentration and oxygen saturation of a blood sample without affecting the geometry of the red blood cells (and thus the scattering properties of the blood). The model is used to increase understanding of the scattering and absorption effects of the flowing blood, but the model does not include such confounding effects as the polarization influences of the cornea and nerve fiber layer, the optical properties of the vessel wall, the irregular choroidal blood vessels beneath the retinal pigmented epithelium, and the scattering properties of the crystalline lens or vitreous.

Materials and Methods:

A 5 μl micropipette (Fisherbrand disposable micropipettes, Cat. # 21-164-2B, Fisher Scientific) was chosen as the retinal vessel model. The 10 cm length facilitated mounting and grasping, and the 268 μm inner-diameter is slightly larger than the largest retinal veins (212 μm) and arteries (150 μm). [7] To more closely approximate these dimensions, the pipettes were gently pulled on a lathe while softened with a Bunsen burner. The resulting tapered pipettes had inner diameters ranging from 110 to 268 μm .

These micropipettes are manufactured from a borosilicate glass with a nominal refractive index of $n_d = 1.4712$. As a result, the pipette acts as a powerful cylindrical lens, and this optical power must be removed in order to be useful as a model. Standard Type A immersion oil (Cargille Laboratories, Cedar Grove, NJ) was purchased as an inexpensive replacement for more expensive index matching fluids. The index of Type A oil is $n_d = 1.5150$, which is slightly too high to provide a good index match to the pipettes. We titrated the Type A oil with mineral spirits ($n_d = 1.438$ as measured by an Abbe refractometer) and index matched the pipette such that it was completely invisible to visual inspection when immersed in the fluid.

We used a slab of Spectralon (Labsphere, Inc.) adhered to an aluminum plate as a tissue phantom simulating the retinal layers. Spectralon is a diffusely reflective, spectrally neutral material typically used in integrating spheres. By modifying the thickness of the Spectralon slab, we were able to control the size of the diffusion-enlarged point spread function on the simulated retina. We use a 4 mm thick slab of Spectralon that results in a diffusion enlarged point spread function (PSF) that is ~ 40 μm FWHM. This compares well with estimated retinal PSFs for

visible wavelengths reported in the literature.[8] Using thicker slabs of Spectralon results in larger PSFs. Alternately, other researchers have suggested latex microspheres suspended in epoxy as a useful phantom to simulate the diffuse reflectance properties of tissues.[9,10]

We constructed a mechanical housing which simulates the eyeball (See Fig. 1). The housing is filled with the index matching fluid. A plano-convex lens (Royln Optics, #10.0025) adhered to the housing with MIL-Bond is used to simulate the cornea. This lens has a focal length of 17.2 mm in air, but closely approximates the 23 mm focal length of the average human eye when the planar side of the lens is immersed in the index matched fluid. The entrance pupil diameter was set to 6 mm. The center of the pipette is located 22.6 mm behind the planar surface of the lens, and the Spectralon slab is positioned directly behind the pipette. An infinitely distant object that subtends 1° will form an $294\text{ }\mu\text{m}$ image on the retina of the model eye. This corresponds closely to the typical magnification ($297\text{ }\mu\text{m}$ per degree) of the normal human eye.[11] The model eye was constructed such that the pipettes could be positioned in various locations both on-axis and off-axis since the major vessels of the human eye are approximately 15° off-axis. Bead blasting and black anodizing the inside of the mechanical housing prevents multiple reflections within the eye from exiting the pupil.

To simulate blood flow through the retinal vessel, a syringe pump (Harvard Apparatus, Model # 55-1111) was used to pump whole human blood through a short length of tubing, and through the pipette. The pump was set to deliver blood at a typical value of retinal blood flow ($34\text{ }\mu\text{l/min.}$).[12] A catch basin collected the blood after it passed through the eye and was disposed of via approved methods.

Preparation of blood samples was carefully conducted to assure that a single variable was being modified throughout a given test. Whole human blood (500 cc) was drawn from a healthy donor according to an Internal Review Board (IRB) approved protocol. The blood was anticoagulated (citrated dextrose) to prevent clotting during the measurement. The anticoagulant is not expected to affect the scattering measurement since it does not alter the red blood cell size or shape, and its small volume fraction will not significantly alter either the refractive indices of the components or their relative concentrations. The whole blood was immediately packed in ice and samples were drawn and prepared as needed. A sample of blood was centrifuged for approximately 5 minutes to separate the plasma from the cellular component of the blood. The packed blood cells and plasma were mixed volumetrically to make different concentrations of blood cells in plasma. The use of the patient's own plasma to dilute the blood minimizes changes in the size and shape of the red blood cells and possible color changes which may occur when isotonic salt solutions are used to dilute the blood.

A three-gas mixer was used to individually set the oxygen, nitrogen and carbon dioxide concentrations of a combined gas. The total flow rate for the gas mixture was set at three liters per minute. The CO₂ flow was adjusted (~0.1 l/min.) to ensure the partial pressure of CO₂ in the blood was maintained at 35-45 mmHg, as measured by a blood gas machine (Corning 280 pH / Blood Gas Analyzer). The ratio between N₂ and O₂ flow rates was varied in order to set the oxygen saturation of the blood sample. This gas mixture was bubbled through a warm water bath saturating the gas with water vapor and warming it to body temperature. The warmed, humidified gas mixture was passed over the blood sample in a counter current exchange system

as the blood was pumped through a closed circuit. A subsection of the blood circuit tubing was passed through a warm water bath (39° C) to keep it at body temperature during the oxygenation procedure. The blood was pumped through the system at a rate of 1000 ml/hour. This system is illustrated in Figure 2. The blood was allowed to flow through the circuit for as long as is required to obtain the desired oxyhemoglobin saturation level, generally about 15 minutes. We used a CO-Oximeter (Corning 2500 CO-Oximeter) to measure the oxygen saturation and hemoglobin concentration of the prepared blood samples.

Results:

Our primary purpose for developing this model was to test a scanning laser retinal vessel oximeter that we are developing.[4,5,6] The Eye Oximeter (EOX) shines low-power lasers into a subject's eye, and scans the beams across the retinal vasculature. The light that is scattered back out of the eye is collected and analyzed. Performing this measurement at multiple wavelengths allows spectroscopic determination of the oxygen saturation of blood contained within the arteries and veins of the retina. In Figure 3, we compare EOX scans acquired from a human eye to scans acquired from the model eye. These scans are one-dimension profiles of the collected intensity as a beam is scanned perpendicularly across the vessel. The similarity between the scans is obvious. The primary difference between the scans is that those acquired from the model eye have uniform intensity in regions lateral to the vessel, while human scans can be quite irregular in regions lateral to the vessel due to underlying choroidal vessels and variations in retinal pigmentation.

In a recent set of experiments [13], we used this model eye apparatus to calibrate a four-wavelength version of the EOX. We generated an array of blood samples with oxygen saturation values ranging from 6 to 87 %O₂Sat and hemoglobin concentrations ranging from 5.0 to 27.2 g/dl, and we used a variety of vessels with diameters ranging from 110 to 268 μ m. A total of 187 different combinations were generated. This large array of known samples was used to develop equations that allow that accurate calculation of oxygen saturation. For demonstration, we show the results this calibration experiment in Figure 4.

Discussion and Conclusions:

By using the model eye and blood preparation system described in this paper, we were able to develop an increased understanding of oximetry in the ophthalmic environment. This system is useful for testing systems that use light to study the blood and blood flow in retinal vessels. Such systems include fluorescent dye photography, laser doppler flow experiments, and spectroscopic studies of blood constituents.

In this model we did not attempt to model the coloration of the retina (pigment epithelium), the choroidal circulation (an absorptive and scattering function as apposed to simply scattering with Spectralon), scattering from the lens and vitreous, and the vessel wall (a vessel wall in water as apposed to a pipette in index matching solutions). These interactions make the eye a complex environment, and we used this in an attempt to decrease the number of these variables. As we increase our understanding of the light-eye interaction, these more complex models will likely be required for further hypothesis testing. An extension of this work will be the creation of phantoms that model both the scattering properties and the coloration of

the human ocular fundus. Alternately, human retinal tissue samples embedded in epoxy might prove to be ultimate model for this system. Another improvement that should be made to the mode is the inclusion of an adjustable pupil diameter. Simulating the vessel wall and scattering from the lens and vitreous will prove to be more challenging, and we currently have no plans to attempt these models.

A good *in vitro* model is imperative in the development of noninvasive techniques for measuring physiologic parameters. This is particularly true in the retina because actual values of the parameters being measured often cannot be measured directly for comparison. The inexpensive model described here has proven invaluable for advancing our understanding of retinal vessel oximetry.

References:

1. A. Harris, L. Kagemann, G.A. Cioffi, "Assessment of human ocular hemodynamics," *Survey of Ophthalmology* **42**(6), 509-533 (1998).
2. D. Schweitzer, M. Hammer, M. Scibor, "Imaging spectrometry in ophthalmology-- principle and applications in microcirculation and in investigation of pigments," *Ophthalmic Research* **28 Suppl 2**, 37-44 (1996).
3. J.M. Beach, K.J. Schwenzer, S. Srinivas, D. Kim, J.S. Tiedeman, "Oximetry of retinal vessels by dual-wavelength imaging: calibration and influence of pigmentation," *Journal of Applied Physiology* **86**(2), 748-758 (1999).
4. K.R. Denninghoff, M.H. Smith, R.A. Chipman, L.W. Hillman, P.M. Jester, C.E. Hughes, F. Kuhn, L.W. Rue, "Retinal large vessel oxygen saturations correlate with early blood loss and hypoxia in anesthetized swine," *Journal of Trauma-Injury Infection & Critical Care* **43**(1), 29-34 (1997).
5. M.H. Smith, K.R. Denninghoff, L.W. Hillman, C.E. Hughes, T.E. Minnich, R.A. Chipman, "Technique for noninvasive monitoring of blood loss via oxygen saturation measurements in the eye," *Invited Paper in Optical Diagnostics of Biological Fluids II, Prezzhev AV, Asakura T Eds., Proc. SPIE* **2982**, 46-52 (1997).
6. K.R. Denninghoff, M.H. Smith, L.W. Hillman, D. Redden, L.W. Rue, "Retinal venous oxygen saturation correlates with blood volume," *Academic Emergency Medicine* **5**(6), 577-582 (1998).

7. H.C. Chen, V. Patel, J. Wiek, S.M. Rassam, E.M. Kohner, "Vessel Diameter Changes during the cardiac cycle," *Eye* **8**, 97-103 (1994).
8. I.J. Hodgkinson, P.B. Greer, A.C. Molteno, "Point-spread function for light scattered in the human ocular fundus," *Journal of the Optical Society of America A-Optics & Image Science* **11**(2), 479-486 (1994).
9. P. Danilova, S.P. Chernova, A.B. Pravdin, "Tissue-like phantoms: fluorescence under 405 nm excitation," *Saratov Fall Meeting 1998: Light Scattering Technologies for Mechanics, Biomedicine, and Material Science*, Valery V. Tuchin, Vladimir P. Ryabukho, Dmitry A. Zimnyakov, Eds., *Proc. SPIE* **3726**, 410-414 (1999).
10. S.T. Flock, B.C. Wilson, M.S. Patterson, "Total attenuation coefficients and scattering phase functions of tissues and phantom materials at 633 nm," *Medical Physics* **14**(5), 835-841 (1987).
11. D. Sliney, M. Wolbarsht, "Safety with Lasers and Other Optical Sources," Chap. 3, *Plenum Press, New York*, 1980.
12. T.F. Gilbert, T. Hiroshi, D.M. Deupree, D.G. Goger, J. Sebag, J.J. Weiter, "Blood Flow in the Normal Human Retina," *Investigative Ophthalmology and Visual Science* **30**, 58-65 1989.
13. J. D. Drewes, M. H. Smith, D. R. Denninghoff, L. W. Hillman, "An Instrument for the Measurement of Retinal Vessel Oxygen Saturation," in *Optical Diagnostics of Biological Fluids IV*, Alexander V. Priezzhev, M. V. Lomonosov, Toshimitsu Asakura, eds., *Proceedings of SPIE* **3591**, 114-120 (1999).

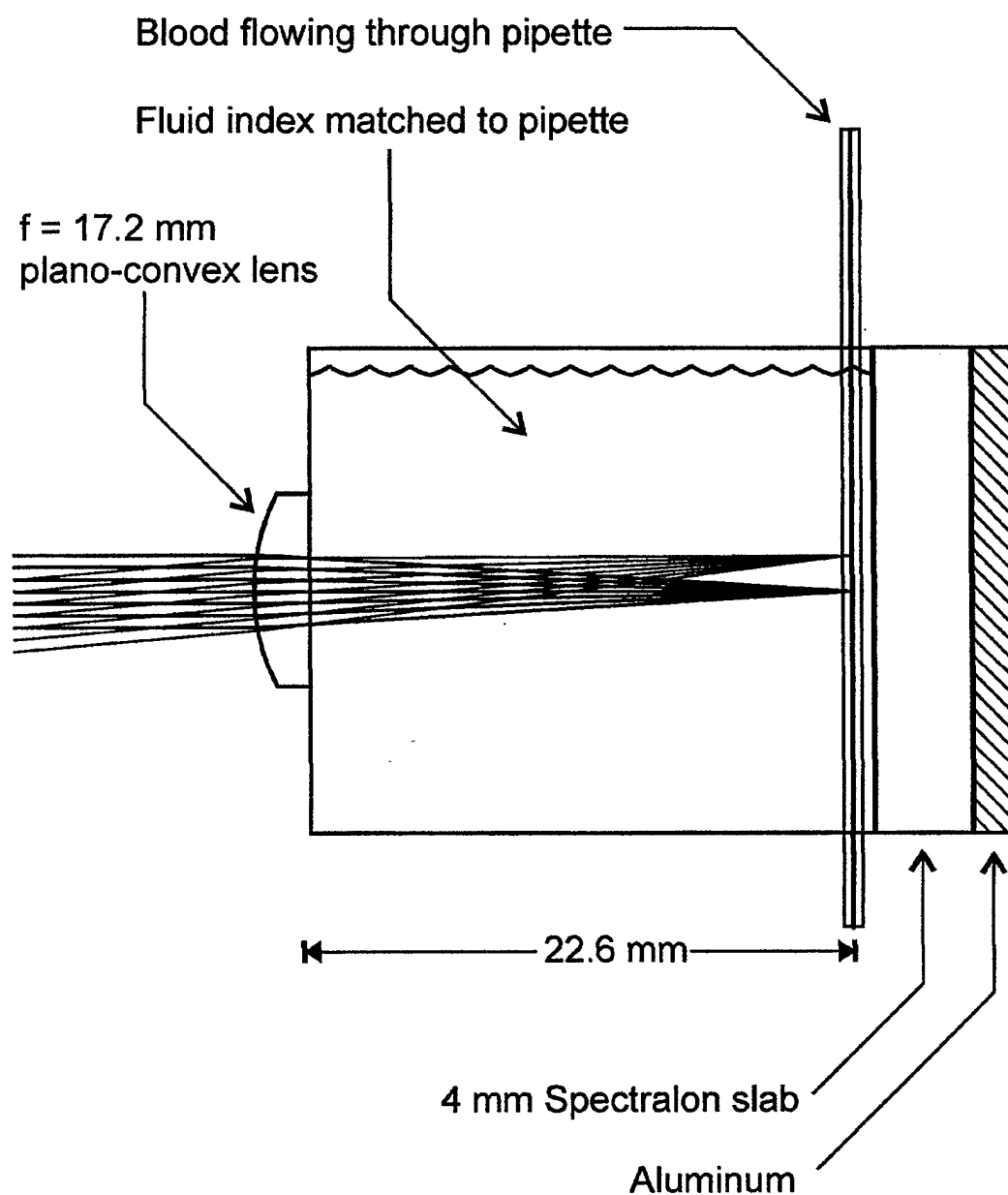


Figure 1:

Schematic of the model eye and blood vessel. A pipette filled with whole blood is immersed in index matched fluid and positioned in front of a piece of Spectralon. A plano-convex lens simulates the refractive power of the cornea and lens. Incoming rays from infinitely distant objects that are on-axis and 5° off-axis are shown.

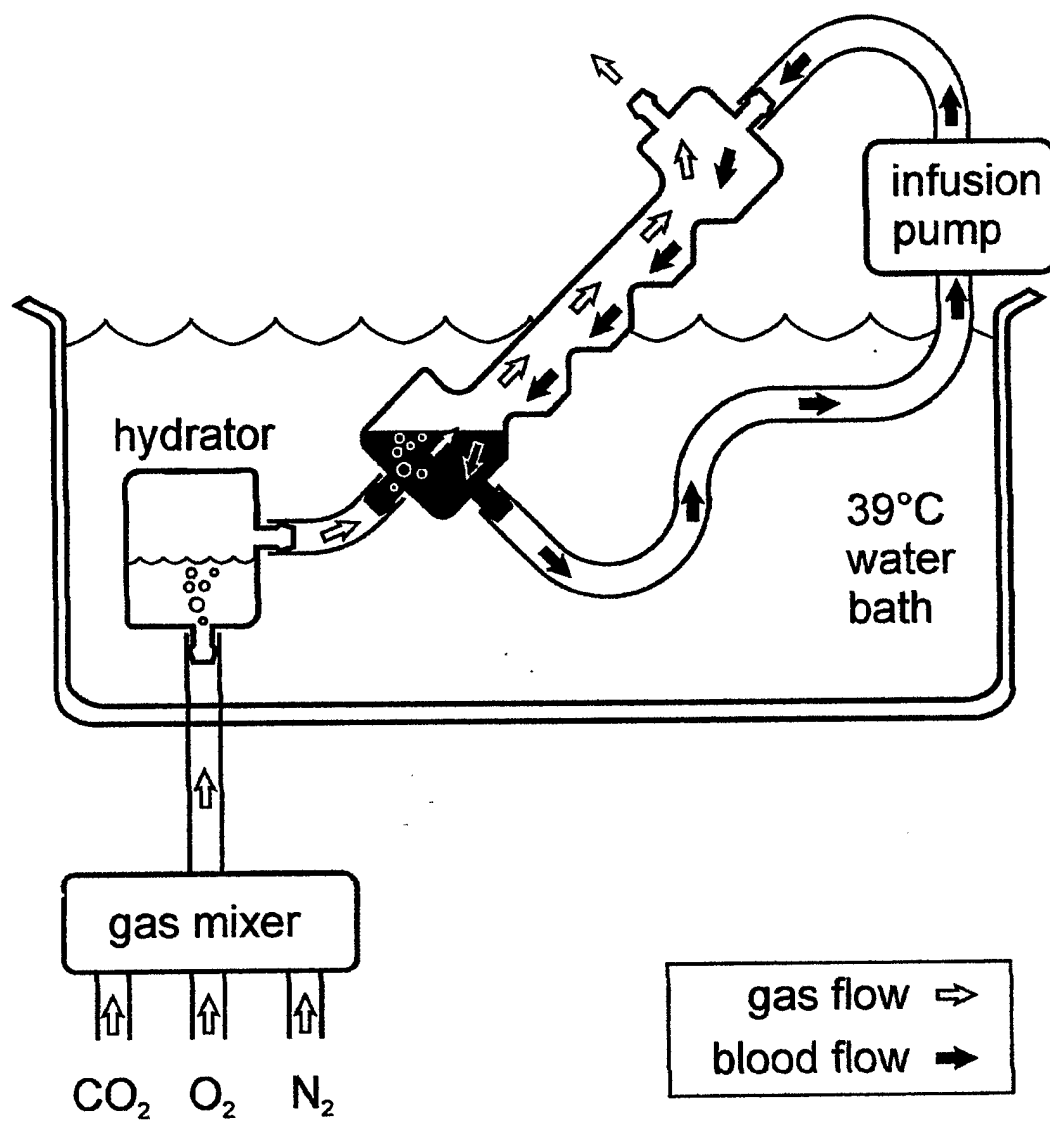


Figure 2:

Schematic of the apparatus for setting the oxygen saturation of whole blood. The apparatus allows the CO_2 , O_2 , and N_2 gas levels to be set while keeping the blood hydrated and at body temperature.

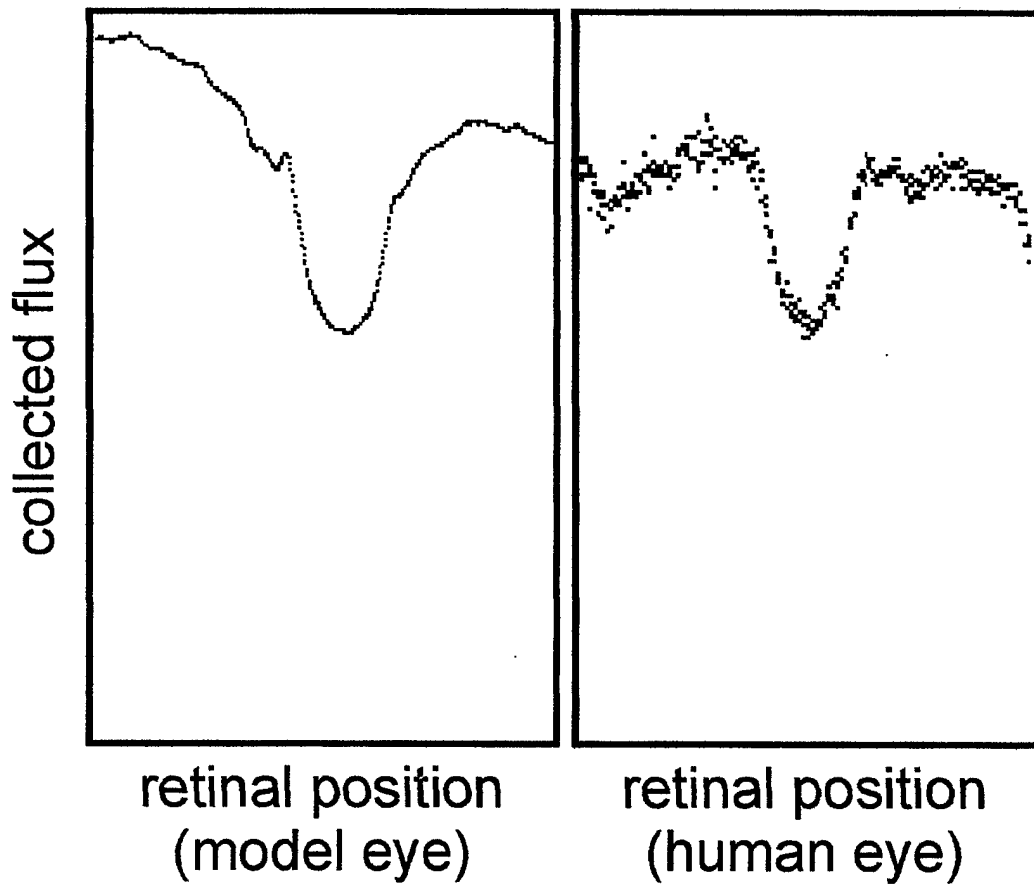


Figure 3:

Comparison of one-dimensional retinal vessel intensity profiles. The scan on the left was acquired in the model eye and the scan on the right was acquired in a human eye. Note the decreased noise in the model eye scan that is due to the high reflectivity of Spectralon.

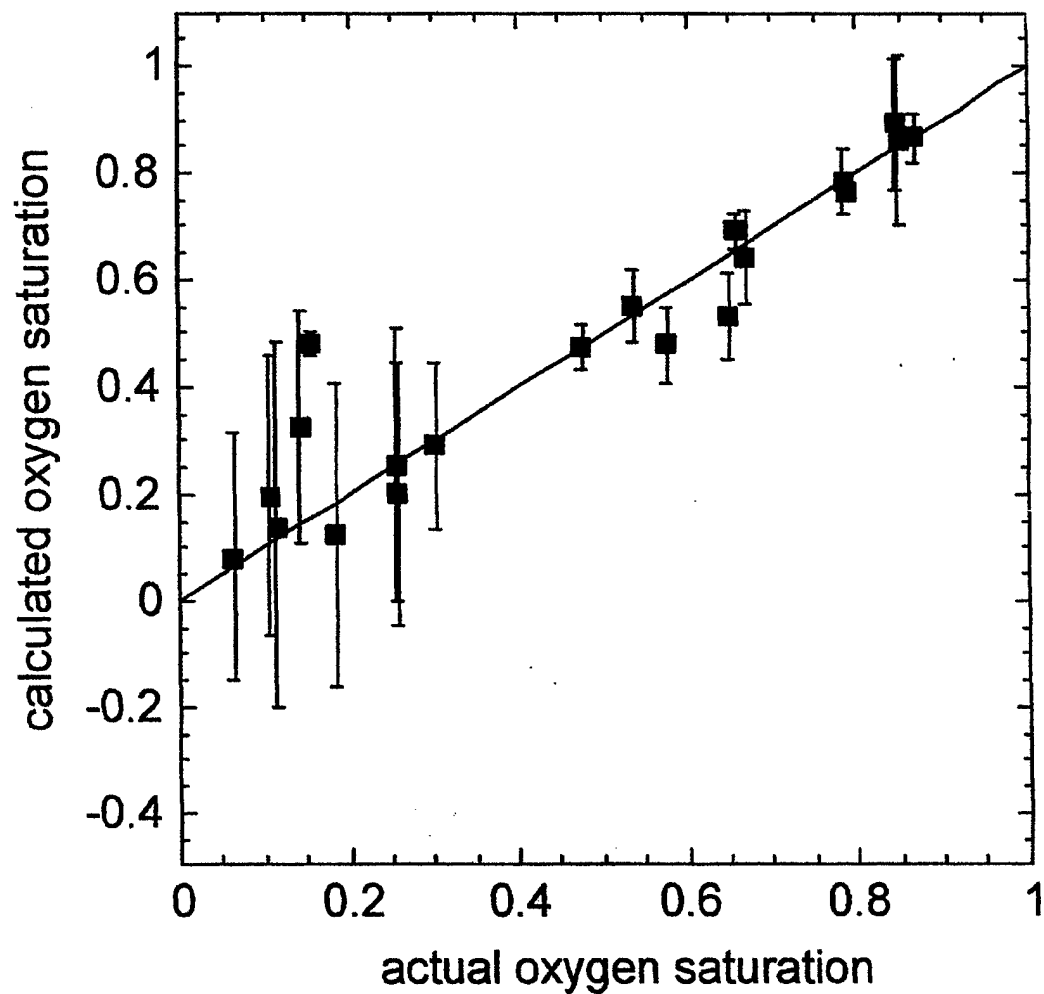


Figure 4:

Example of data acquired in the model eye. This graph is the result of the Eye Oximeter calibration experiment described in Ref. 13. Each data point represents a blood sample with different oxygen saturation and hemoglobin concentration. The error bars indicate the standard deviation of measurements made at different vessel diameters ranging from 110 to 268 μm .

Four Wavelength Data Reduction Using the EOX

Introduction

Using the model eye, we obtained transmittance measurements at the four wavelengths (629, 678, 821 and 899) for 211 different combinations of oxygen saturation, hemoglobin, and diameter. In our analysis of this data, we have constructed model functions to describe the transmittance as a function of these parameters and wavelength. Mathematica® (software by Wolfram Research, Inc.) was used throughout this analysis and calibration procedure. We document, here, several of the attempts at generating an accurate model function for transmittance and discuss the method which performed best to calibrate the model eye data set.

Modeling the Transmittance

At a given wavelength, transmittance T measured by the EOX of a targeted vessel within the model eye is considered to be a product of the transmittance due to the optical absorption T_a and a transmittance caused by the optical scattering T_s from the blood inside the vessel, $T = T_a T_s$. We will consider the absorption transmittance to take the form of Beer's Law written for a two-component absorber

$$T_a = 10^{-cd[s\epsilon_{HbO_2} + (1-s)\epsilon_{Hb}]} \quad (1)$$

where c is the concentration of hemoglobin, d is the length of the physical path through the vessel, s is the oxygen saturation of the hemoglobin, and the ϵ 's are the absorption coefficients of oxyhemoglobin and reduced hemoglobin at a given wavelength. This transmittance describes only the absorption process by the hemoglobin components within the retinal vessel.

To model the scattering transmittance, we first chose to make T_s a constant¹⁷. The model function then becomes

$$T = T_a T_s^o \quad (2)$$

Applying this to the calibration data set yielded inaccurate calculations of oxygen saturation. The model function did not fit the transmittance data points well.

Next, we allowed each of the scattering transmittances at our wavelengths to vary discretely through an optimization procedure which found the best compromise for the entire data set. The resulting empirical functionality for the scattering transmittance increases with wavelength as seen in Figure 8. The calculated oxygen saturation using this model,

$$T = T_a T_s^o k(\lambda) \quad (3)$$

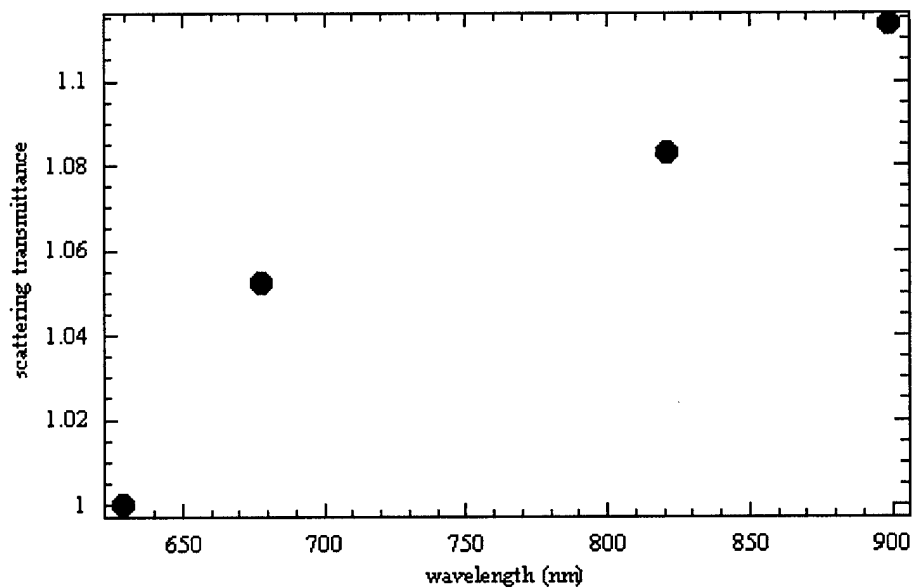


Figure 8. Discrete wavelength dependence of scattering found by optimization of the model eye data set.

where $k(\lambda)$ represents this discrete wavelength factor, normalized with respect to the value at 629 nm, still yielded inaccurate model fits to transmittance data. Further, we find that for actual saturations which were below 50 %, this model would consistently calculate a saturation value no lower than about 40 %. At higher actual saturation values, the model gave nearly correct values for saturation.

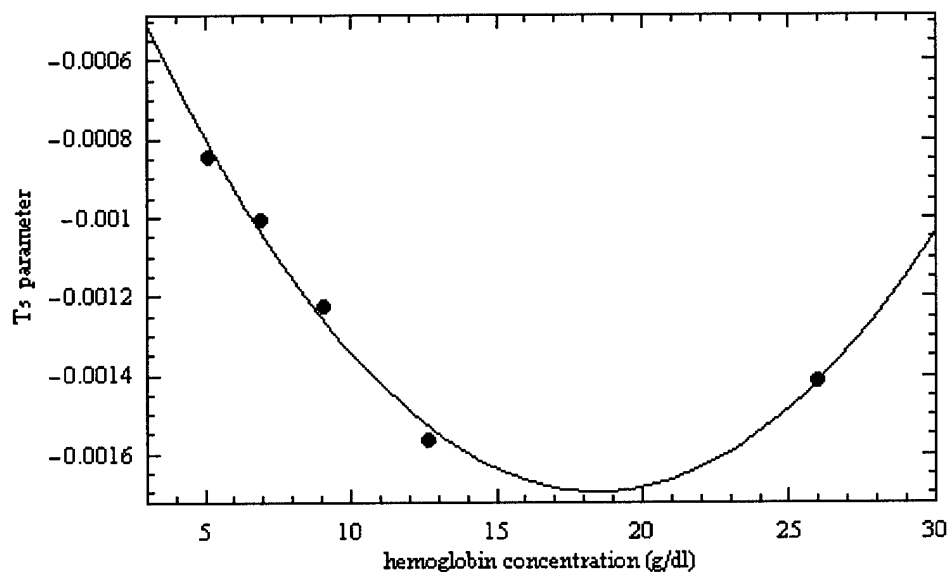


Figure 9. A parabolic nature of the scattering transmittance was seen with concentration.

Next, we investigated the relationship between the scattering transmittance and the concentration and diameter parameters. To do this, we used the constant scattering model (Eqn. 2) looking at the relationship between the calculated value for T_s^o and c and d . The dependance calculated as a function of concentration looked parabolic, with a minimum at 18 g/100mL and increasing on both sides of that value (Figure 9). This dependance agrees with other investigators¹⁷ measurements, having a minimum value at a hematocrit (fractional volume) of about 50 % (or a hemoglobin concentration of about 16 g/100mL). The scattering transmittance relationship as a function of the diameter was found to be linear, increasing with decreasing diameter. Using this empirical function for $T_s(c,d)$, we calculated saturation. The calculated values for saturation were similar to those found using the previously described method with discrete λ dependance.

Finally, we attempted an empirically-determined scattering correction that was linear with wavelength. Our model function for the scattering transmittance is:

$$T_s = T_s^o \left[1 + m \frac{(\lambda - \lambda_o)}{(\lambda_n - \lambda_o)} \right] \quad (4)$$

where m is a slope factor, λ_o is the shortest measuring wavelength, and λ_n the longest measuring

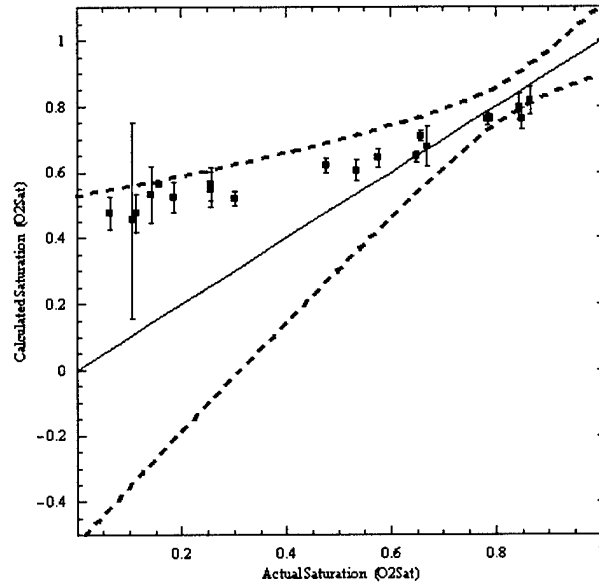


Figure 10. Model eye calibration with linear wavelength dependance of scattering transmittance. The dashed curves represent the expected error in saturation given a 1 % error in the transmittance measurement.

wavelength. Here, $\lambda_o = 629$ nm and $\lambda_n = 899$ nm, and with $m \sim 0.03$, T_s goes from T_s^o to $1.03 T_s^o$ linearly over our wavelength range. We optimized the value of m to the model eye data

using the known s , c , and d parameters. Applying the new model to the data results in more accurate fits over the previous models. Our total transmittance model function now requires that we solve for the three unknowns s , cd , and T_s^o .

When this model is applied to the data set, the actual saturations below 60% map to calculated values which do not go below the 40% level. This resulted in a “bowed” calibration curve (Figure 10). At this point, we began seeking explanations for this unexpected behavior. Finally, we questioned the accuracy of the blood absorption coefficient data we had been using. This led us to try to calibrate and solve for the 8 absorption coefficients that we were using.

Calibration to Determine the Absorption Coefficients

Using the linear wavelength dependant scattering transmission model, we tried several methods to determine what the absorption coefficients were given the known values for the saturation, concentration, and diameter. Writing the oximetry equations in matrix form for four wavelengths enabled quick calculations of the absorption coefficients. In order to solve for them, the scattering optical density had to be given some functionality. We chose to make it take the form

$$D_s = \text{Sin}^{\frac{1}{3}} \left(\frac{c}{3} \right) \quad (5)$$

which approximates the expected behavior with concentration for $c < 15$ g/100mL. Calculating the 8 ϵ 's which give the best results for the model eye data set, we found that the calibration curve of saturation no longer exhibited the "hook" feature seen previously. In fact, the r^2 value of the fit was 0.95. However, many of the resulting values for the 8 ϵ 's were too far from their referenced values to be legitimate measurement error. Some of them were 200% of their reported values. We concluded that there were too many degrees of freedom in this optimization

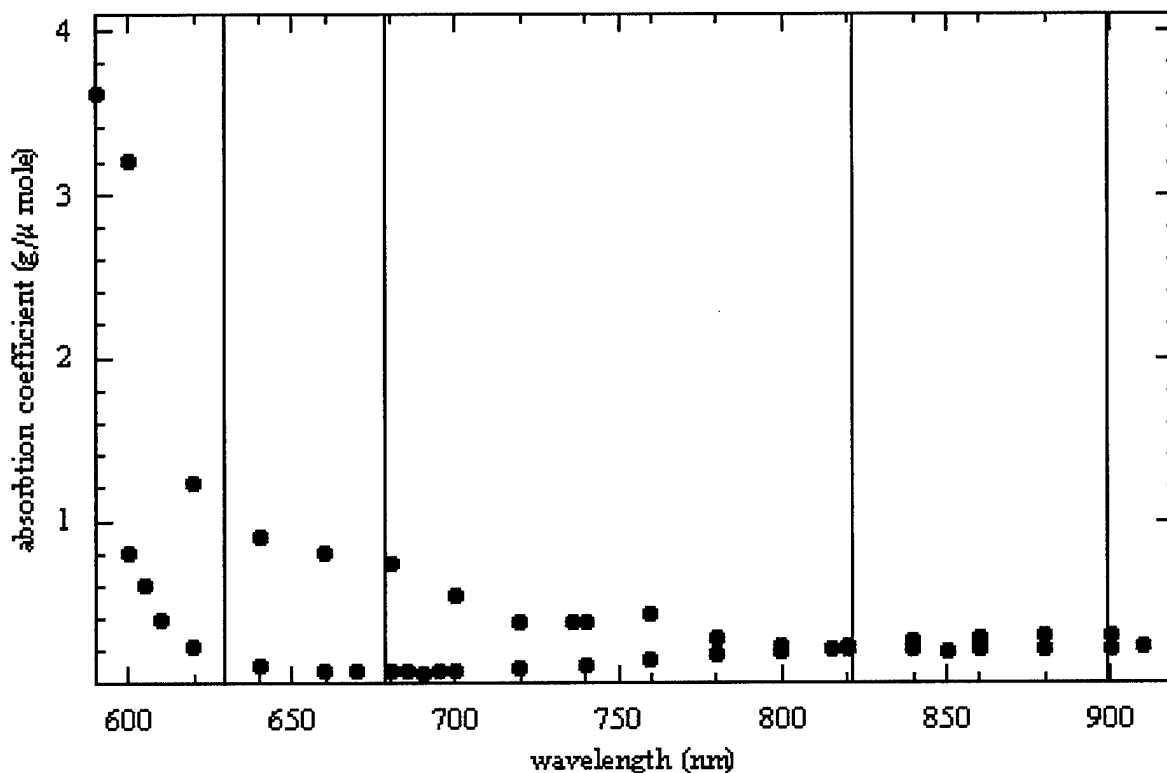


Figure 11. Absorption spectra of oxyhemoglobin (red) and deoxyhemoglobin (blue) from VanAssebedekt's data²². The discrete nature of the data requires that we perform a parabolic interpolation of the data. Our measuring wavelengths are indicated by the vertical lines.

procedure which resulted in this outcome. Further, we applied this calibration to human eye data only to find that the resulting fit parameters were nonphysical. Another method of removing this "hook" in the calibration was required.

We expect that the most likely extinction coefficients to be in error are those in which $\partial\epsilon/\partial\lambda$ are the greatest. Also, the absorption data we use is given at discrete wavelengths²² and we perform a parabolic interpolation of the data to approximate intermediate values (Figure 11). Therefore, the absorption coefficient at 629 nm of deoxyhemoglobin was thought to contain the largest probable error. If this was in fact the primary error in the calibration of the data set, we would expect the "hook" to be corrected with the value of ϵ_{Hb}^{629} actually being larger than determined from the reported value, 1.06 g/ μ mole.

We developed an optimization routine to find the value of ϵ_{Hb}^{629} which best calibrates the data set from the model eye experiment. We found that a value of $1.42 \text{ g}/\mu\text{mole}$ for this coefficient produced a very good calibration line, with $r^2 = 0.89$ (Figure 12). Our calculated

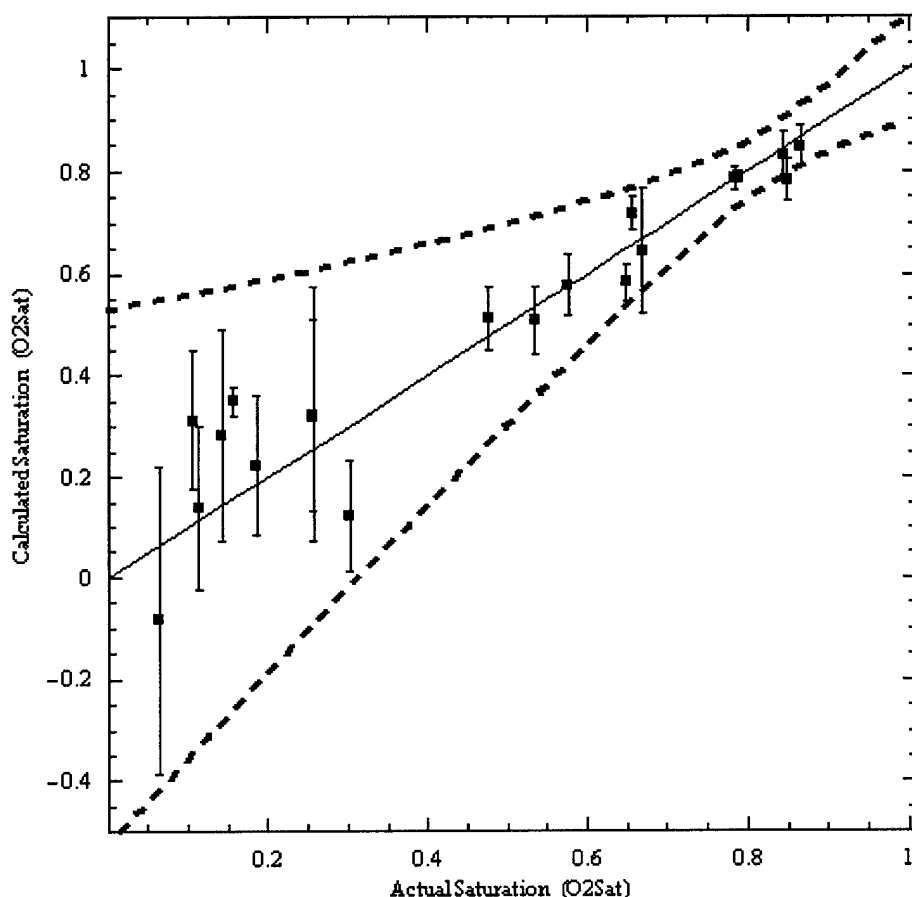


Figure 12. Model eye calibration when ϵ_{Hb} at 629 nm has been adjusted.

value of ϵ_{Hb}^{629} is larger than the value from the reported data, and it is larger than $\epsilon_{Hb}^{620} = 1.23$. It is possible that there is some feature present in the absorption spectra in the vicinity of the 629 nm wavelength which would account for this difference.

We cannot be certain that our calculated value for ϵ_{Hb}^{629} is correct until we perform spectroscopic measurements at our measuring wavelength(s) for these blood components. However, we do seem to be calibrated within the expected experimental error of the saturation measurement as seen in Figure 12. Preliminary applications of this new model to human eye transmittance data yield saturation values that we expect.

Summary

We have completed an analysis of data from a model eye using the EOX which has resulted in an *in vitro* calibration of a four wavelength scan analysis. This is one of our project milestones for year one of this contract. We used this model eye in a similar manner to test the EOX-2 described later in this report. The *in vivo* testing of this device is described in later sections of this report. See "Retinal vessel oximetry: Toward absolute calibration" for a detailed description of the use of the model eye to calibrate the EOX-2.

Optimum Wavelength Combinations

One of the most important aspects of retinal vessel oximetry is the choice of the optical wavelengths used for the measurement. Previous work performed by our group²³ has indicated that a combination including one blue-green laser, one red laser, and one infrared laser may result in oxygen saturation measurements with extremely high accuracy. Over the past 10 months, we have written a manuscript detailing the optimization procedure and presenting optimum wavelength triads.²⁴ (See appendix for this article). This paper has been accepted for publication in *Applied Optics*. This technique was originally laid out in our U. S. Patent #5,776,060.²⁵

The technique described in this manuscript is straightforward. When selecting wavelengths for oximetry, one must *not* simply choose wavelengths where the extinction coefficients between hemoglobin and oxyhemoglobin are large. Also, the inclusion of an isobestic wavelength is not helpful. These choices do not guarantee high sensitivity to oxygen saturation. Instead, the goal is to choose wavelengths that minimize the error in the calculated saturation due to small errors in measured vessel transmittance. Wavelength combinations are chosen such that the error $\partial s / \partial T$ is small across a broad range of vessel diameters and oxygen saturation levels, where the error is calculated from the equation

$$\Delta s = \sqrt{\left(\frac{\partial s}{\partial T^{\lambda_1}} \Delta T^{\lambda_1} \right)^2 + \left(\frac{\partial s}{\partial T^{\lambda_2}} \Delta T^{\lambda_2} \right)^2 + \dots + \left(\frac{\partial s}{\partial T^{\lambda_n}} \Delta T^{\lambda_n} \right)^2}. \quad (1)$$

The expression for the saturation s can either be a closed-form expression (so that there are closed form expressions for the partial derivatives) or the result of a curve fitting algorithm. If s is determined from a fit, then the partial derivatives need to be calculated numerically.

As part of the peer review process, two points were brought to our attention. First, the target vessel diameters for our optimization were about 50% too large. As such, we re-tuned the optimization using 160 μm and 120 μm as targets for retinal vein and artery diameters, respectively. It turns out that this had almost no effect on our optimum wavelength choices. Next, it was pointed out that the media of the eye absorbs light significantly at 960 nm (double-pass transmissions as low as 10%). Since our original optimization indicated 960 nm was an excellent wavelength, we investigated shorter wavelengths and found that a 905 nm laser could be used without a significant reduction in performance.

We find an optimum wavelength triad for retinal vessel oximetry to be 488, 635 & 905 nm. Figure 13 is a plot of our expected measurement error for this triad as a function of oxygen saturation and vessel diameter. Each of these wavelengths can currently be generated by a laser; 635 and 905 nm diode lasers are available, and 488 nm is the primary line of an argon ion laser. One of the primary motivations for developing the EOX-2 is that it will allow the use of any wavelength between 450 and 1000 nm. The data collected from the EOX-2 will then be used

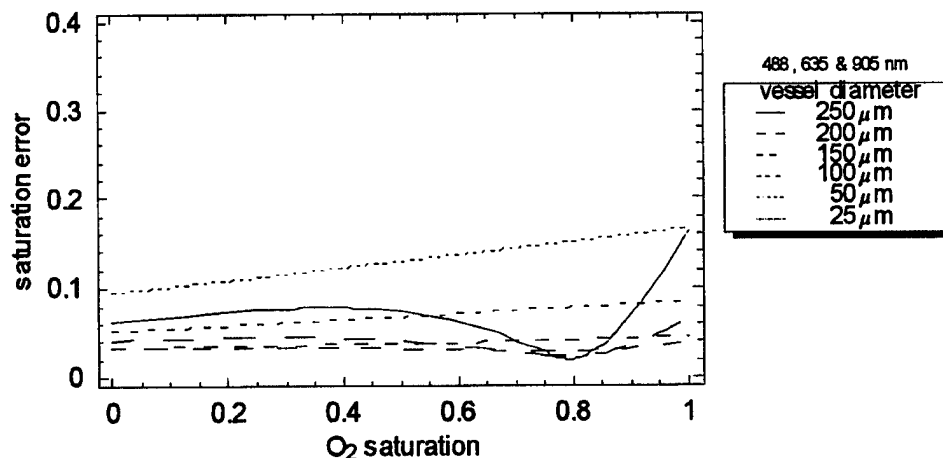


Figure 13. The expected absolute error (in %O₂Sat.) in calculated oxygen saturation using the optimized wavelength triad 488, 635, 905 nm.

to determine the minimum requirements for a battlefield device. For example, while the Ar⁺ laser would not be useful in a battlefield instrument, frequency-doubled 980 nm diode lasers that operate at ~490 nm are becoming commercially available. If the blue wavelength is found to be sufficiently important, then the additional cost of a 490 nm solid state laser might be justified in a product.

As a comparison, the errors associated with the current EOX wavelengths (629, 678, 821 & 899 nm) are plotted in Fig. 14. Due to these larger errors, we typically average 16 or more measurements in order to achieve a sufficiently low standard error of the mean. The motivation for including the 488 nm laser is to reduce the required number of scans for an accurate measurement.

It is important to note that the only parameter used in this optimization study was the

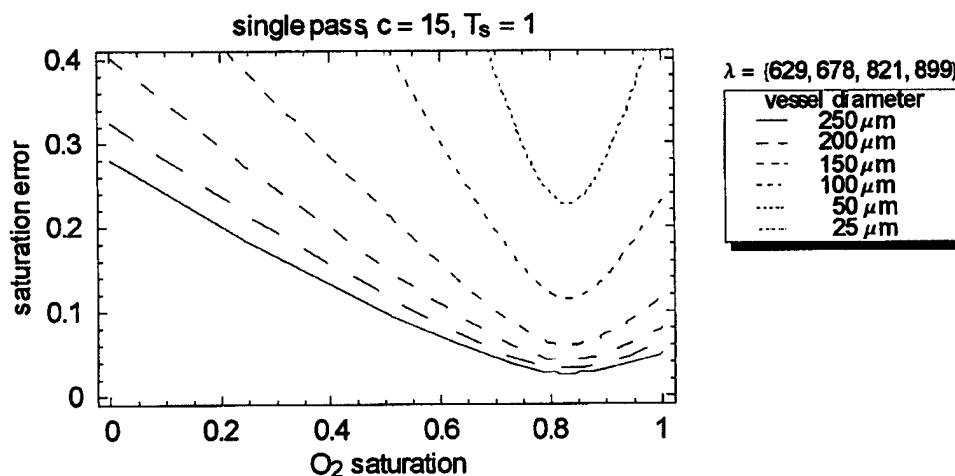


Figure 14. The saturation error (%O₂Sat.) associated with the current EOX wavelengths (629, 678, 821, 899 nm).

sensitivity to oxygen saturation. Since it is known that the spatial irregularity of the fundus varies with wavelength, it is expected that there will be wavelengths that make it difficult to estimate the vessel transmittance accurately. Our studies are ongoing in an attempt to quantify this parameter.

Another parameter that is useful to consider is whether or not the entire wavelength range can be coupled into a single fiber optic. In discussions with the fiber manufacturer, we find that the range from 488 to 905 nm *cannot* be coupled into one single-mode fiber. As such, we continued our wavelength optimization study to try to compress the wavelength range as small as possible. We did find a wavelength combination that offers excellent performance and should be able to be coupled into a fiber. **We find 488, 600 and 635 nm to be an excellent wavelength**

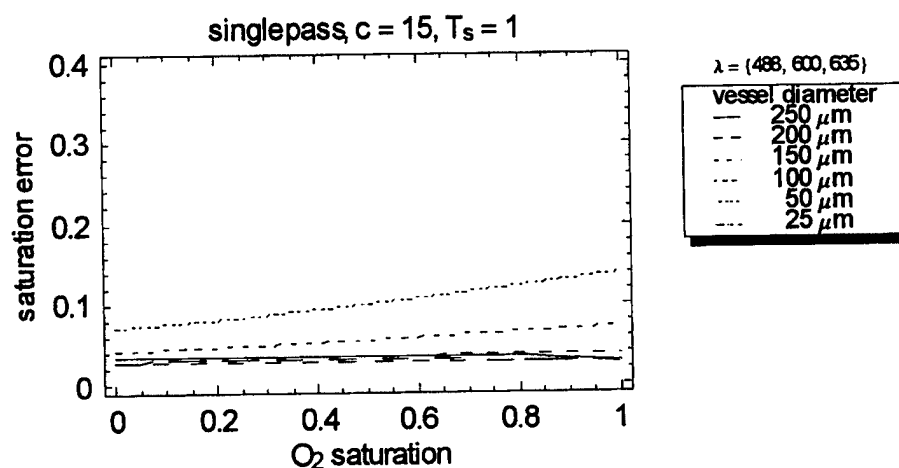


Figure 15. Although not yet viable in an instrument, the 488, 600 & 635 nm wavelength combination yields excellent sensitivity to oxygen saturation, and it could possibly be coupled into a single fiber optic.

combination for retinal vessel oximetry. Figure 15 contains the error plot for this combination. *(NOTE: The 488, 600, 635 nm wavelength combination was discovered after our paper submission. Due to the market potential of an instrument using these wavelengths, this combination is currently **proprietary**.)* The most significant difficulty with using this combination is that 600 nm laser light cannot be economically generated. We expect to test this combination in the EOX-2 using a tunable dye laser, and we are currently considering the issue of generating 600 nm light in a product.

Some other issues that must be considered are those involving the comfort of the patient. It would be preferable if all of the wavelengths used by the EOX were infrared. Three significant advantages are gained by using infrared light. First, since the beams are not visible, the patient is unlikely to react to the measurement (by moving, etc.). Second, infrared light will not constrict

the patient's pupil. This may allow us to make measurements without chemically dilating the subject eyes. (Note: The white light used to view the retina in the current EOX prototype is sufficiently bright to constrict the pupils of about 20% of the population when used in a semi-darkened room. This limitation must eventually be overcome either through chemical dilation or the use of infrared light.) Third, our data indicates that the retinal background becomes more uniform beyond ~800 nm, allowing more accurate transmittance measurements.

A study was undertaken to determine if oximetry measurements could be made solely with infrared diode lasers. The results of this study indicate an "optimum" wavelength

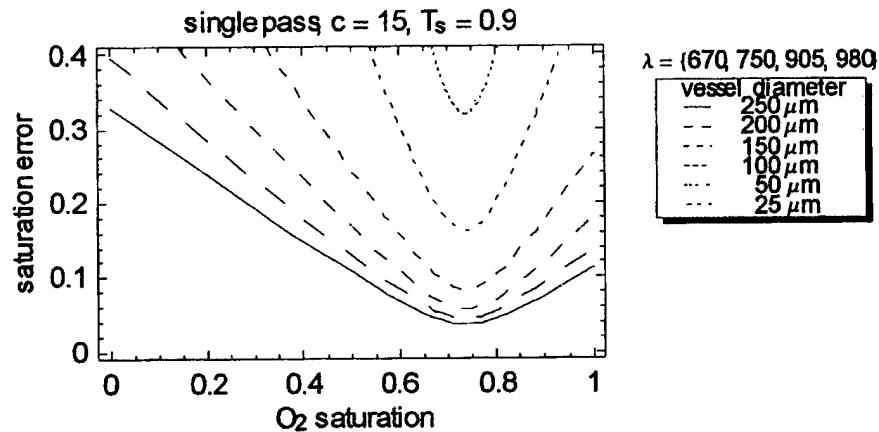


Figure 16. Saturation error for the near-infrared wavelength combination.

combination of 670, 750, 905 & 980 nm might provide useful saturation measurements. The error associated with this wavelength combination is presented in Figure 16. Although these wavelengths are not as oxygen sensitive as those combinations including the 488 nm wavelength, it appears that useful oxygen saturation data can be acquired at this combination. We anticipate averaging up to 64 measurements in order to achieve a sufficiently accurate oxygen saturation value.

Summary

During the two years we have worked on this project, we have improved our understanding of wavelength optimization, published a peer review articles on the subject, and tested our theorys in a model eye, animal models and in the human eye. We have demonstrated that there are variables which are not accounted for in our optimization analysis. Specifically, we assumed a fixed error in the vessel profile across wavelengths, minimal back scattering of light and wavelength independent background variability. In our analysis of actual retinal vessel scans, we have found that the background variability is wavelength dependent. We are actively testing methods to adapt to these significant variables. For an in depth description of our work on this problem to date please see the papers we have published on this subject "Retinal vessel

oximetry: Toward absolute calibration” and “Multi-spectral confocal scanning laser ophthalmoscope for retinal vessel oximetry” in the appendix.

Multipass Transmission in Oximetry

Please see the appended article "Effect of multiple light paths on retinal vessel oximetry" for the in depth discussion of this topic as completed in year two of this grant.

There are a number of issues that significantly complicate the practice of measuring retinal vessel oxygen saturation. Such issues include, but are certainly not limited to, the wavelength dependence of red blood cell scattering; scattering from other sources (the crystalline lens, etc.); absorption, reflection, and scattering effects of the vessel walls; and the diffusion of light in the underlying retinal layers. A theoretical study was completed that investigated one of these effects, specifically the diffusion of light in the ocular fundus.

Figure 17 illustrates the primary light paths that must be considered in retinal vessel oximetry. A beam of light I_o is directed into the pupil of the eye and is focused onto a retinal vessel. A retinal oximeter system then collects whatever fraction of light that is reflected back out of the pupil of the eye. There are several factors responsible for determining this collected power. There is typically a specular reflection from the apex of the vessel I_{glint} that is collected back out of the pupil.²⁶ As the incident beam passes through the blood within the vessel, its intensity is decreased via the Lambert-Beer Law due to absorption by hemoglobin and oxyhemoglobin within the red blood cells (RBCs). Additionally, light is scattered by the RBCs. Some quantity of this light, I_{scat} , is scattered into angles that cannot be collected by the instrument, causing an apparent increase in absorption. There is also a much smaller (perhaps negligible) quantity of light, I_{bs} , that is directly back-scattered toward the instrument resulting in an apparent *decrease* in absorption.

The beam that emerges from the other side of the vessel has been broadened due to scattering and attenuated due to absorption. This beam then reaches the retinal pigmented epithelium (RPE) and choroid (~240 μm posterior to the vessel).²⁷ For wavelengths lower than 575 nm, there is little penetration of the light through the RPE into the choroid. This low penetration results in a tightly localized point spread function (PSF) on the RPE. Wavelengths much longer than 575 nm penetrate the choroid deeply, eventually reflecting off of the sclera and passing back through the choroid. The resulting laterally diffused PSF is much larger than that of shorter wavelengths. Reasonable estimates for the standard deviation of the diffusion enlarged PSF in the nasal fundus (near the optic nerve head) are ~60 μm from 450 to 575 nm and ~180 μm from 600 to 750 nm.²⁸ A fraction of this diffused light I_{dp} will pass back through the vessel to be absorbed and scattered in double pass, while another fraction I_{sp} will extend beyond the edge of the vessel and exit the pupil in single pass.

To demonstrate the likely existence of both single pass and double pass components of the collected light, consider the illustration in Figure 18 (drawn to scale). A 100 μm retinal vessel positioned 240 μm anterior to the reflecting layers of the ocular fundus is considered. Two separate diffusion enlarged point spread functions are considered, a 60 μm (standard deviation) PSF typical of blue wavelengths and a 150 μm PSF typical of red and near infrared

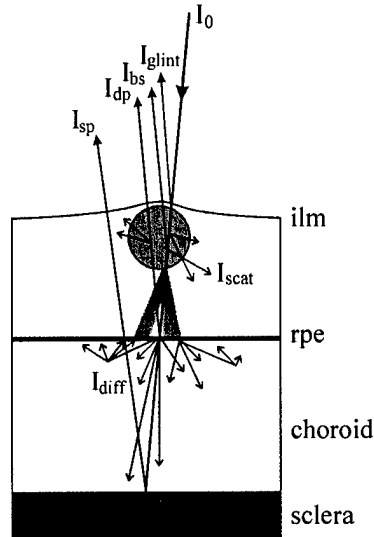


Figure 17. The primary light paths associated with retinal vessel oximetry; I_0 , incident light; I_{glint} , specular reflection from the inner limiting membrane (*ilm*); I_{scat} , light scattered away by red blood cells (RBCs) within the vessel; I_{bs} , light back-scattered to the detector by RBCs; I_{sp} , light collected that has traversed the vessel in single pass; I_{dp} , light collected that has traversed the vessel in double pass; I_{diff} , light diffused laterally in the choroid.

wavelengths. Finally, 10° cones of light are illustrated that indicate the acceptance angle of a ~ 4 mm diameter pupil located 22 mm away. Thus, only the light in these cones could be collected by a retinal vessel oximeter. From this illustration, it is clear that significant amounts of both single pass and double pass light could exist for typical retinal geometries. The relative magnitudes of these components depend on numerous factors including the point spread function, size, the diameter of the pupil, the vessel diameter, and the specular/diffuse reflectance properties of the ocular fundus. We have not yet attempted to quantify this ratio.

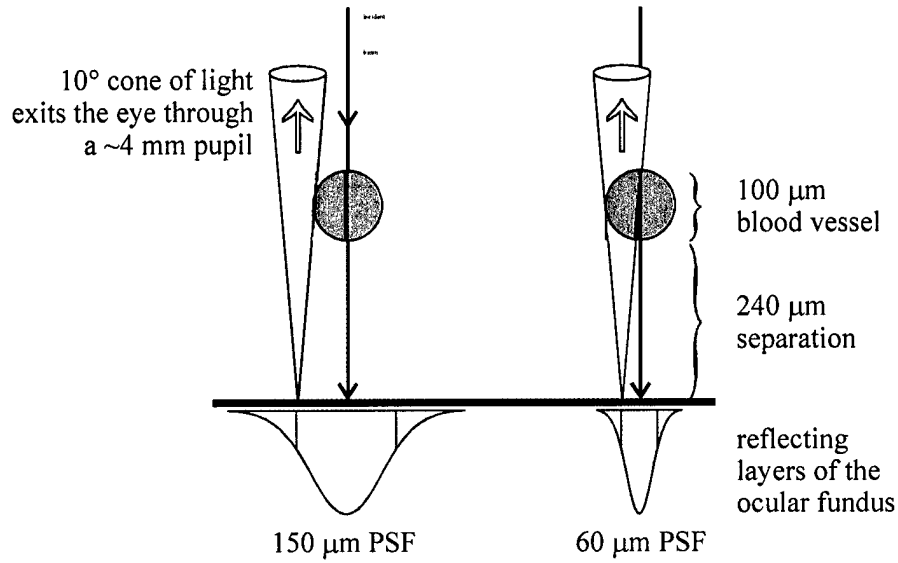


Figure 18. When illuminating a retinal vessel with a scanning retinal vessel oximeter, the light collected back out of the pupil will contain components that traversed the vessel in single pass and in double pass. The relative magnitudes of these components depend on numerous factors including the point spread function size, the diameter of the pupil, the vessel diameter, and the specular/diffuse reflectance properties of the ocular fundus.

For our mathematical model, we define a parameter ρ that represents the ratio of single-pass to double-pass transmission, where $1 \leq \rho \leq 2$. For $\rho = 1$, the collected light is entirely single-pass, and for $\rho = 2$ it is double-pass.

The ρ parameter is incorporated into the oximetry equation as

$$T = (2 - \rho) 10^{-\epsilon c l} + (\rho - 1) 10^{-2\epsilon c l}$$

where ϵ is the extinction coefficient (which contains the saturation information), c is hemoglobin concentration, and l is the sample thickness. (Note that in this study, the effects of red blood cell scattering are not considered.)

The apparent optical density of the vessel can then be written as

$$D = -\log((2 - \rho) 10^{-\epsilon c l} + (\rho - 1) 10^{-2\epsilon c l}).$$

Note that this equation cannot be simplified any further. The important implication of this equation is that *the optical density is not linear with the extinction coefficient*. This equation also prevents a closed form solution for the oximetry equation, implying that some form of iterative regression may be required in order to calculate the saturation.

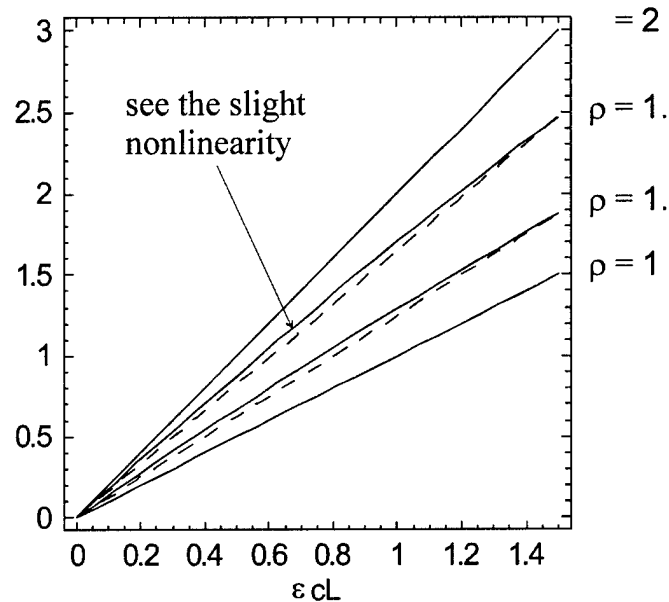


Figure 19. For values of ρ between 1 and two, it is found that the optical density of a vessel is *not* linear with the extinction coefficient ϵ of the blood.

Before developing iterative regression techniques for calculating the oxygen saturation, it was important to quantify the expected magnitude of this effect. Figure 19 illustrates the magnitude of the nonlinearity of optical density. This is plotted across the range of optical densities that are reasonable of blood in a retinal vessel ($0 \leq D \leq 2$), and for four different ρ values between 1 and 2. From this figure, it seems that the nonlinearity of optical density is quite small (a few percent at maximum), and that the nonlinearity is zero when $\rho = 1$ or $\rho = 2$ (as expected from the equation for D). From this figure, however, one cannot estimate the magnitude of the error introduced into the saturation calculation.

Figure 20 plots the expected error in calculated oxygen saturation due to multipass transmission. To determine the error in calculated oxygen saturation due to these nonlinearities, we simulate optical density data using the multi-pass equation, and then analyze this data using the traditional oximetry equations. The simulation assumes a 100 μm vessel with 15 g/100ml hemoglobin concentration. We do this for the wavelength combination currently used by the EOX, and for the wavelength combinations used by Delori.²⁰

From these plots, it is found that Delori potentially had a significant calibration problem with his retinal vessel oximeter. At his wavelengths (558, 569 & 586 nm), an error in saturation as large as 20 %O₂Sat. could be expected. This may have contributed to the difficulty he experienced in performing accurate saturation measurements.

For the wavelengths used in the EOX (629, 678, 821 & 899 nm), we find that the expected error due to multi-pass transmittance is actually quite low (a maximum of 1.7%O₂Sat.). *This is an important result because it indicates that an iterative solution for calculating the*

oxygen saturation should not be necessary for the EOX.

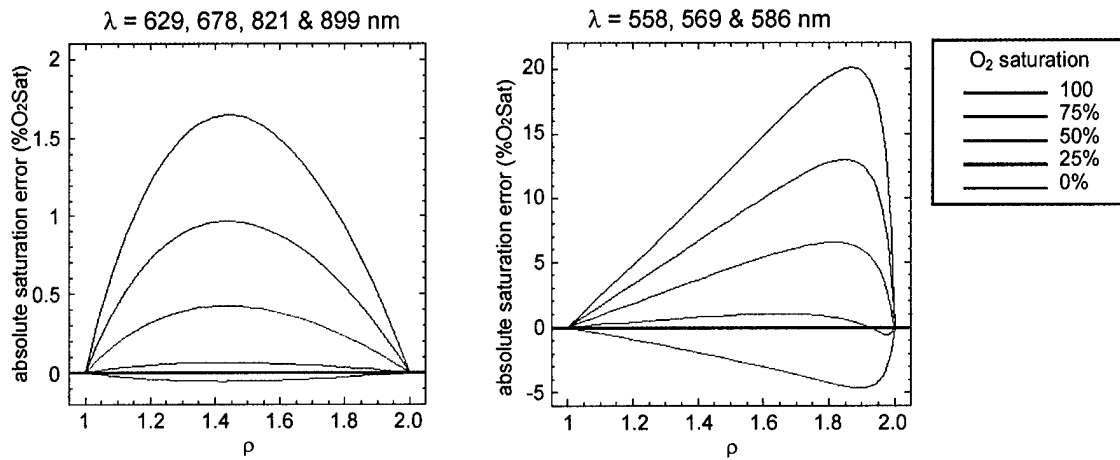


Figure 20. Estimation of the error in calculated oxygen saturation due to multi-pass (ρ) transmission. Calculations are made for the EOX wavelengths (left) and for Delori's wavelengths (right).

Finally, it is important to make one last note about this subject. Throughout, we have assumed that ρ was constant across the wavelength range of interest. While this is quite likely to be accurate in the red and infrared wavelengths used by the EOX, it will probably *not* be the case once a blue-green laser (488 nm) is included in the EOX-2. Once that system is completely online, this study will need to be expanded to attempt to quantify the spectral variation in ρ across these wavelengths.

Summary

In this body of work we have addressed the optical geometry of the eye and the possible light paths involved in retinal vessel oximetry measurements. By increasing our understanding of the double pass phenomenon, we have increased our ability to calibrate retinal oximetry and have added a blue-green wavelength to our oximeter. We describe this work in detail in the appended articles, "Retinal vessel oximetry: Toward absolute calibration" and "Effect of multiple light paths on retinal vessel oximetry."

Construct and Test EOX-2 Prototype

Please see the paper in the appendix "Multi-spectral confocal scanning laser ophthalmoscope for retinal vessel oximetry" for the description of the final EOX-2 and year 2 efforts in this system development.

System Description and Specifications

The EOX-2 is the experimental platform which we are using to test the oximeter modifications which we proposed in this contract. The EOX incorporates several of these changes in a device which is similar to our original breadboard instrument. Important new attributes found in the EOX-2 include two dimensional laser scanning, confocal optics, increased capacity for laser wavelengths and improved retinal imaging. Two dimensional laser scanning allows more complete imaging of the subject's retina, producing a larger region for targeting and subsequent data acquisition and analysis. Confocal optics²⁹ permits a more precise study of the effect of the retinal structure on the incident laser light by localizing³⁰ the returned light within the ocular fundus. Secondary modifications include converting the optical system to a reflective design to minimize image quality degradation due to chromatic aberration and using aspheric optics to reduce spherical aberration.³¹ The optical system, its design, and function will be described in this section.

The choice of wavelengths employed in the EOX-2 has been changed in an effort to test our wavelength selection hypothesis. The system not only uses three diode lasers in the red and near-infrared part of the spectrum (635 nm, 670 nm, and 830 nm) but also includes the 488 nm laser line from an argon ion laser. The system is capable of incorporating up to two more lasers if required. A laser multiplexing subsystem is used to toggle the on-off state of the source lasers to create a vertically interlaced image. The data reduction routines then separate the individual

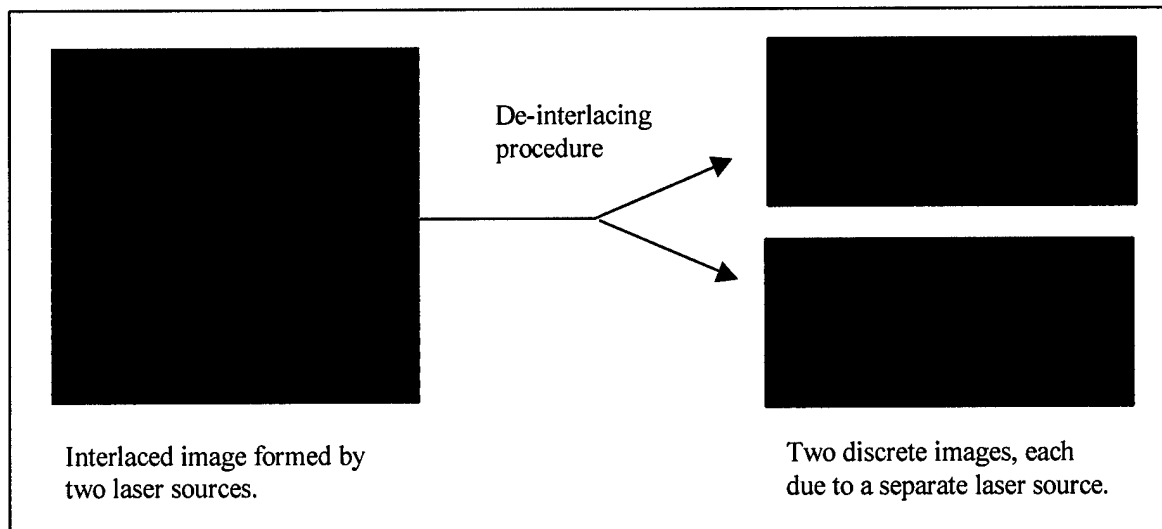


Figure 21. Example of de-interlacing procedure for two incident wavelengths

single-laser images for analysis. This spatial interlacing scheme insures that individual horizontal lines that are illuminated by a single laser are displaced from each other by no more than two rows (for the case when four lasers are used). The subsequent spectral analysis for the four separate lasers then occurs at essentially the same position on the retina. An example of the de-interlacing procedure for the simple case of two source wavelengths is shown in Figure 21 below.

EOX-2 Optical System Design

The main portion of the EOX-2 optical system is a traditional afocal telescopic design, but there are a number of limitations which increase the complexity of the entire system. Most of the limitations are imposed by the fact that an important part of the system depends on the optical response of the subject's eye. These include issues ranging from the subject's capability to focus a collimated beam to a sharp point on the retina to the spatial variability of the subject's retinal pigmentation. Inherent aberrations in the average (or "standard") human eye comprising primarily spherical aberration and defocus (in the form of myopia or hyperopia) tend to degrade a subject's capability to focus sharply. The resulting blur spot on the retina is more difficult to re-image at the detector plane due to its extended size. The spherical aberration problem is addressed in the EOX-2 by simply illuminating a small central region of the subject's cornea. Since the cornea is the major contributor to spherical aberration, and the effects worsen with increased aperture, illuminating a small central region helps to minimize the effect. Defocus is tended to by allowing some adjustment capability in the optical power of the telescope to compensate for a subject's refractive error. The wide variability in the response between subjects ensures that all possible subjects could not be accommodated. In fact, the focusing capability of the EOX-2 is postulated to be too limited to allow its application to extreme myopic or hyperopic subjects. However, the system has been used on subjects who have maintained their corrective eyewear, indicating that it may still be useful on subjects who require extreme defocus correction, provided eyewear is available.

A problem encountered during the design of the optical system was that the system is bidirectional in the sense that the laser source light propagates to the subject's retina, where it may be treated as a new light source, and must then be re-imaged through the detection path of the system (some of which is coincident with the illumination arm). This bidirectionality necessitates designing two separate optical systems as modern lens design programs cannot accommodate such a two-way design. Moreover, these subsystems have a common path throughout most of the primary system (e.g., through the telescope and the subject's eye) requiring that they employ the same optical elements for this region. Optimizing the system in the "forward" direction typically causes a degradation of the image quality in the "rearward" system so that a performance tradeoff becomes inevitable. Accordingly, the optics of the EOX-2 will be described in sections: the illumination module, the forward propagating subsystem, and the rearward propagating subsystem with its associated detection arm.

Illumination module

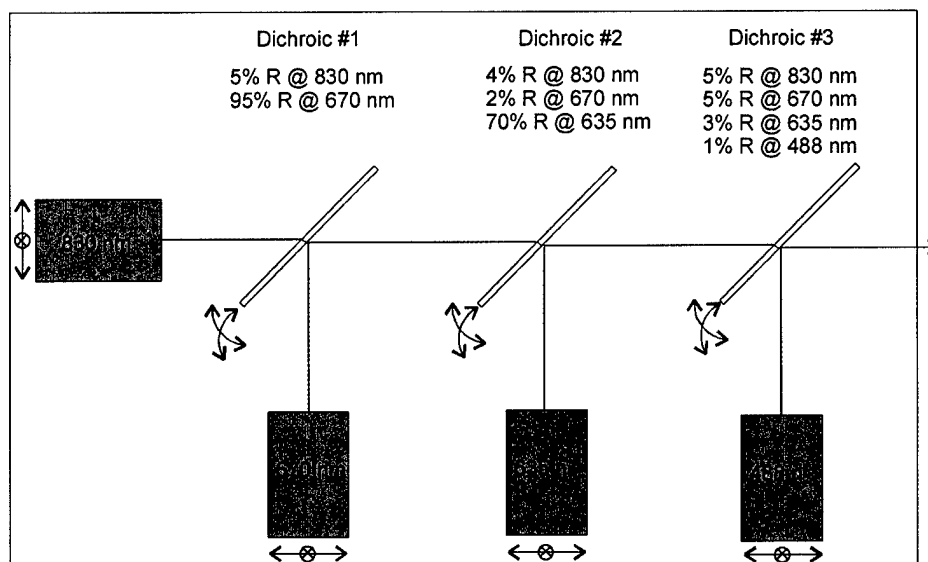


Figure 22. EOX-2 laser source module. Dichroic reflectance values are for p-polarized light.

The illumination module is depicted in Figure 22. Source light from the four lasers is combined via a cascade of three dichroic beam combiners. The 830 nm beam, shown propagating from left to right in the figure, defines the optical axis of the system and is the reference beam to which the others are added. The beam combiners are coated to operate at a 45° angle of incidence, transmit 830 nm light, and reflect the wavelength which is being added. As well, the second and third beam combiners must transmit light which has already been added to the initial beam. The laser beams are made coaxial using the pitch and yaw adjustments on the beam combiners coupled with the transverse translation capabilities of the source beams. All lasers are polarized in the plane of the figure (p-polarized) and the reflectance values of the dichroics listed in the figure apply to p-polarized incident light. The output beam, consisting of four coaligned laser beams is next folded off of a broadband reflector and proceeds into the forward propagating subsystem.

Forward Propagating Subsystem

Once the light reflects from the above mentioned mirror, it next strikes a beam splitter

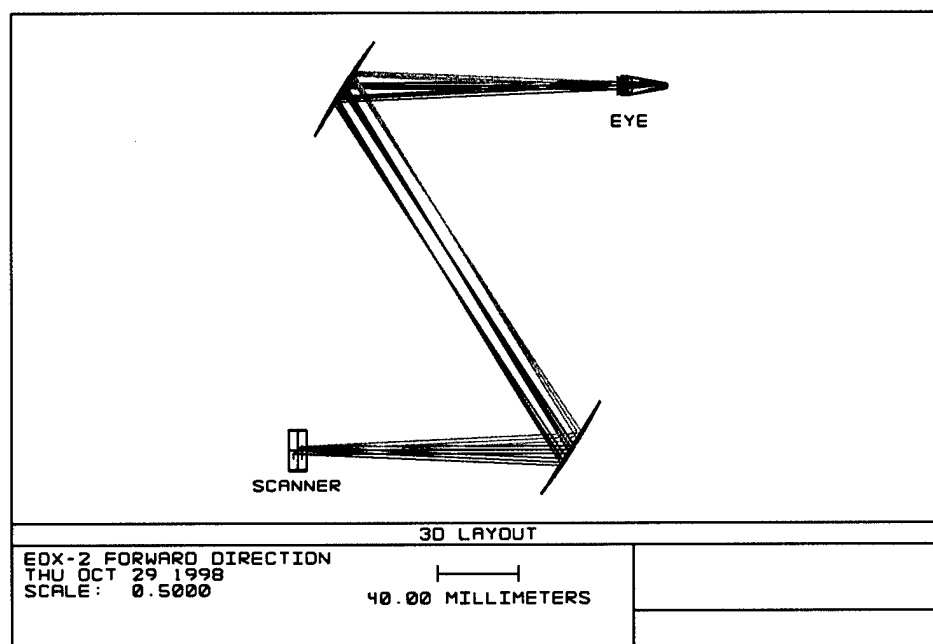


Figure 23. Optical design of EOX-2. Forward direction.

which will eventually act as a discriminator between the common path and the detector arm for the returned light. Continuing in the forward direction however, the beam passes through the splitter and on to the forward propagating subsystem. The beam encounters the two dimensional scanner which rotates it through a small angle in orthogonal directions, causing it to traverse a square area. Presently, we only consider the on-axis beam (i.e., the beam resulting from the scanner mirrors both being in the central scan position) to simplify the discussion. The beam then propagates through the telescope, composed of two off-axis parabolic mirrors, and is emitted in a collimated fashion for introduction into the subject's eye. The choice of a broadband reflective off-axis aspheric system was made to minimize the aberrations in the image contributed by the optical system itself. The system is designed such that once the scanning mirrors are allowed to rotate, a scanning pupil plane is located in this collimated space at a comfortable position for the subject. The subject's physiological pupil is then made coincident with the scanning pupil plane to insure maximum efficiency for coupling of laser energy into the eye. The resulting scanned region on the subject's pupil is a square with sides of length ≈ 4 mm. Figure 23 is the output from the optical system design software used to optimize the chosen system showing a layout of the system as seen from above. The input beam from the above mentioned beam splitter is incident on the scanner in a direction normal to the plane of the figure. Hence, the laser source module, fold mirror, and beam splitter are omitted from the figure for

clarity. The scanning mirrors are represented by the rectangle in the lower left corner of the drawing, followed by the two parabolic mirrors and a "standard" human eye. The figure shows three possible positions of the scanning beam: the blue rays correspond to the on-axis beam whereas the gray and yellow rays represent the two non-axial horizontal positions for a centered vertical mirror position.

Rearward Propagating Subsystem

The rearward propagating subsystem is exactly the same as the forward system in the region between the retina and the beam splitter. At the beam splitter, a portion of the light energy returned from the eye is folded into the detector arm comprising a focusing mirror, confocal pinhole, relay lens and avalanche photodiode. The system is shown in Figure 24. Once again, as in Figure 23 the three groups of rays correspond to three angular positions of the horizontal scanner mirror. In this case however, the source is the retina and the ray trace propagates back through the telescope, reflects off the scanner mirror in the lower left corner, and on to the detector arm. For simplicity, the scanner mirror, which oscillates the beam into and out of the plane of the figure, and the beam splitter, which also takes the beam out of the figure plane, have been omitted. Note that the scanner mirror descans the three input beams so that its output is always a collimated beam propagating in the same direction. After the (de)scanner mirror another off-axis parabolic mirror is used to focus the incident beam onto a pinhole, whose position is indicated in the figure. This pinhole has the effect of spatially filtering any light that did not originate at the source point (e.g., any scattered light or light displaced axially from the source point) and is referred to as a confocal pinhole. Also omitted from the figure are the last

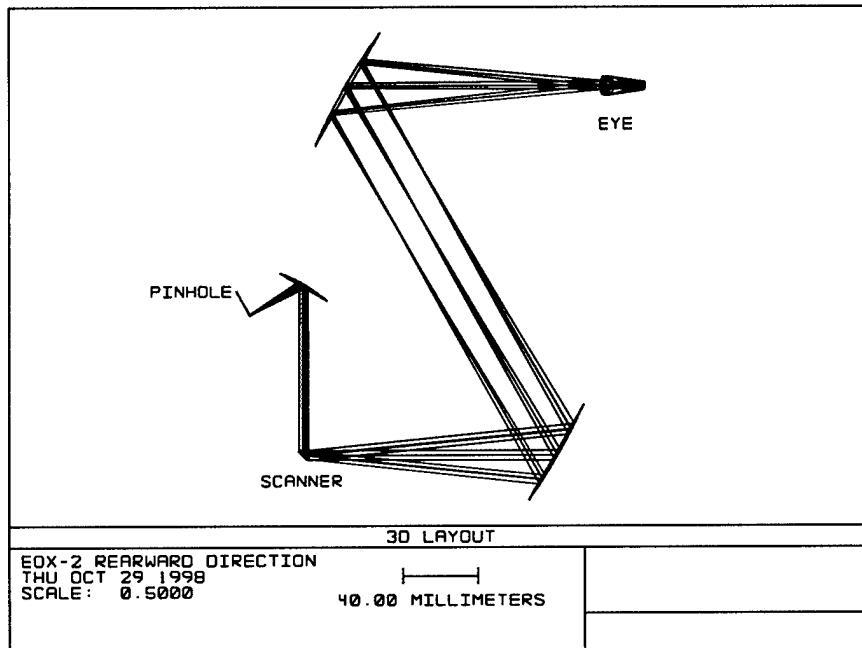


Figure 24. Optical design of the EOX-2. Rearward direction.

optical element of the system and the detector. The simple relay lens images the light which does transmit through the pinhole onto the detector. The active area of the detector is relatively large at 1.5 mm in diameter and this has several important ramifications for the system. First, the large detector size can easily accommodate the relayed spot diameter considering that the pinhole diameter never exceeds 200 μ m and the lens is working at 1:1 conjugates (magnification = 1). This remains true even though the lens will impart some chromatic aberration to the beam because this aberration will not be enough to exceed the substantially larger detector size.

Electronics Design

The electronics of the EOX-2 allow the user control of the various subsystems. These may be broken down into the following sections: scanner electronics, multiplexer electronics, detector electronics and computer control system.

The scan mirrors are driven by an integrated scan control head called the Video Scan Head Controller (VSH) manufactured by General Scanning (Watertown, MA). The scan system consists of one galvanometric paddle mirror and an orthogonally oriented resonant mirror. The paddle mirror oscillates about one of the short ends of its rectangular profile at a rate of 13 Hz while the resonant mirror oscillates about the minor axis of its elliptical profile at 8 kHz. A 15 MHz pixel clock temporally tracks a scanned square area that is 512 x 512 pixels. The VSH drives the paddle mirror linearly and the resonant mirror sinusoidally. Since typical video processing electronics expect linear signals, the resonant mirror driver electronics compensate for the sinusoidal driving signal before producing the required linear pixel clock signal. The

horizontal and vertical synchronization signals and the linearized pixel clock are the available outputs for subsequent video processing electronics. The VSH also is capable of taking the detector signal as an input, amplifying it, and outputting it along with the timing signals to produce a complete (non-composite) video signal. The EOX-2 uses these outputs for two purposes: first to drive the framegrabber board (timing and detector signals) in the computer control system and second to provide reference timings for the laser multiplexer (timing signals only) electronics. The VSH is also capable of panning and zooming the scanned area through hardware to help target the subject's retina. Signal communications can be performed in analog or digital (RS-422) mode.

The laser multiplexing subsystem electronics consist of a customized six channel controller manufactured by ABR Inc. (Huntsville, AL) specifically for the EOX-2. This controller was completed prior to the beginning of this contract. The laser multiplexer uses the timing signals from the VSH (specifically the horizontal and vertical timings) to vertically interlace the laser sources during a frame acquisition. The multiplexer does not actually perform the acquisition but merely switches the laser states while the framegrabber acquires the measures intensity data. The desired source interlacing configuration is entered via the computer control system (described below) and transmitted to the multiplexer using an RS-232 bus connection. The multiplexer processes the received interlace scheme and uses the timing signals from the VSH to turn the laser sources on and off during the frame acquisition. The step response of the laser drivers is far shorter than the flyback time for a horizontal line scan so that a different laser may be used to scan each horizontal line. This may be done for a maximum of 6 different lasers, after which the cycle repeats until all 512 rows which make up the image have been acquired. The multiplexer is initiated by a trigger signal which indicates that the next available frame should be acquired. This trigger may either come from the computer control system (i.e., operator activated) or from an external hardware device (e.g., an electrocardiogram). The trigger to the multiplexer initiates a second trigger to the framegrabber indicating that the next available video frame should be recorded. This next frame is the one in which the laser sources are modulated by the multiplexer. The multiplexer is also capable of inserting a time delay of up to 2 s between the time when it receives a trigger signal and when it calls to acquire a frame. Note that the frame acquisition cannot occur instantaneously upon reception of the initial trigger signal so the multiplexer will time the delay between the trigger arrival and the frame call and report it to the user. This delay is typically on the order of tens of milliseconds.

The detection system of the EOX-2 consists of an avalanche photodiode (APD) and the signal processing electronics in the VSH mentioned above. The APD, manufactured by Hamamatsu (Bridgewater, NJ), is a sensitive high speed photodetector capable of handling the EOX-2 video rate signal (15MHz) with good responsivity (10^6 V/W). This is important since the return signal from the human eye is typically a factor of 10^4 - 10^5 less than what is incident (which itself must necessarily be fairly low due to safety considerations). Even the APD is strained by the low return light levels however and the detector gain must be increased above the factory preset to obtain a useable signal. This unfortunately increases the system noise and thereby decreases the overall signal to noise ratio of the device. Reduction of system noise is

something that must be addressed, and filtering techniques as well as multiple frame averaging are methods being investigated for this purpose.

The computer control of the EOX-2 is provided by a 200 MHz Pentium (Dell Computer Co., Austin, TX) IBM PC compatible computer which houses the framegrabber (Matrox Electronic Systems, Quebec, Canada) and synchronizes all of the data acquisitions. Two computer programs written in Visual BASIC (Version 5.0, Microsoft Co., Redmond, WA) specifically for the EOX-2 oversee the interactions. The first program provides an interface for the EOX-2 operator to allow live targeting of the subject's retina, selection of the interlacing scheme, and data acquisition and storage facilities. The scan interlace scheme is delivered to the multiplexer via the RS-232 communications bus, and triggers for data acquisition are generated and received via the framegrabber. The framegrabber uses the timing and detector signals from the VSH to acquire a frame temporally. The frame is built up one pixel at a time as the scanner translates the incident beam over a square area on the subject's retina.

An example of the output from the user interface for the data acquisition program is shown in Figure 25. This image of a human retina is overlaid with a horizontal red line. The data analysis program takes the acquired data and de-interlaces it as shown earlier in Figure 21. The data analysis program then allows the user to select a subsection of the image for oximetric analysis. Incorporation of this final analysis step is not completed yet but is expected to be finished shortly. Figure 25 below shows an example of a plot of the intensity as a function of position across the scan line indicated in red. This data has been smoothed with a Savitsky-Golay slope preserving filter.

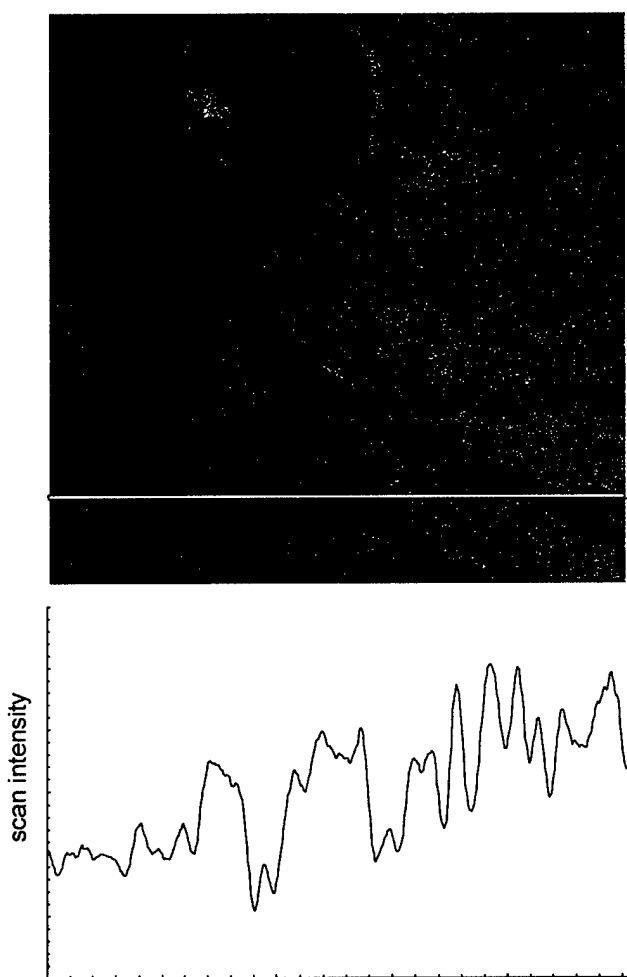


Figure 25. Early scan data from the EOX-2. A retinal image acquired at 635 nm is shown. The graph is an intensity profile through the indicated scan line.

Summary

In this section we have described the design and development of the EOX-2 as anticipated in our contract statement of work. The preliminary testing of the breadboard instrument has demonstrated that the device functions as expected optically. The testing of this instrument in the model eye, animals, and humans is under way. The use of this system is described in "Multi-spectral confocal scanning laser ophthalmoscope for retinal vessel oximetry."

Light Scattering by Blood in a Retinal Vessel

Introduction

There are a number of optical effects that must be understood in order to make accurate retinal vessel oxygen saturation measurements. The "multi-pass transmission" and "wavelength optimization" sections of this report outlined advanced topics of retinal oximetry that had not been considered by previous investigators. The red blood cell scattering compensation that was discussed in the "model eye" section of this report is an extension of the work of previous investigators.²⁰ The idea of this scattering compensation is that some of the light that passes through the retinal vessel is scattered into the eye and never returns back out of the pupil. This results in vessel absorption profiles that are deeper than they would be if only absorption had occurred. The oximetry equations required for measuring saturation become complicated because the instrumentation has no way of knowing whether this lost light was scattered or absorbed.

We believe that the studies performed to date by previous investigators have not considered blood cell scattering in a sufficiently rigorous manner. Specifically, the contribution of light that is directly backscattered by the blood has never been considered. The effect of backscattered light would be to *increase* the collected signal, resulting in *less* deep vessel absorption profiles. In this section, we describe our efforts to better understand these scattering effects. The analysis of these data is still underway, however a few significant findings have already been made. First, the scattering is not dependent on oxygen saturation. Second, while the backscattered component is small, it does not appear to be negligible. We are in the process of developing models that include backscattering as a term in our oximetry equations. We believe that this will help solve some of the difficulties we have experienced making accurate saturation measurements across different degrees of retinal pigmentation.

Theory

The propagation of light through an inhomogeneous medium has been studied for many years and in most real world cases, is a difficult system to model. Scattering and absorption of the incident energy by inhomogeneities in a medium has been treated in different ways with varying degrees of success. For materials with a low particle concentration, single scattering (as opposed to multiple scattering) prevails wherein the scattered field due a particle is assumed to have propagated to the point of measurement without suffering a second scattering event. Moreover, random particle separation distance (and/or orientation) usually eliminates the possible coherent phase relationship between a number of scatterers and such a material is said to scatter incoherently. The study of incoherent, single scattering materials has seen much success in the literature in terms of the correlation with theoretical predictions. Specifically for spherical and cylindrical particles, Mie theory has been shown to adequately describe the magnitude, directionality, and polarization characteristics of the transmitted radiation. Propagation of radiation through such systems is described by certain fundamental measurable quantities of the

particles such as their scattering and absorption coefficients, σ_s and σ_a ; their cross sections, C_{sca} and C_{abs} , and the single particle scattering phase function $p(\theta, \phi)$. The coefficients are the inverse of the respective mean free paths between scattering and absorption events and are related directly to the cross sections. The total extinction of a beam of radiation as it passes through an inhomogeneous material is related to both the scattering and absorption characteristics via a simple summation. Hence, the total extinction coefficient and cross section are given by

$$\begin{aligned}\sigma_{ext} &= \sigma_s + \sigma_a \\ C_{ext} &= C_{sca} + C_{abs}\end{aligned}\tag{1}$$

The phase function is a description of the distribution of scattered radiation as a function of angular position in the scattering plane, that which contains the incident and scattered rays. Assuming an incident beam of unit amplitude, the integral of the phase function over all space for a nonabsorbing material must also be unity. Hence, we write the normalization condition for the phase function as

$$\int_{4\pi} p(\theta, \phi) d\Omega = 1\tag{2}$$

For systems where multiple scattering dominates, the theory of Mie does not directly apply, but the fundamental particle parameters are still important. This is also referred to as the radiation transfer problem and has been studied extensively. In general the equation of radiative transfer, which describes the propagation of light through a multiply scattering medium, is an intractable mathematical discourse. There are situations however, notably the diffusion approximation, where this equation may be solved. Unfortunately, an analytical solution only makes itself obvious for situations with strong symmetries and simple boundary conditions. For example, the case of a semi-infinite half space of scattering material with a planar interface to some initial scattering or nonscattering medium is addressable.

The situation of retinal blood flow for a physiologically healthy specimen is one where the scatterer density is so high as to render Mie theory essentially useless, and the required symmetries and simple boundary conditions for a well behaved radiative transport model are absent. The Mie theory can however provide a guide as to what may be expected as shown in previous research. Hence, we attempt here not to specifically resolve the scatter measurements with some theory, but rather to accurately quantify the scattering due to the blood in the vessel in an attempt to incorporate the results into the required oximetric calculations so as to improve the overall accuracy of the system.

Construction of Scatterometer (Concept and Design)

Quantifying the scattered energy from an assembly of scattering particles in a surrounding medium requires a nephelometer or scatterometer. Whole human blood is composed of $\approx 50\%$ by volume red blood cells (RBCs) surrounded by a matrix of essentially transparent plasma. The plasma does contain a small amount of other scattering elements (e.g., white blood cells, lipids etc.) although these comprise only a small amount of the remaining volume and are neglected in our analysis. An automated scatterometer was constructed which simulates the environment of a retinal vessel and is capable of measuring the scattered intensity as a function of angles of a sample out to $\pm 168^\circ$ from the axis of the incident beam. An overhead view of the scatterometer system is illustrated in Figure 26. Light from a 5 mW HeNe laser is spatially filtered and then re-collimated (not shown) with a beam diameter of 3mm. This beam is incident from the left side of the figure and initially encounters a focusing lens with an focal length of 30 mm. This beam-lens combination gives an $f/\#$ of 10 which is similar to a relaxed human eye. The beam next passes through a flat Pyrex window in the side of a spherical ampule, also made of Pyrex. The ampule has two Pyrex tubes emerging radially from the sphere that intersect a full diameter of the sphere (29.6 mm) in the direction orthogonal to the figure. Rubber septum stoppers with centered feedthrough holes are set in the ends of the tubes. These feedthroughs allow insertion of a micropipette (also made of Pyrex) through the center of the ampule which has an inner diameter of $270\text{ }\mu\text{m}$ and acts as a channel for the blood. A side view of the ampule with the pipette inserted is shown in Figure 27. After a slight refraction from the flat window, the beam comes to focus at the center of the micropipette at which point the blood scatters the light. The red lines emerging from the pipette indicate the scattered light in the figure and their density is proportional to the scattered intensity for a typical blood sample. To limit the system's signature on the measured data, the sphere is filled with an index matching fluid, eliminating any refractions at the inside surface of the sphere (and the flat window) and the outside surface of the pipette. Centering the pipette within the sphere and adjusting the focal plane to the central

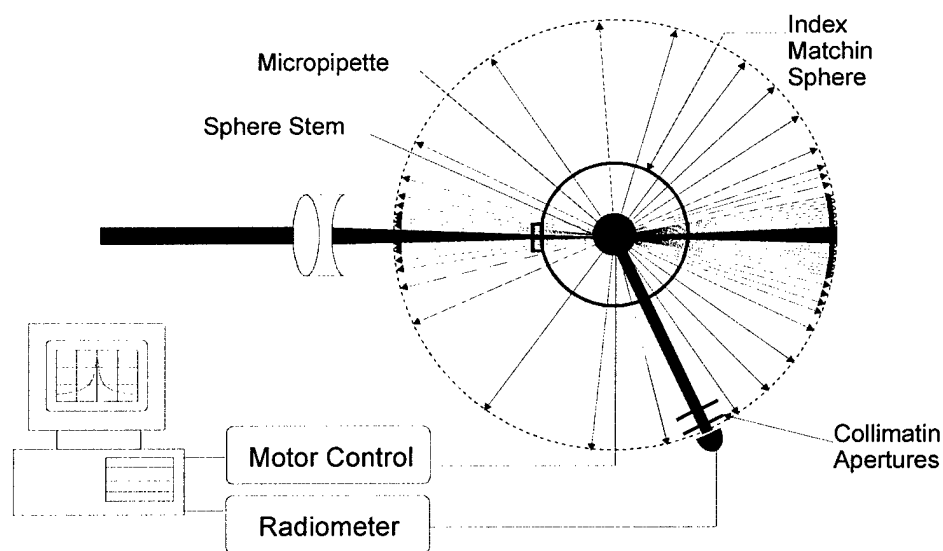


Figure 26. Over head view of scatterometer. See text for description.

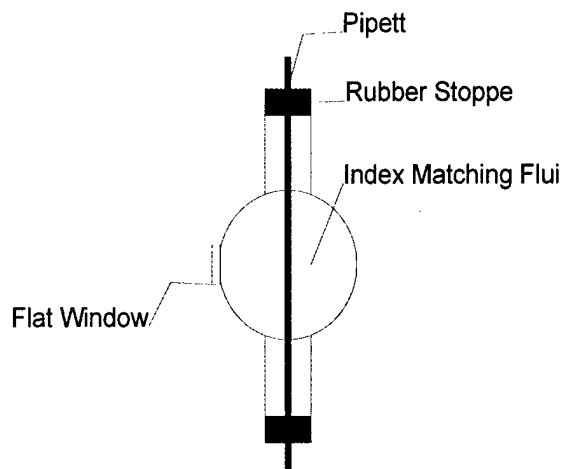


Figure 27. Side view of spherical ampule.

position (using the lens) also minimizes any refractive error contributed by the inner pipette and outer sphere surfaces. Coaxial with the pipette and sphere feedthrough axis is the axis of rotation of a stepper motor controlled rotation stage. Secured to this stage and oriented radially to its rotation axis is a boom arm, the distal end of which supports a photodetector at a distance of 13.5 cm from the blood filled pipette. The photodetector is preceded by two collimating circular apertures which assure that the measured light at a given angular position originates within a small solid angle (1.1×10^{-5} sr) at the sample. These apertures have a diameter of 0.5 mm giving the system an angular resolution of less than 0.5° . The angular resolution of the stepper motor is below 0.1° . By stepping the angular position of the stage, the photodetector can scan a circular locus around the sample and accumulate the scattered intensity distribution to a range of $\pm 168^\circ$ from the original beam direction. The system is automated by monitoring the rotating stage position and the photodetector with a control computer. A customized program written in Visual BASIC (version 5.0 Microsoft Corp., Redmond, WA) allows the operator to choose the angular range and angular resolution for a scan, after which the system will collect the phase function automatically. A provision is made in the software to measure and subtract out a background signal thereby increasing the signal to noise ratio of the measurement.

Human Blood Studies

One pint of whole human blood was drawn from a healthy donor according to an Internal Review Board approved protocol. The whole blood was immediately packed in ice and samples were drawn and prepared as needed. The two independent variables in this study were blood oxygenation and scatterer concentration. Assuming that scattering is due primarily to red blood cells and that the ratio of hemoglobin to hematocrit remains constant in a single sample diluted with the donors plasma, we refer to the scatterer concentration as the hemoglobin concentration. We modified the red blood cell concentration in the sample by mixing the cellular component of the blood with varied amounts of blood plasma. The oxyhemoglobin level in the sample was

varied using the gas exchange technique described previously in the section of this report "Model Eye Calibration Experiments".

After a DC background scan with no sample in a darkened laboratory was acquired, the system was ready to measure the blood samples. 1.0 ml of a prepared blood sample was placed in a 10 cc syringe which was then mounted in a calibrated syringe pump. 1.0 ml of the same sample was analyzed in a CO-oximeter obtaining the hemoglobin concentration and the percent oxyhemoglobin saturation. The first syringe was connected to the top of the micropipette via small diameter tubing and the waste blood from the bottom of the pipette was collected and discarded. The average blood flow rate in the retinal vessels of healthy males has been reported³² and this flow rate was entered into the automatic syringe pump. The air was purged from the system by pumping a small aliquot of the blood through the tubing and the pipette. The scatterometer measurement was initiated while the blood flowed continuously. Intensity measurements were made in 1° intervals over the full range of the device. Multiple readings (2-8) were taken at each position and the average intensity was calculated and stored.

Figure 28 is a scattering diagram which plots the normalized measured phase function for three blood samples whose hemoglobin concentration was kept constant at ~8.7 g/dl and whose

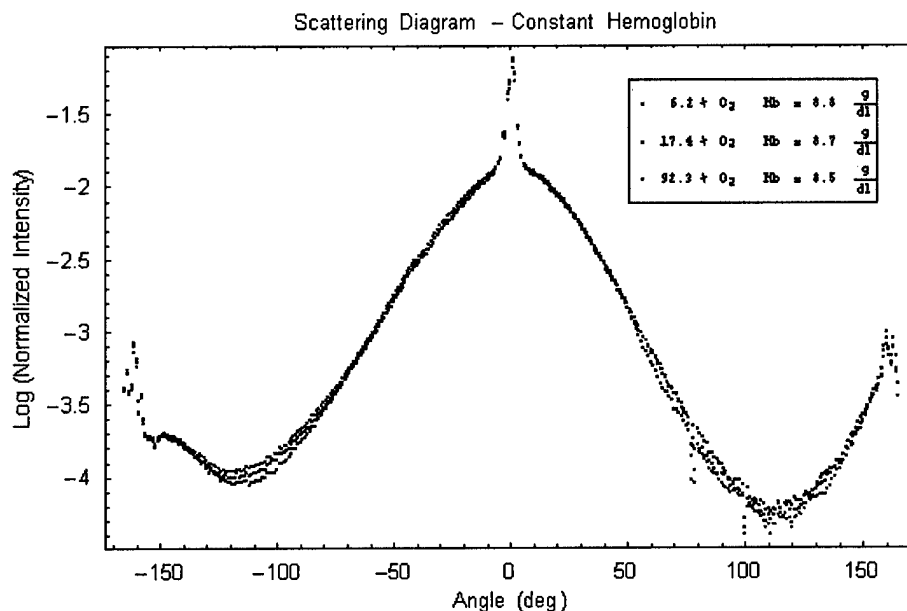


Figure 28. Scattering diagram for three blood samples with equivalent hemoglobin concentrations (≈ 8.7 g/dl) and varying degrees of oxygen saturation.

oxygenation level varied from 6.2% to 92.3%. Normalization of each measurement is performed by dividing the intensity at each position by the integral of the data across the range, and the data are plotted on a logarithmic scale due to the large measured dynamic range. We first

notice that each function is fairly symmetric about the incident direction as would be expected from the sample and the experimental configuration. However, the measured intensity minimum in the negative direction is slightly higher than its symmetric counterpart. There is no theoretical reason to expect this, and since the artifact appears in all of the plots of highly scattering media which are presented in this work, it is assumed that this is a minor systematic contribution.

It is immediately obvious that the oxygen level of the sample does not have a noticeable effect on the shape or normalized amplitude of the measured phase function. Also, all samples exhibit a strong central peak is evident out to the range of $\pm 6^\circ$ corresponding to the unscattered (i.e., transmitted) incident beam. The data is then seen to monotonically decrease until an angle of $\approx 115^\circ$, at which point it begins to increase. The position of this minimum and the increased backscatter are expected effects which will be discussed later. Finally, the scatter in the data at the extreme edges of the measured range is instrument signature due to light reflecting off the system lens mount.

Figure 29 is a similar diagram to Figure 28 in that the hemoglobin concentration is kept constant while the blood oxygen level is varied. In this case however, the hemoglobin concentration is only ≈ 3.9 g/dl for an oxygen range of 15.6 % to 95.9 %. Once again the curves are symmetric and the effect of varied oxygenation has a negligible effect on both the curve shape and amplitude. In this case, however, the curve shape is decidedly different in that there is no discernable central peak. That is not to say that there is no transmitted beam for there surely is. It simply implies that the scattered radiation is less pronounced at small angles. Although there is substantially less scattered energy in these samples, a measured profile of a sample consisting

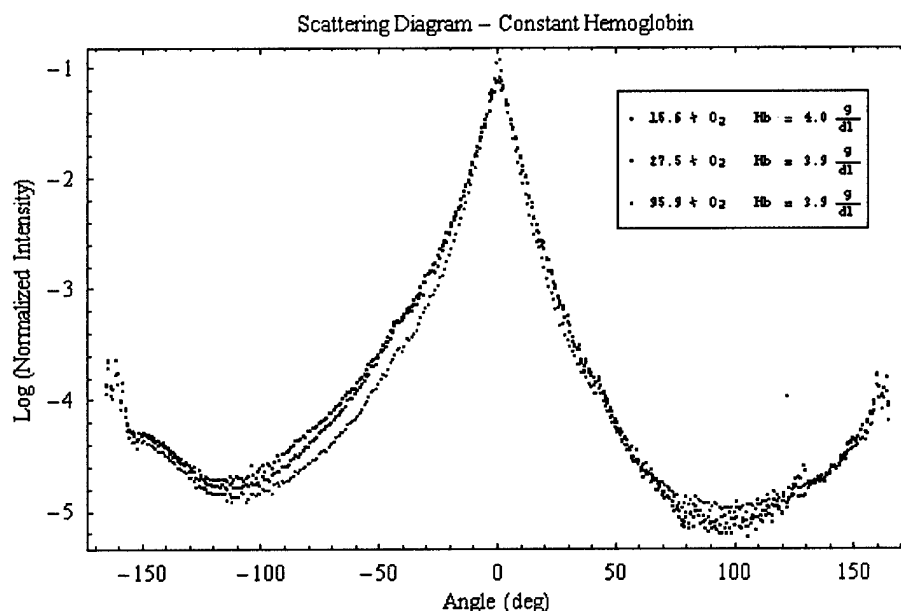


Figure 29. Scattering diagrams for three blood samples with equivalent hemoglobin concentrations (≈ 3.9 g/dl) and varying degrees of oxygen saturation.

of index matching fluid shows that the present blood scatter data is far above the system noise level. This plot will be shown below in conjunction with a sample that actually encroaches on the minimum measurable signal.

The obvious deviation between the two sets of curves in Figures 28 and 29 led to an experiment which measured the scattering function shape vs. hemoglobin concentration. Figure 30 shows the scattering functions for three samples whose oxygen level was maintained at $\approx 95\%$ while the hemoglobin concentration was varied from 3.9 g/dl to 13.9 g/dl. The scattering function shapes trend as would be expected; the sample with the highest scatterer concentration scatters more energy laterally and transmits less in the forward direction than that with the lowest concentration, with the third sample lying in between.

Figure 31 is a graph of the scattering diagram due to some of the whole plasma which was decanted from a centrifuged blood sample. Along with the plasma profile is a system profile showing the absolute minimum measurable signal as a function of angular position. It is seen that the sample is highly transparent, approaching the system profile in the angular range of $\pm 55^\circ$ and equivalent to the system noise in the range beyond this. Even though it is likely that the plasma contains some scattering centers such as lipid spheres and suspended cellular debris, the scattered energy due to these elements is negligible compare to that of the cellular component removed by centrifugation. As alluded to above, it can be seen that the system profile does not encroach on any of the measured scatter profiles of the blood cell containing samples.

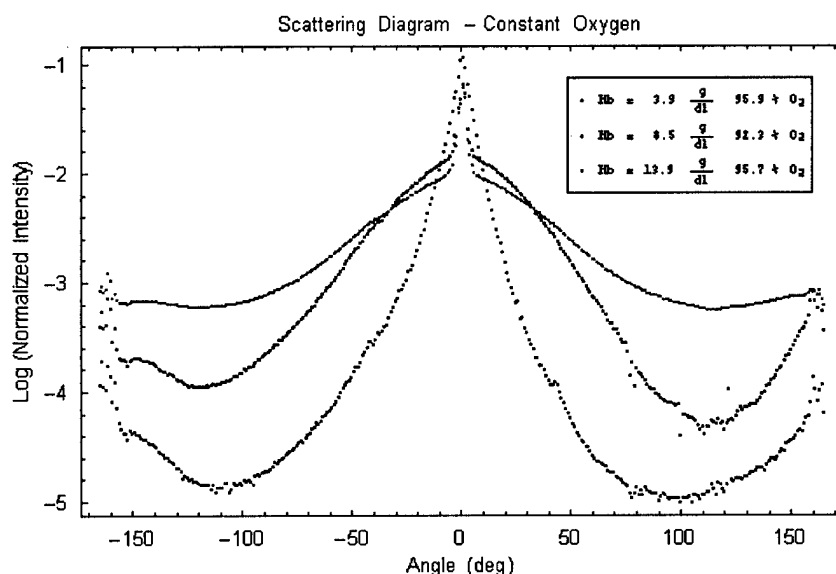


Figure 30. The scattering functions for three samples whose oxygen level was maintained at $\sim 94.6\%$ while the hemoglobin concentration was varied from 3.9 g/dl to 13.9 g/dl.

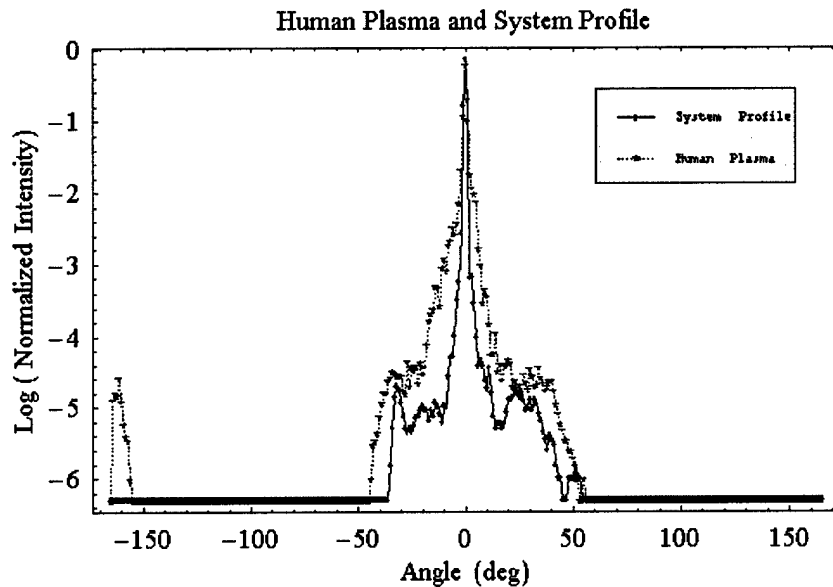


Figure 31. Scattering diagram of whole plasma and system profile. Data beyond -45 and 50 are at the noise floor of the measurement. The increased intensity at the extreme negative angles is an instrument artifact.

Analysis

The weak dependence of the scattering phase function on blood oxygenation was a reassuring discovery since anything else would have complicated the data reduction of the retinal vessel oximetry technique. The dependence was expected to be weak since the known parameters which effect the scattering phase function (scattering cross-section and coefficient, size parameter and geometric shadow) are not modified as the oxygenation of the blood changes. The absorption of the blood does change with oxygenation and its dependence on the fractional percentage of oxy- and deoxygenated hemoglobin in the cells is the mechanism that permits the oximetry measurement technique. The strong dependence on scatterer concentration was also an expected result since the concentration of scattering particles is known to profoundly effect the scattering phase function (e.g., converting a sample from single to multiple scattering regime). What was surprising was the change in shape of the scattering function as the scatterer concentration became low (incidentally, a hemoglobin concentration of 4g/dl is at the extreme of pathologically low levels). It is known that the scattering of light by whole blood with hemoglobin values that are near the norm (12 g/dl to 17.2 g/dl) is a multiple scattering process due to the proximity of the cellular component of the blood. The evident change in the scattering function shape for the samples with low hemoglobin concentrations may be an indication of the conversion from multiple to single scattering.

Summary

The purpose of the investigations reported in this section was to aggressively define the interaction between the blood column and incident light. This understanding is essential for us to answer the questions in our technical objectives: "do these measurements depend on hematocrit?" and "do these measurements depend on vessel diameter?". This group of studies allowed us to quantify the relationship between scattering of light and the blood column in the geometry of the retinal vessel. In these studies, we have demonstrated that the scattering of light by blood in a model vessel was not dependant on oxygen saturation. Scattering was sensitive to changes in the concentration of red blood cells and there appears to be a phase response to changes in concentration in the physiologic range. We have incorporated these findings in our oximetry equations and studied scattering as a function of wavelength and of vessel diameter. As we continue to improve our understanding of this effect, we have improved our ability to measure retinal vessel saturation across broad ranges of vessel diameter, blood cell concentration, and fundus pigmentation. Please see a detailed description of this work in "In-plane scatterometry of a small caliber blood column."

Four-Wavelength Saturation Measurements on Human Subjects

Introduction

The procedure for acquiring scan profiles from human subjects is summarized here. Also, the technique for the analysis of the human scan profiles is presented. This technique includes an important detail that significantly influences the saturation measurement. An experiment to investigate the repeatability and accuracy of the oxygen saturation measurement is presented and its results examined.

Acquiring Scans on the Human Subject

When scanning human subjects, the EOX is mounted to a slit lamp base which provides a chin rest support, helping to stabilize the patient's head from movement. With the subject's eye placed at the exiting window of the EOX, the patient is asked to follow a fixation target (a dim light bulb) with the opposite eye. The operator positions the target in order to aim the EOX at particular retinal vessels. The operator can translate the EOX on its mount to position it with the subject's pupil. Focus adjustment is made with an external knob allowing the operator to see an image of the retina. Once the operator has the vessel of interest centered on the cross-hairs, the scan sequence is initiated. Adjustment of the laser focus may then be made by repeatedly adjusting the externally mounted laser focus knob and viewing scans on the retina. The human measurements are best made in a dimly lit room so that the subjects' pupils are sufficiently large. A larger pupil ensures that all of the white light and laser light enters the pupil, and it maximizes the signal at the EOX detector. Once the scan has been taken, the operator looks at the scan profile on the computer screen, saving only those which are analyzable.

Data Analysis

The vessel transmittance is measured using the scan analysis software. As in the analysis of the model eye scans, we are required to choose the background signal of the vessel. These are the intensity values chosen on both sides of the vessel to approximate the value of the intensity at the center of the vessel in its absence. Figure 32 shows a typical scan at a retinal location that has both an artery and a vein together (the artery is on the left side). The background has been chosen to extend across both vessels. Frequently, we find that when two vessels become close enough together, the intensity between them seen in the scan increases far above the background values. We feel that this increase does not approximate the background signal at the center of the vessel. Thus, we chose to select the background points beyond the lateral extent of both vessels. Additionally, we almost always observe an increase in intensity next to the artery. We do not know the cause of this increase, but we choose our background line far from the artery in order to reject this artifact. These "glints" are more pronounced at 629 nm and decrease with increasing wavelength. They are nearly nonexistent at 821 and 899 nm. Occasionally, the magnitude of the glint next to the artery is so severe at 629 nm that we are not confident in our ability to acquire an accurate arterial saturation measurement. The source of these glints and means to account for

them, either optically or through signal processing, will be a major research area in the next year.

Once the vessel transmittances are measured at each wavelength, the four wavelength oximetry equations discussed in the previous section are employed to calculate the saturation. Again, this model gives a linear wavelength dependence to the scattering transmittance and uses a value for the absorption coefficient of reduced hemoglobin at 629 nm found through the model eye experiment calibration. This model fits the parameters s , cd , and T_s to the oximetry equation given the four transmittances. In the following, only the calculated saturation is discussed.

Repeatability Study

We performed an experiment on one human subject. With this experiment, we sought to verify our model eye calibration with human eye measurements. We wanted to investigate the repeatability of the saturation measurement and get an idea of how many scans are needed to generate an accurate saturation value.

In this study, the subject was in a dimly lit room and breathing room air. For both eyes, several locations on the subject's fundus were chosen to be scanned and recorded on a fundus photograph for reference (Figure 33). These scan sites allowed the simultaneous measurement of both an artery and vein and were chosen within the optic disk, outside but near the disk, and up to about 3 disk diameters away from the disk. The largest vessels present were chosen for measurement, and 32 scans were acquired at each selected site. The scanning procedure was conducted each of four consecutive days and the calculated saturation from all four days averaged to report the values given in Table 1. For each of the 32 scans acquired per site, the saturation was calculated and the saturation reported in the table is the average of these 32 measurements.

From this experiment, we see that the arteries have been measured with a saturation in the upper 90's and the veins around 60 %. Considering the venous measurements first, we expect the saturation to be nearly the same for sites 2 and 3, as the two are very near each other and no branching has taken place between them. Since the saturation is different, we believe that noise in the measurement may still be present. Increasing the number of scans taken to report a saturation may serve to decrease this noise. It is reported in the literature that the retinal veins have a saturation of 45 %²⁰ and 55 %³³. Our mean value was measured to be 62%.

The arterial saturation was expected to be roughly 97%. The mean arterial saturation that we measured was 97 %. Again, measurement noise is likely the cause of the difference seen between retinal sites.

From this *in vivo* experiment, we have measured the saturation of the retinal arteries to be about 97% and veins 62%. The oximetry equations used to calculate saturation were found to fit the transmittance data well, with the mean transmittance difference between the measurement and the model being approximately 1%. Based on this, we are reassured of the validity of the

Table 1 At each scan sit in the subject's eye, 32 scans were taken on four occasions. Saturation was calculated for each scan and the average saturation and standard deviation of the group reported.

Scan Site	Measured Saturation (%O₂Sat)	Standard Deviation (%O₂Sat)	Standard Error (%O₂Sat)
Vein 1	65	14	2.5
Vein 2	58	25	4.4
Vein 3	65	5	0.9
Vein 4	58	24	4.2
Artery 1	97	3	0.5
Artery 2	102	5	0.9
Artery 3	89	7	1.2
Artery 4	101	3	0.5
Mean Vein	62		
Mean Artery	97		

transmittance model function.

Summary

In analyzing human scan profiles, we have found features that influence the background signal. In this study, we measured the retinal arterial and venous saturation to be 97 % and 62 %, respectively.

We are in the process of acquiring data from additional subjects. We have found that there are locations on some retinas that do not yield scans that can be analyzed with our algorithms. We are working to better understand when accurate measurements can be made, and how to maximize our ability to acquire meaningful scans. The EOX-2 allows us to scan an entire region of the retina and to study these focal effects. These studies are under way. Please see "An Instrument for the Measurement of Retinal Vessel Oxygen Saturation" for a detailed description of this work.

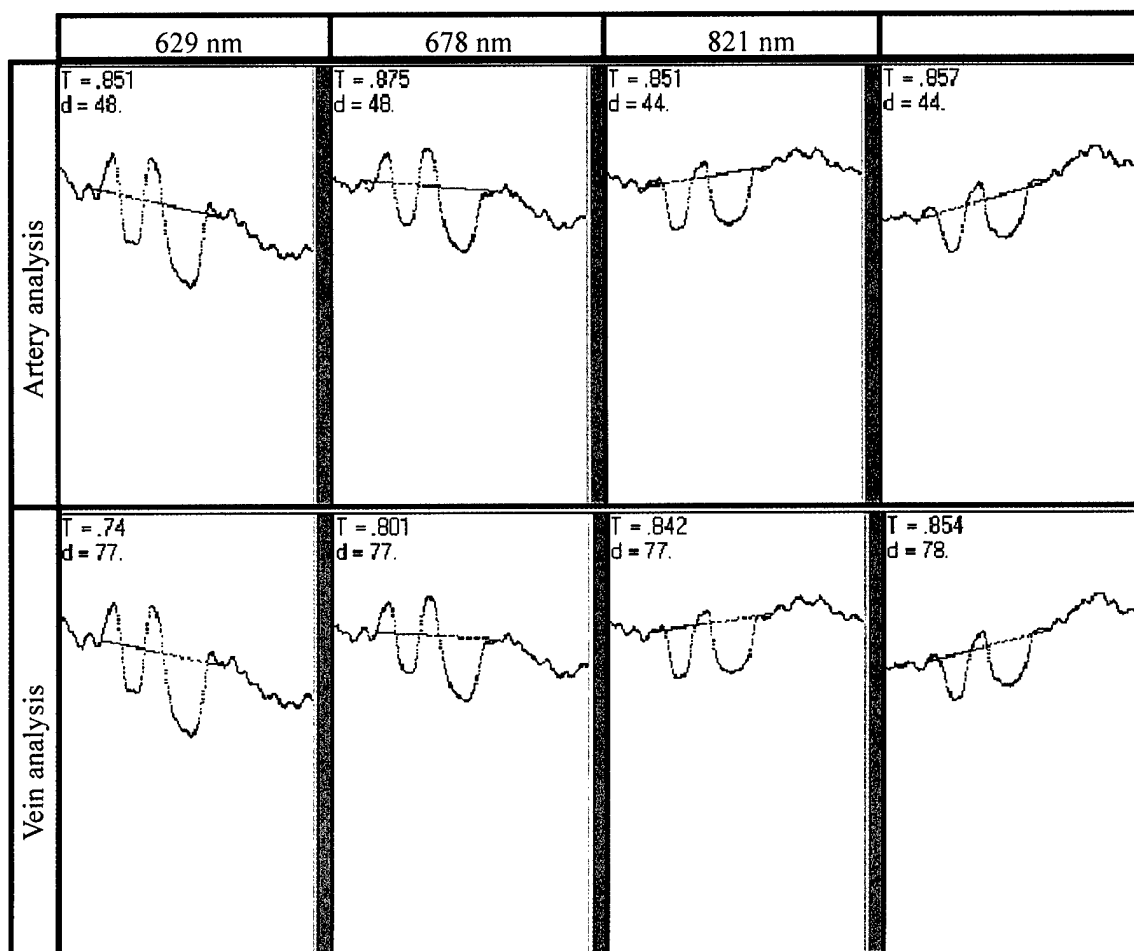


Figure 32. Typical scans from a human eye. An artery is on the left (analyzed in the top row) and a vein is on the right (analyzed on the bottom row). Notice the significant increase in intensity between the vessels and to the left of the artery for the 629 and 678 nm lasers.

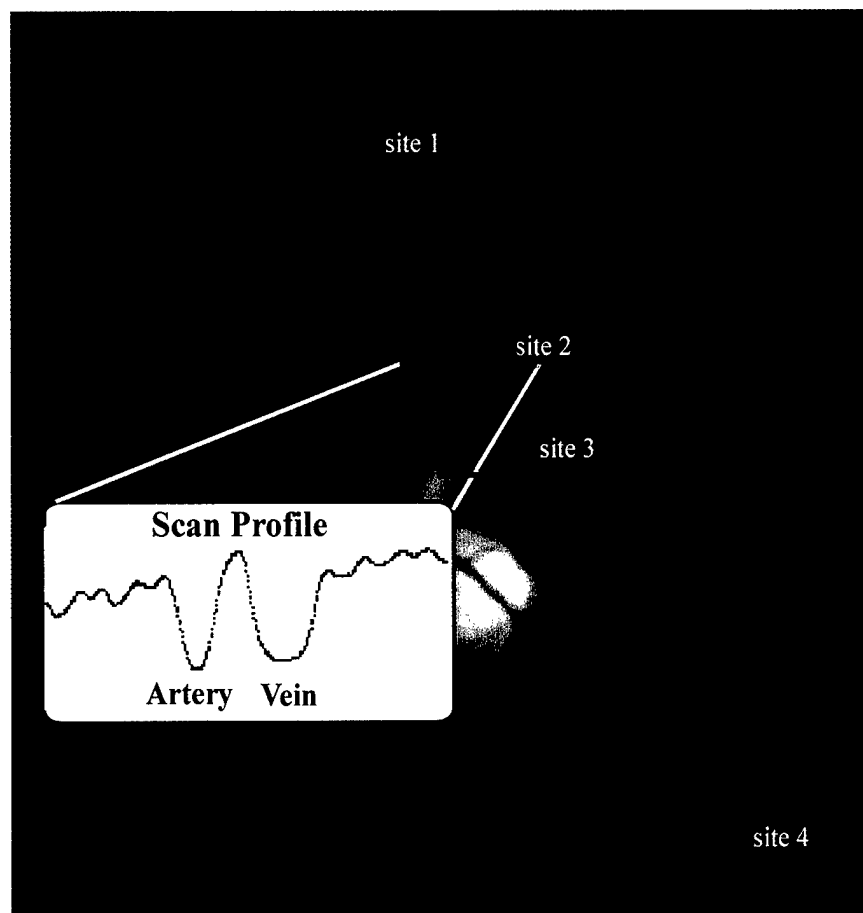


Figure 33. Fundus photograph used to mark the locations of the scan site of the subject's eye. This typical scan profile at 821 nm shows that the diameter of the vein is measured to be larger than the artery.

Swine Four-Wavelength Studies

Background

The primary motivation for developing the Eye Oximeter has been the noninvasive monitoring of blood loss. Prior to this grant from the USAMRMC, our research group had constructed a breadboard EOX and tested it in a swine model of blood loss. The breadboard oximeter, which we used for these pilot studies, allowed us to measure relative changes in oxygen saturation. Since it used only two wavelengths (670 nm and 803 nm), it could only follow trends in oxygen saturation, and the instrument could not be calibrated. In addition, the scan length of the early instrument was not large enough to reliably scan the area of the retina around the vessel(s) of interest. Finally, the early instrument could not be easily focused to allow accommodation for refractive errors in a subject's eye. Nevertheless, our pilot studies indicated a significant decrease in retinal venous oxygen saturation during the first 20% of blood loss in anesthetized swine and a high correlation between retinal artery oxygen saturation and femoral artery oxygen saturation during graded hypoxia.^{21,34,35}

At the beginning of this USAMRMC grant, we had nearly completed our current EOX prototype. This is a rugged, portable four-wavelength instrument. As described in the section *EOX Prototype Modifications*, some final work was done on this instrument under this grant. This EOX now scans approximately 1 mm of the retina, allowing large portions of the retina on either side of a vessel to be observed (typical retinal vessels are $\geq 150 \mu\text{m}$ in diameter). This instrument also incorporates four wavelengths (629, 678, 821, and 899 nm) to allow calibrated measurements of oxygen saturation. During the first seven months of this grant, we performed model eye calibration experiments, developed our four-wavelength analysis routines, and demonstrated the EOX calibration *in vitro*. We began swine studies during the 8th month of this grant to verify that the instrument was working properly, to make any necessary signal analysis modifications, to duplicate our pilot results, and to measure the retinal venous oxygen saturation during profound blood loss.

Retinal Scans from Swine

In our early experiments with the original breadboard oximeter, we generally had difficulty collecting high quality scans from the eyes of anesthetized swine. The optical quality of the cornea and lens of the swine eye is so bad that retinal vessels were barely discernable in the white-light image of the retina presented to the operator. In addition, the lasers of the original instrument could not be focused to accommodate for the significant myopia we observe in swine. Finally, the polarizers used in the original EOX did not perform well at the wavelengths used in the instrument (670 and 803 nm). This often resulted in severe specular reflections ("glints") from the cornea and from the apex of the retinal vessels. Despite these difficulties, we were able to eventually acquire scans in nearly all of the animals tested. In order to measure the transmittance of swine retinal vessels, we needed to overcome the glints from the vessel apex.

To do this, aggressive curve -fitting techniques were employed as described in our pending U. S. patent³⁴ and in the attached paper by Smith.²¹ This technique was used to generate all of the pilot data in the attached papers.^{35,36}

The current EOX allows us to finely focus the laser beams in order to account for refractive errors in the swine eyes. In addition, high-quality broad-band polarizers are used in the EOX. By illuminating the eye with vertically polarized light and collecting only horizontally polarized light, the EOX is quite effective at eliminating the glints from a subject's cornea and retinal vessels. Typical scans in *human* eyes show little if any glint from the apex of the vessel (see, for example, the artery and vein pair scanned in Fig. 32). Unfortunately, we still observe significant vessel glints at 629 and 678 nm in *swine* eyes (although the glints at 821 and 899 nm are minimal). We are not certain why the glints are still so large in the swine eyes for the red wavelengths. As discussed in the next subsection, we have attempted to improve the cornea and lens of the swine in an attempt to eliminate effects such as strain birefringence in the cornea; however, the glints still remain in the scans using red wavelengths.

We have applied our curve fitting routines to calculate the transmittance of the vessel for the swine data presented in this report. The technique involves fitting a cubic polynomial to the steepest portions of the vessel absorption profile. The most critical aspect of this fitting procedure is the selection of the data windows used for the fit. This is illustrated in Fig. 34. In this figure, the same scan is analyzed using two different data ranges for the cubic fit (this is a scan acquired at 670 nm in a swine eye). In (a), a large data range is chosen and the fitted cubic is seen to "cut through" the left edge of the vessel. This results in a transmittance value of $T = 0.837$, which we believe is too high for this scan profile. In (b), a smaller data range is used to achieve the

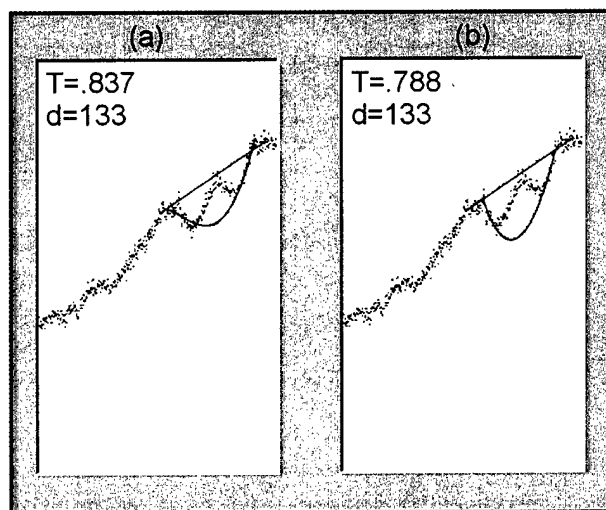


Figure 34 This figure illustrates the difficulty in fitting curves to vessel absorption profiles to eliminate glints from the vessel center. In (a), a large range of data points are used in the curve fit resulting a too high of a transmittance T . In (b), a smaller data range is used to achieve the "correct" transmittance value.

selected and the curve appears to fit the vessel edges better. We believe that the transmittance of $T = 0.778$ is "correct." We have routines in place that select these data ranges based on the fractional variation in slope at the vessel edges. However, this technique as a whole introduces more variability into our measurements than we desire, and it requires a trained operator to confirm the computer's selection.

We are working on theories to explain the increased vessel glints for red wavelengths in swine. We believe the glints occur due to the significantly higher light absorption of the swine retinal pigmented epithelium at these wavelengths.

In addition to having large glints, the red wavelengths pose additional difficulties. In both human and swine scans, the background reflectance becomes more spatially variable for the 678 and 629 nm lasers (it is the worst at 629 nm). The scans from humans are generally still acceptable for analysis, however the scans from swine frequently become so irregular that analysis at 629 nm is impossible. Figure 35 illustrates this problem. First, note the central glint at 629 nm. Once this much of the absorption profile has been obscured, we have little if any confidence in the cubic fit routine. Notice also the small feature immediately to the right of the vessel that is clearly visible at 629 and 678 nm, but less visible at 821 and 899 nm. These features appear frequently and make placement of the assumed background line difficult for the red wavelengths.

Due to the difficulties associated with scanning swine retinæ at 635 nm, we have ordered two additional diode lasers to be tested in the EOX (750 and 980 nm). As described in the *Optimum Wavelength Combinations* section, these wavelengths will replace the 635 and 820 nm lasers. The resulting instrument will be slightly less sensitive to oxygen saturation; however, we

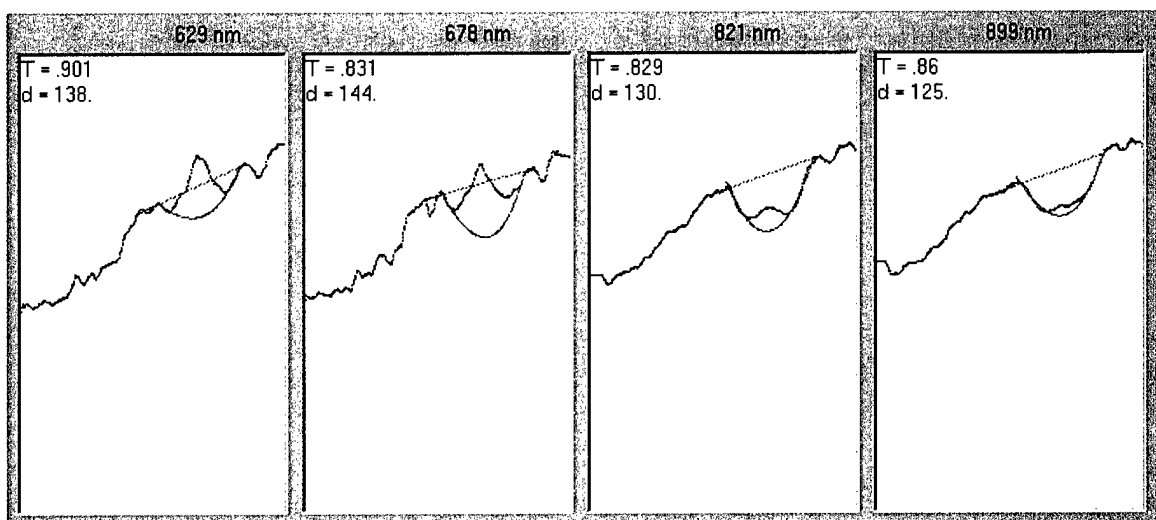


Figure 35. Typical EOX scans of a large vein in a swine eye. Notice that at 635 nm, the glint from the vessel center overwhelms the absorption signal and the background irregularity makes determining the transmittance difficult.

expect that the increased quality of scans will provide an overall improvement for our swine data.

Improving the Swine Ocular Model

As noted previously, we observed a significant increase in instrument noise when scanning swine eyes which led to unanalyzable scans in several animals.

The quality of the yorkshire swine cornea was assessed optically and found to be similar to the human eye. The swine eye lens was found to have aberrations in it which caused degradation of the image obtained with the EOX. To evaluate this effect, we dissected the swine eye and examined the lens. Unlike the human crystalline lens, the swine lens was found to contain three parts shaped like a clover leaf fused together. We believe that the area between these compartments in the lens is generating optical aberrations in the swine eye. In addition to the aberrations from the lens of the eye, we have found that the swine are profoundly myopic. We felt that this could be solved by removing and replacing the swine lens.

In order to address these problems we performed a lensectomy on a swine and replaced the natural lens with a prosthesis. This procedure was performed in the same manner as it is routinely performed on humans with cataracts. The optical quality of the eye was improved markedly as demonstrated by direct ophthalmoscopy. We were also able to identify veins and arteries in the swine eye using the EOX by direct visualization as we do in the human eye after this procedure.

Even with the new lens in place we continued to have unacceptable central glints in the swine eyes. The yorkshire swine has a significantly higher density of pigmentation when compared to the human eye (we measured the absolute reflectivity of the fundus to be about 5-10 times higher in the human eye). As a result of the significant differences between the swine eye and the human eye we began looking of a different model.

The Sinclair mini-pig swine spontaneously develops melanoma which the animal reacts to immunologically and develops variable vitiligo. About half of the animals will develop retinal vitiligo (no pigment in the retina) after two years. We were able to purchase eight vitiligo swine from Sinclair Research for our studies. The lens and cornea quality in this breed were excellent and the scan profiles from these animals were very similar to the scans which we obtained from the human eye.

Profound Blood Loss Studies

After completing the model eye experiments with the EOX, we started animal experimentation. The purpose of these experiments is to verify the efficacy of the enhancements in the EOX. In addition to answering this important question, we tested the changes in retinal venous oxygen saturation seen with profound blood loss. In order to test these hypotheses, we have designed an experiment using swine similar to that used in the second set of pilot work performed using the EOX breadboard. In this previous study we removed 16 cc/kg of blood and

reinfused it at varied rates. In these experiments, we are removing 28 cc/kg and attempting reinfusion. This profound blood loss (about 40% of total blood volume) is removed at 1.4 cc/kg/minute and subsequently reinfused at the same rate.

Materials and Methods

The EOX scans low power lasers across the retinal vasculature. The light scattered and reflected back out of the eye is collected and analyzed, and the optical density of the blood within the vessels is determined from the collected signals. These optical density measurements are made at multiple wavelengths and a biophysical model is used to calculate the oxygen saturation of the blood within the vessels.^{10,14,16,17,19}

Through an eyepiece, the EOX provides an image of the subject's ocular fundus to the operator. The operator then targets a retinal artery or vein and initiates the measurement procedure. A full data set is acquired within 0.1 seconds. Typically, eight to sixteen data sets are averaged to comprise a single saturation determination.¹⁷

This study adhered to NIH guidelines for the use of laboratory animals and was approved by the Institutional Animal Care and Use Committee.

Nine adult female Sinclair swine with retinal vitiligo weighing 55-95 kg, were fasted overnight but allowed water *ad libitum*. On the morning of the experiment, the animals were given intramuscular pre-anesthetic ketamine 20mg/kg and xylazine 5mg/kg. The swine were placed in the supine position, intubated endotracheally and placed on a ventilator. The swine were placed on 2-4% isoflurane during the surgical procedures and the depth of anesthesia was monitored using web space stimulation. An esophageal temperature probe was used to monitor core body temperature and continuous electrocardiographic monitoring was utilized. The eyes were treated with two drops of 1% cyclopentolate hydrochloride. At the beginning of the surgical preparation the animal was given a bolus of 1000 cc's of normal saline. A solution of five percent dextrose in half normal saline with 10 milliequivalents of KCl/liter was infused at 80-110 cc/hr. A celiotomy was performed using an infra-umbilical approach, the bladder exposed and a Foley catheter placed in the bladder via cystotomy. The abdominal wall was closed around the bladder catheter. A femoral cut down was performed, a 7.0 French catheter was placed in the femoral artery and an 8.0 French introducer was placed in the femoral vein. The femoral artery catheter was connected to a Hewlett Packard 78203 physiological pressure monitoring system and a 7.5 French Abbott continuous mixed venous oxygen saturation monitoring catheter was placed in the central circulation via the introducer in the femoral vein. The distal port of the central venous catheter was connected to a Hewlett Packard 78203 physiological pressure monitoring system. Placement of the central venous catheter was verified by waveform. The catheter oximeter calibration was verified using mixed venous blood obtained from the distal port. All blood gas analysis was performed using an IL 482 CO-Oximeter system. The eyelids were sutured open and sutures were placed in the conjunctiva to hold the eye in place. A catheter, attached to a 60cc syringe filled with buffered 0.9% saline (pH = 7.0), was sutured to the periocular skin and used to bathe the eye every 30 - 45 seconds to maintain corneal hydration throughout the experimental protocol.

When the surgical prep was completed, the isoflurane was decreased to 1.0%-1.5% as needed to maintain anesthesia. The respiratory rate was adjusted such that arterial CO_2 tension (P_aCO_2) between 36-44 Torr and the blood pH between 7.35-7.45. At least 10 minutes was allowed from the time of a ventilator adjustment to the time of arterial blood gas (ABG) measurement. The end tidal CO_2 was measure continuously and the respiratory rate was adjusted throughout the experiment such that the etCO_2 was maintained between 36-44 Torr. An Abbot central venous catheter was used to record continuous mixed venous oxygen saturation (S_vO_2). Femoral arterial blood samples were drawn every 5 minutes during exsanguination and reinfusion. The EOX was then aimed at a large vein near the optic disk. The retinal venous oxygen saturation (S_{rv}O_2) was measured every minute to obtain baseline data. Then the animal was exsanguinated at 1.4 cc/kg/min until a total of 28 cc/kg had been removed or the animal became premonitory by developing significant EKG changes such as ST segment elevations, QRS widening or loss of central arterial pressure waves. The shed blood was anti-coagulated using ACD solution. When the exsanguination was complete, the animal was resuscitated by reinfusing the anti-coagulated blood at 1.4 cc/kg/min.

After the final exsanguination and re-infusion, the retina was examined for laser damage using ophthalmoscopy. At the conclusion of the experimental protocol, the anesthetized swine was euthanized using supersaturated potassium chloride.

RESULTS

Cardiac output measures were normalized by dividing baseline cardiac output into all subsequent measures obtained for each animal. Figure 36 shows S_{rv}O_2 ($\pm\text{S.D.}$), and normalized cardiac output ($\pm\text{S.D.}$) measured in 8 swine during blood removal and subsequent resuscitation. Similarly, figure 37 shows the S_vO_2 ($\pm\text{S.D.}$), and normalized cardiac output ($\pm\text{S.D.}$) measured in the same 8 swine. Figure 38 shows the correlation between retinal venous oxygen saturation and mixed venous oxygen saturation during exsanguination and resuscitation. The mean S_{rv}O_2 , as measured using the EOX, correlated with blood loss ($r=-0.91$) and with re-infusion of autologous blood ($r=0.67$) during exsanguination and resuscitation. Two swine died during exsanguination preventing data collection during resuscitation. The central venous catheter failed in one animal preventing the collection of mixed venous oxygen saturations, this animal was excluded. The correlation between the normalized cardiac output and retinal venous oxygen saturation ($r = 0.92$) during profound blood loss and resuscitation from shock is shown in figure 39. We have compared retinal venous oxygen saturation to mean arterial pressure, cardiac output, mixed venous oxygen saturation, heart rate, and pulmonary artery pressure during bleeding using Friedman's exact test and found no significant difference between these monitoring modalities in this model.

SUMMARY

We have demonstrated in these animal studies that the retinal oximeter must have improvements made which correct for retinal pigmentation and vessel glints. The Sinclair animal study demonstrated significant correlations between cardiac output and mixed venous oxygen saturation during profound blood loss. In addition, we have compared retinal venous oxygen saturation to mean arterial pressure, cardiac output, mixed venous oxygen saturation, heart rate, and pulmonary artery pressure during bleeding in Sinclair swine and the monitoring tools were equivalent in detecting blood loss. The use of a non-invasive tool equivalent to mixed venous oxygen saturation for detecting active bleeding was our primary objective.

Changes in Retinal Venous Oxygen Saturation During Exsanguination and Reinfusion

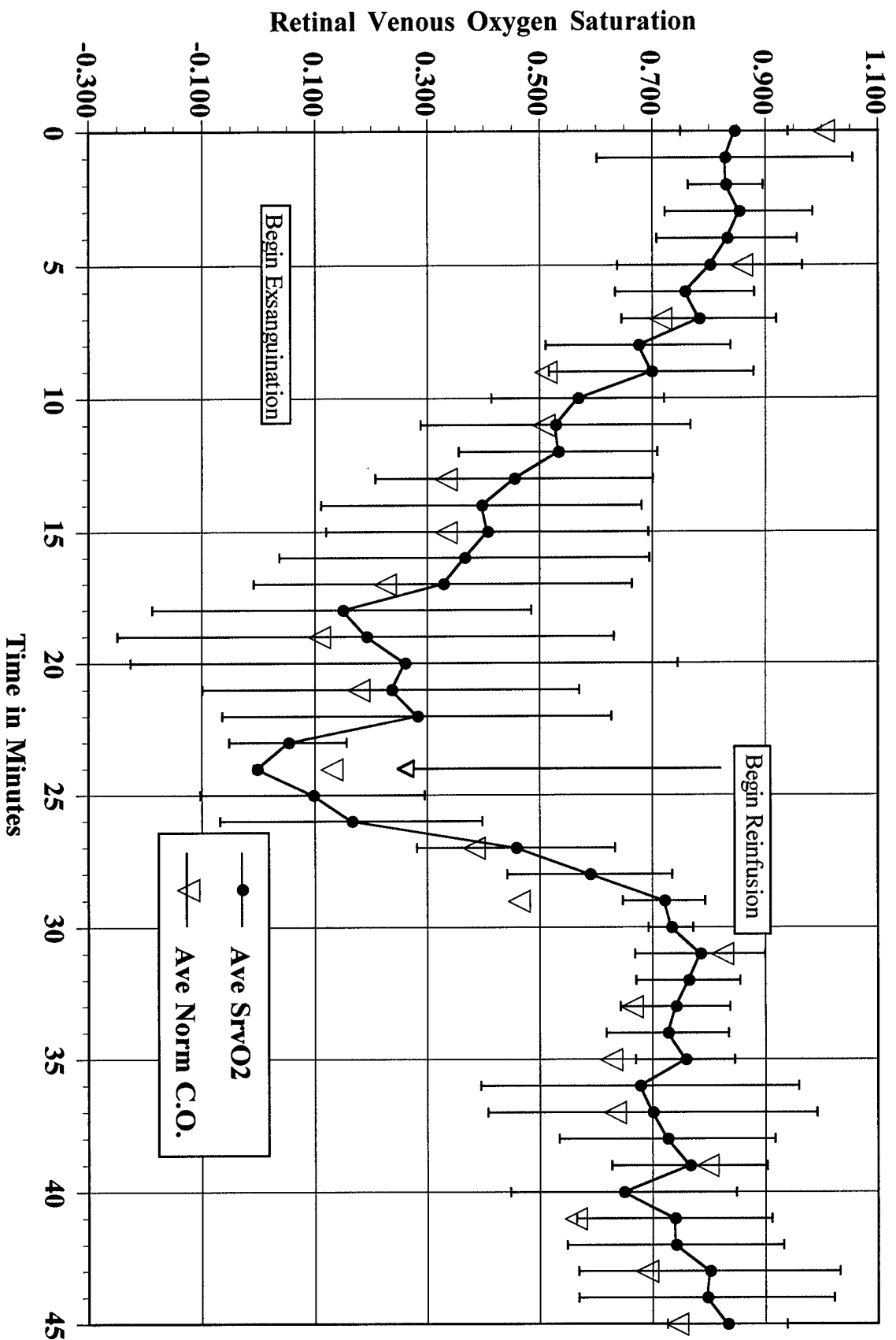


Figure 36

Mixed Venous Oxygen Saturation Changes During Exsanguination and Reinfusion

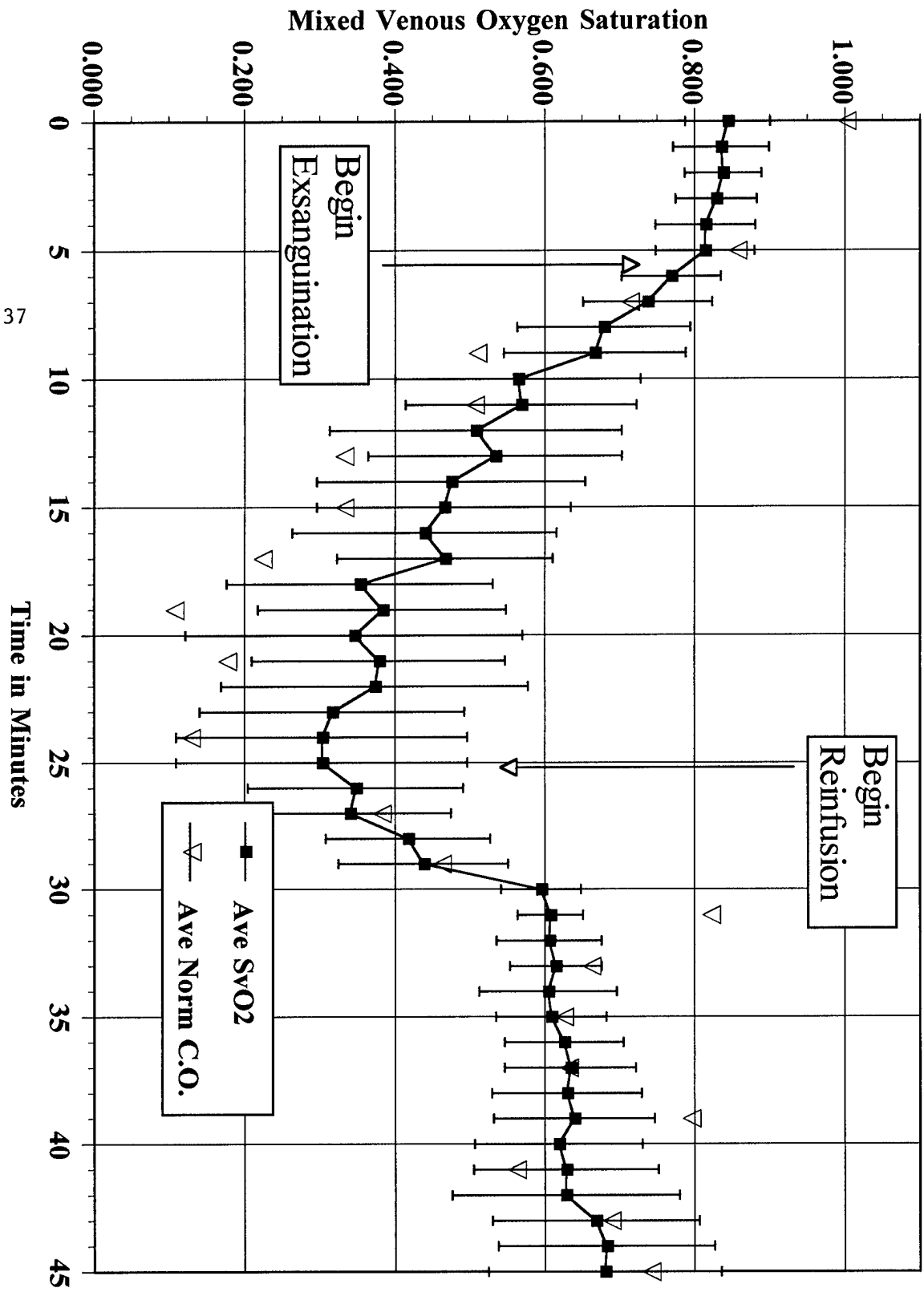


Figure 37

SvO2 vs SrVO2 During Exsanguination and Reinfusion

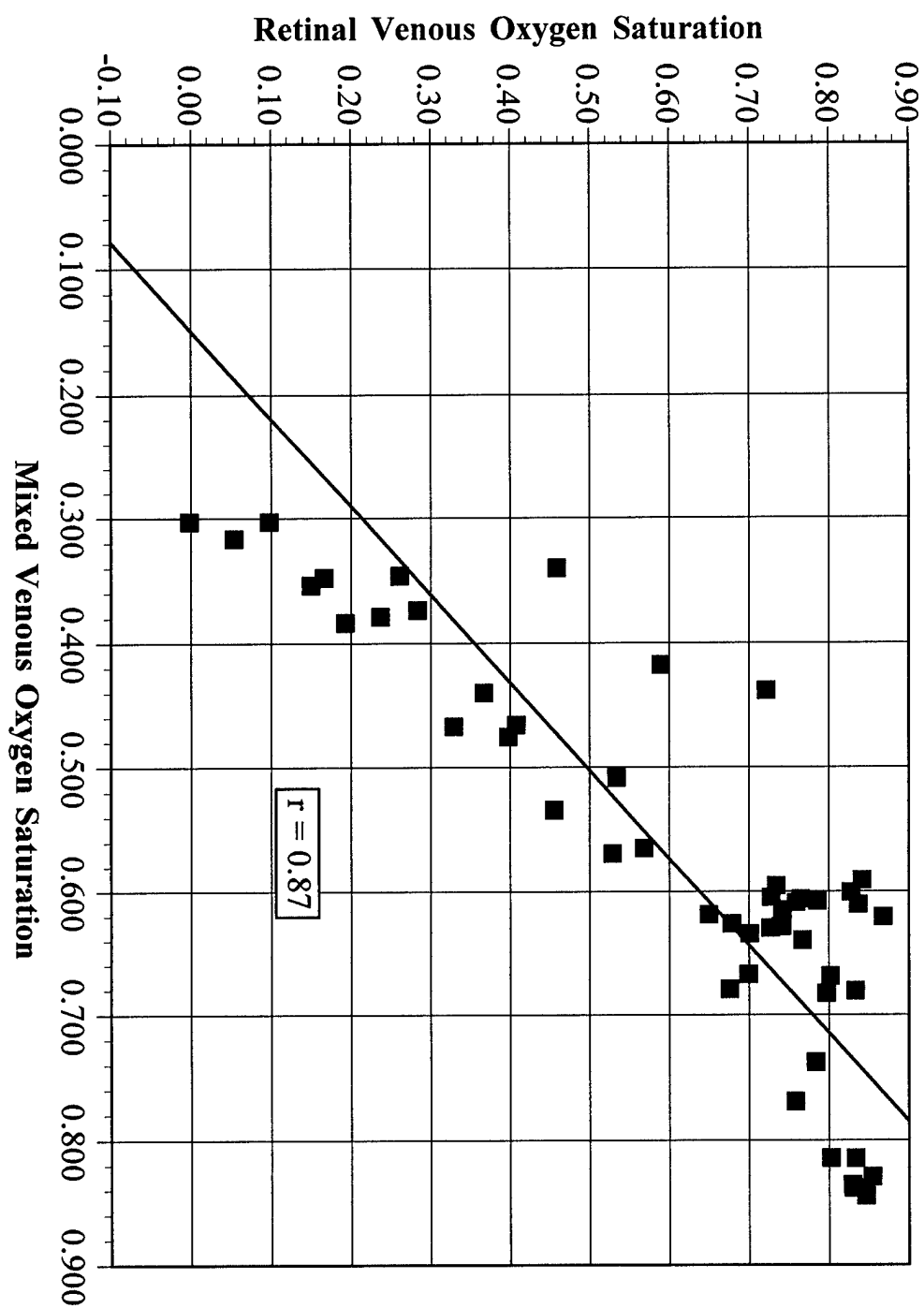


Figure 38

SrVO2 vs Normalized Cardiac Output During Exsanguination and Reinfusion

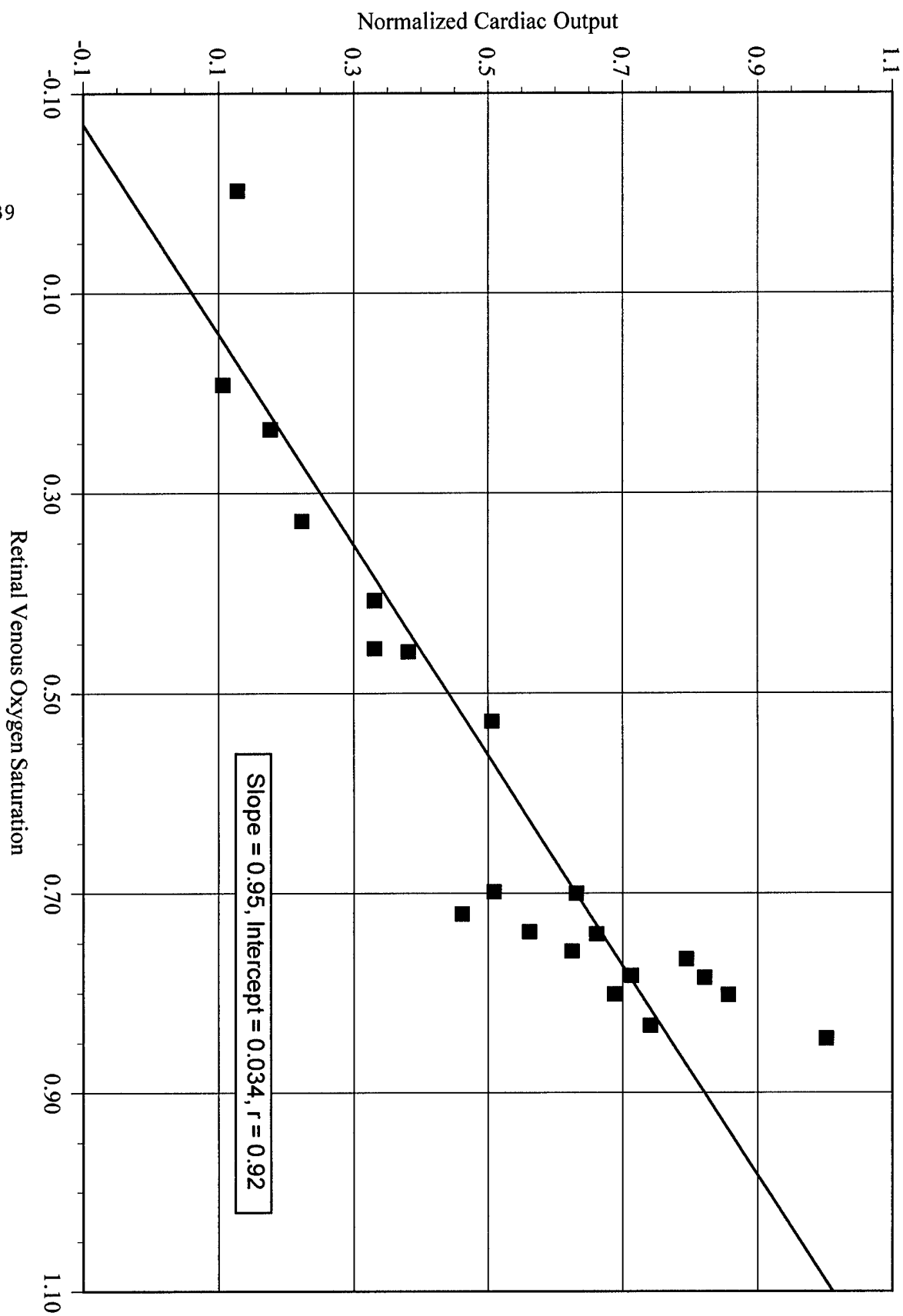


Figure 39

Key Research Accomplishments:

- Demonstrated a significant correlation between retinal venous oxygen saturation and cardiac output during profound blood loss.
- Demonstrated a significant correlation between mixed venous oxygen saturation and cardiac output during profound blood loss.
- Identified a species of swine that allowed the EOX to give approximately calibrated measurements of retinal arterial and venous oxygen saturation.
- Performed a series of swine studies with the EOX to examine changes in retinal oxygen saturation during blood loss and hypoxia.
- Completed the development of the EOX, including the incorporation of an r-wave trigger.
- Developed a model eye to simulate blood flow through a retinal vessel.
- Obtained an accurate calibration of the EOX in the model eye.
- Used the EOX and model eye to advance our understanding of the physics of retinal vessel oximetry (red blood cell scattering, photon diffusion into tissues, etc).
- Developed and tested a prototype EOX-2, and verified improved oxygen sensitivity from the use of a 488 nm laser.
- Designed and constructed the EOX-2 clinical instrument, including packaging and ergonomic considerations, an articulated arm, and a fiber coupled 488 nm laser.
- Performed theoretical work indicating that back-scattering from red blood cells may prevent instrument calibration.
- Developed an “annular confocal” technique to optically reject light back-scattered from red blood cells.
- Performed a calibration study in the model eye with the “annular confocal” technique and the 488nm laser that showed calibration to $\pm 5\%$ oxygen saturation on a single measurement, independent of hemoglobin concentration.
- Began investigating variations in calibration due to fundus pigmentation.

Reportable Outcomes:

Manuscripts, abstracts and presentations:

"An instrument for the measurement of retinal vessel oxygen saturation" J.D. Drewes, M.H. Smith, K.R. Denninghoff, L.W. Hillman, Invited paper in *Optical Diagnostics of Biological Fluids IV*, Proc. SPIE 3591 (1999).

"Handheld four-wavelength eye oximeter" C. Heaton, M.H. Smith, K.R. Denninghoff, L.W. Hillman, in Ophthalmic Technologies X, P. O. Rol, K.M. Joos, eds., *Proceedings of SPIE Vol. 3908*, January, (2000).

"Retinal vessel oximetry: Toward absolute calibration" M.H. Smith, K.R. Denninghoff, A. Lompado, L.W. Hillman, in Ophthalmic Technologies X, P. O. Rol, K. M. Joos, eds., *Proceedings of SPIE Vol. 3908*, January, (2000).

"In-plane scatterometry of small caliber blood column" A. Lompado, M.H. Smith, K.R. Denninghoff, L.W. Hillman, in Optical Diagnostics of Biological Fluids V, A. V. Priezzhev, T. Asakura, eds., *Proceedings of SPIE Vol. 3923*, January, (2000).

"Multispectral confocal scanning laser ophthalmoscope for retinal vessel oximetry" A. Lompado, M. H. Smith, K.R. Denninghoff, L W. Hillman, in Spectral imaging: Instrumentation, applications, and analysis, G. H. Bearman, D. Cabib, R. M. Levenson, eds., *Proceedings of SPIE Vo. 3920*, January, (2000).

"Effect of multiple light paths on retinal vessel oximetry" M.H. Smith, K.R. Denninghoff, J.E. Drewes, A. Lompado, L.W. Hillman, *Applied Optics* (In press).

"Retinal Imaging Techniques in Diabetes" K.R. Denninghoff, M.H. Smith, L.W. Hillman, *Diabetes Technology and Therapeutics* (In press).

"An Optical Model of the Blood in the Large Retinal Vessels" K.R. Denninghoff, M.H. Smith. Submitted to *Journal of Biomedical Optics*, November, (1999).

"Retinal vessel diameter correlates with blood volume in a swine model" K.R. Denninghoff, *Acad. Emerg. Med.* Annual Meeting, Boston, MA, (1999)

"Eye Oximeter for Combat Casualty Care 1999-I" L.W. Hillman, K.R. Denninghoff, M.H. Smith, *Advanced Technology Applications to Combat Casualty Care*, Proc., Fort Walton Beach, FL (1999)

"Eye Oximeter for Combat Casualty Care 1999-II" K.R. Denninghoff, M.H. Smith, L.W.

Hillman, *Advanced Technology Applications to Combat Casualty Care*, Proc., Fort Walton Beach, FL (1999)

"Noninvasive optical systems in systemic and ophthalmic diseases" K.R. Denninghoff, M.H. Smith, L.W. Hillman, *Optical Society America*, Annual Meeting, Santa Clara, CA, (1999)

"A scanning laser ophthalmoscope for retinal vessel oximetry" M.H. Smith, A. Lompado, K.R. Denninghoff, L.W. Hillman, *Optical Society America*, Annual Meeting, Santa Clara, CA (1999)

"Multiple light paths in retinal vessel oximetry" M.H. Smith, K.R. Denninghoff, A. Lompado, L.W. Hillman, *Optical Society of America*, Annual Meeting, Santa Clara, CA (1999)

"An eye oximeter for combat casualty care" K.R. Denninghoff, M.H. Smith, L.W. Hillman, *ATACCC98*, Proc., Fort Walton Beach, Florida (1998).

"The effect of a diffusion-enlarged point spread function on retinal vessel oximetry" M.H. Smith, J.E. Drewes, L.W. Hillman, K.R. Denninghoff, *Optical Society of America*, Annual Meeting, Baltimore, MD (1998).

Patents applied for and/or issued:

"Technique for two-dimensional scanning spectroscopy of the ocular fundus" M.H. Smith, K.R. Denninghoff, Issued October, (1999).

"Retinal 'autoregulatory state' as an indicator of perfusion status in systemic and ocular disease states" K.R. Denninghoff, M.H. Smith, T.E. Minnich, Provisional Patent submitted March, (1999).

Degrees obtained:

Jonathon Drewes: Awarded PhD in Optical Science and Engineering, May 1999.

Arthur Lompado: Awarded PhD in Optical Science and Engineering, May 1999.

Funding applied for and/or received:

ONR Grant No. N00014-99-1-0226, "An Eye Oximeter for Noninvasive Physiologic Monitoring." \$1,000,000 over three years.

U.S. Army Combat Casualty Care, "Evaluation of Lower Body Negative Pressure as a Surrogate Model of Hemorrhagic Shock in Human Subjects."

Employment and/or research opportunities applied for and/or received:

Kurt R. Denninghoff, MD: Tenure Tract, Assistant Professor; Tenure Earning, Associate Professor, The University of Alabama at Birmingham.

Penny Jester, RN, MPH: Assistant Director of The Office of Clinical Research, The University of Alabama at Birmingham.

Matthew Smith, PhD: Assistant Research Professor of Physics, The University of Alabama in Huntsville.

Arthur Lompado, PhD: Research Assistant, The University of Alabama in Huntsville.

Jonathon Drewes, PhD: Optical Design Scientist, Industry.

Conclusions:

This grant was concluded one year early to take advantage of potential synergies obtained by combining the effort performed under ONR grant # N00014-99-1-0226. The two grants were added together and the statement of work adapted to allow us to continue our work and reach the important milestones anticipated in year three of this grant. We have achieved a significant number of key outcomes in the last two years. Specifically we have:

1. Demonstrated that we can obtain calibrated measurements from a specialized swine eye.
2. Made the largest contribution to the literature on retinal vessel oximetry to date.
3. Demonstrated that retinal venous oxygen saturation decreases predictably across the spectrum of blood loss, from early blood loss in young swine to profound blood loss in mature animals.
4. Used the knowledge we have created in optics to design and build a new scanning laser oximeter which we will use to test our theoretical calibration models.
5. Developed a model eye which can be used to test our theories inexpensively and which allows for model variations without significant expense.
6. Demonstrated that retinal venous oxygen saturation correlates with cardiac output and mixed venous oxygen saturation during blood loss in a swine model.
7. Demonstrated that retinal venous oxygen saturation is as reliable an indicator of bleeding as mixed venous oxygen saturation and cardiac output during profound blood loss in a fixed rate swine exsanguination model.
8. Patented the use of retinal autoregulation changes measured using a retinal oximeter to evaluate the physiology of the whole body and the eye.

“So what?”

This work is still in progress, but, the overarching goal of developing a noninvasive monitoring tool has been significantly advanced. The question has been asked “will Doppler retinal tissue flow measurements change during blood loss as well”. This is an example of what we have achieved. We are no longer wondering if retinal circulation will be an avenue for monitoring but are rather wondering if there might be other means for capturing this information. We are actively testing this question now under the continued grant as anticipated in the joint effort with the U.S. Army and Navy.

The need for a reliable noninvasive tool for evaluating the combat casualty as far forward as possible is significant. We are actively moving toward the development of one such modality. This tool may help to triage the casualty as stable, stable but bleeding, unstable, and unstable and bleeding. The use of such a tool will be beneficial in the care of civilian casualties as well and this technology has significant dual use potential. The possibility of partnering with industry in the future elaboration of this technology decreases the risk associated with its development.

References

1. Rignault DP: Abdominal trauma in war. *World J Surg* 1992; 16:940-946.
2. Course Overview: The purpose, history and concepts. In. Alexander RH, Proctor HJ (eds): *Advanced Trauma Life Support, Course for Physicians*, Chicago, Illinois, American College of Surgeons, 1995, pp 10-16
3. Rozin R, Kleinman Y: Surgical priorities of abdominal wounded in a combat situation. *J Trauma* 1987; 27:656-660.
4. Scalea TM, Holman M, Fuortes M, Baron BJ, Phillips TF, Goldstein AS, Sclafani SIA, Shaftan GW: Central venous blood oxygen saturation: An early, accurate measurement of volume during hemorrhage. *J Trauma* 1988; 28(6):725-732.
5. Wo CJ, Shoemaker WC, Appel PL, Bishop MH, Kram HB, Hardin E: Unreliability of blood pressure and heart rate to evaluate cardiac output in emergency resuscitation and critical illness. *Crit Care Med* 1993; 21(2):218-223.
6. Dries DJ, Waxman K: Adequate resuscitation of burn patients may not be measured by urine output and vital signs. *Crit Care Med* 1991; 19:327-329.
7. Luna GK, Eddy AC, Copass M: The sensitivity of vital signs in identifying major thoracoabdominal hemorrhage. *Am J Surg* 1989; 157:512-5515.
8. Scalea TM, Hartnett RW, Duncan AO, et al: Central venous oxygen saturation: A useful clinical tool in trauma patients. *J Trauma* 1990; 3(12):1539-1549.
9. Scalea TM, Simon HM, Duncan AO, et al: Geriatric blunt multiple trauma: Improved survival with early invasive monitoring. *J Trauma* 1990; 30:129-136.
10. Trouborst A, Tenbrinck R, van Woerkens E: Blood gas analysis of mixed venous blood during normoxic acute isovolemic hemodilution in pigs. *Anesth Anal* 1990; 70:523-529.
11. Rasanen J: Supply-dependent oxygen consumption and mixed venous oxyhemoglobin saturation during isovolemic hemodilution in pigs. *Chest* 1992; 101:1121-1124.
12. Connors F, Speroff T, Dawson N, et al: The effectiveness of right heart catheterization in the initial care of critically ill patients. *JAMA* 1996; 276:889-897.
13. Abou-Khalil B, Scalea TM, Trooskin SZ, et al: Hemodynamic responses to shock in young trauma patients: Need for invasive monitoring. *Crit Care Med* 1994;22:633-639.

14. Swan H, Sanchez M, Tyndall M, et al: Quality control of perfusion: Monitoring venous blood oxygen tension to prevent hypoxic acidosis. *J Thora Cardiovasc Surg* 1990: 99:868-872.
15. Rady R, Rivers EP, Martin GB, et al: Continuous central venous oximetry and shock index in the emergency department. *Am J Emer Med* 1992: 20:538-541.
16. Healthcare Knowledge Resources, HCIA Inc.: *Hospital inpatient charges*. Baltimore, Maryland, 1993, pp 238-239.
17. Pittman R.N., Duling B.R.: A new method for the measurement of percent oxyhemoglobin. *J Appl Physiol* 1975: 38:315-319.
18. Hickam J, Frayser R, Ross J: A study of retinal venous oxygen saturation in human subjects by photographic means. *Circ* 1963: 27:275-285.
19. Cohen AJ, Laing RA: Multiple scattering analysis of retinal blood oximetry. *Biomed Eng* 1976: 23(5):391-400.
20. Delori FC: Noninvasive technique for oximeter of blood in retinal vessels. *Appl Optics* 1988: 27:1113-1125.
21. Smith MH, Denninghoff KR, Hillman LW, Chipman RA: Oxygen saturation measurements of blood in retinal vessels during blood loss. *J Biomed Optics* 1998: 3(3):296-303.
22. VanAssendelft OW: *Spectrophotometry of Haemoglobin Derivatives*, Thomas, Springfield, Ill., 1970.
23. Smith MH: *Oximetry of blood in retinal vessels*. PhD. Dissertation (The University of Alabama in Huntsville, Huntsville, AL) 1996.
24. Smith MH: Optimum wavelength combinations for retinal vessel oximetry. *Applied Optics* 1999, 38(1) (in print).
25. "Method and apparatus for measuring blood oxygen saturation within a retinal vessel with light having several selected wavelengths", MH Smith, R.A. Chipman, T.E. Minnich, U.S. Patent No. 5,776,060.
26. Delori FC, Gragoudas ES, Francisco R, Pruett C: Monochromatic ophthalmoscopy and fundus photography. *Arch Ophthalmol* 1977: 95:861-868.
27. Delori FC, Pfibsen KP. Spectral Reflectance of the Human Ocular Fundus. *Applied*

- Optics*. 1989: 28(6): 1061-77.
28. Hodgkinson IJ, Greer PB: Point-spread function for light scattered in the human ocular fundus. *Journal of the Optical Society of America* 1994: 11(2):479-486.
 29. Webb RH, Hughes GW, Delori FC: Confocal scanning laser ophthalmoscope. *Applied Optics*. 26(8):1492-1499, 1987.
 30. Wilson T: *Theory and Practice of Scanning Optical Microscopy*. Orlando, Academic Press, 1984.
 31. Smith W: *Modern Optical Engineering, The Design of Optical Systems*, McGraw-Hill, New York, 1997.
 32. Riva CE, Pournaras CJ, Tsdacopoulos M: Regulation of local oxygen tension and blood flow in the inner retina during hyperoxia. *J Appl Physiology* 1986: 61(2):592-598.
 32. Schweitzer D, Leistritz L, Hammer M, Scibor M, Bartsch U, Strobel J: Calibration-free measurement of the oxygen saturation in retinal vessels of men. In *Ophthalmic Technologies V*, J-M. Parel, Q. Ren, and K.M. Joos, eds., Proc. 1995: **SPIE 2393**, 210-218, 1995.
 33. "Method and apparatus for accurately measuring the transmittance of blood within a retinal vessel." M.H. Smith, R.A. Chipman, L.W. Hillman, K.R. Denninghoff, T.E. Minnich; U.S. Patent Pending No. 08/803,065.
 34. Denninghoff KR, Smith MH, Hillman LW, Redden D, Rue LR: Retinal venous oxygen saturation correlates with blood volume. *Academic Emergency Medicine* 1998: 5:577-582.
 35. Denninghoff KR, Smith MH, Hillman LW, Jester PM, Kuhn F, Rue LW, Redden D.: Retinal large vessel oxygen saturation correlates with early blood loss and hypoxia in anesthetized swine. *J Trauma* 1997: 43(1):29-34.

Retinal Large Vessel Oxygen Saturations Correlate with Early Blood Loss and Hypoxia in Anesthetized Swine

Kurt R. Denninghoff, MD, Matthew H. Smith, PhD, Russell A. Chipman, PhD, Lloyd W. Hillman, PhD,
Penelope M. Jester, RN, MPH, Charles E. Hughes, Ferenc Kuhn, MD, and Loring W. Rue, MD, FACS

Background: Noninvasive monitoring would likely improve trauma care. Using laser technology, we monitored the oxygen saturation in retinal vessels during exsanguination and hypoxia.

Methods: Seven anesthetized swine were bled at 0.4 mL/kg/min for 40 minutes. During exsanguination, retinal venous saturation ($S_{rv}O_2$) was measured using an eye oximeter, and central venous saturation (S_{vo_2}) was measured using a fiber-optic catheter. After the shed blood was reinfused, the F_{iO_2} was progressively decreased from 0.97 to 0.07. Femoral artery oxygen saturation (S_{fo_2}) and retinal artery oxygen saturation (S_{rao_2}) were measured at each increment.

The basic principle of shock resuscitation is to ensure that the delivery of oxygen to peripheral tissues is sufficient to maintain aerobic metabolic functions. During shock, therapeutic maneuvers attempt to improve oxygen delivery by optimizing cardiac performance or improving the oxygen-carrying capacity of blood.^{1,2} Several outcome studies have shown central venous oxygen saturation (S_{vo_2}) to be a reliable index of oxygen delivery, enabling the assessment of the response to specific therapeutic maneuvers during shock.³⁻⁷ Unfortunately, obtaining S_{vo_2} requires invasive monitoring, which is time-consuming,² costly,⁸ and has associated complications.^{1,3,9} Consequently, a noninvasive, rapidly applicable technique that provides a reliable index of oxygen delivery during early shock would be a valuable adjunct to patient management.²⁻⁵

The retinal vasculature is a potential source of noninvasive perfusion data and one that is easily accessible.¹⁰⁻¹² A study of the delivery of oxygen to the retina has shown a correlation between retinal perfusion and brain blood flow.¹³ Because of the preservation of blood flow to the central circulation during shock states,^{1,4} perfusion of the retina is preserved during early shock. There have been previous attempts at retinal vessel oximetry, which were able to detect changes in oxygen saturation as small as $\pm 4\%$.^{10,14-16} These devices were not

Results: During exsanguination, $S_{rv}O_2$ correlated with blood loss ($r = -0.93$) and S_{vo_2} ($r = 0.94$). S_{rao_2} correlated with S_{fo_2} during incremental hypoxia ($R^2 = 0.93 \pm 0.15$).

Conclusions: In this model of exsanguination, retinal venous oxygen saturation correlates with blood volume and with central venous oxygen saturation. The S_{rao_2} correlates with S_{fo_2} during graded hypoxia. Use of an eye oximeter to noninvasively monitor trauma patients appears promising and warrants further study.

utilized to monitor retinal saturation during shock states and were not used in clinical practice.

During the last 3 years we have developed an experimental, noninvasive eye oximeter (EOX). This innovative medical device attempts to quickly and noninvasively measure the oxygen saturation of blood in the retinal arteries and veins. This spectroscopic measurement is made by scanning low-power lasers into the eye and across the large vessels near the optic nerve head. In this report we present the results of a pilot test of this device using a swine model of early shock and hypoxia.

MATERIALS AND METHODS

The EOX scans low-power lasers across the retinal vasculature, the light scattered and reflected back out of the eye is collected and analyzed, and the optical density of the blood within the vessels is determined from the collected signals. These measurements of optical density are made at multiple wavelengths, and standard spectrophotometric oximetry equations are used to calculate the oxygen saturation of the blood within the vessels.^{10,14,16,17}

Through an eyepiece, the EOX provides an image of the subject's ocular fundus to the operator. The operator then targets a retinal artery or vein and initiates the measurement procedure. A full data set is acquired within 0.1 seconds. Typically, 8 to 16 data sets are averaged to constitute a single saturation determination.

This study adhered to National Institutes of Health guidelines for the use of laboratory animals and was approved by the University of Alabama at Birmingham Institutional Animal Care and Use Committee. Young female swine, weighing 18 to 32 kg, were fasted overnight but allowed water ad libitum. On the morning of the experiment, the animals were given intramuscular preanesthetic ketamine 600 mg and xy-

From the Department of Emergency Medicine and the Section of Trauma (K.R.D., P.M.J., F.K., L.W.R.), Burns and Surgical Critical Care, Department of Surgery, University of Alabama at Birmingham, Birmingham, Alabama; and The Department of Physics (M.H.S., R.A.C., L.W.H., C.E.H.), University of Alabama in Huntsville, Huntsville, Alabama.

This study was supported by The University of Alabama at Birmingham Research Foundation, The University of Alabama at Birmingham Department of Emergency Medicine, The University of Alabama in Huntsville, Haemonetics Corp., and Abbott Labs.

Address for reprints: Kurt R. Denninghoff, MD, JTN 266, 619 South 20th Street, Birmingham, AL 35233-7013.

lazine 100 mg. The swine were placed in the supine position, intubated endotracheally, and placed on a ventilator with initial settings of $\text{Fio}_2 = 0.9$ and tidal volume = 10 to 15 mL/kg. The swine were placed on 2 to 4% isoflurane during the surgical procedures, and the depth of anesthesia was monitored using web-space stimulation. An esophageal temperature probe was used to monitor core body temperature, and continuous electrocardiographic monitoring was used. The eyes were treated with two drops of 1% cyclopentolate hydrochloride. An intravenous infusion of 5% dextrose in half normal saline solution with 10 mEq of KCl/L was given at 80 to 110 mL/h. A celiotomy was performed using an infraumbilical approach, the bladder was exposed, and a Foley catheter was placed in the bladder via cystotomy. The abdominal wall was closed around the bladder catheter. A femoral cut down was performed, a 7.0 French catheter was placed in the femoral artery, and an 8.0 French introducer was placed in the femoral vein. The femoral artery catheter was connected to a Hewlett-Packard 78203 physiological pressure monitoring system, and an Abbott 7.5 French continuous mixed venous oxygen-saturation monitoring catheter was placed in the central circulation via the introducer in the femoral vein. The distal port of the central venous catheter was connected to a Hewlett-Packard 78203 physiological pressure monitoring system. Placement of the central venous catheter in the pulmonary artery was verified by wave form. The catheter oximeter calibration was verified using mixed venous blood obtained from the distal port. All blood gas analysis was performed using an IL 482 CO-Oximeter system. The eyelids were sutured open, and sutures were placed in the conjunctiva to hold the eye in place. A catheter, attached to a 60-mL syringe filled with 0.9% saline, was sutured to the periocular skin and used to bathe the eye every 45 to 60 seconds to maintain corneal hydration throughout the experimental protocol.

When the surgical preparation was completed, the Fio_2 was decreased to 0.21 and the isoflurane was decreased to 1.25 to 2% as needed to maintain anesthesia. The respiratory rate was adjusted to maintain arterial CO_2 tension (PaCO_2) between 36 and 44 mm Hg and blood pH between 7.35 and 7.45. At least 10 minutes was allowed from the time of a ventilator adjustment to the time of arterial blood gas (ABG) measurement. The central venous catheter was used to record continuous mixed venous oxygen saturation (SvO_2). The EOX was then aimed at a large vein near the optic disk. The retinal venous oxygen saturation (SrvO_2) was measured every 2 minutes. Immediately after each SrvO_2 measurement, 0.8 mL/kg of blood was removed from the pig. A total of 16 mL/kg of blood was removed over 40 minutes. The shed blood was heparinized and washed in 0.9% normal saline using a Haemonetics Cell Saver I system. When the exsanguination was complete, the animal was resuscitated by reinfusing the red cell mass with saline in a 1:3 ratio. ABCs were obtained and the respiratory rate adjusted to keep the PaCO_2 between 36 and 44 mm Hg.

After the resuscitation of the swine from exsanguination, the EOX was aimed at a large artery near the optic disk. The Fio_2 was then decreased incrementally from 0.97 to 0.07. At

each Fio_2 level, the femoral artery oxygen saturation (SaO_2) was obtained from an ABG and, at the same time, the retinal arterial saturation (SraO_2) was measured with the EOX.

After the EOX scans were completed, the retina was examined for laser damage using indirect ophthalmoscopy. At the conclusion of the experimental protocol, the anesthetized swine were euthanized using supersaturated KCl.

RESULTS

The SrvO_2 and SvO_2 measured during blood loss in each swine are shown in Figure 1. The best fit line for SrvO_2 in each swine is also shown in Figure 1. The rate of decrease in retinal saturation over 16 mL/kg blood loss was $1.4 \pm 0.9\%$ saturation for each mL/kg blood loss. Figure 2 shows the graph of the mean values for SrvO_2 and SvO_2 during blood loss. Mean retinal venous oxygen saturation, as measured using the EOX, correlates with blood loss ($r = -0.93$; $n = 7$; $p < 0.001$) when 16 mL of blood/kg total body weight is removed over 40 minutes in anesthetized swine. Retinal venous oxygen saturation is also found to correlate with mixed venous saturation ($r = 0.94$; $n = 6$; $p < 0.001$) during the 16 mL/kg blood loss. Figure 3 shows the average data from six swine. (Because of a system failure, mixed venous oxygen saturation data were not available from one swine.)

The arterial saturation of six swine was varied via graded hypoxia (one swine was excluded because the retinal arteries in the 18-kg swine were too small for analysis). Figure 4 displays the data from a single swine. The SraO_2 , which was measured with the EOX, is plotted versus SaO_2 , which was measured with the blood gas analyzer. Strong correlation ($R^2 = 0.956$; $p \ll 0.001$) is found between the two measurements. The graded arterial hypoxia experiment was performed on six swine. In each case, the correlation between SraO_2 and SaO_2 was excellent ($R^2 = 0.93 \pm 0.072$; range, 0.8–0.998; $n = 6$). The correlation plot slopes and intercepts were similar from animal to animal, with an average slope of 0.80 ± 0.11 and an average intercept of 0.06 ± 0.17 . All errors reported are the standard deviation from the mean.

DISCUSSION

The ability to accurately and rapidly identify occult blood loss would be an invaluable adjunct to the management of patients with multiple injuries.¹ Conventional vital signs, which are prone to compensatory maintenance during hemorrhage, are particularly unreliable in the early period of blood loss when intervention is the most efficacious.^{2,18,19} The alteration of vital signs seen in response to the cascade of acidosis, vascular collapse, and death occurs late in the process of blood loss and is variable from patient to patient.² There have been several studies published advocating the use of central venous oxygen-saturation measurements as a means of identifying occult blood loss early in the time course to lethal exsanguination.^{1,3,4,20,21} Drawbacks of central catheter monitoring include the known associated complications and the skill and time required for proper insertion.^{1,9} As a result of these limitations, central monitoring cannot be used in the prehospital setting, tends to be em-

on (S_{aO_2})
he retinal
OX.
i was ex-
scr. At
es zed

ach swine
ach swine
in retinal
.9% satu-
e graph of
ss. Mean
using the
n = 7;
weight is
etinal ve-
ith mixed
ng the 16
from six
is oxygen
)
ia graded
al arteries
Figure 4
which was
hich was
lat' R^2
me. are-
was per-
between
'2; range,
intercepts
e slope of
0.17. All
mean.

ult blood
ement of
tal signs,
ing hem-
period of
ous.^{2,18,19}
ascade of
the pro-
patient.²
ing the use
nts as a
the time
s of cen-
ted com-
er. r-
om. ing
be em-

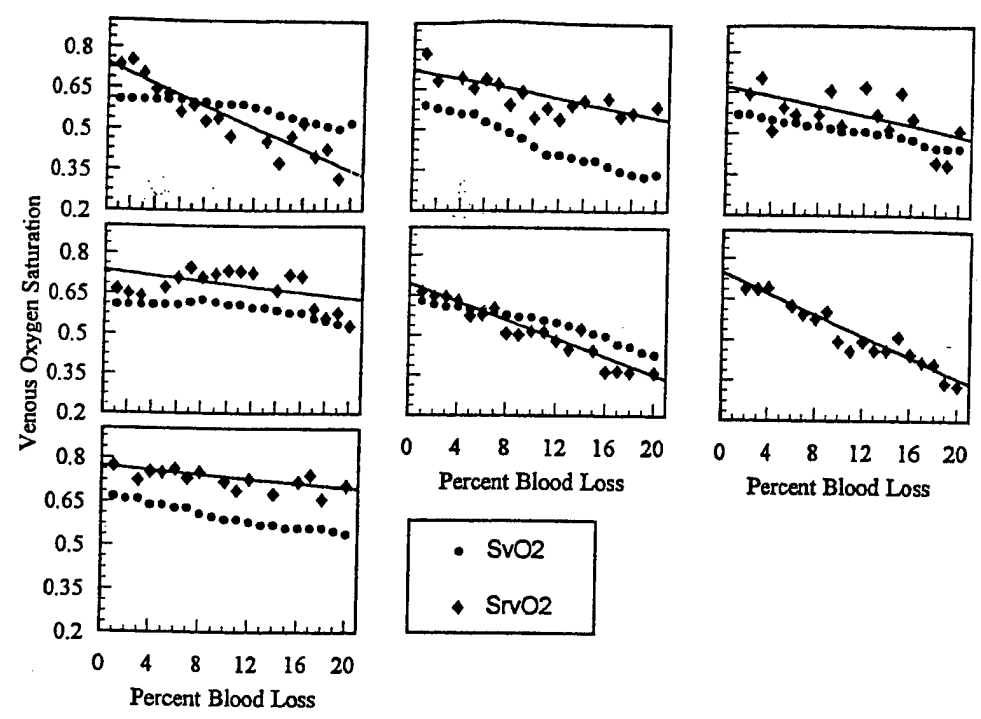


FIG 1. Retinal and mixed venous oxygen saturation measured in each of seven swine during removal of 20% of total blood volume (16 mL/kg). The best-fit line for the retinal venous oxygen saturation is also shown.

ployed late in the emergency stay of trauma victims, and is rarely used in victims of blunt trauma without signs of significant injury. The need for a method to identify ongoing occult blood loss of trauma patients with a noninvasive device that is fast, accurate, and simple to use is apparent.² Previously, noninvasive blood-oxygenation measurements have been attempted.^{22,23} Weaknesses have been found with these approaches. Near-infrared spectroscopy is potentially erroneous because of differences in the thickness of the skull

and the scalp, which alter path length.²² Pulse oximetry is sometimes inaccurate as a result of optical shunting (the presence of light that alters the true reading)^{24,25} and has been associated with skin burns.²⁶⁻²⁸ The device measures peripheral perfusion only²⁹ and has limited efficacy for patients with anemia or hypoxia.^{29,30}

We used this animal model because of the similarities between the swine and the human eye.³¹ We chose to leave the spleen intact because the removal of the spleen might lead

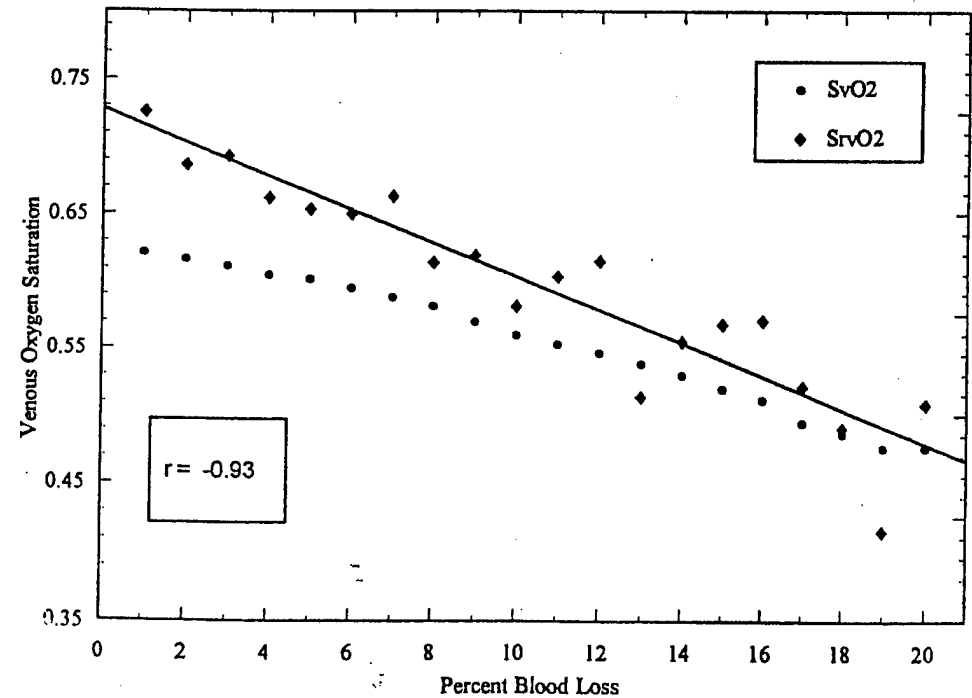


FIG 2. Average retinal and mixed venous oxygen saturation measured during removal of 20% of total blood volume (16 mL/kg). The best-fit line for the retinal venous oxygen saturation is also shown.

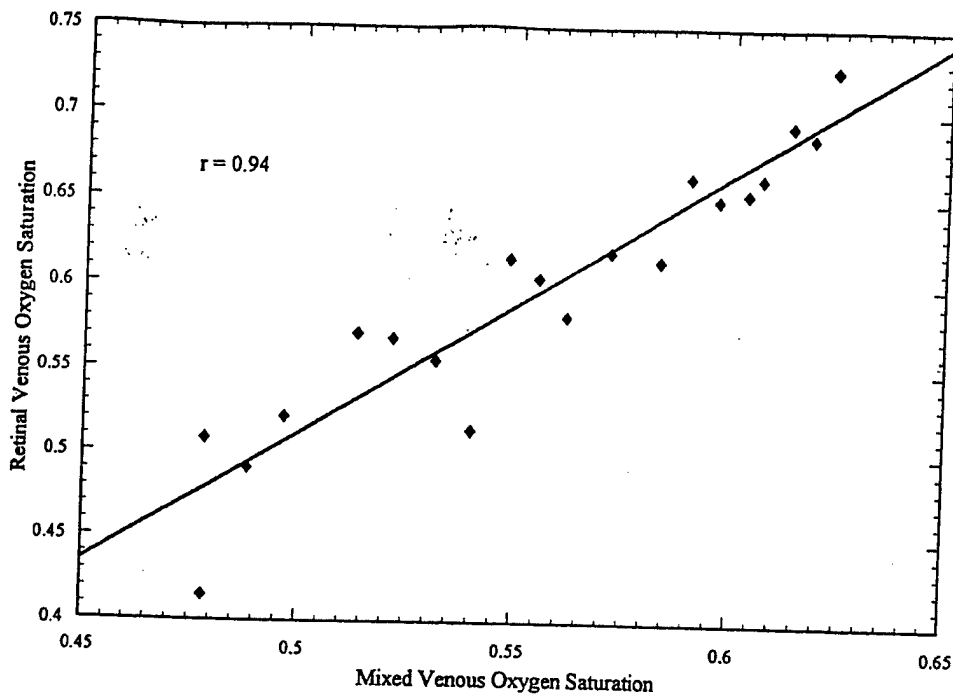


FIG 3. Scatter plot of retinal venous and mixed venous oxygen saturation measured during a 40-minute period of 0.4 mL/kg/min blood loss.

to a functional decrease in circulating blood volume and because the response to early blood loss by the splanchnic circuit is not expected to completely compensate for blood loss.^{32,33} Specifically, we felt that this was a better model because testing the retinal venous saturation's sensitivity to early blood loss was our primary objective. We used a slow rate of exsanguination and a modest end point for blood removal (0.4 mL/kg/min over 40 minutes for a total blood loss of 16 mL/kg) because we felt that this would more accurately reflect the occult bleeding of trauma patients who appear hemodynamically stable and who compensate for

slow blood loss. Changes in retinal venous saturation with more profound blood loss and correlation with cardiac index, lactate, base deficit, and tonometry remain to be studied.

As currently configured, the EOX requires a skilled operator. For this device to be useful in the prehospital setting, it will need to be more fully automated.

This pilot study demonstrates the potential value of a device that uses spectrophotometric technology to evaluate oxygen saturation in the large vessels of the eye. The EOX has an eyepiece that allows the operator to view the laser scans on the retina. Thus, we were able to verify that the

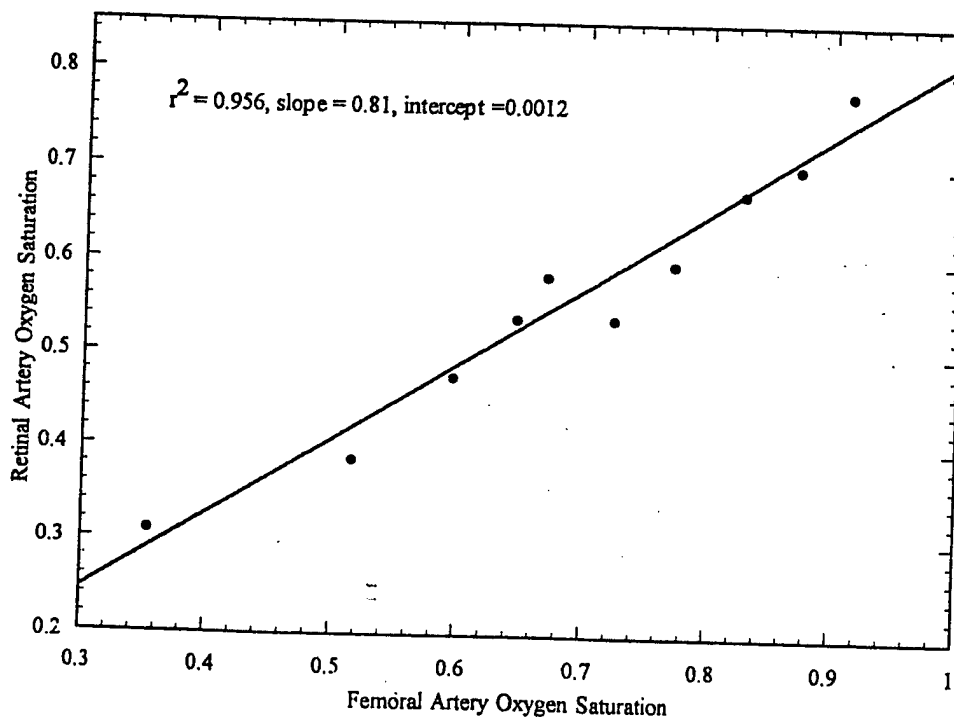


FIG 4. Femoral artery oxygen saturation correlates with retinal artery oxygen saturation measured using the EOX over a broad range of oxygen saturations.

artery or vein in question was being scanned by direct visualization. The EOX is completely noninvasive in that it projects light into the eye and measures the light returning from the eye without touching the patient. We sutured the animals' eyes open and in place because the animals are not cooperative. This necessitated our use of an irrigation system to keep the cornea moist. Similar scanning devices used on the retina (i.e., the scanning laser ophthalmoscope) do not require these measures for humans. We do not expect this to be a problem with awake, cooperative patients. For patients who have altered mental states, the use of the device may be limited. The light levels used by the EOX are lower than the class I laser limits (no significant risk) set forth by the Food and Drug Administration.³⁴ As such, the device could be tested on humans with institutional review board approval.

In the configuration used for this study, the EOX is capable of analyzing vessels ranging from approximately 50 to 300 μm in diameter. Veins and arteries in this diameter range were readily accessible near the optic nerve heads of all of the swine used in this study. (An 18-kg swine was excluded from the arterial hypoxia study because of insufficient retinal arteriolar diameter). This diameter restriction, however, prevents the use of the current device on vessels far from the optic disk and may prevent its use on the retinal arteries of small children.

The eye provides a relatively clear window to the arteries and veins of the retina, with little intervening tissue that would promote light scattering. The optical quality of the eye/EOX system contributes to the accuracy of the device. However, because of this need for a clear optical window, this instrument may not be useful for elderly patients with cataracts or for patients with corneal opacities.

The retinal venous oxygen saturation measured using this device appears to be very sensitive to early blood loss. In some cases, we were able to detect a 1.6 mL/kg decrease in blood volume. This would equate to a blood loss of 112 mL over 4 minutes in a 70-kg patient. There was considerable variability in the response to blood loss seen from animal to animal. This is similar to results seen in exsanguination studies using central venous oximetry.¹

The retinal arterial oxygen saturation measured using the EOX correlated well with progressive hypoxia. The consistently strong correlation between $S_{ra}O_2$ and S_aO_2 in the graded-hypoxia experiment demonstrates the potential for the EOX to become a clinically viable diagnostic instrument. This would allow for an end-organ arteriovenous oxygen-saturation difference in a preserved circuit. The correlation between this retinal arteriovenous saturation difference, cardiac output, systemic vascular resistance, and brain blood flow remains to be tested.

CONCLUSION

We have demonstrated the use of an experimental eye oximeter during blood loss and hypoxia in an anesthetized swine model. Changes in retinal venous saturation correlated with blood loss and retinal venous saturation correlated with mixed venous saturation during blood loss. The retinal artery

saturation correlated with femoral artery saturation during graded hypoxia. The use of such a device as a noninvasive monitoring tool for occult blood loss and hypoxia appears promising and warrants further study.

Acknowledgments

The authors thank Mr. Ronnie J. Brown, Senior Research Associate, The University of Alabama at Birmingham Department of Surgery, for technical support and several late nights in the lab.

REFERENCES

1. Scalea TM, Holman M, Fuortes M, et al. Central venous blood oxygen saturation: an early, accurate measurement of volume during hemorrhage. *J Trauma*. 1988;28:725.
2. Wo CJ, Shoemaker WC, Appel PL, Bishop MH, Kram HB, Hardin E. Unreliability of blood pressure and heart rate to evaluate cardiac output in emergency resuscitation and critical illness. *Crit Care Med*. 1993;21:218.
3. Scalea TM, Hartnett RW, Duncan AO, et al. Central venous oxygen saturation: a useful clinical tool in trauma patients. *J Trauma*. 1990;3:1539.
4. Scalea TM, Simon HM, Duncan AO, et al. Geriatric blunt multiple trauma: improved survival with early invasive monitoring. *J Trauma*. 1990;30:129.
5. Abou-Khalil B, Scalea TM, Trooskin SZ, et al. Hemodynamic responses to shock in young trauma patients: need for invasive monitoring. *Crit Care Med*. 1994;22:633.
6. Swan H, Sanchez M, Tyndall M, et al. Quality control of perfusion: monitoring venous blood oxygen tension to prevent hypoxic acidosis. *J Thorac Cardiovasc Surg*. 1990;99:868.
7. Rady M, Rivers EP, Martin GB, et al. Continuous central venous oximetry and shock index in the emergency department. *Am J Emerg Med*. 1992;10:538.
8. *Hospital Inpatient Charges*. Baltimore, Md: Healthcare Knowledge Resources; 1993:238.
9. Connors F, Speroff T, Dawson N, et al. The effectiveness of right heart catheterization in the initial care of critically ill patients. *JAMA*. 1996;276:889.
10. Delori FC. Noninvasive technique for oximeter of blood in retinal vessels. *Appl Optics*. 1988;27:1113.
11. Delori FC, Gragoudas ES, Francisco R, et al. Monochromatic ophthalmoscopy and fundus photography. *Arch Ophthalmol*. 1977;95:861.
12. Hickam JB, Frayser R. Studies of the retinal circulation in man: observations on vessel diameter, arteriovenous oxygen difference, and mean circulation time. *Circulation*. 1966;33:302.
13. Harris A, Arend O, Kopecky K, et al. Physiological perturbation of ocular and cerebral blood flow as measured by scanning laser ophthalmoscopy and color Doppler imaging. *Surg Ophthalmol*. 1994;38(suppl):S51.
14. Hickam JB, Frayser R, Ross J. A study of retinal venous oxygen saturation in human subjects by photographic means. *Circulation*. 1963;27:275.
15. Delori FC, Pflibsen KP. Spectral reflectance of the human ocular fundus. *Appl Optics*. 1989;28:1061.
16. Cohen AJ, Laing RA. Multiple scattering analysis of retinal blood oximetry. *Biomed Eng*. 1976;23:391.
17. Van Assendelft OW. *Spectrophotometry of Haemoglobin Derivatives*. Springfield, Ill: Charles C Thomas; 1970:8.
18. Dries DJ, Waxman K. Adequate resuscitation of burn patients may not be measured by urine output and vital signs. *Crit Care Med*. 1991;19:327.
19. Luna GK, Eddy AC, Copass M. The sensitivity of vital signs in identifying major thoracoabdominal hemorrhage.

- Am J Surg.* 1989;157:512.
20. Trouwborst A, Tenbrinck R, van Woerkens E. Blood gas analysis of mixed venous blood during normoxic acute isovolemic hemodilution in pigs. *Anesth Analg.* 1990;70:523.
 21. Rasanen J. Supply-dependent oxygen consumption and mixed venous oxyhemoglobin saturation during isovolemic hemodilution in pigs. *Chest.* 1992;101:1121.
 22. Kurth CD, Steven JM, Benaron D, Chance B. Near infrared monitoring of the cerebral circulation. *J Clin Monit.* 1993; 9:163.
 23. Poets CF, Southall DP. Noninvasive monitoring of oxygenation in infants and children: practical considerations and areas of concern. *Pediatrics.* 1994;93:737.
 24. Kelleher JF, Ruff RH. The penumbra effect: vasomotion-dependent pulse oximeter artifact due to probe malposition. *Anesthesiology.* 1989;71:787.
 25. Southall DP, Samuels M. Inappropriate sensor application in pulse oximetry. *Lancet* 1992;340:481.
 26. Murphy KG, Secunda JA, Rockoff MA. Severe burns from a pulse oximeter. *Anesthesiology.* 1990;73:350.
 27. Sloan TB. Finger injury by an oxygen saturation monitor probe. *Anesthesiology.* 1988;68:936.
 28. Sobel DB. Burning of a neonate due to a pulse oximeter: arterial saturation monitoring. *Pediatrics.* 1992;89:154.
 29. Severinghaus JW, Spellman MJ. Pulse oximeter failure thresholds in hypotension and vasoconstriction. *Anesthesiology.* 1990;73:532.
 30. Jay GD, Hughes L, Renzi FP. Pulse oximetry is accurate in acute anemia from hemorrhage. *Ann Emerg Med.* 1994; 24:32.
 31. De Schaepdrijver L, Simoons P, Pollet L, et al. Morphologic and clinical study of the retinal circulation in the miniature pig: fluorescein angiography of the retina. *Exp Eye Res.* 1992;54:975.
 32. Carneiro JJ, Donald DE. Blood reservoir function of dog spleen, liver, and intestine. *Am J Physiol* 1977;232:H67.
 33. Hartwig H, Hartwig HG. Structural characteristics of the mammalian spleen indicating storage and release of red blood cells: aspects of evolutionary and environmental demands. *Experientia.* 1985;41:159.
 34. Standards for light-emitting products. In: *Code of Federal Regulations.* Title 21, Food, and Drugs, Part 1040.10, Laser Products. Washington, DC: US Government Printing Office 1994.

The 1998 Tanner-Vandeput-Boswick Burn Prize

The 1998 Tanner-Vandeput-Boswick Burn Prize will be awarded during the 10th Quadrennial Congress of the International Society for Burn Injuries to be held November 1-6, 1998 in Jerusalem, Israel. The Prize consists of a gold pin and a cash payment anticipated to be in excess of \$100,000.

The Prize will go to a person (or persons) who in the opinion of the Prize Committee has made an outstanding contribution to any aspect of the burn field. This could be a specific achievement or might represent a body of work over a period of years. The recipient does not have to be a physician or a member of the ISBI.

Nominations for the 1998 Prize may be made by colleagues of those who have made such major contributions, or a candidate may make application on his or her own behalf. Anyone interested in making a nomination should request an application form from the International Burn Foundation at the address below.

Information required to apply for the 1998 prize includes 1) a completed application, 2) a letter of nomination, 3) a description of the person's work, 4) a current CV, and 5) letters of support from colleagues. The deadline for submission of applications is January 30, 1998.

For application forms or further information, contact Dr. John Boswick, Chairman, Board of Directors, International Burn Foundation, P.O. Box 24386, Denver, CO 80224. Phone: (303) 839-1694; FAX: (303) 839-1695.

OXYGEN SATURATION MEASUREMENTS OF BLOOD IN RETINAL VESSELS DURING BLOOD LOSS

Matthew H. Smith,[†] Kurt R. Denninghoff,[‡] Lloyd W. Hillman,[†] and Russell A. Chipman[†]

[†]The University of Alabama in Huntsville, Department of Physics, Huntsville, Alabama 35899;

[‡]The University of Alabama at Birmingham, Department of Emergency Medicine, Birmingham, Alabama 35226

(Paper JBO-160 received Jun. 18, 1997; revised manuscript received Jan. 5, 1998; accepted for publication Jan. 28, 1998.)

ABSTRACT

We describe a noninvasive technique and instrumentation for measuring the oxygen saturation of blood in retinal arteries and veins. The measurements are made by shining low-power lasers into the eye, and scanning the beams across a retinal blood vessel. The light reflected and scattered back out of the eye is collected and measured. The oxygen saturation of blood within the vessel is determined by analyzing the vessel absorption profiles at two wavelengths. A complete saturation measurement can be made in less than 1 s, allowing real-time measurement during physiologic changes. The sensitivity of this measurement technique to changes in retinal saturation has been demonstrated through a series of pilot studies in anesthetized swine. We present data indicating that retinal venous oxygen saturation decreases during ongoing blood loss, demonstrating a potential application of an eye oximeter to noninvasively monitor blood loss. © 1998 Society of Photo-Optical Instrumentation Engineers. [S1083-3668(98)01403-8]

Keywords: oximetry; retina; eye; blood loss; noninvasive monitoring.

1 INTRODUCTION

Early detection of internal bleeding during trauma resuscitation could significantly improve the outcome of a patient's condition.¹ Unfortunately, traditional vital signs such as pulse rate and blood pressure are insensitive indicators of ongoing blood loss.^{2,3} As a result, trauma victims presented to the emergency department may die when physicians are unable to identify internal bleeding, or may require costly and invasive surgery to determine if bleeding is present.

There presently are technologies that can monitor blood loss in the hospital setting. For example, fiber optic catheters can be threaded through the heart and into the pulmonary artery to measure the amount of oxygen in the mixed venous blood (recall that the pulmonary artery carries deoxygenated venous blood from the heart back to the lungs). Arterial blood oxygenation, measured through blood gas analysis or pulse oximetry, gives a supply-side measure of how well the lungs are oxygenating the blood. However, mixed venous blood oxygenation represents a demand-side measure of how much of the available oxygen is being used by the body. As a patient loses blood, and thus loses oxygen carrying capacity, the mixed venous oxygen saturation is known to decrease. From these mixed venous measurements, physicians can determine if a patient is bleeding.¹ Unfortunately, it is logistically difficult to

insert these catheters in an ambulance or during the early period of emergency care. Therefore, a need exists for a technology that could make quick and noninvasive (i.e., without entering the body or puncturing the skin) measurements of blood loss.²⁻⁶

Previous noninvasive techniques for monitoring blood loss have been attempted, but each approach had associated weaknesses. Near-infrared spectroscopy is potentially erroneous due to differences in skull and scalp thickness that alter the optical path length.⁷ Transcutaneous oxygen saturation measurements are made at peripheral vascular beds and have not been widely accepted despite data suggesting sensitivity to early blood loss.⁸ Conjunctival pO_2 measurements have demonstrated sensitivity to blood loss in animal exsanguination studies similar to this study.⁹ The conjunctival oximeter is somewhat invasive, however, as it requires a probe to be placed directly on the conjunctiva of the patient's eye.¹⁰ While a significant need exists for an accurate blood loss monitor, the lack of acceptance of each of these technologies emphasizes that such a monitor must be truly noninvasive, must monitor a central perfusion bed, and must be easy to use.¹¹

The arteries and veins of the retina can be directly imaged through the pupil of the eye, and they are not obscured by thick layers of highly scattering tissues. Additionally, studies have shown that the metabolism and perfusion of the retina and of the cerebrum are similar across a range of normal and

Address all correspondence to Matthew H. Smith. E-mail: SmithM1@email.uah.edu

adverse conditions.¹²⁻¹⁴ The optical accessibility of the retina, coupled with the preservation of retinal circulation during early stages of shock, has led to the hypothesis that retinal venous oxygen saturation may be a valuable parameter for monitoring blood loss.^{15,16}

To investigate this hypothesis, we are developing an instrument called the eye oximeter (EOX).^{17,18} The EOX shines low-power lasers into a subject's eye. The laser beams are scanned across the veins and arteries lying on the retina, and the light that scatters back out of the eye is collected and analyzed. These scans are made at multiple wavelengths, allowing spectroscopic determination of the oxygen saturation of the blood contained in the vessels. Experiments in swine have demonstrated the ability of the EOX to measure the oxygen content of blood in retinal arteries and veins. This article details the instrumentation and signal processing used to make these measurements, and reports the results of animal studies intended to calibrate the EOX¹⁹ and determine the effect of blood loss on retinal venous oxygen saturation.¹¹

2 THE EYE OXIMETER INSTRUMENTATION

Previous retinal vessel oximeters²⁰⁻²² developed by other investigators have been based on modified fundus cameras. These instruments either exposed photographic film at multiple wavelengths or scanned slits of filtered light across retinal vessels. While each of these techniques demonstrated sensitivity to changes of oxygen saturation in human subjects, to the best of our knowledge, the eye oximeter is the first such instrument to be used in an animal model of blood loss. The EOX is a portable device (30×30×12 cm) tethered to an electronics package and laptop computer. The EOX is mounted on a slit lamp base that allows it either to be translated across the cornea and pivoted about the pupil of an immobilized eye or to be used with a fixation target on a cooperative patient.

The EOX instrumentation measures the transmittance of retinal blood vessels at multiple wavelengths. These measurements are then used to calculate the oxygen saturation of blood within the retinal arteries and veins. To achieve this goal, we established a number of design criteria for a prototype instrument. The ultimate requirement, of course, is that the measurement must cause no harm to the patient. Furthermore, the optical system of the EOX should provide a view of the subject's retina to the operator, shine lasers into the eye and scan them across the veins and arteries of the retina, and collect and measure the laser light reflected and scattered back out of the eye. Additionally, data reduction algorithms must analyze the collected scans to determine the percent transmittance of blood within the scanned vessels, and calculate the oxygen saturation of the blood from these measured transmittances. Finally, the eye of

the subject should not need to be chemically dilated, the scans should be fast enough to minimize problems associated with eye movements, and the instrument should accommodate for a range of patient refractive errors. An operational prototype was constructed in accordance with these goals. The device was tested and shown to measure changes in retinal oxygen saturation. The implementation of each subsystem is considered below.

Figure 1 contains a schematic of the eye oximeter breadboard. In Figure 1, all planes marked *r* are conjugate with the subject's retina, and all planes marked *p* are conjugate with the pupil of the subject's eye. A small, 6 V incandescent lamp (IL) and a series of two lenses illuminate a ~2 mm diam circular area of the subject's retina. An image of the lamp filament (1 mm×4 mm) is formed at the center of the subject's pupil, while an image of the uniformly illuminated first lens surface is formed at the subject's retina. The pupil image is formed 25 mm beyond the cube beamsplitter (BS).

A fraction (~50%) of the light scattered back out of the eye is reflected by the cube BS toward an eyepiece (EP). A white-light retinal image is formed for the operator. By placing a vertical polarizer after the lamp and a horizontal polarizer before the eyepiece, reflections from the cornea are greatly reduced, providing a high-contrast retinal image. Translating the eyepiece provides focus through a wide range of patient and operator refractive errors.

Intertwined with the retinal illumination/imaging subsystem is the laser delivery/collection subsystem. Any number of lasers can be coaligned and directed into the EOX prototype. For all of the animal data presented in this report, two astigmatically corrected diode lasers were used due to their portability and ruggedness. The two wavelengths used were 670 and 803 nm. The 670 nm laser is chosen as a wavelength at which the extinction coefficient of reduced hemoglobin is much greater than the extinction coefficient of oxygenated hemoglobin.²³ At 803 nm, the extinction coefficients of reduced hemoglobin and oxygenated hemoglobin are nearly the same. A galvanometer scanning mirror (SM) that is conjugate to the patient's pupil is used to scan the laser beams. The beams pivot about the center of pupil of the eye (25 mm beyond the cube BS). The beams are focused to a point at the subject's retina, and scanned in a line approximately 400 μ m in length. The cube BS directs a fraction of the laser light scattered back out of the eye to a silicon photodiode (PD) for detection. A cross-polarizer scheme is again used to minimize corneal reflections. A limitation of the current instrument is that no means of adjusting laser collimation to accommodate for patient refractive errors exists. However, the beams entering the eye are only 1.25 mm in diameter, providing a very large depth of field. We have had little difficulty acquiring high spatial resolution scans in each of the swine tested

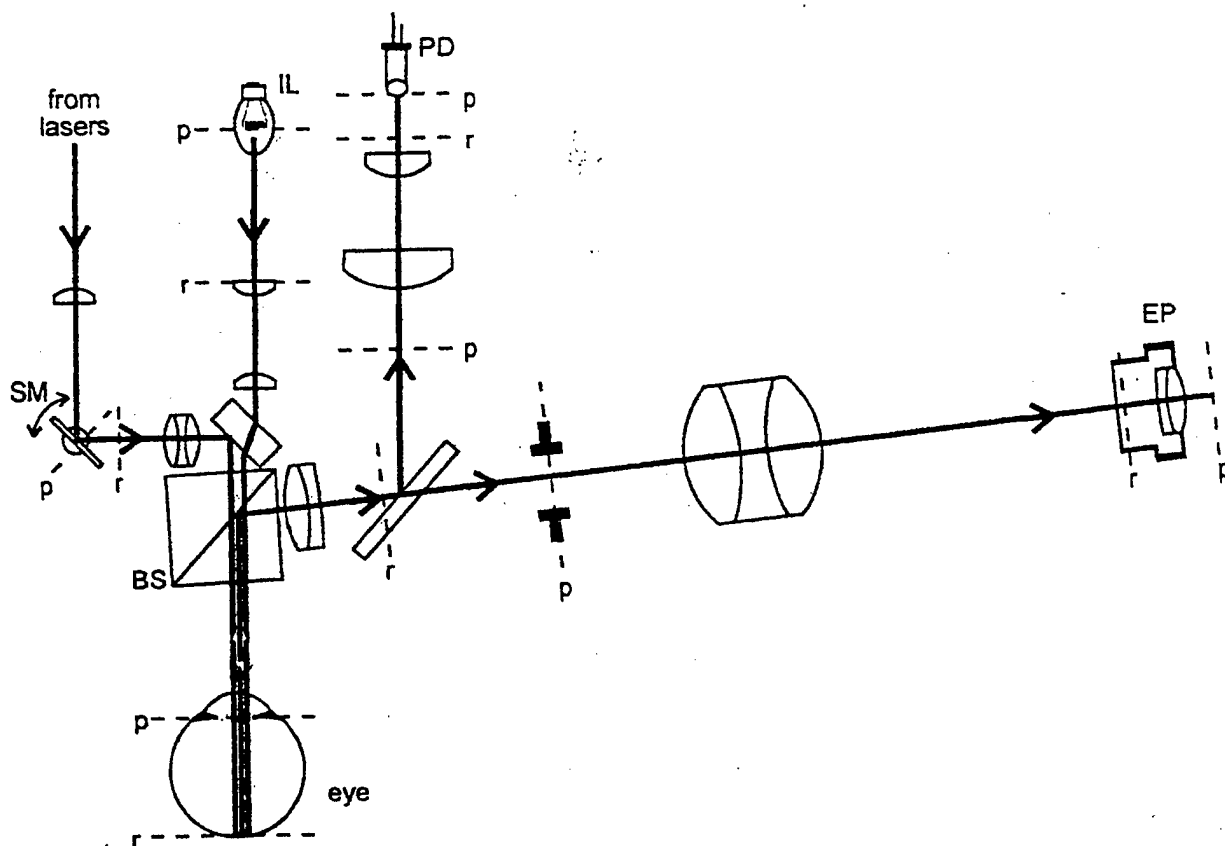


Fig. 1 Schematic of the eye oximeter prototype. Planes marked *p* are conjugate with the patient's pupil, and planes marked *r* are conjugate with the patient's retina.

with this device. Future versions of the EOX will provide focusing ability to the lasers, allowing high spatial resolution scans across a wide range of subject refractive errors.

The measurement sequence involves illuminating a spot on the retina with each of the lasers in turn, and measuring the returned flux from each laser. The signals from PD are digitized with a 14-bit analog-to-digital converter and uploaded to a laptop computer. The scanning mirror is then moved to the next scan location and each of the lasers are again measured in sequence. The procedure is repeated 256 times. The resulting linear scan on the retina contains each of the laser wavelengths. This procedure requires ~ 0.1 s. Generally, eight such scans are made in sequence, resulting in eight individual scans for each of the lasers acquired in ~ 0.8 s. These scans are stored in the computer for post-processing.

To perform a measurement, an operator observes the subject's retina through the eyepiece and chooses a retinal artery or vein. Since the operator is directly observing a white-light retinal image, arteries and veins are easily distinguished by their color and size, and by comparison of the EOX image with the image provided by direct ophthalmoscopy. Once the intended vessel is targeted by cross hairs in the eyepiece, the operator initiates the scanning sequence. The operator is able to faintly see the eight consecutive laser scans across the vessel

(of the 670 nm laser), and can immediately compare this with the vessel profiles displayed graphically on the computer. If the vessel profiles are visible in the scans, the data are saved for later analysis. If the vessel is missed (due to misalignment, eye motion, severe corneal glints, etc.), then the measurement is immediately repeated by the operator.

Since the eye oximeter shines lasers directly into a subject's eye, it is of utmost importance that the laser power levels are at or below safe levels. All laser safety considerations for the eye oximeter are derived from 21 CFR 1040.10, in the Code of Federal Regulations.²⁴ All laser products with viewports that allow direct retinal exposure to laser radiation must limit the level of laser radiation to less than the emission limits of class I. Class I levels of laser radiation are not considered to be hazardous. In all cases, the maximum permissible laser exposure is calculated assuming a failure mode of the EOX not scanning (i.e., a single retinal location illuminated continuously throughout an experiment). The lasers in the EOX were set to $\sim 130 \mu\text{W}$. This is approximately one-tenth of the class I limit, given the modulation frequency, duty cycle, scan time, and experiment length used by the EOX.

Additionally, the white-light exposure level is set to a retinal irradiance less than 1.4 mW cm^{-2} . This exposure level is not uncomfortable to a subject in a

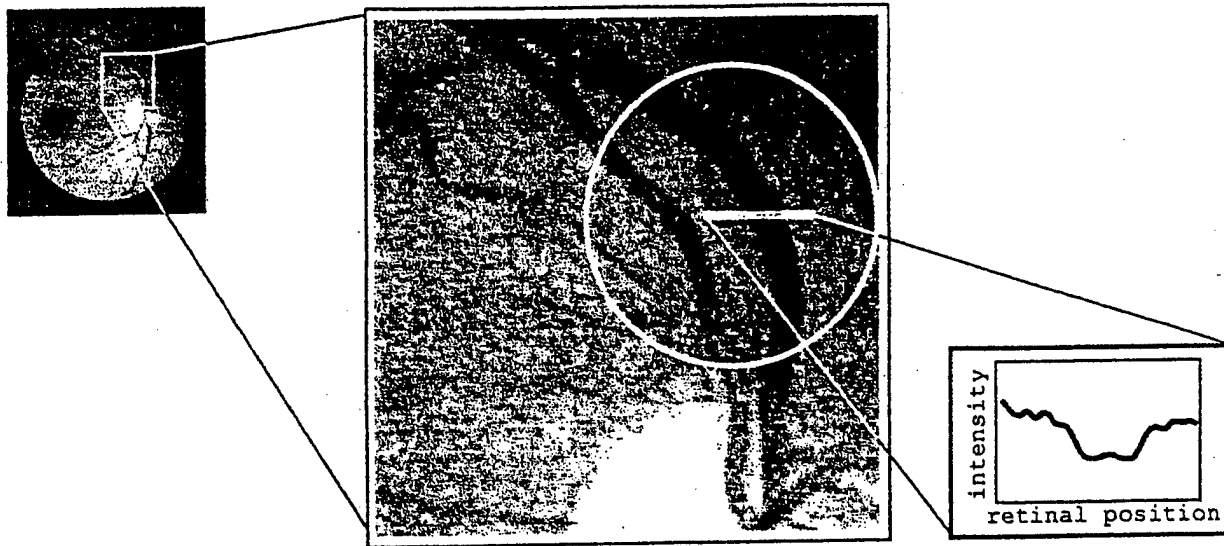


Fig. 2 Illustration of the signals collected by the eye oximeter. The white circle represents the field of view observable by the operator. The white line represents the length of a retinal scan (about 400 μm). The graph is the one-dimensional vessel absorption profile that is analyzed to determine the percent transmittance of the blood within the vessel.

darkened room. The maximum exposure time for this irradiance significantly exceeds the experiment time (about 1 min) that would be typical for human patients.²⁵

3 SIGNAL ANALYSIS AND DATA REDUCTION

Figure 2 illustrates the type of one-dimensional intensity profile that is measured when scanning a focused laser across a retinal blood vessel. The eye oximeter is generally used to measure the larger veins ($\sim 200 \mu\text{m}$ diam) and arteries ($\sim 150 \mu\text{m}$ diam) near the optic nerve head. The white circle in Figure 2 represents the size of the retinal image that the EOX operator observes. The white line is the approximate relative length of the laser scans. As seen in the graph in Figure 2, the collected intensity decreases as the scan crosses a vessel, and increases as the scan emerges from the opposite side of the vessel. Also note that there is generally a small increase in intensity at the center of the vessel. This increase is believed to be caused by the irregular specular reflections often observed along the apex of retinal vessels.²⁶

We believe that the vessel absorption profile in Figure 2 results from a complex combination of numerous light paths within the eye. There is light that is absorbed by the vessel, reflected from the underlying retinal layers, and absorbed again by the vessel in double pass. There is likely also light absorbed by the vessel, laterally diffused in the retinal layers, and scattered back out of the eye in single pass. Specular reflections from the inner limiting membrane, scattered light from red blood cells, and the absorption and scattering properties of vessel walls also influence the signal. As a final difficulty, the coloration of the retinal layers can vary significantly across the length of our retinal scans.

Efforts to incorporate each of the suspected light paths into our analysis are underway. However, in the analysis that follows we assume that the observed optical density of a vessel obeys Lambert-Beer's law. That is, the optical density is linearly related to both the thickness and the concentration of the medium. The optical density D of a vessel is, therefore, assumed to be described by

$$D = s\epsilon_{\text{HbO}_2}cl + (1-s)\epsilon_{\text{Hb}}cl, \quad (1)$$

where $D = -\log(T)$, T is the measured transmittance of the vessel, s is the oxygen saturation of the blood, c is the total hemoglobin concentration of the blood, l is optical path length, and ϵ_{Hb} and ϵ_{HbO_2} are the millimolar extinction coefficients of reduced hemoglobin and oxy-hemoglobin, respectively.²⁶ By measuring D at two wavelengths, Eq. (1) is easily solved for oxygen saturation s :

$$s = \frac{D^{\lambda_2}\epsilon_{\text{Hb}}^{\lambda_1} - D^{\lambda_1}\epsilon_{\text{Hb}}^{\lambda_2}}{D^{\lambda_1}(\epsilon_{\text{HbO}_2}^{\lambda_2} - \epsilon_{\text{Hb}}^{\lambda_2}) - D^{\lambda_2}(\epsilon_{\text{HbO}_2}^{\lambda_1} - \epsilon_{\text{Hb}}^{\lambda_1})}. \quad (2)$$

Note that Eqs. (1) and (2) assume Beer's law is valid in whole blood, which is not the case due to scattering caused by red blood cells. Previous studies^{21,22} have applied multiple scattering theory²⁷ to retinal vessel oximetry; however, it is not clear that this theory was well suited to the specific geometry of retinal vessels. While the Beer's law assumption in this study has produced encouraging results at 670/803 nm, we are continuing our work developing improved models that will improve the accuracy and precision of retinal oximetry.

Figure 3 illustrates the technique used to determine the percent transmittance of a vessel. This method performs curve fits to compensate for reflections from the vessel center, and for variation in retinal pigmentation. A line is calculated that connects the edges of the vessel profile (where the vessel slope approaches zero). This line estimates what the collected intensity of the retinal background would have been in the absence of the vessel. A cubic function is then linearly fitted to the vessel data. Only the data points within small regions centered on the slope extrema are used in the fit calculation. This cubic function estimates the depth of the absorption profile in the absence of the central glint. Dividing the vessel curve by the background line, and finding the minimum of this ratio, gives an estimate of the percent transmittance of blood within the vessel. This percent transmittance is the physical measurement made by the eye oximeter.

For a single oxygen saturation calculation, eight scans of each wavelength are acquired and analyzed as described above. The measured transmittance values are averaged to obtain a single transmittance value T for each wavelength. The transmittance values are converted into optical densities via the equation $D = -\log(T)$. Equation (2) is then used to calculate the oxygen saturation. Finally, the standard deviations of the transmittances are propagated through Eq. (2) to determine the uncertainty in the saturation calculation.

4 ARTERIAL CALIBRATION DATA

To establish the oxygen sensitivity of the eye oximeter, a series of arterial calibration experiments were performed in anesthetized swine.¹⁹ Swine were chosen for these studies due to similarity between swine and human retinal vasculature,²³ and because they provided a good cardiovascular model for blood loss studies. All animal protocols described in this report were approved by the Institutional Animal Care and Use Committee (IACUC) of The University of Alabama at Birmingham. All Public Health Services (PHS) guidelines regarding the care and use of laboratory animals were followed.

Seven young, female swine (18–32 kg) were used in this experiment. The 18 kg animal was excluded from this protocol because its retinal arteries were too small for analysis (see Sec. 6). The swine were placed in the supine position, intubated endotracheally, and placed on a ventilator. The swine were put on 2%–4% isoflurane anesthesia during surgical procedures. A femoral cut down was performed, and the femoral artery and vein were accessed. A maintenance solution of 5% dextrose in half normal saline with 10 mEq/L of KCl was infused intravenously at 80–110 mL/h. A fiber optic mixed venous oxygen saturation catheter was placed in the pulmonary artery (which contains venous blood) via the femoral vein. (This catheter was used for the

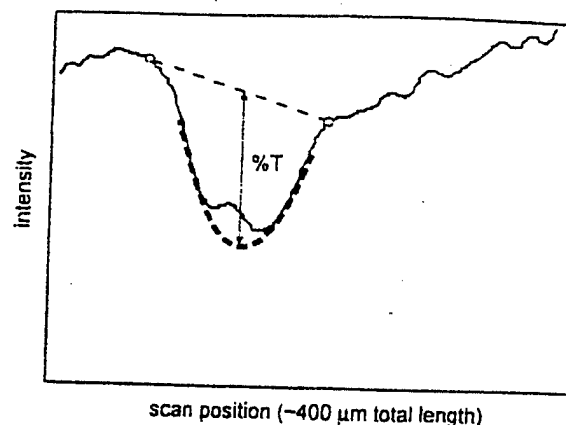


Fig. 3 Vessel profile analysis technique used to analyze the raw data. This method performs curve fits to compensate for vessel-center reflections and variations in fundus pigmentation. The transmittance of the blood within the vessel is calculated from the ratio of these curves.

blood loss study described in the next section.) When needed, arterial blood samples were drawn from the femoral artery. Blood samples were measured using an IL 482 CO-Oximeter system. Once the surgical preparation was completed, isoflurane was maintained at 1.25%–2% as needed to maintain anesthesia. The respiratory rate was adjusted to maintain arterial CO_2 tension between 36 and 44 mm Hg, and blood Ph between 7.35 and 7.45.

During the surgical preparation, the eyes of the swine were dilated using two drops of 1% cyclopentolate. The eyelids were then sutured open, and one or two sutures were placed in the conjunctiva to prevent the eye from drifting during the experiment. In order to reduce corneal stresses and irregularities that can cause significant optical aberrations, these sutures were placed as far from the cornea as possible, and as few sutures as possible were used. Once sutured open, the eye was bathed with 0.9% saline at least every 45 s to prevent corneal dehydration. The EOX was positioned, and the white-light image of the retina provided to the operator allowed selection of arteries or veins by direct observation of color (veins are darker) and size (veins are larger). The instrument was aimed at a large artery near the optic disk.

To perform this calibration study, the arterial saturation of the swine was varied via graded hypoxia. The oxygen was decreased incrementally from 100% to 7%. At each increment, the EOX scanned a large retinal artery, and samples drawn from the femoral artery were measured on the CO-Oximeter system. Retinal arterial oxygen saturation was calculated from the EOX scans in the method described in the previous section.

Figure 4 displays the correlation between femoral artery saturation and retinal artery saturation in a single swine. Error bars on this graph represent the standard error of each calculated saturation (derived from the eight EOX scans). Strong correlation

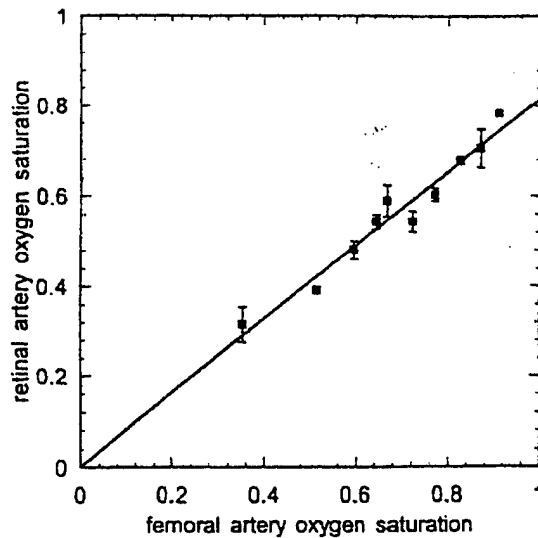


Fig. 4 Arterial calibration line from a single swine. The correlation between retinal arterial oxygen saturation (measured with the EOx) and femoral arterial oxygen saturation was very strong ($r^2 = 0.956$, $p < 0.001$). Error bars are standard error of the mean.

($r^2 = 0.956$, $p < 0.001$) was found between the two measurements. This calibration line has a slope of 0.81, and a y intercept of 0.0012.

This experiment was performed on all six swine. Table 1 summarizes the calibration lines calculated in each of these experiments. As demonstrated by the consistently high correlation values, the EOx measurements are able to follow saturation trends within a single animal. There is, however, variation in the slopes and y intercepts of these lines. Figure 5 contains plots of all six calibration lines. The average of the slopes of these six lines was $m = 0.80 \pm 0.11$, and the average y intercept was $b = 0.06 \pm 0.17$. From Figure 5 it is seen that four of the lines fell quite close together, while two had large differences in their y intercept. One of our current research efforts includes determining the cause of this variation and working to reduce it.

Table 1 Eye oximeter arterial calibration line data from six swine. The data from subject 4 are shown in Figure 4. The six calibration lines are plotted individually in Figure 5.

Subject	Slope	y intercept	r^2	Number of data points
1	0.734	0.160	0.957	6
2	0.812	0.100	0.897	7
3	0.831	0.770	0.998	6
4	0.814	0.001	0.956	10
5	0.976	-0.237	0.800	7
6	0.696	0.200	0.979	5

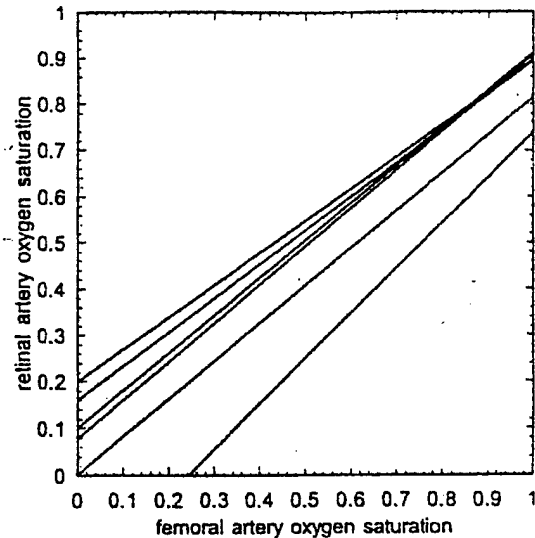


Fig. 5 Arterial calibration lines from six different swine. These lines illustrate the interanimal variability of the EOx calibration.

5 BLOOD-LOSS DATA

A series of exsanguination studies were performed in anesthetized swine to determine if the eye oximeter can detect ongoing blood loss.¹⁴ Mixed venous oxygen saturation (measured in the pulmonary artery) is known to decrease predictably during blood loss.¹ As blood volume decreases, the body's oxygen carrying capacity decreases. As a result, a higher percent of O_2 is extracted at the end-body level (i.e., at the pulmonary artery). Unfortunately, making mixed venous saturation measurements requires catheterizing the heart, thus precluding this measurement during the early stages of trauma. It has been hypothesized that retinal venous saturation ($SrvO_2$) may also decrease predictably during blood loss.¹⁶ A primary motivation for developing the eye oximeter has been to investigate this hypothesis.

Seven young, female anesthetized swine were used in this study. The surgical preparation described in the previous section was performed. The EOx was positioned and aimed at a large retinal vein near the optic disk.

The swine were placed on 21% oxygen and bled at a controlled rate of approximately 0.5% of total blood volume every minute. This was continued for 40 min, resulting in a 20% blood loss. Throughout the experiment, mixed venous oxygen saturation was measured via a fiber optic Swan-Ganz catheter placed in the pulmonary artery. The eye oximeter scanned the retinal vein every 2 min throughout the experiment. Retinal venous oxygen saturation ($SrvO_2$) was calculated as described in Sec. 3. The $SrvO_2$ calculations in this section have not been adjusted based on the arterial calibration study in Sec. 4, and are therefore not expected to be well calibrated.

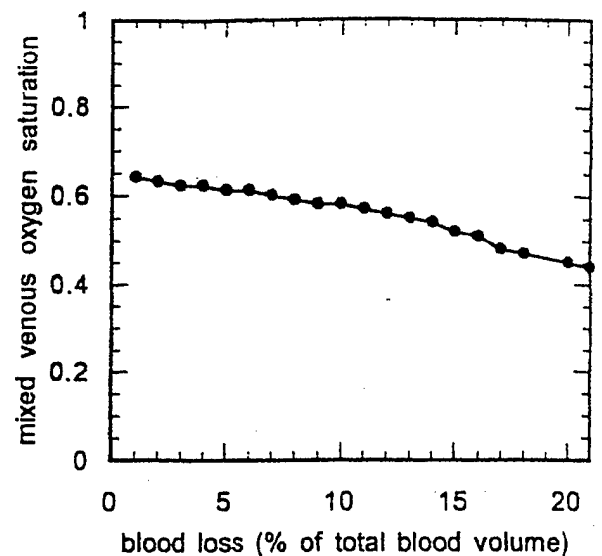
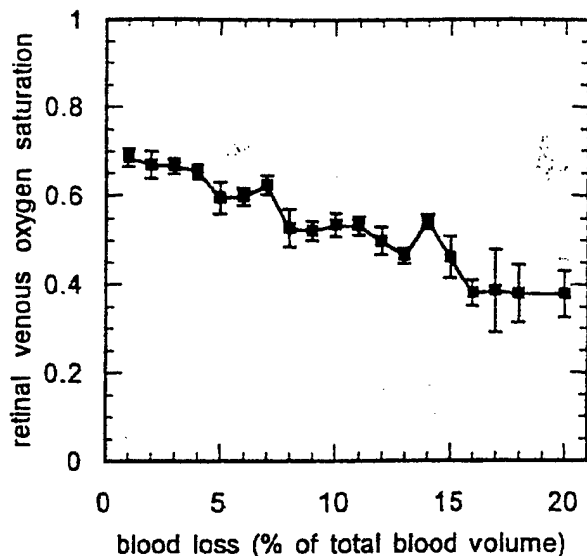


Fig. 6 Retinal venous oxygen saturation and mixed venous oxygen saturation both decrease with blood loss. These data are from a single swine, bled at a rate of 0.5% of total blood volume per minute. Error bars on the retinal saturations indicate uncertainty in the calculated oxygen saturation made with the eye oximeter.

The data in Figure 6 were collected from a single swine. As expected, mixed venous saturation measured with the pulmonary catheter decreases predictably with blood loss ($r^2=0.96$, $p<0.001$). Retinal venous saturation also correlates strongly with blood loss ($r^2=0.93$, $p<0.001$). The error bars on the $SrVO_2$ values indicate the standard error of the calculated saturation mean due to measurement variability in the eight EOX scans comprising each data point.

Figure 7 contains the results of averaging all seven swine in this study. In Figure 7, the error bars are the standard deviation of the population mean (note that to avoid overlap, only one half of each error bar is plotted). Since the calibration of the pul-

monary catheter was verified prior to each use, the variability in the mixed venous saturation is expected to be a result of physiologic variability between animals. In addition to physiologic variability, the retinal venous saturation is also likely affected by the interanimal calibration variability observed in the arterial calibration experiment.

The average mixed venous saturation values correlate strongly ($r^2=0.96$, $p<0.001$) with blood loss. In addition, the average retinal venous saturation values, as measured with the EOX, are found to correlate strongly ($r^2=0.86$, $p<0.001$) with blood loss.

6 DISCUSSION AND CONCLUSIONS

We have established the feasibility of making fast, precise measurements of the oxygen saturation of blood within the large veins and arteries of the retina. Our arterial calibration lines were each found to be strongly linear; however, variations in the slopes and intercepts of these lines were observed. It is unclear whether this variation is an instrumental effect, a physiologic effect, or a combination of the two. Improved models of the light-vessel interaction, the incorporation of additional wavelengths, and an *in vitro* calibration study may lead to a more consistent intersubject calibration.

Our pilot animal data suggest that retinal venous saturation may be a sensitive indicator of blood loss. Retinal venous oxygen saturation measured with the eye oximeter decreased predictably as blood volume decreased. This resulted from proportionally more oxygen being extracted at the capillary beds as the bleeding ensued. However, this study was performed in anesthetized swine, and the response of retinal venous saturation to blood loss may be different in human trauma victims.

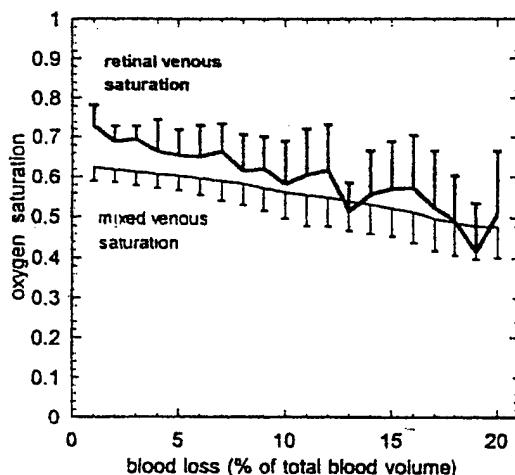


Fig. 7 The average results of seven swine are shown. Both mixed venous oxygen saturation and retinal venous oxygen saturation are found to correlate strongly with blood loss. The error bars represent standard deviations between subjects. (Note that only one half of each error bar is drawn in order to prevent overlap.)

The red and near-infrared wavelengths used in the EOX restrict its use to retinal vessels larger than about 50 μm in diameter. Vessels smaller than 50 μm typically absorb less than 3% of the incident light at our wavelengths. This low absorbance makes vessel identification difficult, and results in large variations in the calculated saturation. The use of more highly absorbed wavelengths would allow the EOX to be tuned for these smaller vessels. In one of the swine used in this study, no retinal artery greater than 50 μm was present and the arterial calibration protocol could not be performed. This limitation may also prevent the use of the EOX (in its current configuration) on small children.

In this study, we sutured the anesthetized animals' eyes open and irrigated the cornea because the animals could not cooperate with an ophthalmic examination. Cooperative human patients will not require these measures. However, a method for immobilizing the eye or a complex tracking system would be required for uncooperative or unconscious patients, and use of the EOX on combative patients presents significant difficulties. The eyes of the swine in this study were dilated to facilitate alignment of the EOX. The eyes of human patients can generally be scanned by the EOX without dilation, unless their pupil diameter is less than about 2 mm. Finally, because of the need for a clear retinal image, the EOX may not be useful in patients with cataracts or corneal opacities. Despite these limitations, the EOX technology is noninvasive, and monitoring retinal versus saturation as an indicator of occult bleeding appears promising and warrants further investigation.

Acknowledgments

This work was supported by grants from The University of Alabama in Huntsville and The University of Alabama at Birmingham, and by a contract from Vectranetics, Inc. (Madison, AL 35899).

REFERENCES

1. T. M. Scalea, M. Holman, M. Furtes, B. J. Baron, T. F. Phillips, A. S. Goldstein, S. I. A. Sclafani, and G. W. Shaftan, "Central venous blood oxygen saturation: An early, accurate measurement of volume during hemorrhage," *J. Trauma* 28(6), 725-732 (1988).
2. C. J. Wo, W. C. Shoemaker, P. L. Appel, M. H. Bishop, H. B. Kram, and E. Hardin, "Unreliability of blood pressure and heart rate to evaluate cardiac output in emergency resuscitation and critical illness," *Crit. Care Med.* 21(2), 218-223 (1993).
3. G. K. Luna, A. C. Eddy, and M. Copass, "The sensitivity of vital signs in identifying major thoracoabdominal hemorrhage," *Am. J. Surg.* 157, 512-515 (1989).
4. T. M. Scalea, R. W. Hartnett, A. O. Duncan, N. A. Atweh, T. F. Phillips, S. J. Sclafani, M. Fuortes, and G. W. Shaftan, "Central venous oxygen saturation: A useful clinical tool in trauma patients," *J. Trauma* 30(12), 1539-1543 (1990).
5. T. M. Scalea, H. M. Simon, A. O. Duncan, N. A. Atweh, S. J. Sclafani, T. F. Phillips, and G. W. Shaftan, "Geriatric blunt multiple trauma: Improved survival with early invasive monitoring," *J. Trauma* 30, 129-136 (1990).
6. B. Abou-Khalil, T. M. Scalea, S. Z. Trooskin, S. M. Henry, and R. Hitchcock, "Hemodynamic responses to shock in young trauma patients: Need for invasive monitoring," *Crit. Care Med.* 22, 633-639 (1994).
7. C. D. Kurth, J. M. Steven, D. Benaron, and B. Chance, "Near infrared monitoring of the cerebral circulation," *J. Clin. Monit.* 9, 163-170 (1993).
8. S. C. Dronen, P. A. Maningas, and R. Fouch, "Transcutaneous oxygen tension measurements during graded hemorrhage and reinfusion," *Ann. Emerg. Med.* 24, 534-539 (1984).
9. M. Klein, D. Hess, D. Eitel, D. Bauernshub, and N. Sabulsk, "Conjunctival oxygen tension monitoring during controlled phlebotomy," *Am. J. Emerg. Med.* 6, 11-13 (1988).
10. E. Abraham, "Conjunctival oxygen tension monitoring," *Int. Anesthesiol. Clin.* 25(3), 97-112 (1987).
11. K. R. Denninghoff, M. H. Smith, R. A. Chipman, L. W. Hillman, P. M. Jester, F. Kuhn, D. Redden, and L. W. Rue, "Retinal venous oxygen saturation correlates with blood volume," *Acad. Emerg. Med.* (to be published).
12. A. Harris, O. Arend, K. Kopecky, K. Caldemeyer, S. Wolf, W. Sponsel, and B. Martin, "Physiological perturbation of ocular and cerebral blood flow as measured by scanning laser ophthalmoscopy and color Doppler imaging," *Surv. Ophthalmol. (Suppl.)* 38, S81-S86 (1994).
13. M. Laughlin, W. M. Harold, and R. N. Whittaker, "Regional cerebral blood flow in conscious miniature swine during high sustained +G, acceleration stress," *Aviat. Space Environ. Med.* 50(11), 1129-1133 (1979).
14. A. Ames, "Energy requirements of CNS cells as related to their function and to their vulnerability to ischemia: A commentary based on studies on retina," *Can. J. Physiol. Pharmacol.* 70, S158-S164 (1992).
15. T. E. Minnich, "Method and apparatus for monitoring the arteriovenous oxygen difference from the ocular fundus via retinal venous oxygen saturation," U.S. Patent No. 5,308,919 (1994).
16. T. E. Minnich, "Method and apparatus for monitoring blood loss via retinal oxygen saturation," U.S. Patent No. 5,119,814 (1992).
17. L. W. Hillman, S. C. McClain, M. H. Smith, and R. A. Chipman, "Eye oximeter for the noninvasive measurement of cardiac output," in *Vision Science and its Applications*, 1994 Technical Digest Series, Vol. 2, pp. 151-154, Optical Society of America, Washington DC (1994).
18. M. H. Smith, K. R. Denninghoff, L. W. Hillman, C. E. Hughes, T. E. Minnich, and R. A. Chipman, "Technique for noninvasive monitoring of blood loss via oxygen saturation measurements in the eye," *Proc. SPIE* 2982, 46-52 (1997).
19. K. R. Denninghoff, M. H. Smith, R. A. Chipman, L. W. Hillman, P. M. Jester, C. E. Hughes, F. Kuhn, and L. W. Rue, "Retinal large vessel oxygen saturation correlates with early blood loss and hypoxia in anesthetized swine," *J. Trauma* 43(1), 29-34 (1997).
20. J. B. Hickam, R. Frayser, and J. C. Ross, "A study of retinal venous blood oxygen saturation in human subjects by photographic means," *Circulation* 27, 375-385 (1963).
21. A. I. Cohen and R. A. Laing, "Multiple scattering analysis of retinal blood oximetry," *IEEE Trans. Biomed. Eng.* 23(5), 391-400 (1976).
22. F. C. Delori, "Noninvasive technique for oximetry of blood in retinal vessels," *Appl. Opt.* 27(6), 1113-1125 (1988).
23. O. W. Van Assendelft, *Spectrophotometry of Haemoglobin Derivatives*, Charles C. Thomas, Springfield, IL (1970).
24. *Code of Federal Regulations*, Title 21, Food and Drugs, Part 1040.10, Performance Standards for Light-Emitting Products, laser products, U.S. Government Printing Office (1994).
25. F. C. Delori, J. S. Parker, and M. A. Mainster, "Light levels in fundus photography and fluorescein angioplasty," *Vision Res.* 20, 1099 (1980).
26. F. C. Delori, E. S. Gragoudas, R. Francisco, and C. Pruett, "Monochromatic ophthalmoscopy and fundus photography," *Arch. Ophthalmol.* 95, 861-868 (1977).
27. V. Twersky, "Absorption and multiple scattering by biological suspensions," *J. Opt. Soc. Am.* 60, 1084-1093 (1970).
28. L. De Schaepe-drijver, P. Simoons, L. Pollet, H. Lauwers, and J. De Lay, "Morphologic and clinical study of the retinal circulation in the miniature pig. B: Fluorescein angiography of the retina," *Exp. Eye Res.* 54, 975-985 (1992).

Retinal Venous Oxygen Saturation Correlates with Blood Volume

KURT R. DENNINGHOFF, MD, MATTHEW H. SMITH, PHD,
LLOYD W. HILLMAN, PHD, DAVID REDDEN, PHD, LORING W. RUE, MD

Abstract. **Objectives:** To evaluate the sensitivity of retinal venous O₂ saturation (SrvO₂) for early blood loss and reinfusion. A secondary objective was to measure the correlation between SrvO₂ and mixed venous O₂ saturation (SvO₂) during blood loss and reinfusion. **Methods:** Seven anesthetized swine were bled at 0.8 mL/kg/min to 16 mL/kg. Shed blood was re-infused at the same rate and the swine were allowed to equilibrate. After equilibration, repeat hemorrhages were performed at 1.6 mL/kg/min and 2.4 mL/kg/min. SrvO₂ was measured using an eye oximeter (EOX) and SvO₂ was measured using a fiber-optic catheter. **Results:** During blood loss, SrvO₂ correlated with blood removed ($r = -0.88, -0.97, -0.96$) and SvO₂ ($r = 0.87, 0.98, 0.92$). During reinfusion, SrvO₂ correlated with blood re-infused ($r = 0.63, 0.76, 0.82$) and SvO₂ ($r = 0.80, 0.93, 0.96$). SrvO₂ decreased $1.22 \pm 0.60\%/mL/kg$ of blood removed. The rate of decrease

in SrvO₂ per minute ($\Delta SrvO_2$) when blood was removed at 2.4 mL/kg/min was significantly greater than $\Delta SrvO_2$ when blood was removed at 0.8 mL/kg/min ($p < 0.007$). The rates of change in blood pressure (BP) and pulse were not significantly different at any rate of blood removal. **Conclusions:** In this model, retinal venous O₂ saturation correlated with blood volume and central venous O₂ saturation. Unlike the rate of change in BP and heart rate, $\Delta SrvO_2$ values were significantly different at different rates of blood removal. Use of an EOX to monitor for blood loss, estimate the rate of hemorrhage, and evaluate the response to therapy during resuscitation warrants further study. **Key words:** shock; blood loss; noninvasive monitoring; retinal vessel; oxygen saturation; swine. ACADEMIC EMERGENCY MEDICINE 1998; 5:577-582

DURING shock resuscitation, the clinician seeks to ensure that the delivery of O₂ to the tissues is sufficient to maintain aerobic metabolic functions. To this end, the clinician improves O₂ delivery by optimizing cardiac performance and/or increasing the O₂-carrying capacity of blood.^{1,2} Several outcome studies have shown central venous O₂ saturation (SvO₂) to be a reliable index of the balance between O₂ delivery and consumption, enabling the assessment of the response to specific

therapeutic maneuvers during shock.³⁻⁷ However, obtaining SvO₂ is time-consuming² and costly,⁸ and has associated complications.^{1,3,9}

The retinal vasculature offers a potential site for noninvasive monitoring of perfusion data.¹⁰⁻¹² Retinal perfusion has been used associated with cerebral perfusion under adverse conditions.¹³⁻¹⁵ Retinal vessel oximetry can detect changes in O₂ saturation as small as $\pm 4\%$.^{10,16-18} In a study of large retinal vessel saturations, the retinal venous O₂ saturation (SrvO₂) was found to be sensitive to hyperoxia, hypoxia, hyperventilation, hypercarbia, and hyperglycemia.¹²

We have developed an experimental, noninvasive eye oximeter (EOX). This innovative medical device quickly and noninvasively measures the O₂ saturation of blood in the retinal arteries and veins. The EOX scans low-power lasers into the eye and across the large vessels near the optic nerve head. A biophysical model is used to analyze the signals obtained and to calculate the O₂ saturation.¹⁹ A detailed description of the device, its function, and ease of use has been published elsewhere.^{19,20}

In a pilot test of the device, swine were bled at a slow rate (0.4 mL/kg/min) to a modest end point (16 mL/kg).²⁰ In the pilot study, there was a strong negative correlation between the amount of blood removed and SrvO₂ ($r = -0.93$). We also described

From the Department of Emergency Medicine (KRD), Department of Hematology/Oncology (DR), and Department of General Surgery (LWR), University of Alabama at Birmingham, Birmingham, AL; and the Department of Physics (MHS, LWH), University of Alabama in Huntsville, Huntsville, AL.

Received: June 4, 1997; revision received: October 29, 1997; accepted: December 14, 1997. Presented at the SAEM annual meeting, Washington, DC, May 1997.

Supported by the University of Alabama at Birmingham Research Foundation, the University of Alabama at Birmingham Department of Emergency Medicine, the University of Alabama in Huntsville, Hacmonetics Corp., and Abbott Labs. Penelope M. Jester, RN, MPH, and Ferenc Kuhn, MD, also provided valuable support.

Address for correspondence and reprints: Kurt Denninghoff, MD, Department of Emergency Medicine, University of Alabama at Birmingham, JTN 266, 619 South 20th Street, Birmingham, AL 35233-7013. Fax: 205-975-4662; e-mail: kurt@qs2b.his.uab.edu

a strong correlation between retinal artery O₂ saturation and femoral artery O₂ saturation during graded hypoxia. This pilot study demonstrated that the measurements made with this device were sensitive to changes in O₂ saturation and to slow rates of blood loss.

In the current study, our primary objective was to evaluate the sensitivity of SrvO₂, measured using the EOX, to more rapid rates of early blood loss and to reinfusion. A secondary objective was to measure the correlation between SrvO₂ and SvO₂ during blood loss and reinfusion.

METHODS

Study Design. A controlled, operator-unblinded, porcine investigation was performed of the sensitivity of SrvO₂ for detection of early blood loss during rapid hemorrhage and reinfusion. A secondary objective was to measure the correlation between SrvO₂ and SvO₂ during these conditions. This study adhered to NIH guidelines for the use of laboratory animals and was approved by the Institutional Animal Care and Use Committee.

Animal Subjects and Instrumentation. Seven young female swine, weighing 23–44 kg, were fasted overnight but were allowed water ad libitum. On the morning of the experiment, the animals were given IM preanesthetic ketamine 600 mg and xylazine 100 mg. The swine were placed in the supine position, intubated endotracheally, and placed on a ventilator (AirShields Ventimeter Ventilator, Hatboro, PA). The swine were placed on 2–4% isoflurane during the surgical procedures (Daytex-254 Airway Gas Monitor, Helsinki, Finland) and the depth of anesthesia was monitored using web space stimulation. An esophageal temperature probe was used to monitor core body temperature. Continuous ECG monitoring was used (101T, IVY Biomedical Systems, Inc., Branford, CT). The eyes were treated with 2 drops of 1% cyclopentolate hydrochloride. A maintenance solution of 5% dextrose in half normal saline with 10 mmol/L of KCl was infused at 80–110 mL/hr.

A celiotomy was performed using an infraumbilical approach, the bladder was exposed, and a Foley catheter was placed in the bladder via cystotomy. The abdominal wall was closed around the bladder catheter. A femoral cutdown was performed, a 7.0-Fr catheter was placed in the femoral artery, and an 8.0-Fr introducer was placed in the femoral vein. The femoral artery catheter was connected to a physiologic pressure monitoring system (Hewlett Packard 78534, Andover, MA), and a 7.5-Fr continuous mixed venous O₂ saturation monitoring catheter (P575-10CM-EH, Abbott Critical Care System, Sandy, UT) was placed in the central

circulation via the introducer in the femoral vein. The distal port of the central venous catheter was connected to a Hewlett Packard 78203 physiologic pressure monitoring system. Placement of the central venous catheter in the pulmonary artery was verified by waveform. The catheter oximeter calibration was verified using mixed venous blood obtained from the distal port. All blood gas analysis was performed using a standard co-oximeter system (IL 482 CO-Oximeter, Instrumentation Laboratory, Lexington, MA). The eyelids were sutured open and sutures were placed in the conjunctiva to hold the eye in place. A catheter, attached to a 60-mL syringe filled with 0.9% saline, was sutured to the periocular skin and used to bathe the eye every 45 seconds to maintain corneal hydration throughout the experimental protocol.

When the surgical prep was completed, the isoflurane was decreased to 1.25% to 2% as needed to maintain anesthesia. The respiratory rate was adjusted to maintain arterial CO₂ tension (PaCO₂) between 36 and 44 torr and the blood pH between 7.35 and 7.45. At least 10 minutes was allowed from the time of a ventilator adjustment to the time of arterial blood gas measurement. The central venous catheter was used to record continuous SvO₂. The EOX was then aimed at a large vein near the optic disk. The EOX was used to obtain an SrvO₂ measurement every minute.

Study Protocol. The animal was exsanguinated at 0.8 mL/kg/min until a total of 16 mL/kg had been removed. The shed blood was anticoagulated using anticoagulant citrate phosphate dextrose (ACD) solution. When the exsanguination was complete, the animal was resuscitated by reinfusing the anticoagulated blood at 0.8 mL/kg/min. The animal was allowed to equilibrate for 20 minutes after reinfusion was completed [in pilot testing of this protocol, 20 minutes was sufficient to allow for stabilization of SrvO₂, SvO₂, blood pressure (BP), and heart rate (HR)]. This process was repeated at 1.6 mL/kg/min and 2.4 mL/kg/min.

After the final exsanguination and reinfusion, the retina was examined for laser damage using ophthalmoscopy. At the conclusion of the experimental protocol, each anesthetized swine was euthanized using supersaturated KCl.

Data Analysis. To summarize the data, means with SDs were calculated for SrvO₂ and SvO₂ during exsanguination and reinfusion. To quantify the relationship between SrvO₂ and SvO₂ during blood loss at 0.8, 1.6, and 2.4 mL/kg/min, Pearson correlation coefficients were calculated at each exsanguination rate. Due to the small sample size ($n = 7$) and pilot nature of the data, nonparametric procedures were used, making no assumptions about

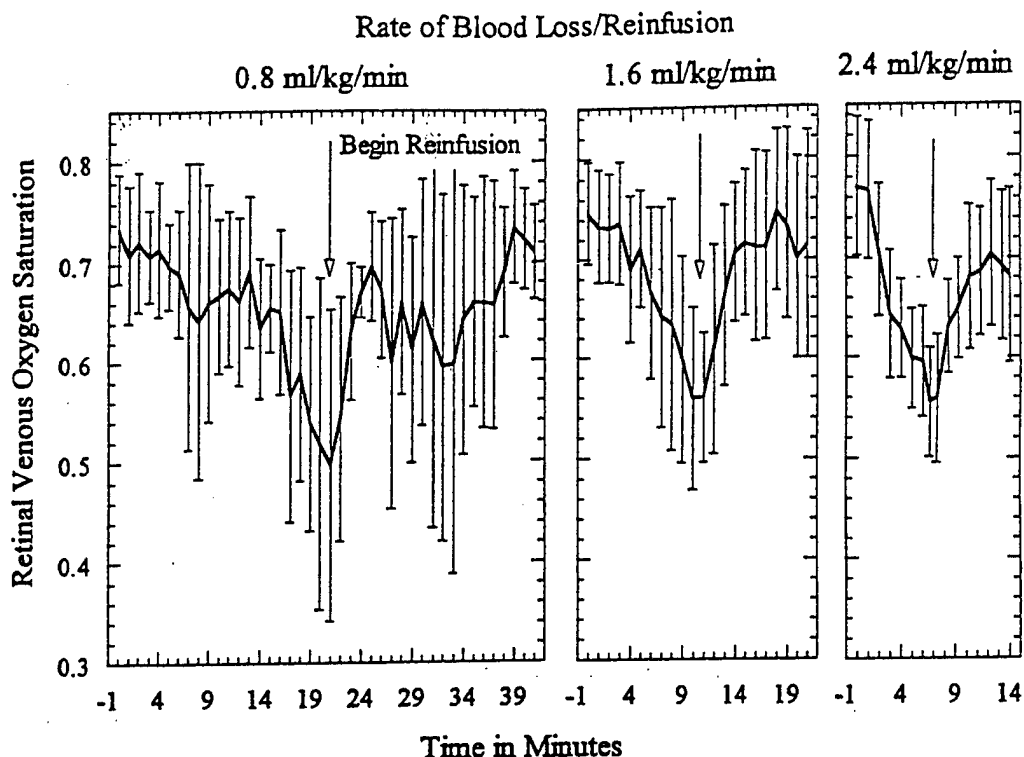


Figure 1. The average retinal venous O_2 saturation values determined for 7 swine at each of 3 exsanguination and reinfusion rates. Error bars are the SD.

the distributional properties of the data. Specifically, Friedman 2-way analysis of variance (ANOVA) by ranks was used to determine whether the different exsanguination rates of 0.8, 1.6, and 2.4 mL/kg/min could be distinguished one from another when observing $SrvO_2$, BP, and HR. If Friedman's test indicated that a difference could be observed based on exsanguination rates, multiple comparisons, controlling for the overall type I error rate, were used to determine which pairs of exsanguination rates could be distinguished.

RESULTS

The $SrvO_2$ correlated with SvO_2 and blood volume during blood loss and reinfusion of autologous blood. Figure 1 shows the $SrvO_2$ (\pm SD) values measured in 7 swine during blood removal and reinfusion at 0.8 mL/kg/min, 1.6 mL/kg/min, and 2.4 mL/kg/min. Figure 2 shows the mean $SrvO_2$ and SvO_2 during exsanguination and reinfusion. $SrvO_2$ correlated with SvO_2 during changes in blood volume. Over all rates of blood removal tested, the rate of decrease in $SrvO_2$ was $1.22 \pm 0.6\%$ saturation for each mL/kg of blood removed ($n = 21$). Table 1 shows the Pearson correlation coefficients when $SrvO_2$ is compared with blood volume and SvO_2 during 3 different rates of blood removal and reinfusion.

Table 2 shows the mean rate of decrease in retinal venous saturation ($\Delta SrvO_2$), heart rate (ΔHR), and mean arterial pressure (ΔMAP) for each rate

of blood loss. Follow-up multiple comparisons after a Friedman's 2-way ANOVA by ranks ($p = 0.007$) showed the rate of decrease in $SrvO_2$ at 2.4 mL/kg/min blood loss is significantly greater than the rate of decrease seen at 0.8 mL/kg/min. There was no significant difference between the rates of decrease in HR or BP at the 3 rates of blood removal tested ($p > 0.10$).

There were no signs of acute laser damage noted on ophthalmic examination at the conclusion of these experiments.

DISCUSSION

The ability to accurately and rapidly identify occult blood loss would be an invaluable adjunct to the management of the multiply injured patient.¹ Conventional vital signs, which are prone to compensatory maintenance during hemorrhage, are particularly unreliable in the early period of blood loss when intervention is the most efficacious.^{2,21,22} The alteration of vital signs seen in response to the cascade of acidosis, vascular collapse, and death occurs late in the process of blood loss and is variable from patient to patient.²

There have been several studies published advocating the use of central venous O_2 saturation measurements as a means of identifying occult blood loss early in the time course to lethal exsanguination.^{1,3,4,23,24} Limitations of central catheter monitoring include the known associated complications of central line placement, as well as the

TABLE 1. Correlation of Retinal Venous Oxygen Saturation with Blood Volume and Mixed Venous Oxygen Saturation during Changes in Blood Volume

Rate of Change in Blood Volume	Retinal Venous O ₂ Saturation vs Blood Volume		Retinal Venous O ₂ Saturation vs Mixed Venous O ₂ Saturation	
	During Removal	During Reinfusion	During Removal	During Reinfusion
0.8 mL/kg/min	$r = -0.88$	$r = 0.63$	$r = 0.87$	$r = 0.80$
1.6 mL/kg/min	$r = -0.96$	$r = 0.76$	$r = 0.98$	$r = 0.93$
2.4 mL/kg/min	$r = -0.97$	$r = 0.82$	$r = 0.92$	$r = 0.96$

skill and time required for proper insertion.^{1,9} As a result, central vascular monitoring cannot be used in the out-of-hospital setting, tends to be used late in the emergency stay of trauma victims, and is rarely used in blunt trauma victims without signs of significant injury. The need for a method to identify ongoing occult blood loss in trauma victims that is noninvasive, fast, accurate, and simple to use is apparent.² Previously, noninvasive blood oxygenation measurements have been attempted.²⁵⁻²⁸ The various weaknesses of these approaches have been summarized elsewhere.^{20,27,29}

This study demonstrates the potential value of a device that uses spectrophotometric technology to evaluate O₂ saturation in the large vessels of the eye. The rate of decrease in retinal venous O₂ saturation seen in these animals was consistent and rate-dependent. In addition, early blood loss was detected at all of the rates tested. This has important implications in out-of-hospital, combat casu-

alty, and emergency care. If a subject is bleeding quite slowly (i.e., <0.4 mL/kg/min), then a less urgent response is required. Conversely, if a subject is bleeding >2.4 mL/kg/min, the subject must receive rapid treatment if he or she is expected to survive.

The change in retinal venous O₂ saturation and central venous O₂ saturation seen during reinfusion emphasizes the monitoring capacity of these tools. Both indicated a rapid response to initial reinfusion and a marked flattening of this response after about 5-6% of total blood volume had been re-infused. The nonlinear response to the reinfusion of autologous blood seen in this model has been described in a study using autologous blood transfusions in swine.³⁰

There is considerable variability in the physiologic response to blood loss seen from animal to animal in this study. These observations are similar to results seen in exsanguination studies using animal models published elsewhere.^{1,29,31-34}

LIMITATIONS AND FUTURE QUESTIONS

This animal model was chosen because of the similarities between the swine eye and the human eye.³⁵ The spleen was left intact, since the removal of the spleen might lead to a functional decrease in circulating blood volume and because the response to early blood loss by the splanchnic circuit is not expected to completely compensate for blood loss.^{36,37} Specifically, we thought that this was a

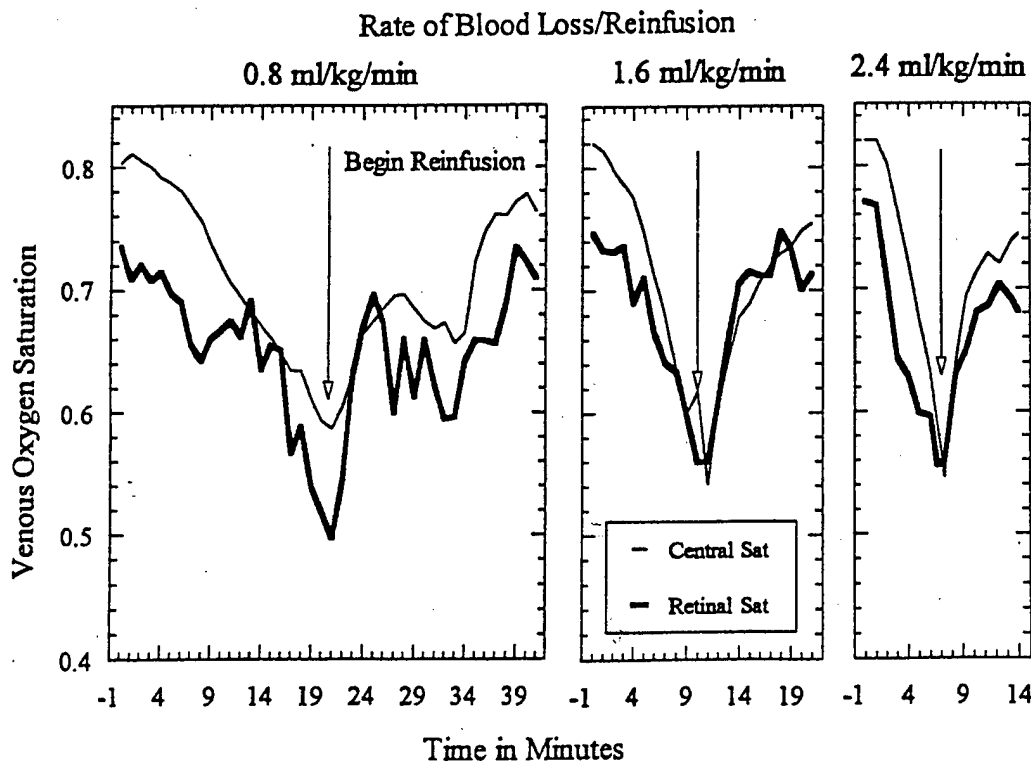


Figure 2. The average SrvO₂ and SvO₂ during 3 rates of blood removal and reinfusion.

TABLE 2. The Rates of Change in Retinal Venous Oxygen Saturation (SrvO₂), Heart Rate (HR), and Mean Arterial Pressure (MAP) at Different Rates of Blood Removal

	0.8 mL/kg/min	1.6 mL/kg/min	2.4 mL/kg/min
ΔSrvO ₂ (%sat/min)	-0.846 ± 0.57*	-2.03 ± 1.0	-3.2 ± 1.25*
ΔHR (beats/min) [†]	0.049 ± 0.85	0.57 ± 1.97	1.52 ± 2.59
ΔMAP (mm Hg/min) [†]	-2.51 ± 1.08	-4.94 ± 4.94	-5.66 ± 4.16

*These values are significantly different ($p < 0.007$, Friedman's test).

†Values in these groups are not significantly different ($p > 0.10$).

better model because testing the sensitivity of SrvO₂ for early blood loss and reinfusion was our primary objective. We chose rates of exsanguination that model the occult bleeding in trauma patients who appear hemodynamically stable and who compensate for slow blood loss. A person bleeding $\leq 0.25\%$ of total blood volume (TBV) per minute (0.2 mL/kg/min) does not reach life-threatening levels of blood loss for ≥ 2 hours. An individual bleeding $> 3\%$ of TBV/min (2.4 mL/kg/min) reaches life-threatening levels of blood loss in < 10 minutes and should be rapidly diagnosed because of dramatic changes in BP and pulse. Because we had already measured retinal venous O₂ saturation when blood was removed at 0.5% of TBV/min (0.4 mL/kg/min),²⁰ we chose to exsanguinate swine at 1%, 2%, and 3% of TBV/min.

We sutured the eyelids open and the eye in place because the animals are not able to cooperate with an ophthalmic examination. This required the use of an irrigation system to keep the cornea moist. Similar scanning devices used on the retina (i.e., the scanning laser ophthalmoscope) do not require these measures in humans. We do not expect this to be a problem in awake cooperative patients. In patients who are uncooperative, the use of the device will require a method for immobilizing the eye or a complex targeting system. Methods for immobilizing the eye will be at least semi-invasive, and a targeting system has yet to be developed for this device. For these reasons, the use of the EOX in patients who are combative is problematic. The device could be used on an unconscious patient since the EOX is aimed by the operator and the lids are retracted manually.

In the configuration used for this study, the EOX is capable of analyzing vessels ranging from approximately 50 to 300 μ m in diameter. Veins in this diameter range were readily accessible near the optic nerve heads of all of the swine used in this study. However, this diameter restriction prevents the use of the current device on vessels far from the optic disk and may prevent its use on the retinal arteries of small children.

The eye provides a relatively clear window to the arteries and veins of the retina, with little intervening tissue that would promote light scattering. The optical quality of the eye/EOX system con-

tributes to the accuracy of the device. However, because of the need for a clear optical window, the EOX may not be useful in elder patients with cataracts or in patients with corneal opacities. In fact, in one swine, excluded from this study, that had a cataract and corneal opacity, we were unable to obtain data during reinfusion at 0.8 mL/kg/min and 2.4 mL/kg/min. We were able to find a path past both of these defects and obtain meaningful data during exsanguination at 0.8, 1.6, and 2.4 mL/kg/min and during reinfusion at 1.6 mL/kg/min.

In this study we used a controlled rate of exsanguination that does not model the nonlinear response to injury seen in trauma victims. This was another reason to test the device across a range of blood loss rates. The reliability of SrvO₂ measurements as an indicator of blood loss during uncontrolled hemorrhage needs to be tested in both animals and humans. In all of the studies that we have done to date measuring SrvO₂ changes during blood loss, we have used a modest endpoint for exsanguination (i.e., 16 mL/kg). We need to study changes in SrvO₂ during profound blood loss. Changes in cardiac index, lactate level, base deficit, and gastric tonometry seen during profound blood loss need to be correlated with SrvO₂ as well.

Since the present device has limited use on vessels < 50 μ m in diameter and since small children may benefit greatly from a noninvasive means for monitoring perfusion in the eye, we need to investigate possible modifications in the device that may allow us to accurately scan smaller retinal vessels.

The retinal arteriovenous saturation difference (SavO₂) has not been studied using this device. The associations of retinal SavO₂ with cardiac index, systemic vascular resistance, blood volume, and brain blood flow remain to be studied.

In this study we used controlled ventilation and oxygenation. We attempted to change one parameter, blood volume. This model does not represent the complex trauma patient with varying respiratory function leading to changes in CO₂ and pH. The retinal circulation is known to respond to changes in O₂ tension and CO₂.¹² The effects of changing arterial O₂ saturation, CO₂, and pH on changes in retinal large-vessel saturations with and without blood volume changes need to be tested.

CONCLUSION

We have demonstrated the use of an experimental eye oximeter during variable rates of blood loss and reinfusion in an anesthetized swine model. Changes in $SrVO_2$ correlated with blood volume and mixed venous O₂ saturation during blood removal and subsequent reinfusion. Unlike vital signs, the rate of change in $SrVO_2$ was significantly greater when blood was removed more rapidly. There was a nonlinear response to the reinfusion of autologous blood seen in this model. This nonlinear response has been described elsewhere and is probably a physiologic response to autologous blood transfusions in swine.³⁰ It is unclear whether this response is present in humans. Use of $SrVO_2$ to monitor for unrecognized blood loss, to estimate the rate of blood loss during hemorrhage, and to evaluate the response to therapy during resuscitation warrants further study.

The authors thank Mr. Ronnie J. Brown, Senior Research Associate, UAB Department of Surgery, for technical support and several late nights in the lab.

References

1. Scalea TM, Holman M, Fuortes M, et al. Central venous blood oxygen saturation: an early, accurate measurement of volume during hemorrhage. *J Trauma*. 1988; 28:725-32.
2. Wo CJ, Shoemaker WC, Appel PL, Bishop MH, Kram HB, Hardin E. Unreliability of blood pressure and heart rate to evaluate cardiac output in emergency resuscitation and critical illness. *Crit Care Med*. 1993; 21:218-23.
3. Scalea TM, Hartnett RW, Duncan AO, et al. Central venous oxygen saturation: a useful clinical tool in trauma patients. *J Trauma*. 1990; 30:1539-43.
4. Scalea TM, Simon HM, Duncan AO, et al. Geriatric blunt multiple trauma: improved survival with early invasive monitoring. *J Trauma*. 1990; 30:129-36.
5. Abou-Khalil B, Scalea TM, Trooskin SZ, Henry SM, Hitchcock R. Hemodynamic responses to shock in young trauma patients: need for invasive monitoring. *Crit Care Med*. 1994; 22: 633-9.
6. Swan H, Sanchez M, Tyndall M, et al. Quality control of perfusion: monitoring venous blood oxygen tension to prevent hypoxic acidosis. *J Thorac Cardiovasc Surg*. 1990; 99:868-72.
7. Rady M, Rivers EP, Martin GB, Smithline H, Appleton T, Nowak RM. Continuous central venous oximetry and shock index in the emergency department. *Am J Emerg Med*. 1992; 10: 538-41.
8. Healthcare Knowledge Resources, HCLIA Inc. Hospital inpatient charges. Baltimore, MD, 1993, pp 238-9.
9. Connors AF, Speroff T, Dawson N, et al. The effectiveness of right heart catheterization in the initial care of critically ill patients. *JAMA*. 1996; 276:889-97.
10. Delori FC. Noninvasive technique for oximeter of blood in retinal vessels. *Appl Optics*. 1988; 27:1113-25.
11. Delori FC, Gragoudas ES, Francisco R, Pruett RL. Monochromatic ophthalmoscopy and fundus photography. *Arch Ophthalmol*. 1977; 95:861-8.
12. Hickam JB, Frayser R. Studies of the retinal circulation in man: observations on vessel diameter, arteriovenous oxygen difference, and mean circulation time. *Circulation*. 1966; 33: 302-16.
13. Harris A, Arend O, Kopecky K, et al. Physiological perturbation of ocular and cerebral blood flow as measured by scanning laser ophthalmoscopy and color Doppler imaging. *Surv Ophthalmol*. 1994; 38(suppl):S81-S86.
14. Laughlin M, Witt WM, Whittaker RN. Regional cerebral blood flow in conscious miniature swine during high sustained +G_z acceleration stress. *Aviat Space Environ Med*. 1979; 50: 1129-33.
15. Ames A. Energy requirements of CNS cells as related to their function and to their vulnerability to ischemia: a commentary. *Can J Physiol Pharmacol*. 1992; 70(suppl):S158-S164.
16. Hickam JB, Frayser R, Ross J. A study of retinal venous oxygen saturation in human subjects by photographic means. *Circulation*. 1963; 17:375-84.
17. Delori FC, Pflibsen KP. Spectral reflectance of the human ocular fundus. *Appl Optics*. 1989; 28:1061-77.
18. Cohen AJ, Laing RA. Multiple scattering analysis of retinal blood oximetry. *Biomed Eng*. 1976; 23:391-400.
19. Smith MH, Denninghoff KR, Hillman LW, et al. Technique for noninvasive monitoring of blood loss via oxygen saturation measurements in the eye. Invited paper in: Priezzhev AV, Asakura T, Leif RC (eds). *Optical diagnostics of biological fluids and advanced techniques in analytical cytology*. Proceedings of SPIE. 1997; 2982:46-52.
20. Denninghoff KR, Smith MH, Chipman RA, et al. Retinal large vessel oxygen saturations correlate with early blood loss and hypoxia in anesthetized swine. *J Trauma*. 1997; 43:29-34.
21. Dries DJ, Waxman K. Adequate resuscitation of burn patients may not be measured by urine output and vital signs. *Crit Care Med*. 1991; 19:327-9.
22. Luna GK, Eddy AC, Copass M. The sensitivity of vital signs in identifying major thoracoabdominal hemorrhage. *Am J Surg*. 1989; 157:512-5.
23. Trouwborst A, Tenbrinck R, van Woerkens E. Blood gas analysis of mixed venous blood during normoxic acute isovolemic hemodilution in pigs. *Anesth Analg*. 1990; 70:523-9.
24. Rasanen J. Supply-dependent oxygen consumption and mixed venous oxyhemoglobin saturation during isovolemic hemodilution in pigs. *Chest*. 1992; 101:1121-4.
25. Kurth CD, Steven JM, Benaron D, Chance B. Near infrared monitoring of the cerebral circulation. *J Clin Monit*. 1993; 9:163-70.
26. Poets CF, Southall DP. Noninvasive monitoring of oxygenation in infants and children: practical considerations and areas of concern. *Pediatrics*. 1994; 93:737-46.
27. Gibson BE, McMighan JC, Cucchiara RF. Lack of correlation between transconjunctival O₂ and cerebral blood flow during carotid artery occlusion. *Anesthesiology*. 1986; 64:277-9.
28. Kram HB, Appel PL, Fleming AW, Shoemaker WC. Conjunctival and mixed-venous oximeters as early warning devices of cardiopulmonary compromise. *Circ Shock*. 1986; 19:211-20.
29. Klein M, Hess D, Eitel D, Bauernshub D, Sabulsk N. Conjunctival oxygen tension monitoring during controlled phlebotomy. *Am J Emerg Med*. 1988; 6:11-3.
30. Filos KS, Vagianos CE, Stravropoulos M, et al. Evaluation of the effects of autotransfusion of unprocessed blood on hemodynamics and oxygen transport in anesthetized pigs. *Crit Care Med*. 1996; 24:855-61.
31. Dronen SC, Maningas PA, Fouch R. Transcutaneous oxygen tension measurements during graded hemorrhage and reinfusion. *Ann Emerg Med*. 1984; 14:534-9.
32. Guerri AD, Thomas K, Hess D, et al. Correlation of transconjunctival PO₂ with cerebral oxygen delivery during cardiopulmonary resuscitation in dogs. *Crit Care Med*. 1988; 16: 612-4.
33. Kram HB, Appel AW, Fleming AW, Shoemaker WC. Conjunctival and mixed venous oximeters as early warning devices of cardiopulmonary compromise. *Circ Shock*. 1986; 19:211-20.
34. Abraham E, Finks S. Conjunctival oxygen tension monitoring in emergency department patients. *Am J Emerg Med*. 1988; 6:549-54.
35. De Schaepdrijver L, Simoons P, Pollet L, Lauwers H, DeLacey J. Morphologic and clinical study of the retinal circulation in the miniature pig: fluorescein angiography of the retina. *Exp Eye Res*. 1992; 54:975-85.
36. Carneiro JJ, Donald DE. Blood reservoir function of dog spleen, liver, and intestine. *Am J Physiol*. 1977; 232:H67-H72.
37. Hartwig H, Hartwig HG. Structural characteristics of the mammalian spleen indicating storage and release of red blood cells. Aspects of evolutionary and environmental demands. *Experientia*. 1985; 41:159-63.

Optimum wavelength combinations for retinal vessel oximetry

Matthew H. Smith

Several investigators have demonstrated techniques for noninvasive measurement of the oxygen saturation of blood in retinal arteries and veins. These techniques have been based on measuring the optical density of a retinal vessel at multiple wavelengths and on calculating the oxygen saturation on the basis of the known absorption coefficients of hemoglobin and oxyhemoglobin. A technique is presented for determining the optimum wavelengths for retinal oximetry measurements. What is believed to be a novel wavelength combination of 488, 635, and 905 nm is found to provide excellent oxygen sensitivity across a broad range of typical vessel diameters and saturations. The use of this wavelength combination should allow for the most accurate retinal saturation measurements made to date. © 1999 Optical Society of America

OCIS codes: 170.1470, 170.4460, 300.1030.

1. Introduction

Spectroscopic oximetry is the technique of determining the percentage of oxygen saturation of blood by means of spectroscopic analysis. The Lambert-Beer law is used to determine the relative concentrations of hemoglobin (Hb) and oxyhemoglobin (HbO₂) in a solution; however, care must be taken to ensure the validity of the assumptions and limitations inherent in this law. Specifically, scattering caused by red blood cells (RBC's) places severe restrictions on the applicability of the Lambert-Beer law in whole blood oximetry. Nevertheless, commercially available instruments such as fingertip pulse oximeters and fiber-optic pulmonary artery catheter oximeters have had great success in making *in vivo* oxygen saturation measurements.

Since 1963, several investigators have developed techniques for noninvasive measurement of the oxygen saturation of blood within the arteries and veins of the retina.¹⁻⁶ The eye is a particularly attractive noninvasive monitoring site, because the blood vessels of the retina are not obscured by thick layers of highly scattering tissue. The proposed uses for ret-

inal oxygenation measurements have ranged from the identification of patients at risk for glaucoma and diabetic retinopathy to the detection of internal bleeding in trauma victims.⁷

As with any spectroscopic technique, the careful choice of optical wavelengths is critically important to the field of retinal oximetry. For *in vitro* measurements, the traditional method of choosing oximetric wavelengths depends on controlling the thickness or concentration of the blood sample. However, *in vivo* techniques do not allow for the control of the sample thickness or concentration. Here a procedure is described that allows for the calculation of optimum wavelength combination for configurations in which the ranges of sample concentration and thickness are known but cannot be controlled. Results of this optimization are presented for the specific case of retinal blood vessels.

2. Retinal Oximetry

A. Overview

The principles of retinal oximetry seem straightforward. An instrument must image the retina and measure the apparent optical density of a retinal vessel at multiple wavelengths. This is done typically by division of the signal intensity at the center of the vessel by the signal intensity on either side of the vessel. The resulting ratio is the apparent transmittance T of the vessel, and the optical density is defined as $-\log(T)$. The oxygen saturation of the blood within the vessel is calculated from these optical den-

The author is with the Department of Physics, The University of Alabama in Huntsville, Huntsville, Alabama 35899. His e-mail address is SmithMH@email.uah.edu.

Received 2 July 1998; revised manuscript received 9 October 1998.

0003-6935/99/010258-10\$15.00/0

© 1999 Optical Society of America

sities and from the known extinction coefficients of Hb and HbO₂ (Ref. 8). Some of the difficulties encountered in making this measurement include light scattering by RBC's, lateral diffusion of light in the choroid, irregularities in the pigmentation of the ocular fundus, glints from the cornea and the apex of the vessel, and a wide range of possible vessel diameters. To date, two theories have been used to calculate oxygen saturation from the measured optical densities of retinal vessels. The two- and three-wavelength oximetry equations are presented in Subsections 2.B and 2.C.

The first retinal oximetry experiments, reported by Hickam *et al.* in 1963, used two different wavelength combinations.¹ Broadband (>100-nm FWHM) Wratten filters centered at 800 and 640 nm were used in a red-infrared instrument. A red-green instrument used interference filters (10-nm FWHM) centered at 640 and 510 nm. Both instruments were fundus cameras modified to take dual, quasi-monochromatic retinal photographs. Optical densities of the vessels were measured through manual analysis of the exposed film.

Cohen and Laing² reported an instrument in 1976 that was similar to the device of Hickam *et al.* This instrument employed a blue-green combination, with interference filters (20-nm FWHM) centered at 470 and 515 nm.

In 1988, Delori³ reported a three-wavelength retinal vessel oximeter. This device scanned a slit of filtered light across the retina and interpreted collected data automatically by means of a computer algorithm. Three green wavelengths (558, 569, and 586 nm) were chosen for this measurement.

Schweitzer *et al.*⁴ demonstrated a retinal imaging spectrometer in 1995. This technique was unique in that it determined retinal vessel oxygen saturation by means of transmittance measurements at 2-nm increments from 400 to 700 nm.

A recent photographic retinal oximeter was described in 1998 by Tiedeman *et al.*⁵ This instrument illuminated the retina with filtered light (8-nm FWHM) at 569 and 600 nm and acquired images on a high-dynamic-range CCD camera.

Finally, Smith *et al.*⁶ described the first retinal vessel oximeter to use diode lasers as its light source. Two lasers (670 and 803 nm) were focused onto a subject's retina and scanned across a retinal vessel. Curve-fitting routines were applied to the collected signals to determine the optical density of the vessel.

To understand the wavelength selections made by each investigator, consider the millimolar extinction coefficients for Hb and HbO₂ shown in Fig. 1. The wavelengths of the maxima and minima of the absorption peaks of Hb and HbO₂ are labeled in Fig. 1, as are the wavelengths at which Hb and HbO₂ have the same absorption. The wavelengths at which two substances, one of which can be converted into the other, have the same extinction coefficients are called isobestic wavelengths. Each wavelength combination that has been used for retinal oximetry included one wavelength for which the difference in the extinc-

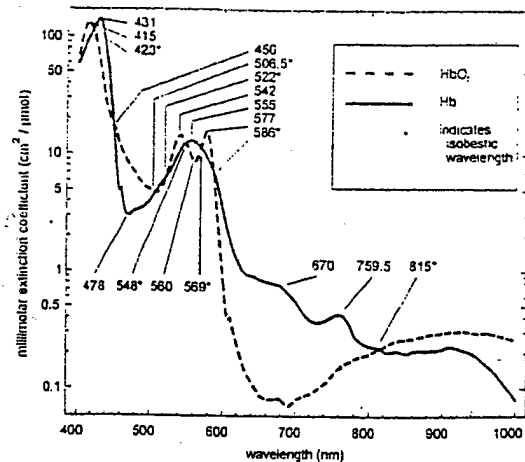


Fig. 1. Millimolar extinction coefficients of Hb and HbO₂ (data from Ref. 8).

tion coefficients $|\epsilon_{\text{HbO}_2} - \epsilon_{\text{Hb}}|$ was large and one or two isobestic wavelengths. It is shown that these wavelength choices are not optimized.

B. Two-Wavelength Oximetry

A blood sample that was hemolyzed and cleaned (i.e., the RBC's were split open and the cell membranes removed) forms a solution composed essentially of two components, Hb and HbO₂. It should be noted that, although numerous other Hb derivatives such as carboxyhemoglobin, methemoglobin, and sulphemoglobin are also generally present in blood, it is assumed throughout this paper that the contribution of these trace components is insignificant. Future retinal oximetry efforts should be focused on this assumption, as the absorption spectra of these components are available.⁸

The Lambert-Beer law for a system that contains a mixture of more than one absorbing substance can be written as

$$D = \epsilon_1 c_1 l + \epsilon_2 c_2 l + \dots + \epsilon_n c_n l, \quad (1)$$

where ϵ_n and c_n are the millimolar extinction coefficient and concentration, respectively, of the n th component and the sample thickness l is the same for each component. Assuming a solution of only Hb and HbO₂, Eq. (1) can be written as

$$D = \epsilon_{\text{Hb}} c_{\text{Hb}} l + \epsilon_{\text{HbO}_2} c_{\text{HbO}_2} l. \quad (2)$$

The oxygen saturation s is defined as

$$s = \frac{c_{\text{HbO}_2}}{c_{\text{HbO}_2} + c_{\text{Hb}}} = \frac{c_{\text{HbO}_2}}{c_{\text{HbTOTAL}}}, \quad (3)$$

such that $s = 1$ for pure HbO₂ and $s = 0$ for pure Hb. Equation (2) can be rewritten as

$$D = s \epsilon_{\text{HbO}_2} c_{\text{HbTOTAL}} l + (1 - s) \epsilon_{\text{Hb}} c_{\text{HbTOTAL}} l \quad (4)$$

or

$$D = s(\epsilon_{\text{HbO}_2} - \epsilon_{\text{Hb}}) c_{\text{HbTOTAL}} l + \epsilon_{\text{Hb}} c_{\text{HbTOTAL}} l. \quad (5)$$

If c_{HbTOTAL} and l are known with sufficient accuracy, then the saturation s can be calculated by measurement of the optical density D of the sample at any wavelength as long as $\epsilon_{\text{HbO}_2} - \epsilon_{\text{Hb}} \neq 0$.

Generally, c_{HbTOTAL} and l are not known accurately (especially *in vivo*), so a two-wavelength oximetry method is used. When D is measured at the two wavelengths λ_1 and λ_2 , Eq. (5) becomes

$$\begin{aligned} D^{\lambda_1} &= m[s(\epsilon_{\text{HbO}_2}^{\lambda_1} - \epsilon_{\text{Hb}}^{\lambda_1}) + \epsilon_{\text{Hb}}^{\lambda_1}], \\ D^{\lambda_2} &= m[s(\epsilon_{\text{HbO}_2}^{\lambda_2} - \epsilon_{\text{Hb}}^{\lambda_2}) + \epsilon_{\text{Hb}}^{\lambda_2}], \end{aligned} \quad (6)$$

where $m = c_{\text{HbTOTAL}} l$. Equations (6) are solved easily for s , resulting in

$$s = \frac{D^{\lambda_2} \epsilon_{\text{Hb}}^{\lambda_1} - D^{\lambda_1} \epsilon_{\text{Hb}}^{\lambda_2}}{D^{\lambda_1} (\epsilon_{\text{HbO}_2}^{\lambda_2} - \epsilon_{\text{Hb}}^{\lambda_2}) - D^{\lambda_2} (\epsilon_{\text{HbO}_2}^{\lambda_1} - \epsilon_{\text{Hb}}^{\lambda_1})}. \quad (7)$$

Equation (7) calculates oxygen saturation of a hemolyzed blood sample and is independent of hemoglobin concentration or sample thickness. Some care must be taken when these wavelengths are chosen, but in general any two wavelengths will work provided $\epsilon_{\text{HbO}_2} - \epsilon_{\text{Hb}} \neq 0$ for at least one wavelength.

It is important to note that the two-wavelength saturation equation of Eq. (7) was derived from the Lambert-Beer law and therefore is valid only for a homogenous, nonscattering solution. Whole blood is primarily a suspension of RBC's in plasma, and there is a refractive-index discontinuity at the interface of the RBC and the surrounding plasma. Scattering caused at these interfaces violates the assumptions of the Lambert-Beer law, thus generally making the two-wavelength oximetry technique invalid for whole blood. As such, whereas two-wavelength retinal

solution is written as a correction to the Lambert-Beer law:

$$D = \epsilon c l + B(\lambda), \quad (8)$$

where $B(\lambda)$ is a complicated function of wavelength. RBC geometry, the geometry of the detector used in a given experiment, and the complex refractive indices of the RBC's and the plasma.

Pittman and Duling¹¹ suggested an oximetric technique in which the scattering term $B(\lambda)$ was assumed to be constant. This assumption is valid across sufficiently narrow wavelength ranges that do not fall near a strong Hb absorption band. Across such a range, the complex refractive indices should remain nearly constant. Experiments performed by Pittman and Duling verify the constancy of B for the green series wavelengths (520, 546, and 555 nm). They also demonstrate that B is not constant across the blue series wavelengths (420, 436, and 450 nm), owing to the Soret absorption band of Hb at ~420 nm. Finally, they hypothesize the validity of this approximation into the near infrared that is due to the lack of strong Hb absorption bands in this region.

As was done for the two-wavelength method in Eq. (7), one can obtain the oxygen saturation by solving the three equations

$$\begin{aligned} D^{\lambda_1} &= m[s(\epsilon_{\text{HbO}_2}^{\lambda_1} - \epsilon_{\text{Hb}}^{\lambda_1}) + \epsilon_{\text{Hb}}^{\lambda_1}] + B, \\ D^{\lambda_2} &= m[s(\epsilon_{\text{HbO}_2}^{\lambda_2} - \epsilon_{\text{Hb}}^{\lambda_2}) + \epsilon_{\text{Hb}}^{\lambda_2}] + B, \\ D^{\lambda_3} &= m[s(\epsilon_{\text{HbO}_2}^{\lambda_3} - \epsilon_{\text{Hb}}^{\lambda_3}) + \epsilon_{\text{Hb}}^{\lambda_3}] + B, \end{aligned} \quad (9)$$

for s by canceling m and B (where $m = c_{\text{HbTOTAL}} l$). This yields the three-wavelength saturation equation

$$s = \frac{D^{\lambda_1}(\epsilon_{\text{Hb}}^{\lambda_3} - \epsilon_{\text{Hb}}^{\lambda_2}) + D^{\lambda_2}(\epsilon_{\text{Hb}}^{\lambda_1} - \epsilon_{\text{Hb}}^{\lambda_3}) + D^{\lambda_3}(\epsilon_{\text{Hb}}^{\lambda_2} - \epsilon_{\text{Hb}}^{\lambda_1})}{D^{\lambda_1}[(\epsilon_{\text{Hb}}^{\lambda_3} - \epsilon_{\text{HbO}_2}^{\lambda_3}) - (\epsilon_{\text{Hb}}^{\lambda_2} - \epsilon_{\text{HbO}_2}^{\lambda_2})] + D^{\lambda_2}[(\epsilon_{\text{Hb}}^{\lambda_1} - \epsilon_{\text{HbO}_2}^{\lambda_1}) - (\epsilon_{\text{Hb}}^{\lambda_3} - \epsilon_{\text{HbO}_2}^{\lambda_3})] + D^{\lambda_3}[(\epsilon_{\text{Hb}}^{\lambda_2} - \epsilon_{\text{HbO}_2}^{\lambda_2}) - (\epsilon_{\text{Hb}}^{\lambda_1} - \epsilon_{\text{HbO}_2}^{\lambda_1})]}. \quad (10)$$

oximetry techniques can monitor changes in retinal saturation, such techniques are not expected to be well calibrated.

C. Three-Wavelength Oximetry

Twersky developed a mathematical formalism that describes the scattering of light by a suspension of slightly absorbing particles⁹ and applied these results to biological suspensions (i.e., whole blood).¹⁰

The oxygen saturation can be calculated from this equation, provided all three wavelengths are not isobestic. Pittman and Duling chose two isobestic wavelengths such that

$$\epsilon_{\text{HbO}_2}^{\lambda_2} = \epsilon_{\text{Hb}}^{\lambda_2}, \quad \epsilon_{\text{HbO}_2}^{\lambda_3} = \epsilon_{\text{Hb}}^{\lambda_3}. \quad (11)$$

This simplifies Eq. (10) to

$$s = \frac{D^{\lambda_1}(\epsilon_{\text{Hb}}^{\lambda_3} - \epsilon_{\text{Hb}}^{\lambda_2}) + D^{\lambda_2}(\epsilon_{\text{Hb}}^{\lambda_1} - \epsilon_{\text{Hb}}^{\lambda_3}) + D^{\lambda_3}(\epsilon_{\text{Hb}}^{\lambda_2} - \epsilon_{\text{Hb}}^{\lambda_1})}{(D^{\lambda_2} - D^{\lambda_3})(\epsilon_{\text{Hb}}^{\lambda_1} - \epsilon_{\text{HbO}_2}^{\lambda_1})}. \quad (12)$$

The significance of Twersky's multiple-scattering theory is that it predicts that the effects of absorption and scattering on the collected flux can be considered independently. The optical density of a scattering

The choice of two isobestic wavelengths provides simplification in the saturation equation and results in the saturation equation being linear in D^{λ_1} , because D^{λ_2} and D^{λ_3} are constant with saturation for isobestic

wavelengths. However, this choice of two isobestic wavelengths is not necessary mathematically, and it does not lead to optimized sensitivity to oxygen saturation.

3. Wavelength Selection

A. Photometric Error

The considerations associated with choosing oximetric wavelengths arise from the errors involved in making optical-density measurements. Ideally, the output signal from an optical detection system is linear with the radiant power incident on the detector element. As such, measurements of the light transmitted through an absorbing sample and of the light incident on the sample allow for direct calculation of the transmittance T of the sample. The absolute photometric error ΔT is some value (e.g., $\Delta T = 0.01$) that represents the uncertainty in the calculated T and is generally independent of the magnitude of T . The signal-to-noise ratio of the measurement system typically determines the magnitude of ΔT .

Recall the general two-wavelength oximetry equation (7). The optical densities D are calculated from the measured transmittances as $D = -\log(T)$. The absolute error in D is expressed as $\Delta D = (dD/dT)\Delta T$. Van Assendelft suggests that the relative density errors $\Delta D/D$ should be minimized to minimize the measurement error in ϵ , which subsequently minimizes the error in calculated oxygen saturation.⁸

Minimizing the relative density errors is straightforward. The optical density D is rewritten in terms of natural logarithms as

$$D = -\log(T) = -\frac{\ln(T)}{\ln(10)}. \quad (13)$$

The absolute density error is

$$\Delta D = \frac{dD}{dT} \Delta T = -\frac{\Delta T}{\ln(10)} \frac{1}{T}, \quad (14)$$

and the relative density error is found by division of Eq. (14) by Eq. (13):

$$\frac{\Delta D}{D} = \frac{\Delta T}{T \ln(T)}. \quad (15)$$

To minimize the relative error, set its first derivative to zero:

$$\frac{d(\Delta D/D)}{dT} = -\frac{\ln(T) + 1}{[T \ln(T)]^2} \Delta T = 0. \quad (16)$$

The trivial solution of $\Delta T = 0$ is, unfortunately, unrealizable. The relative error also minimizes as the denominator of Eq. (16) approaches infinity; however, this does not occur across the allowed range of transmittance $0 \leq T \leq 1$. The remaining solution $\ln(T) + 1 = 0$ yields an important result:

$$\begin{aligned} T &= (1/e) = 36.8\%, \\ D &= 0.434. \end{aligned} \quad (17)$$

Thus the most accurate optical-density measurements are made if the transmittance is $T = 36.8\%$. In general, the analysis error is acceptably small if the spectrophotometric measurement is made in the range $10\% < T < 70\%$.³

This effect of T on optical-density error is understood easily through an example. Consider a sample that undergoes a 0.3 change in optical density, from $D = 0.2$ to $D = 0.5$. The corresponding change in transmittance is $T = 63.10\%$ to $T = 31.62\%$. A measurement error of 1% T will have only a slight effect on this measurement. Next, consider another sample that also undergoes a 0.3 change in optical density, but this sample changes from $D = 2.2$ to $D = 2.5$. The corresponding transmittance change is $T = 0.63\%$ to $T = 0.32\%$. A measurement error of 1% T makes this measurement extremely difficult.

To extend this technique to more than one wavelength, the thickness and concentration of a sample could be adjusted individually for each wavelength within a spectrophotometer to achieve this optimized sensitivity. Unfortunately, retinal vessel oximetry prevents the direct application of this wavelength optimization method, because sample thickness and concentration are fixed. A new method is described in Subsection 3.C that extends this principle for application to retinal oximetry.

B. Isobestic Wavelengths

The historical reason for choosing isobestic wavelengths is that the extinction coefficients of multicomponent solutions were not always known. In this case an isobestic wavelength could be found experimentally. When one isobestic wavelength is chosen, Eq. (7) simplifies to

$$s = a + b(D^{\lambda_1}/D^{\lambda_2}). \quad (18)$$

The constants a and b can be measured experimentally through two sets of density measurements, one at $s = 1$ (solution fully converted to one component) and the other at $s = 0$ (solution fully converted to the other component). A calibration line is then drawn for subsequent unknown measurements.

To date, all retinal oximetry techniques have employed at least one isobestic wavelength. This choice of an isobestic wavelength, however, is not mathematically necessary. Equations (7) and (10) are solved easily, because the millimolar extinction coefficients of Hb derivatives are well known. As such, there is no obvious advantage offered by use of an isobestic wavelength in retinal oximetry except a modest simplification in the saturation calculation.

C. Wavelength Selection Method

The motivation for developing the new selection criteria was an intuitive assumption with regard to the optimum wavelengths for two-wavelength oximetry calculations. Instead of choosing one wavelength with large $|\epsilon_{\text{HbO}_2} - \epsilon_{\text{Hb}}|$ and one isobestic wavelength, it seemed obvious that two wavelengths with large $|\epsilon_{\text{HbO}_2} - \epsilon_{\text{Hb}}|$ should result in increased saturation

Table 1. Target Values Chosen for Wavelength Optimization

Vessel Type	Diameter (μm)	Saturation (%O ₂ Sat.)	Hb Concentration (g _{Hb} /100 ml _{blood})	Absolute Measurement Error (ΔT)
Retinal vein	160	50	15	0.01
Retinal artery	120	98	15	0.01

sensitivity, provided $\epsilon_{\text{HbO}_2} - \epsilon_{\text{Hb}}$ was positive for one wavelength and negative for the other. Thus a change in saturation causes the transmittance at one wavelength to increase while the transmittance at the other wavelength decreases. This should provide better sensitivity than use of an isobestic wavelength with a transmittance that does not vary with

The error in the calculated saturation is expressed as

$$\Delta s = \left[\left(\frac{\partial s}{\partial T^{\lambda_1}} \Delta T^{\lambda_1} \right)^2 + \left(\frac{\partial s}{\partial T^{\lambda_2}} \Delta T^{\lambda_2} \right)^2 \right]^{1/2} \quad (21)$$

Performing the partial derivatives necessary for Eq. (21) yields

$$\frac{\partial s}{\partial T^{\lambda_1}} = - \frac{\log(T^{\lambda_2})}{T^{\lambda_1}} \frac{\epsilon_{\text{Hb}}^{\lambda_1} \epsilon_{\text{HbO}_2}^{\lambda_2} - \epsilon_{\text{Hb}}^{\lambda_2} \epsilon_{\text{HbO}_2}^{\lambda_1}}{[\log(T^{\lambda_1})(\epsilon_{\text{HbO}_2}^{\lambda_2} - \epsilon_{\text{Hb}}^{\lambda_2}) - \log(T^{\lambda_2})(\epsilon_{\text{HbO}_2}^{\lambda_1} - \epsilon_{\text{Hb}}^{\lambda_1})]^2} \quad (22)$$

saturation. However, the method of setting T near 36.8% provides no mechanism for bearing out this hypothesis.

The importance of the procedure described by Van Assendelft is that the absolute photometric measurement error is some ΔT instead of a ΔD . With this in mind, the criterion for wavelength selection can be stated simply: Choose wavelengths to minimize the error in the saturation calculation caused by transmittance measurement errors ΔT ; that is, minimize

$$\Delta s = \left[\left(\frac{\partial s}{\partial T^{\lambda_1}} \Delta T^{\lambda_1} \right)^2 + \left(\frac{\partial s}{\partial T^{\lambda_2}} \Delta T^{\lambda_2} \right)^2 + \dots + \left(\frac{\partial s}{\partial T^{\lambda_n}} \Delta T^{\lambda_n} \right)^2 \right]^{1/2}, \quad (19)$$

where Δs is the error in calculated saturation and ΔT^{λ} is the measurement error in transmittance at a particular wavelength.

D. Optimum Two-Wavelength Selection for Retinal Vessels

Although two-wavelength oximetry techniques provide accurate results only for hemolyzed blood, they have proven useful in monitoring trends in oxygen saturation in retinal vessels. As such, it is worthwhile to investigate the optimum wavelength pair for retinal vessel oximetry. Rewriting the general two-wavelength oximetry equation (7) in terms of T gives

$$s = \frac{\log(T^{\lambda_2})\epsilon_{\text{Hb}}^{\lambda_1} - \log(T^{\lambda_1})\epsilon_{\text{Hb}}^{\lambda_2}}{\log(T^{\lambda_1})(\epsilon_{\text{HbO}_2}^{\lambda_2} - \epsilon_{\text{Hb}}^{\lambda_2}) - \log(T^{\lambda_2})(\epsilon_{\text{HbO}_2}^{\lambda_1} - \epsilon_{\text{Hb}}^{\lambda_1})}. \quad (20)$$

and a similar expression for $\partial s / \partial T^{\lambda_2}$ (by means of cyclic permutation).

Note that Δs is still a function of T^{λ_1} and T^{λ_2} . As such, values for these transmittances must be estimated in order to calculate Δs . Estimates for these transmittances are made by means of the Lambert-Beer law,

$$T^{\lambda} = 10^{-cl[s\epsilon_{\text{HbO}_2}^{\lambda} + (1-s)\epsilon_{\text{Hb}}^{\lambda}]}, \quad (23)$$

assuming typical values for retinal vessel diameter, Hb concentration, and oxygen saturation. The target values chosen are the listed in Table 1. The absolute measurement error ΔT is assumed to be constant across wavelength and saturation. For wavelengths longer than 600 nm, the coloration of the fundus becomes more spatially variable, possibly resulting in larger measurement errors. This effect, however, cannot be quantified easily and is ignored here.

For the purpose of estimating the transmittances in these calculations, light is assumed to traverse the vessel in double pass. As such, twice the listed diameter is used in all transmittance calculations of Eq. (23). This assumption is not entirely accurate, owing to RBC scattering and lateral diffusion of light in the underlying retinal layers. It is expected that some fraction of the collected signal in retinal oximetry has traversed the vessel in single transmission and some fraction in double transmission. This fraction is likely to be dependant on wavelength and on retinal vessel diameter, but no attempt is made here to quantify this fraction. For the wavelength optimization calculation, double-pass transmission is equivalent mathematically to single-pass transmission at twice the vessel diameter. Final results are always presented for double-pass diameters that range from 25 to 250 μm . Equivalently, these re-

Table 2. Calculated Saturation Error Due to 0.01 Error in T for the Wavelength Combinations Used by Various Investigators^a

Investigator	Wavelengths (nm)	Saturation Error, 120- μ m Artery (%O ₂ Sat.)	Saturation Error, 160- μ m Vein (%O ₂ Sat.)	Saturation Error, 50- μ m Artery (%O ₂ Sat.)	Saturation Error, 50- μ m Vein (%O ₂ Sat.)
Hickam <i>et al.</i> ^b	510 and 640	2.3	6.3	6.3	7.4
Hickam <i>et al.</i> ^b	640 and 800	3.3	6.4	7.5	18.0
Cohen and Laing ^c	470 and 515	22.0	18.0	5.7	4.1
Delori ^d	558, 569, and 586	90.0	>100	11.3	17.8
Tiedeman <i>et al.</i> ^e	569 and 600	17.0	>100	2.9	4.8
Smith <i>et al.</i> ^f	670 and 803	3.4	6.2	7.9	17.5

^aThe target values in Table 1 are used in the error calculation. Values are also presented for 50- μ m vessels, because some investigators' instruments performed significantly better for smaller vessels.

^bRef. 1.

^cRef. 2.

^dRef. 3.

^eRef. 5.

^fRef. 6.

sults could be interpreted as single-pass diameters that range from 50 to 500 μ m.

A MATHEMATICA notebook was developed to calculate the error for any given combination of wavelengths, saturation, vessel diameter, and Hb concentration. A piecewise cubic interpolating function was applied to the millimolar extinction coefficient data of Van Assendelft⁸ to provide ϵ_{Hb} and ϵ_{HbO_2} as functions of wavelength. The millimolar extinction coefficients are presented in units of square centimeters per micromole. From the molecular weight of Hb (64,500 for four polypeptide chains),¹² a conversion factor of 0.0162 g/ μ mol is calculated. This value allows for the use of Hb concentration in the typical units of grams per deciliter.

With the target values in Table 1, the saturation errors are calculated for the two-wavelength combinations used by each of the previous retinal oximetry investigators. In all cases it is assumed that the absolute measurement error is $\Delta T = 0.01$, regardless of the experimental instrumentation. These results are presented in Table 2. Because some investigators' instruments perform significantly better for smaller vessels, error values are also listed for 50- μ m retinal arteries and veins.

For the optimum wavelength combination to be determined, an examination of all possible combinations of two wavelengths within a suitable wavelength range was performed. Wavelengths between 400 and 450 nm are strongly absorbed by the Soret band of Hb (see Fig. 1), and tight retinal exposure limits exist below 400 nm. Low Hb absorption and deep tissue penetration prevent the use of wavelengths greater than 1000 nm. These criteria prescribe the acceptable range of wavelengths for retinal oximetry as $450 \text{ nm} \leq \lambda \leq 1000 \text{ nm}$.

Figure 2 contains gray-scale maps that represent the calculated error in the two-wavelength saturation equation. Gray level decreases from black to white linearly with $1/\Delta s$. As such, areas of large error are black and areas of low error are white. Figure 2(a) displays the saturation errors for a typical retinal vein (see Table 1). The saturation error for a typical

retinal artery is shown in Fig. 2(b). A number of local minima are observed in each map.

No well-defined criteria were developed to determine the wavelength pair that represented the best choice for use on both arteries and veins. Because many of these wavelengths are red or near infrared, diode lasers are an excellent choice as light source for use in an instrument. The commercial availability of the wavelengths is therefore used as one selection criterion. In addition, the human ocular media transmittance is quite low at wavelengths longer than $\sim 920 \text{ nm}$ (Ref. 13). The 635- and 905-nm pair appears promising, because both wavelengths are commercially available from diode lasers and have high media transmittance. The 488- and 905-nm pair is another potentially useful pair, because 488-nm light can be created with an argon-ion laser.

Figure 3 contains plots of saturation error for the 635- and 905-nm wavelength pair and for the 488- and 635-nm pair. The error Δs is plotted versus saturation s for a range of vessel diameters from 25 to 250 μ m. The 635- and 905-nm combination performs well across the entire range of oxygen saturation, but the error increases for smaller vessels and lower saturations. Vessels with diameters less than 100 μ m will have unacceptably large associated errors, thus limiting an instrument to use on vessels near the optic nerve head. The 488- and 635-nm pair offers significant improvement for lower saturations and smaller vessels.

Finally, recall that the Hb concentration c is assumed to be 15 g_{Hb}/100 ml. Changes in c are mathematically equivalent to changes in vessel diameter. Therefore a 50- μ m vessel at 15 g_{Hb}/100 ml has the same associated error as a 150- μ m vessel at 5 g_{Hb}/100 ml.

E. Optimum Three-Wavelength Selection for Retinal Vessels

As discussed in Subsection 2.C, the use of a third wavelength might allow for compensation for RBC scattering in oximetry. Delori applied this three-wavelength method to retinal vessel oximetry and

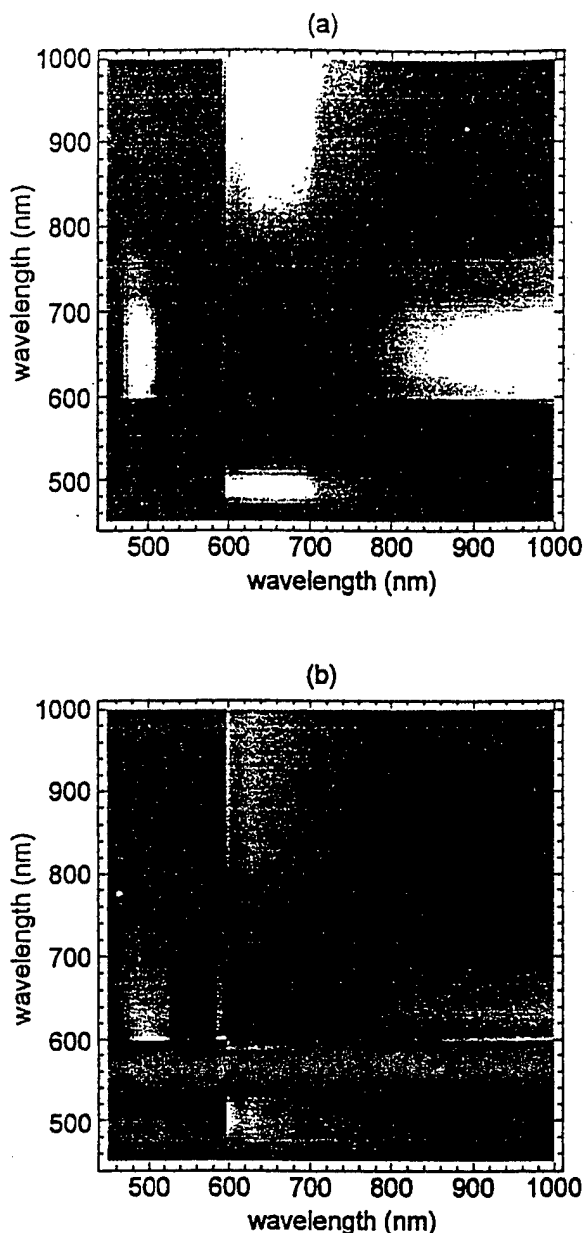


Fig. 2. Relative error in the two-wavelength saturation calculation. Light areas correspond to wavelength pairs with low associated error; dark areas correspond to high error. The error for typical (a) retinal veins and (b) arteries are plotted separately.

reported results that indicated an improvement over two-wavelength measurements, as observed in an instrument calibration that varied only slightly with vessel diameter. This improvement, however, came at the price of decreased sensitivity to oxygen saturation.

Delori used two isobestic wavelengths (569 and 586 nm) and one measurement wavelength (558 nm). When Eq. (19) is extended to three wavelengths, the saturation errors that are due to $\Delta T = 0.01$ measurement errors are calculated for Delori's wavelengths. A 50- μm artery has an associated error of 11.3% O_2Sat , and a 50- μm vein has an associated error of 17.8% O_2Sat , at these wavelengths (see Table

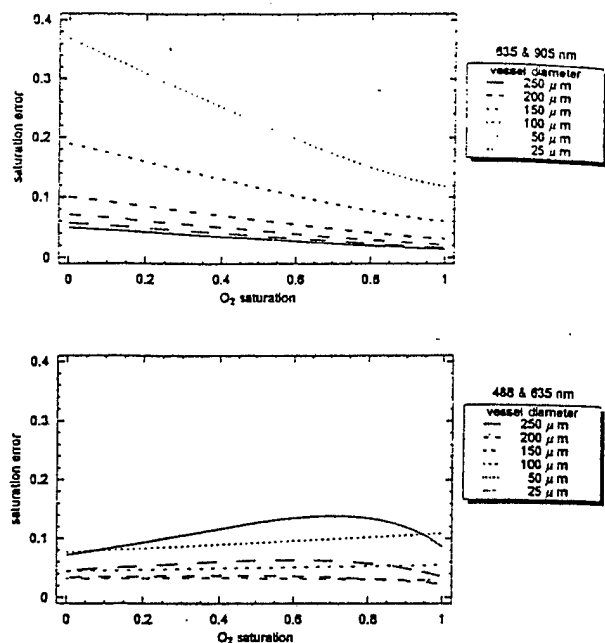


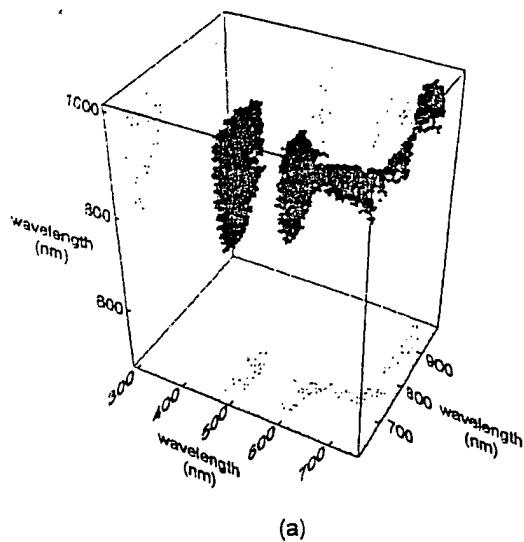
Fig. 3. Variation in the two-wavelength saturation error for the 635- and 960-nm wavelength pair. A Hb concentration of 15 g/100 ml is assumed, and vessel diameter is indicated in the legend.

2). By an average of a large number of scans, the standard error of the mean was decreased to acceptable levels of $\sim 3\% \text{O}_2\text{Sat}$. However, for the largest vessels near the optic disk (vessel diameters greater than $\sim 150 \mu\text{m}$) this wavelength combination yields unacceptably high errors.

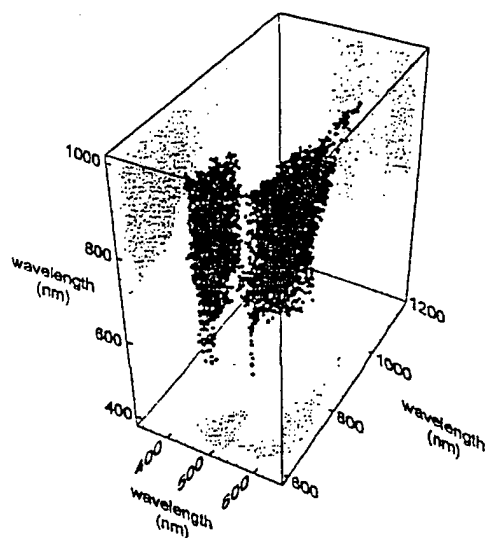
As with the two-wavelength equation in Subsection 3.D, it is useful to find the best possible combination of three wavelengths. The range over which to search for an optimum wavelength triad is limited by the constant-scattering assumption inherent in the three-wavelength method. For this study it is assumed that variations in RBC scattering will be reasonably small across the 450–1000-nm wavelength range, owing to the lack of strong Hb absorption bands in this range.¹¹

As was done for the two-wavelength optimization, values of T must be estimated to calculate the partial derivatives $\partial s / \partial T^\lambda$. For simplicity, the nonscattering Lambert-Beer law of Eq. (23) is again used. At the end of this section it is shown that the inclusion of a constant scattering factor T_s does not significantly affect the results of the optimization.

The computational power to evaluate and display all possible combinations of three wavelengths at sufficiently fine intervals was not available. Instead, a MATHEMATICA routine was written that evaluated the error associated with several thousand randomly selected wavelength triads. Each triad found that had an error less than 5% O_2Sat . (owing to a 1% T measurement error) was recorded. These triads were sorted (lowest to highest wavelength) and the values plotted in a three-dimensional scatterplot. Figure 4(a) contains optimum wavelength triads for typical



(a)



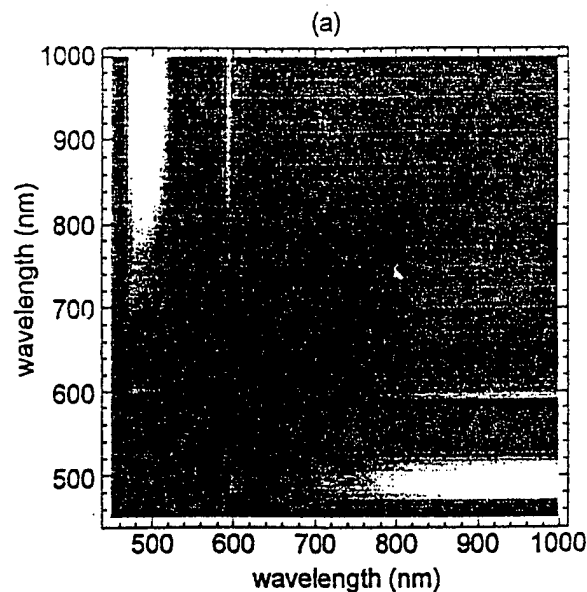
(b)

Fig. 4. Wavelength triads yielding saturation errors less than 5%O₂Sat., owing to transmittance measurement errors of $\Delta T = 0.01$, are plotted. Results are displayed separately for typical retinal (a) veins and (b) arteries.

retinal veins, and Fig. 4(b) is for retinal artery values. The points plotted have saturation errors less than 5%O₂Sat. The shadow of each point is projected onto the three base planes.

Figure 4 provides a starting point for determining the optimum three-wavelength triad. With reference to the results of the two-wavelength optimization of Subsection 3.D, 635 nm was present in all optimum arterial and venous pairs. This wavelength was also present in the 5%O₂Sat. triads. As was done in the two-wavelength optimization, 635 nm was chosen as a compromise between arterial and venous values, because it is commercially available as a diode laser.

Once 635 nm has been chosen as the first wavelength, two-dimensional gray-scale plots that investigate all possible combinations of the second and



(b)

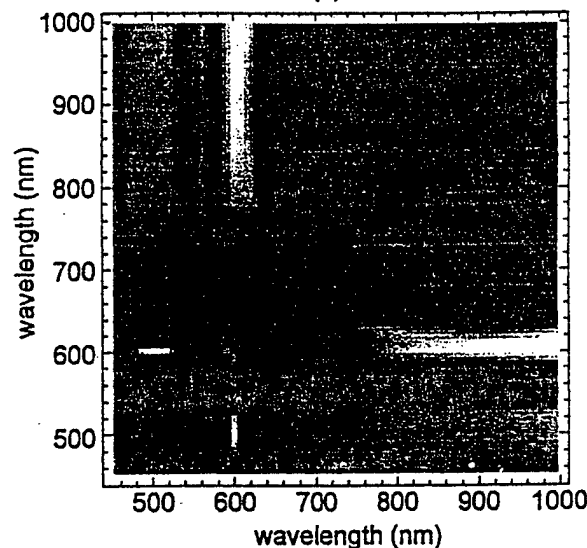


Fig. 5. Relative error in the three-wavelength saturation calculation for 635 nm and two other wavelengths. Light areas correspond to wavelengths with low associated error; dark areas correspond to high error. The error for typical retinal (a) veins and (b) arteries are plotted separately.

third wavelengths are generated. Figure 5 contains the error data for retinal veins and arteries. The gray level decreases from black to white linearly with $1/\Delta s$. Numerous local minima in the error are found in each plot.

Figure 5 shows that 635 and 905 nm are excellent candidates for two of the three wavelengths. However, a number of wavelengths exist that appear to be good third wavelengths for this combination. Figure 6 examines the error associated with all third wavelengths between 450 and 1000 nm when they are used in combination with 635 and 905 nm for measuring retinal arteries or veins. From Fig. 6, three triads of wavelengths appear almost equally opti-

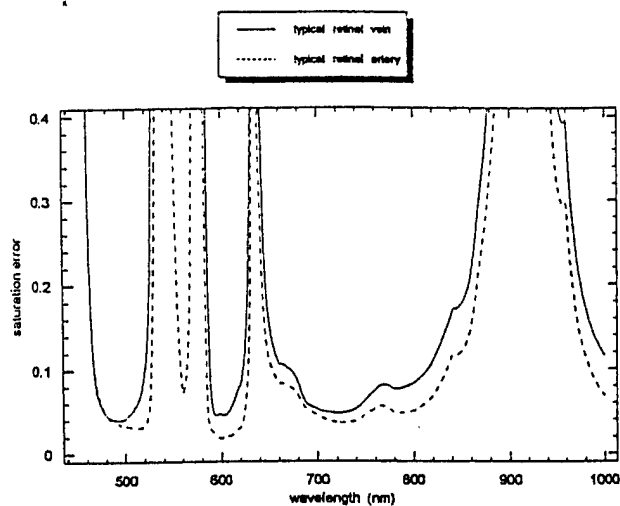


Fig. 6. Error in the three-wavelength saturation equation with 635 nm, 960 nm, and a third wavelength (x axis). Error is calculated for typical retinal veins and arteries.

mized: 488, 635, and 905 nm; 600, 635, and 905 nm; and 635, 720, and 905 nm. None of the three combinations are clearly superior, from this figure.

As the final step in the three-wavelength optimization process, these three triads of wavelengths are examined individually across a range of vessel diameters and saturations. Figure 7 contains the error plots for each of these triads. From this figure, 488, 635, and 905 nm is found to be a remarkably stable wavelength combination. Associated errors are less than 10% O_2 Sat., owing to a $\Delta T = 0.01$ measurement error across typical retinal vessel diameters and across all oxygen saturation values. Diode lasers are currently available that generate 635- and 905-nm light, and 488-nm light can be generated with an argon-ion laser.

Finally, the error for the 488-, 635-, and 905-nm triad is recalculated with the inclusion of a constant scattering term. Instead of using Eq. (23) for our transmittance estimate, we use

$$T^{\lambda} = T_s 10^{-c[\epsilon_{HbO_2}^{\lambda} + (1-s)\epsilon_{Hb}^{\lambda}]} \quad (24)$$

Figure 8 displays the calculated saturation error, assuming a scattering transmittance T_s of 0.75. Whereas the error is $\sim 37\%$ greater than the nonscattering solution of Fig. 7, the same excellent stability across a broad range of saturations and diameters is maintained.

4. Discussion and Conclusions

A new method has been presented that allows for the calculation of the optimum wavelengths for two- and three-wavelength oxygen saturation measurements. The results of this study indicate that a 488-, 635-, and 905-nm wavelength triad might allow for the most accurate oxygen saturation measurements ever made in the retina. At present *in vivo* and *in vitro* experimentation is being performed to determine the value of this wavelength combination.

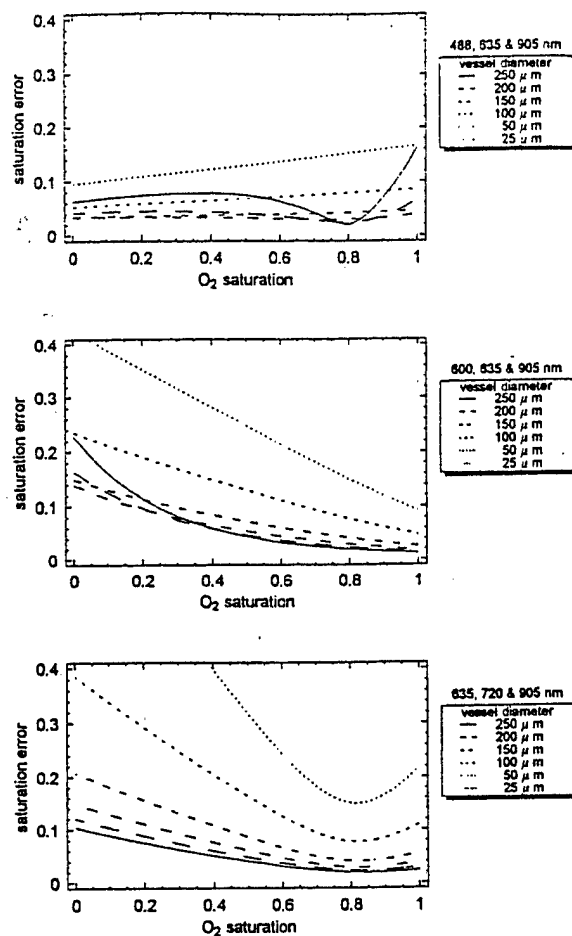


Fig. 7. Variation in the three-wavelength saturation error for three different wavelength triads. Vessel diameters are listed in the legends, and the Hb concentration is assumed to be 15 g/100 ml.

Unfortunately, it seems unlikely that the scattering effects of whole blood will be sufficiently constant across the 488–905-nm wavelength range for the three-wavelength constant-scattering oximetry equation to be valid. However, the lack of strong hemoglobin (Hb) absorption bands in this spectral range suggests that any wavelength-dependant scattering effects should at least behave monotonically. It is therefore reasonable to expect that an experimentally determined wavelength-dependant correction factor

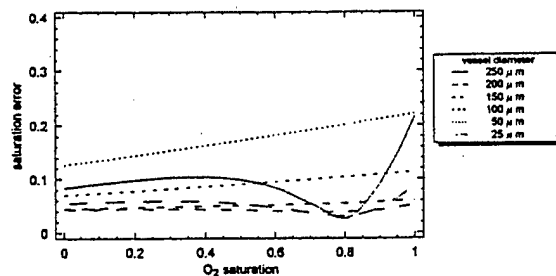


Fig. 8. Error in the three-wavelength saturation calculation for the 488-, 635-, and 905-nm wavelength triad, assuming a 25% scattering loss by the blood vessel. Vessel diameter is indicated in the legend, and the Hb concentration is assumed to be 15 g/100 ml.

could be applied to the transmittance measurements. Or perhaps the 600-, 635-, and 905-nm triad (see Fig. 7) might be considered optimum despite its larger associated errors. The limited wavelength range could minimize spectral variation in RBC scattering and fundus pigmentation.

Finally, the purpose in this paper has been to establish a technique for evaluating the merit of wavelength combinations across a wide range of sample thicknesses and saturations. Although specific wavelength combinations are reported that appear promising for retinal vessel oximetry, the optimization technique is not limited to this application. For example, the technique could be used to find optimum oximetry wavelengths for vessels elsewhere in the body. The technique could also be extended to determine the concentration of other Hb constituents (e.g., methemoglobin).

This study was supported jointly by the U.S. Army Medical Research and Materials Command and by The University of Alabama in Huntsville.

References

1. J. B. Hickam, R. Frayser, and J. C. Ross, "A study of retinal venous blood oxygen saturation in human subjects by photographic means," *Circulation* **27**, 375-385 (1963).
2. A. J. Cohen and R. A. Laing, "Multiple scattering analysis of retinal blood oximetry," *IEEE Trans. Biomed. Eng.* **23**, 391-400 (1976).
3. F. C. Delori, "Noninvasive technique for oximetry of blood in retinal vessels," *Appl. Opt.* **27**, 1113-1125 (1988).
4. D. Schweitzer, L. Leistritz, M. Hammer, M. Scibor, U. Bartsch, and J. Strobel, "Calibration-free measurement of the oxygen saturation in retinal vessels of men," in *Ophthalmic Technologies V*, J.-M. Parel, Q. Ren, and K. M. Joos, eds., *Proc. SPIE* **2393**, 210-218 (1995).
5. J. S. Tiedeman, S. E. Kirk, S. Srinivas, and J. M. Beach, "Retinal oxygen consumption during hyperglycemia in patients with diabetes without retinopathy," *Ophthalmology* **105**, 31-36 (1998).
6. M. H. Smith, K. R. Denninghoff, L. W. Hillman, and R. A. Chipman, "Oxygen saturation measurements of blood in retinal vessels during blood loss," *J. Biomed. Opt.* **3**, 296-303 (1998).
7. K. R. Denninghoff, M. H. Smith, R. A. Chipman, L. W. Hillman, P. M. Jester, C. E. Hughes, F. Kuhn, and L. W. Rue, "Retinal large vessel oxygen saturation correlates with early blood loss and hypoxia in anesthetized swine," *J. Trauma* **43**, 29-34 (1997).
8. O. W. Van Assendelft, *Spectrophotometry of Haemoglobin Derivatives* (Thomas, Springfield, Ill., 1970).
9. V. Twersky, "Multiple scattering of waves and optical phenomena," *J. Opt. Soc. Am.* **52**, 145-171 (1962).
10. V. Twersky, "Absorption and multiple scattering by biological suspensions," *J. Opt. Soc. Am.* **60**, 1084-1093 (1970).
11. R. N. Pittman and B. R. Duling, "A new method for the measurement of percent oxyhemoglobin," *J. Appl. Phys.* **38**, 315-320 (1975).
12. A. L. Lehninger, *Biochemistry* (Worth, New York, 1975).
13. W. J. Geeraets and E. R. Berry, "Ocular spectral characteristics as related to hazards from lasers and other light sources," *Am. J. Ophthalmol.* **66**, 15-20 (1968).

Kurt Denninghoff, MD

An Optical Model of the Blood in Large Retinal Vessels

Kurt R. Denninghoff, M.D.*

Department of Emergency Medicine
University of Alabama at Birmingham

Matthew H. Smith, Ph.D.

Department of Physics
University of Alabama in Huntsville

*Address for Correspondence and reprints:

Kurt Denninghoff, M.D.
Assistant Professor
Department of Emergency Medicine
University of Alabama at Birmingham
JT N. 266, 619 South 19th Street
Birmingham, AL 35233-7013
(205) 975-7458 * FAX (205) 975-4662
kdenning@uabmc.edu

Abstract:

Several optical techniques that investigate blood contained within the retinal vessels are available or under development. We present a mechanical model that simulates the optical properties of the eye, the retinal vessels, and the ocular fundus. A micropipette is chosen as the retinal vessel model, and a mechanical housing is constructed to simulate the eyeball. Spectralon is used to simulate the retinal layers. Filling the eye with fluid index matched to the glass pipette eliminates reflection and refraction effects from the pipette. An apparatus is constructed and used to set the oxygen, nitrogen, and carbon dioxide concentrations in whole human blood. These whole blood samples are pumped through the pipette at 34 $\mu\text{l}/\text{min}$. Measurements made in the model eye closely resemble measurements made in the human eye. This apparatus is useful for testing systems that optically investigate blood and blood flow in the large retinal vessels.

Key Words: retinal vessels, retinal blood flow, oximetry, non-invasive monitoring, tissue phantoms

Introduction:

Several optical techniques that investigate the arteries and veins of the retina are either commercially available or are under development. These techniques include retinal Doppler flowmetry[1], large retinal vessel spectroscopic blood oximetry[2-6] and dynamic measurements of blood vessel pulsations[7]. The optical accessibility of the retina facilitates these techniques, however getting light into and out of the eye presents several interesting problems. Some of these challenges include pigment variability in the retina, lens cataracts, vessel shape, vessel proximity, and large choroidal vessels.

We present an inexpensive mechanical model that simulates the optical geometry of the eye, the blood flowing in a retinal vessel, and the diffuse reflectance properties of the ocular fundus. We also describe an apparatus used to set the hemoglobin concentration and oxygen saturation of a blood sample without affecting the geometry of the red blood cells (and thus the scattering properties of the blood). The model is used to increase understanding of the scattering and absorption effects of the flowing blood, but the model does not include such confounding effects as the polarization influences of the cornea and nerve fiber layer, the optical properties of the vessel wall, the irregular choroidal blood vessels beneath the retinal pigmented epithelium, and the scattering properties of the crystalline lens or vitreous.

Materials and Methods:

A 5 μ l micropipette (Fisherbrand disposable micropipettes, Cat. # 21-164-2B, Fisher Scientific) was chosen as the retinal vessel model. The 10 cm length facilitated mounting and

grasping, and the 268 μm inner-diameter is slightly larger than the largest retinal veins(212 μm) and arteries(150 μm).[7] To more closely approximate these dimensions, the pipettes were gently pulled on a lathe while softened with a Bunsen burner. The resulting tapered pipettes had inner diameters ranging from 110 to 268 μm .

These micropipettes are manufactured from a borosilicate glass with a nominal refractive index of $n_d = 1.4712$. As a result, the pipette acts as a powerful cylindrical lens, and this optical power must be removed in order to be useful as a model. Standard Type A immersion oil (Cargille Laboratories, Cedar Grove, NJ) was purchased as an inexpensive replacement for more expensive index matching fluids. The index of Type A oil is $n_d = 1.5150$, which is slightly too high to provide a good index match to the pipettes. We titrated the Type A oil with mineral spirits ($n_d = 1.438$ as measured by an Abbe refractometer) and index matched the pipette such that it was completely invisible to visual inspection when immersed in the fluid.

We used a slab of Spectralon (Labsphere, Inc.) adhered to an aluminum plate as a tissue phantom simulating the retinal layers. Spectralon is a diffusely reflective, spectrally neutral material typically used in integrating spheres. By modifying the thickness of the Spectralon slab, we were able to control the size of the diffusion-enlarged point spread function on the simulated retina. We use a 4 mm thick slab of Spectralon that results in a diffusion enlarged point spread function (PSF) that is $\sim 40 \mu\text{m}$ FWHM. This compares well with estimated retinal PSFs for visible wavelengths reported in the literature.[8] Using thicker slabs of Spectralon results in larger PSFs. Alternately, other researchers have suggested latex microspheres suspended in epoxy as a useful phantom to simulate the diffuse reflectance properties of tissues.[9,10]

We constructed a mechanical housing which simulates the eyeball (See Fig. 1). The housing is filled with the index matching fluid. A plano-convex lens (Royln Optics, #10.0025) adhered to the housing with MIL-Bond is used to simulate the cornea. This lens has a focal length of 17.2 mm in air, but closely approximates the 23 mm focal length of the average human eye when the planar side of the lens is immersed in the index matched fluid. The entrance pupil diameter was set to 6 mm. The center of the pipette is located 22.6 mm behind the planar surface of the lens, and the Spectralon slab is positioned directly behind the pipette. An infinitely distant object that subtends 1° will form an $294\ \mu\text{m}$ image on the retina of the model eye. This corresponds closely to the typical magnification ($297\ \mu\text{m}$ per degree) of the normal human eye.[11] The model eye was constructed such that the pipettes could be positioned in various locations both on-axis and off-axis since the major vessels of the human eye are approximately 15° off-axis. Bead blasting and black anodizing the inside of the mechanical housing prevents multiple reflections within the eye from exiting the pupil.

To simulate blood flow through the retinal vessel, a syringe pump (Harvard Apparatus, Model # 55-1111) was used to pump whole human blood through a short length of tubing, and through the pipette. The pump was set to deliver blood at a typical value of retinal blood flow ($34\ \mu\text{l}/\text{min}.$).[12] A catch basin collected the blood after it passed through the eye and was disposed of via approved methods.

Preparation of blood samples was carefully conducted to assure that a single variable was being modified throughout a given test. Whole human blood (500 cc) was drawn from a healthy donor according to an Internal Review Board (IRB) approved protocol. The blood was

anticoagulated (citrate dextrose) to prevent clotting during the measurement. The anticoagulant is not expected to affect the scattering measurement since it does not alter the red blood cell size or shape, and its small volume fraction will not significantly alter either the refractive indices of the components or their relative concentrations. The whole blood was immediately packed in ice and samples were drawn and prepared as needed. A sample of blood was centrifuged for approximately 5 minutes to separate the plasma from the cellular component of the blood. The packed blood cells and plasma were mixed volumetrically to make different concentrations of blood cells in plasma. The use of the patient's own plasma to dilute the blood minimizes changes in the size and shape of the red blood cells and possible color changes which may occur when isotonic salt solutions are used to dilute the blood.

A three-gas mixer was used to individually set the oxygen, nitrogen and carbon dioxide concentrations of a combined gas. The total flow rate for the gas mixture was set at three liters per minute. The CO₂ flow was adjusted (~0.1 l/min.) to ensure the partial pressure of CO₂ in the blood was maintained at 35-45 mmHg, as measured by a blood gas machine (Corning 280 pH / Blood Gas Analyzer). The ratio between N₂ and O₂ flow rates was varied in order to set the oxygen saturation of the blood sample. This gas mixture was bubbled through a warm water bath saturating the gas with water vapor and warming it to body temperature. The warmed, humidified gas mixture was passed over the blood sample in a counter current exchange system as the blood was pumped through a closed circuit. A subsection of the blood circuit tubing was passed through a warm water bath (39° C) to keep it at body temperature during the oxygenation procedure. The blood was pumped through the system at a rate of 1000 ml/hour. This system is illustrated in

Figure 2. The blood was allowed to flow through the circuit for as long as is required to obtain the desired oxyhemoglobin saturation level, generally about 15 minutes. We used a CO-Oximeter (Corning 2500 CO-Oximeter) to measure the oxygen saturation and hemoglobin concentration of the prepared blood samples.

Results:

Our primary purpose for developing this model was to test a scanning laser retinal vessel oximeter that we are developing.[4,5,6] The Eye Oximeter (EOX) shines low-power lasers into a subject's eye, and scans the beams across the retinal vasculature. The light that is scattered back out of the eye is collected and analyzed. Performing this measurement at multiple wavelengths allows spectroscopic determination of the oxygen saturation of blood contained within the arteries and veins of the retina. In Figure 3, we compare EOX scans acquired from a human eye to scans acquired from the model eye. These scans are one-dimension profiles of the collected intensity as a beam is scanned perpendicularly across the vessel. The similarity between the scans is obvious. The primary difference between the scans is that those acquired from the model eye have uniform intensity in regions lateral to the vessel, while human scans can be quite irregular in regions lateral to the vessel due to underlying choroidal vessels and variations in retinal pigmentation.

In a recent set of experiments [13], we used this model eye apparatus to calibrate a four-wavelength version of the EOX. We generated an array of blood samples with oxygen saturation values ranging from 6 to 87 %O₂Sat and hemoglobin concentrations ranging from 5.0 to 27.2 g/dl, and we used a variety of vessels with diameters ranging from 110 to 268 μ m. A total of 187 different combinations were generated. This large array of known samples was used to develop

equations that allow that accurate calculation of oxygen saturation. For demonstration, we show the results this calibration experiment in Figure 4.

Discussion and Conclusions:

By using the model eye and blood preparation system described in this paper, we were able to develop an increased understanding of oximetry in the ophthalmic environment. This system is useful for testing systems that use light to study the blood and blood flow in retinal vessels. Such systems include fluorescent dye photography, laser doppler flow experiments, and spectroscopic studies of blood constituents.

In this model we did not attempt to model the coloration of the retina (pigment epithelium), the choroidal circulation (an absorptive and scattering function as apposed to simply scattering with Spectralon), scattering from the lens and vitreous, and the vessel wall (a vessel wall in water as apposed to a pipette in index matching solutions). These interactions make the eye a complex environment, and we used this in an attempt to decrease the number of these variables. As we increase our understanding of the light-eye interaction, these more complex models will likely be required for further hypothesis testing. An extension of this work will be the creation of phantoms that model both the scattering properties and the coloration of the human ocular fundus. Alternately, human retinal tissue samples embedded in epoxy might prove to be ultimate model for this system. Another improvement that should be made to the mode is the inclusion of an adjustable pupil diameter. Simulating the vessel wall and scattering from the lens and vitreous will prove to be more challenging, and we currently have no plans to attempt these models.

A good *in vitro* model is imperative in the development of noninvasive techniques for measuring physiologic parameters. This is particularly true in the retina because actual values of the parameters being measured often cannot be measured directly for comparison. The inexpensive model described here has proven invaluable for advancing our understanding of retinal vessel oximetry.

Acknowledgments:

The authors thank J. E. Drewes for his help designing and constructing the model eye. We gratefully acknowledge the financial support for this work by the U.S. Army Medical Research and Materials Command (DAMD# 17-98-1-8007) and by the Office of Naval Research (ONR# N00014-99-1-0226).

References:

1. A. Harris, L. Kagemann, G.A. Cioffi, "Assessment of human ocular hemodynamics," *Survey of Ophthalmology* 42(6), 509-533 (1998).
2. D. Schweitzer, M. Hammer, M. Scibor, "Imaging spectrometry in ophthalmology-- principle and applications in microcirculation and in investigation of pigments," *Ophthalmic Research* 28 Suppl 2, 37-44 (1996).
3. J.M. Beach, K.J. Schwenzer, S. Srinivas, D. Kim, J.S. Tiedeman, "Oximetry of retinal vessels by dual-wavelength imaging: calibration and influence of pigmentation," *Journal of Applied Physiology* 86(2), 748-758 (1999).
4. K.R. Denninghoff, M.H. Smith, R.A. Chipman, L.W. Hillman, P.M. Jester, C.E. Hughes, F. Kuhn, L.W. Rue, "Retinal large vessel oxygen saturations correlate with early blood loss and hypoxia in anesthetized swine," *Journal of Trauma-Injury Infection & Critical Care* 43(1), 29-34 (1997).
5. M.H. Smith, K.R. Denninghoff, L.W. Hillman, C.E. Hughes, T.E. Minnich, R.A. Chipman, "Technique for noninvasive monitoring of blood loss via oxygen saturation measurements in the eye," *Invited Paper in Optical Diagnostics of Biological Fluids II, Prezzhev AV, Asakura T Eds., Proc. SPIE* 2982, 46-52 (1997).
6. K.R. Denninghoff, M.H. Smith, L.W. Hillman, D. Redden, L.W. Rue, "Retinal venous oxygen saturation correlates with blood volume," *Academic Emergency Medicine* 5(6), 577-582 (1998).

7. H.C. Chen, V. Patel, J. Wiek, S.M. Rassam, E.M. Kohner, "Vessel Diameter Changes during the cardiac cycle," *Eye* **8**, 97-103 (1994).
8. I.J. Hodgkinson, P.B. Greer, A.C. Molteno, "Point-spread function for light scattered in the human ocular fundus," *Journal of the Optical Society of America A-Optics & Image Science* **11**(2), 479-486 (1994).
9. P. Danilova, S.P. Chernova, A.B. Pravdin, "Tissue-like phantoms: fluorescence under 405 nm excitation," *Saratov Fall Meeting 1998: Light Scattering Technologies for Mechanics, Biomedicine, and Material Science*, Valery V. Tuchin, Vladimir P. Ryabukho, Dmitry A. Zimnyakov, Eds., *Proc. SPIE* **3726**, 410-414 (1999).
10. S.T. Flock, B.C. Wilson, M.S. Patterson, "Total attenuation coefficients and scattering phase functions of tissues and phantom materials at 633 nm," *Medical Physics* **14**(5), 835-841 (1987).
11. D. Sliney, M. Wolbarsht, "Safety with Lasers and Other Optical Sources," Chap. 3, *Plenum Press, New York*, 1980.
12. T.F. Gilbert, T. Hiroshi, D.M. Deupree, D.G. Goger, J. Sebag, J.J. Weiter, "Blood Flow in the Normal Human Retina," *Investigative Ophthalmology and Visual Science* **30**, 58-65 1989.
13. J. D. Drewes, M. H. Smith, D. R. Denninghoff, L. W. Hillman, "An Instrument for the Measurement of Retinal Vessel Oxygen Saturation," in *Optical Diagnostics of Biological Fluids IV*, Alexander V. Priezzhev, M. V. Lomonosov, Toshimitsu Asakura, eds., *Proceedings of SPIE* **3591**, 114-120 (1999).

Figure 1:

Schematic of the model eye and blood vessel. A pipette filled with whole blood is immersed in index matched fluid and positioned in front of a piece of Spectralon. A plano-convex lens simulates the refractive power of the cornea and lens. Incoming rays from infinitely distant objects that are on-axis and 5° off-axis are shown.

FIGURE 1:

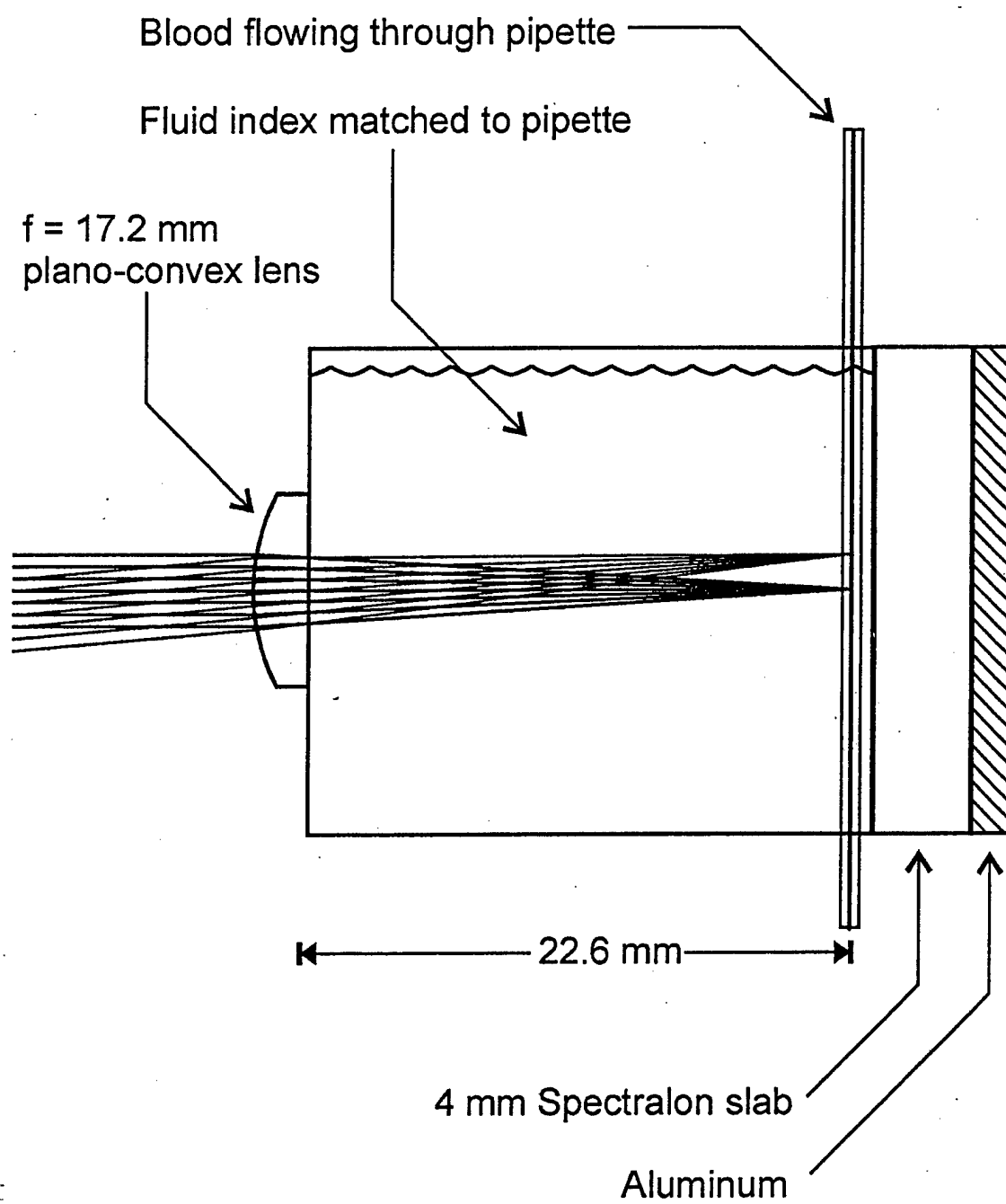


Figure 2:

Schematic of the apparatus for setting the oxygen saturation of whole blood. The apparatus allows the CO₂, O₂, and N₂ gas levels to be set while keeping the blood hydrated and at body temperature.

FIGURE 2:

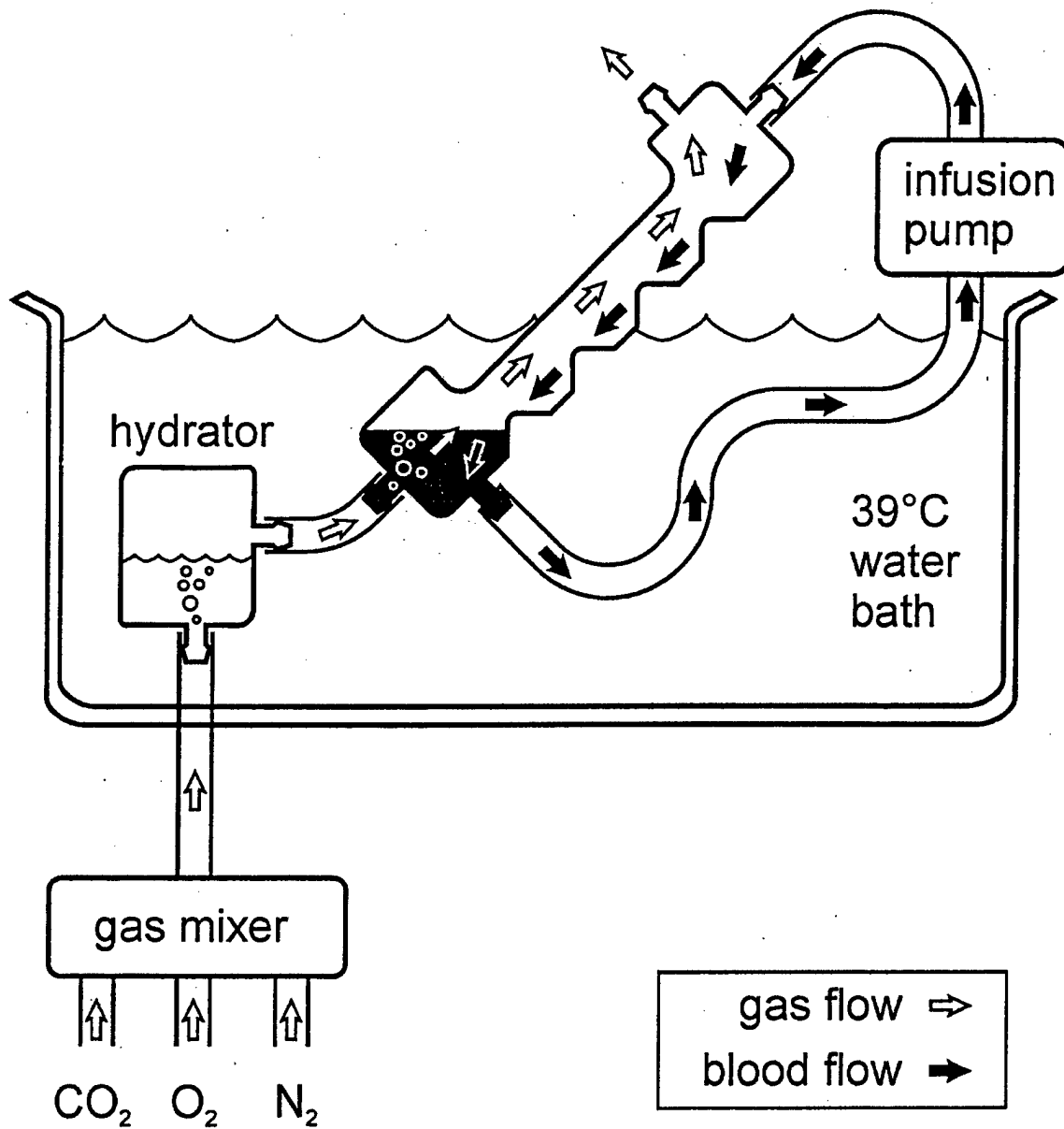


Figure 3:

Comparison of one-dimensional retinal vessel intensity profiles. The scan on the left was acquired in the model eye and the scan on the right was acquired in a human eye. Note the decreased noise in the model eye scan that is due to the high reflectivity of Spectralon.

FIGURE 3:

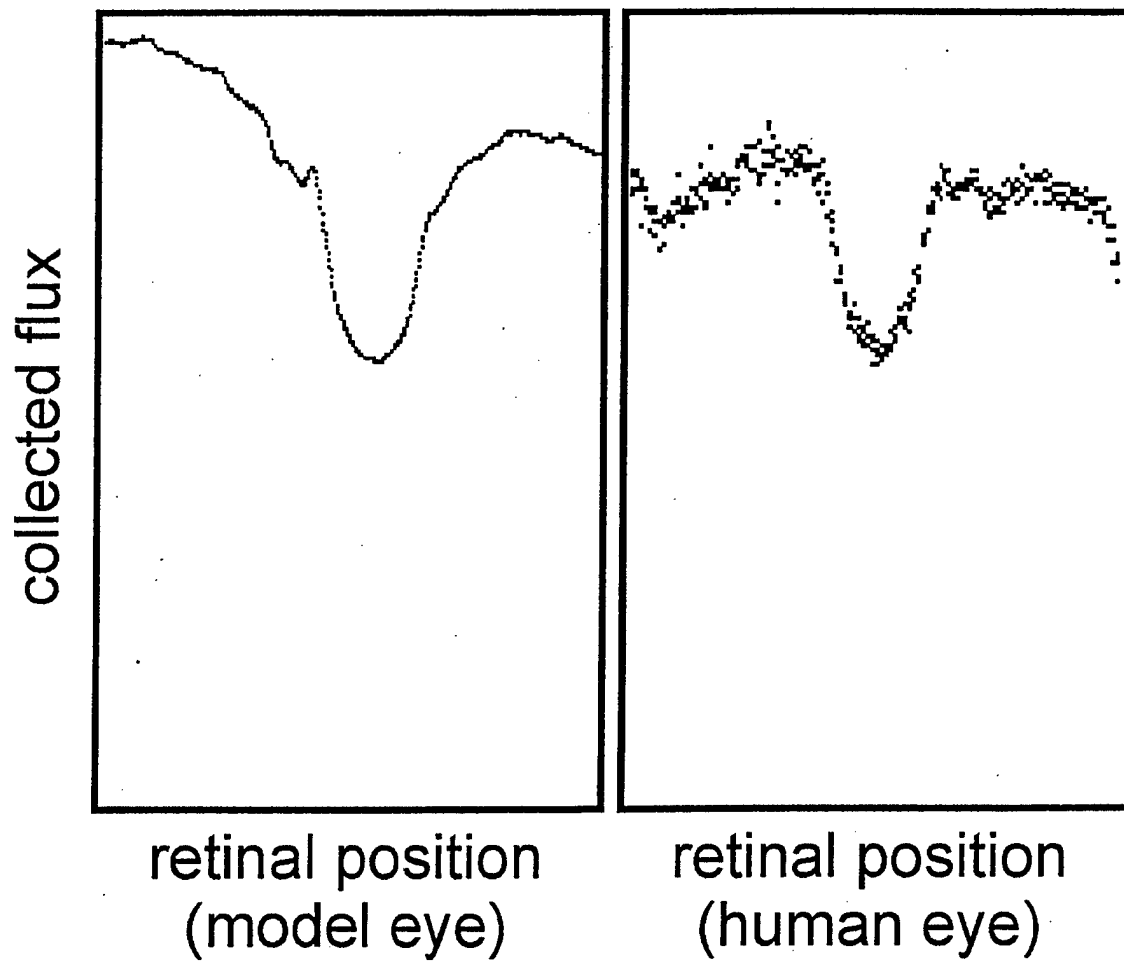
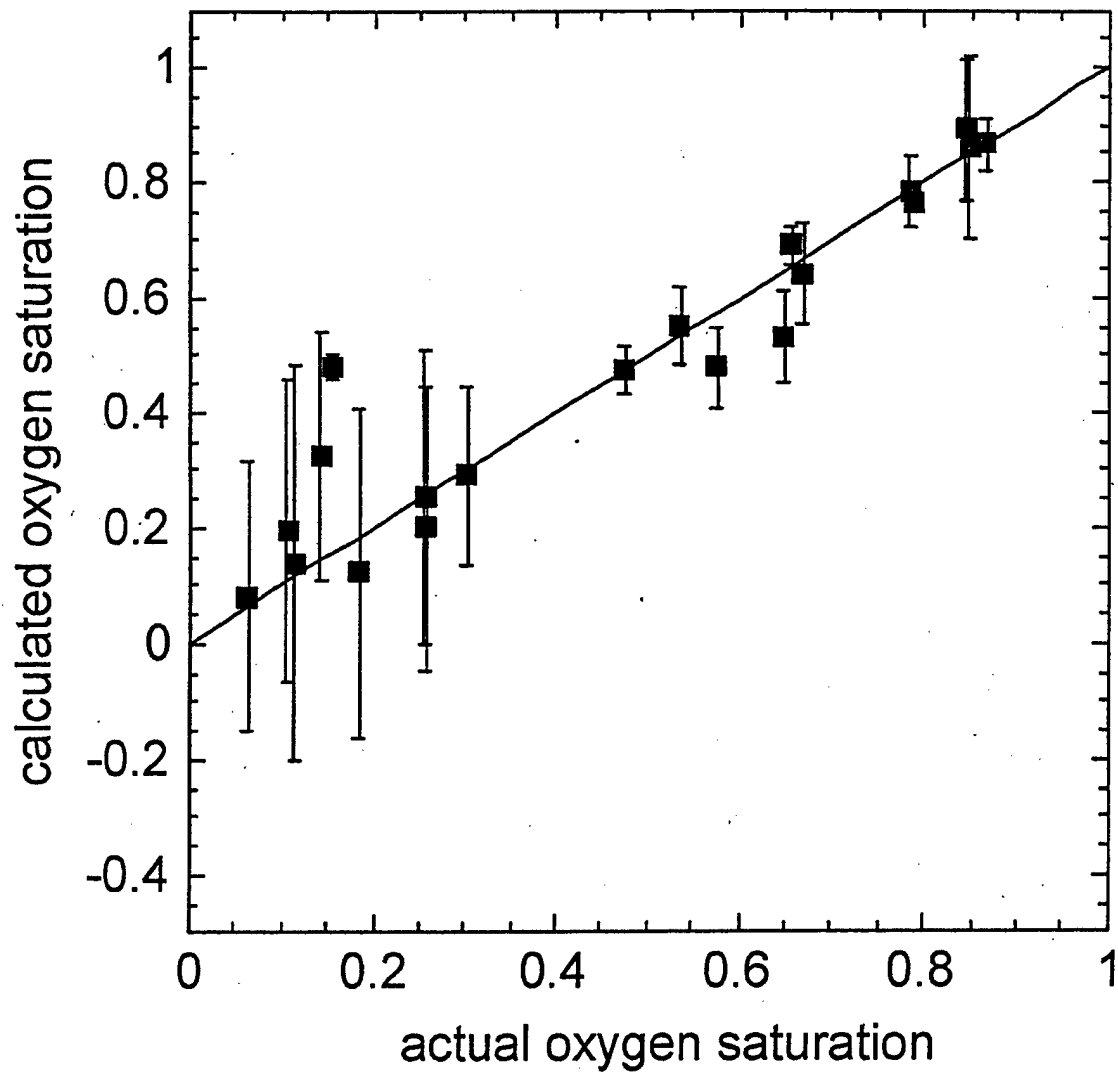


Figure 4:

Example of data acquired in the model eye. This graph is the result of the Eye Oximeter calibration experiment described in Ref. 13. Each data point represents a blood sample with different oxygen saturation and hemoglobin concentration. The error bars indicate the standard deviation of measurements made at different vessel diameters ranging from 110 to 268 μm .

FIGURE 4:



Retinal vessel oximetry: Toward absolute calibration

Matthew H. Smith^{*a}, Kurt R. Denninghoff^b, Arthur Lompadó^a, Lloyd W. Hillman^a

^aDept. of Physics, The Univ. of Alabama in Huntsville, Huntsville, AL 35899

^bDept. of Emergency Medicine, The Univ. of Alabama at Birmingham, Birmingham, AL 35226

ABSTRACT

Accurately measuring the oxygen saturation of blood within retinal arteries and veins has proven to be a deceptively difficult task. Despite the excellent optical accessibility of the vessels and a wide range of reported instrumentation, we are unaware of any measurement technique that has proven to be calibrated across wide ranges of vessel diameter and fundus pigmentation. We present an overview of our retinal oximetry technique, present the results of an *in vitro* calibration experiment, and present preliminary human data.

Keywords: oxygen saturation, spectroscopy, ophthalmic instrumentation, retina

INTRODUCTION

There are numerous clinical applications for measurements of the oxygen saturation of the blood within the arteries and veins of the retina. These applications range from the identification of patients at risk for glaucoma and diabetic retinopathy to the detection of internal bleeding in trauma victims. Additionally, the eye is a particularly attractive noninvasive monitoring site since the blood vessels of the retina are not obscured by thick layers of highly scattering tissue. Given this optical accessibility, it is tempting to expect that spectroscopic analysis of the blood within retinal vessels should allow straightforward determination of the oxygen saturation. However, despite nearly continuous work in the field of retinal vessel oximetry more than 30 years, no technique has proven sufficiently accurate and repeatable to be commercialized.

Retinal vessel oximetry was pioneered in 1963 by Hickham & Frayser¹. Their system was a modified fundus camera that acquired dual quasi-monochromatic fundus photographs. Oxygen saturation was measured by analyzing the optical density of the vessel images at each wavelength, and using oximetry equations² based on the Lambert-Beer Law. Improvements to this fundus photography technique have been offered by Cohen and Laing³, and by Tiedeman, Beach, *et. al.*⁴. The latter has recently identified the influence of fundus reflectivity on these measurements⁵. In addition to photographic retinal oximeters, systems have been developed that scan monochromatic beams across the retinal vasculature and collect the light that is scattered back out of the eye. The earliest scanning oximeter was developed by Delori⁶, and recent advancements have been made by Smith, Denninghoff, *et. al.*^{7,8}. Finally, a retinal oximeter under development by Schweitzer, *et. al.*⁹ uses a diffraction grating and is capable of measuring the full spectrum of a retinal blood vessel in 2 nm increments from 400 to 700 nm.

One of the first hurdles that must be overcome in retinal vessel oximetry is the difficulty of getting light into and back out of a subject's eye. An instrument must be critically aligned to the subject's pupil. This alignment is relatively easy with a chin rest, forehead strap, and fixation target as used in an optometrist's or ophthalmologist's office. This alignment is much more challenging if a hand-held instrument is needed, as might be the case in a primary-care physician's office or in the trauma bay of an emergency department. These engineering challenges can be overcome, and hand-held fundus cameras and scanning laser ophthalmoscopes are now commercially available.

Once the engineering challenges of getting light into and back out of the eye are overcome, there are still several design tradeoffs that must be considered in retinal vessel oximetry.

1. WAVELENGTH TRADEOFFS

^{*}Correspondence: Email: SmithMH@email.uah.edu; WWW: <http://www.osig.uah.edu>

There are several tradeoffs that influence the design of a retinal vessel oximeter. Two of these tradeoffs are the number of wavelengths used in the measurement, and which wavelengths are chosen. We consider these tradeoffs individually below.

1.1. Number of wavelengths

At its heart, retinal vessel oximetry involves performing a least-squares fit of an oximetry equation to measured transmittance data. The oximetry equation will have several unknown parameters that are to be determined via the regression. As an example, the oxygen saturation s , the hemoglobin concentration and vessel diameter product cd , and a scattering coefficient T_s might be unknown. At a minimum, an oximeter must include as many wavelengths as there are unknown parameters. To reduce the uncertainty in the regressed parameters, it is desirable to increase the number of wavelengths used in the measurement.

The advantages of using a large number of wavelengths are reduced due to the *ultimate* design criterion of a retinal vessel oximeter, that is, that the light levels directed into the eye must be kept below safe levels¹⁰. Each additional wavelength increases retinal exposure. As more wavelengths are added, the optical power of each wavelength must be reduced thereby reducing the single-to-noise ratio. In a design solution, a balance must be struck between the desire to use in many wavelengths for analysis purposes, and the desire to use few wavelengths for signal-to-noise improvements.

1.2. Choice of wavelengths

Once it is determined how many wavelengths will be used for analysis, one must determine which wavelengths will be used. Safety issues preclude the use of wavelengths shorter than 400 nm, and wavelengths longer than about 1200 nm are absorbed by the eye. We have previously reported a technique for selecting optimum wavelength combinations for retinal vessel oximetry¹¹. This technique is based on selecting wavelengths they yield small errors in calculated saturation due to measurement errors in vessel transmittance. Careful selection results in saturation errors that are acceptably small across broad ranges of vessel diameter, hemoglobin concentration, and oxygen saturation. For example, we find that the wavelength combination of 488, 635, 670, and 830 nm results in highly accurate oxygen saturation calculations across a wide range of vessel diameters, as indicated in Fig. 1.

While this wavelength combination, spanning from 488 to 830 nm, results in excellent sensitivity to oxygen saturation, it is not necessarily an optimum combination. Particularly, this large wavelength range exceeds the optimum wavelength range of most commercially available achromatic lenses and antireflective coatings. In addition, this wavelength range nearly exceeds the spectral responses of photomultiplier tubes and avalanche photodiodes. Perhaps the most compelling reason to decrease this wavelength range, is that the fundus reflectivity varies significantly across this range¹². Because fundus reflectivity influences the calibration of a retinal vessel oximeter, it would be desirable to choose wavelengths that are closer together if adequate sensitivity to oxygen saturation could be achieved.

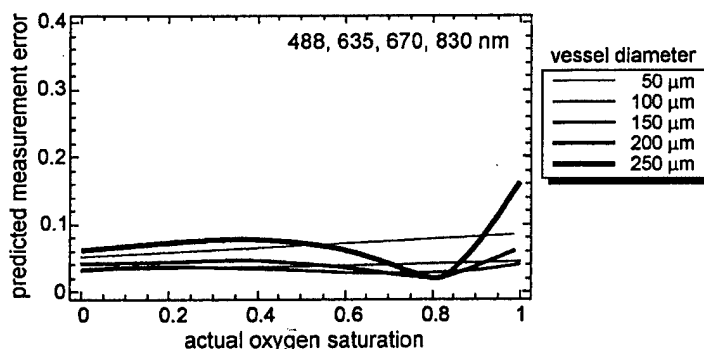


Figure 1. Predicted measurement error in oxygen saturation for the 488, 635, 670, 488 nm wavelength combination. A hemoglobin concentration of 15 g/dl is assumed.

2. THE EYE OXIMETER

2.1. Instrumentation

Our research group has been developing retinal vessel oximeters since 1993, and we are currently testing our Second-Generation Eye Oximeter (EOX-2)¹³. The EOX-2 is based around the existing technology of a scanning laser ophthalmoscope (SLO). A video image of a subject's ocular fundus is acquired by raster-scanning an infrared laser beam across the back of the eye. Laser powers are kept well below the Class I laser limits, and therefore pose no known risk to the eye. Once the retinal features of interest are in the field of view, as determined by an operator, the measurement sequence is initiated. The next available video frame of the scanning system is used for the measurement. Five laser wavelengths (488, 635, 670, 752, and 830 nm) are then multiplexed into this measurement frame. The wavelength multiplexing is achieved as follows: The first scan line of the measurement frame is acquired at a single laser wavelength, the second scan line is acquired at a different laser wavelength, the third line at another wavelength, etc. Once the last measurement wavelength is reached, the system returns to the first wavelength and the process is repeated until all of the scan lines within the video frame have been measured. This acquired video frame contains a number of interlaced monochromatic images.

While the EOX-2 is in targeting mode, the subject can see a faint rectangle of light that is slightly reddish. This rectangle is the result of the infrared beam being raster-scanned across the retina. The rectangle is not bright enough to cause any pupillary constriction of the subjects eye. When the measurement frame is acquired, the subject observes the faint red rectangle to flash white. This white flash is the result of the red and blue lasers firing in rapid succession, and the flash is not uncomfortable. The 67 ms length of the flash is far below the human reaction time of 250 ms, and as such a patient's eye does not typically move until well after the flash is over.

The data is post processed. An operator identifies the desired arteries and veins in the scans. Comparing the light reflected from the vessel to the light reflected from the fundus lateral to the vessel yields transmittance values of the blood within the vessel at each wavelength. These transmittance values are used in our oximetry equations to calculate the oxygen saturation of the blood within the vessels.

2.2. Technique

There are two separate challenges associated with accurately calculating oxygen saturation. The first challenge is measuring the transmittance of the blood vessel in a manner that is not affected by local variations in fundus pigmentation or by glints from the apex of the blood vessel. The second challenge is to develop an oximetry equation that accurately models the light paths associated with making the measurement and that can be used to calculate oxygen saturation. These two issues are addressed separately below.

Figure 2 contains two images acquired with the EOX-2. The image on the left is similar to images acquired by standard scanning laser ophthalmoscopes. The severe reflection observed along the apex of these vessels prevent accurate measurements of the vessel transmittance. The image on the right was acquired by illuminating the retina with vertically polarized light and collecting only horizontally polarized light. Because light that is specularly reflected tends to maintain its polarization state, the glints from the vessel apex is blocked by the crossed polarizer. As such, the image is relatively free of glints.

Figure 3 illustrates our technique for measuring the transmittance, T , of a retinal vessel. The transmittance is defined as $T = \Phi_v / \Phi_f$, where Φ_v is the collected flux from the center of the vessel, and Φ_f is an approximation of the flux that would have been collected from that location in the absence of the vessel. We currently use a linear approximation to determine Φ_f . By acquiring numerous scans along the length of a vessel, we average out any irregularities in fundus pigmentation that could cause systematic errors in our measurement. We measure the transmittance of a vessel at each of our measurement wavelengths. We then fit our oximetry equation to these five transmittance values in order to calculate the oxygen saturation.

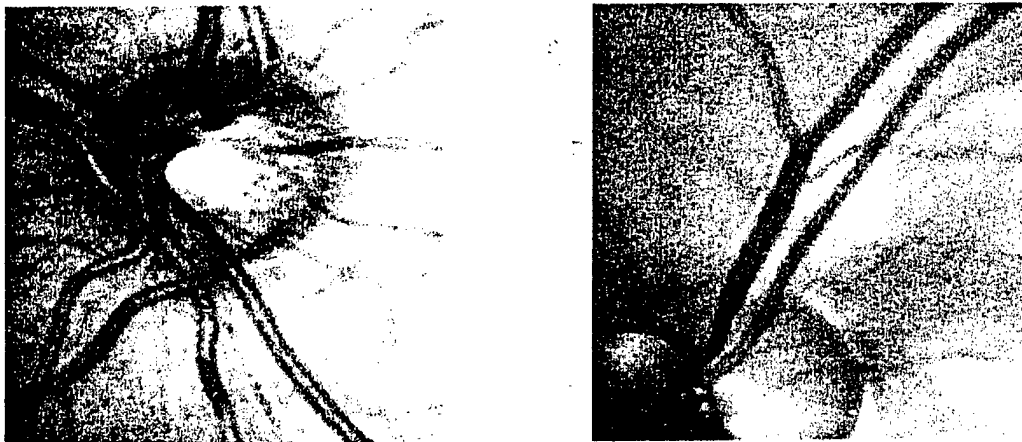


Figure 2. Images acquired with the EOX-2. The image on the right was acquired using crossed polarizers that reduced the glints along the vessel centers.

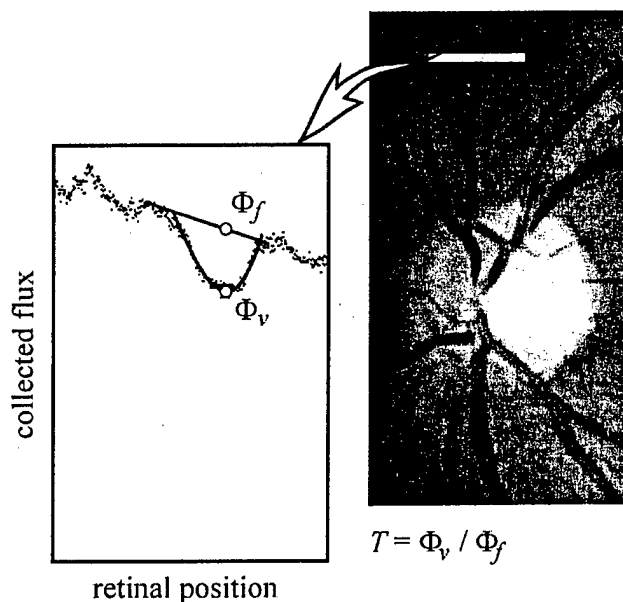


Figure 3. To measure the transmittance of a retinal vessel, we divide the flux collected from the center of the vessel by the estimated flux from the fundus underlying the vessel.

3. LIGHT PATHS

We have recently reported¹⁴ a description of the light paths that comprise a retinal vessel oximetry measurement. From our understanding of these light paths, we developed an oximetry equation that can be used to calculate the oxygen saturation of blood in retinal vessels. We summarize these results below.

A beam of light with flux Φ_o is directed into the pupil of the eye and is focused onto a retinal vessel. A retinal vessel oximeter system then collects the fraction of light that is reflected back out of the pupil of the eye. There are several light paths that contribute to this collected power. First, some quantity Φ_{media} of the incident flux may directly backscatter from the lens or vitreous and be collected. Next, there is a specular reflection from the apex of the vessel, Φ_{glint} , that may exit the pupil and be

collected. This reflection may originate from the inner limiting membrane¹⁵ or from the vessel wall, but any portion of this glint that is caused by backscattering from blood within the vessel is considered in a separate term, Φ_{bs} , below. As the incident beam propagates through the blood within the vessel, the flux of the beam is decreased via the Lambert-Beer Law due to absorption by hemoglobin and oxyhemoglobin within the red blood cells (RBCs). Additionally, light is scattered by the RBCs. Some quantity of this scattered light, Φ_s , is scattered into angles that cannot be collected by the instrument, causing an apparent *increase* in absorption. There is another quantity of light, Φ_{bs} , that is directly backscattered toward the instrument, resulting in an apparent *decrease* in absorption.

The beam that emerges from the other side of the vessel is enlarged due to scattering and attenuated due to absorption. The beam traverses the transparent rods and cones of the retina and finally reaches the scattering layers of the retinal pigment epithelium (RPE) and choroidal plexus that are $\sim 240 \mu\text{m}$ posterior to the vessel. Strong melanin and hemoglobin absorption limits lateral diffusion and result in a tightly localized point spread function (PSF) on the RPE for visible wavelengths shorter than 575 nm. Wavelengths much longer than 575 nm penetrate the choroid deeply, reflecting off of the sclera and passing back through the choroid. As a result, the laterally diffused PSF of these longer wavelengths is much larger than that of shorter wavelengths. Reasonable estimates for the width (twice the standard deviation) of the diffusion enlarged PSF in the nasal fundus (near the optic nerve head) have been reported to be $\sim 60 \mu\text{m}$ from 450 to 575 nm and $\sim 150 \mu\text{m}$ from 600 to 750 nm¹⁶. A fraction of the light, Φ_{dp} , within this diffused PSF will pass back through the vessel to be absorbed and scattered in double pass, and then exit the pupil of the eye. Additionally, a fraction, Φ_{sp} , will extend beyond the edge of the vessel and exit the pupil of the eye in single pass. Note that this geometry is specific to a scanning-beam oximeter. In a photographic oximeter geometry, the single pass component, Φ_{sp} , would be incident on the fundus lateral to vessel and reflect out of the eye through the vessel. The resulting oximetry equations derived in the next section, however, should remain the same.

By summing up these light paths, we derive the equation

$$T_v = \left(\alpha + \frac{a_2}{R_f} \right) \exp \left\{ - \left[s \epsilon_{HbO_2} + (1-s) \epsilon_{Hb} \right] cd \right\} + \beta \exp \left\{ -2 \left[s \epsilon_{HbO_2} + (1-s) \epsilon_{Hb} \right] cd \right\} + \frac{a_1}{R_f} \quad (1)$$

where T_v is the measured transmittance of a blood vessel, s is the oxygen saturation of the blood, c is the hemoglobin concentration, d is the vessel diameter, ϵ_{Hb} is the absorption coefficient of reduced hemoglobin, and ϵ_{HbO_2} is the absorption coefficient of oxygenated hemoglobin. The parameters α and β represent the fraction of light transmitted through the vessel in single-pass and double-pass, respectively. The terms a_1 and a_2 are related to the backscattering of light by red blood cells, as described by Anderson, *et al.*¹⁷ for planar slabs of blood. The factor R_f is the reflectivity of the ocular fundus. During a measurement, we directly measure T_v and R_f . Of the remaining parameters, c , d , and s are constants, while ϵ_{Hb} and ϵ_{HbO_2} are experimentally measured functions of wavelength¹⁸. Unfortunately, the parameters α , β , a_1 , and a_2 are complex functions of λ , c and d that are not currently well understood. As such, eq. (1) has not proven to be useful for calculating s given multi-wavelength transmittance measurements.

A simplification of eq. (1) obtained through a series approximation yields the oximetry equation that we are currently using in our measurements:

$$T_v = f(\lambda) T_s \exp \left\{ - \chi(\lambda) cd \left[s \epsilon_{HbO_2}(\lambda) + (1-s) \epsilon_{Hb}(\lambda) \right] \right\} \quad (10)$$

where T_s is a scattering transmittance describing photons lost due to scattering, $f(\lambda)$ is a wavelength-dependence of the scattering transmittance, and $\chi(\lambda)$ is a function of wavelength that acts to change the effective path length through the sample. This equation indicates that the effective path length through the sample can vary with wavelength. While this seems counter-intuitive, experimental evidence indicates that this is in fact the case¹⁴. This effect is a direct consequence of backscattering of light by red blood cells. As the fundus reflectivity decreases, the relative contribution of backscattered light increases, effectively reducing the path length. Our current research efforts are focused on determining $f(\lambda)$ and $\chi(\lambda)$ as functions of fundus reflectivity, R_f .

4. EXPERIMENTAL RESULTS

We have conducted numerous *in vitro* and *in vivo* experiments in an attempt to derive an absolute calibration for retinal vessel oximetry that is accurate across a large range of vessel diameters (d), hemoglobin concentrations (c), and fundus reflectivities (R_f). Our original Eye Oximeter prototype (EOX) used only red and infrared wavelengths (629, 672, 815, and 899 nm) and performed only one-dimensional linear scans across a retinal vessel¹⁹. This wavelength combination led to large random errors ($>50\%O_2\text{Sat}$) in calculated saturation, and the inability to scan along the length of the vessel generally resulted in systematic errors due to local variations in fundus pigmentation. Despite these limitations, we reported a calibration of the EOX in a model eye that was independent of c and d . Studies performed with the EOX in a swine animal model demonstrated strong correlations (typically $r^2 \sim 0.95$) between measured and actual arterial oxygen saturations during graded hypoxia⁸. However, with the EOX we were never able to achieve sufficient accuracy and repeatability in the measurements. In particular, our calibration lines varied between subjects, necessitating an arterial calibration be performed prior to beginning an experiment. Because this calibration had to be performed at low arterial oxygenation levels (less than about $70\%O_2\text{Sat}$), the EOX was not well suited for human clinical studies.

As described in the previous section, our Second Generation Eye Oximeter (EOX-2) overcomes the wavelength and scanning limitations of the original EOX. Below, we present the results of two experiments performed with the EOX-2.

4.1. Model Eye Experiment

We have constructed a model eye that simulates the flow of blood through retinal vessels. To simulate the vessel, whole blood is pumped through micropipettes with inner diameters ranging from 110 to 270 μm . A 3 mm thick slab of Spectralon (LabSphere Inc.) is placed behind the vessel to simulate the laterally diffusing layers of the ocular fundus. This system is immersed in fluid that is index-matched to the pipette in order to eliminate unwanted reflection and refraction effects. A lens is used to give the model the same effective focal length as a typical human eye.

We create whole human blood samples of varying oxygen saturation, s , and hemoglobin concentration, c . We varied s from 0.11 to 1.0, and created samples with Hb concentrations of 8.5, 10, and 13.5 g/dl. These samples are pumped through the pipette, and scans are acquired with the oximeter. We use Eq. (10), to calculate oxygen saturation s , the product cd , and the scattering transmittance T_s . We arbitrarily assigned $f(\lambda)$ and $\chi(\lambda)$ to be *linear* functions of wavelength, and determined values of the slopes and intercepts that yielded acceptable calibrations. Specifically, we found $f(488) = 0.9$ and $f(830) = 1.1$ for the scattering term, and found $\chi(488) = 1.2$ and $\chi(830) = 1$ for the path-length term.

Figure 4 shows the resulting spectra fits to the transmittance measurements of two blood samples, $c = 13.5$ g/dl and $d = 270$ μm . The calculated saturations are 27.1 and 77.0 $\%O_2\text{Sat}$. From Fig. 2, it is easy to see why accurate measurements can be so difficult. Small errors in calculated transmittance lead to large errors in calculated saturation due to the small variations in the

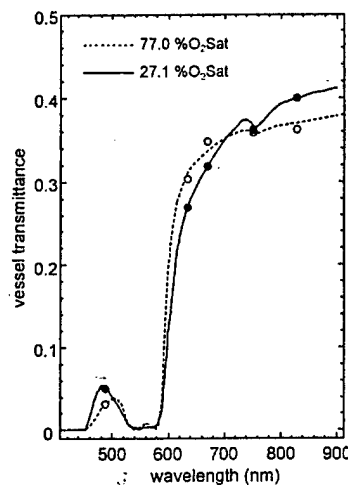


Figure 4. Spectra fit to the measured transmittances from two blood samples in a model retinal vessel.

transmittance spectra at optical wavelengths. Note, however, that the vessel diameter in this experiment was 270 μm , about twice the expected vessel diameter in human eyes. As such, we expect better sensitivity in human measurements.

The results of several measurements at different hemoglobin concentrations are shown in Figure 5. We plot the calculated oxygen saturation versus the known saturation of each sample. As seen from this figure, excellent correlation ($r^2 = 0.968$) was achieved, although a dependence on c is apparent at low saturation, with low hemoglobin concentrations resulting in higher calculated saturations.

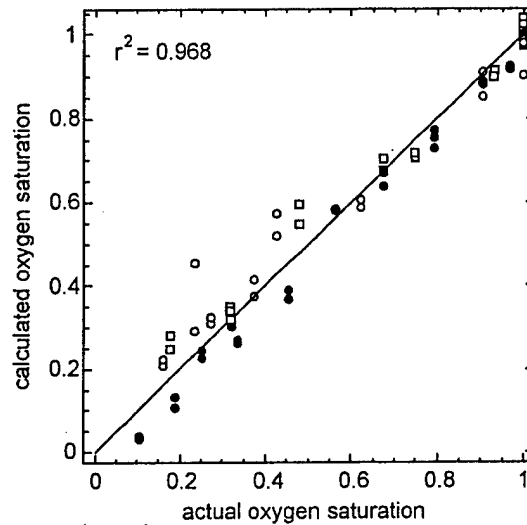


Figure 5. Calibration of the EOX-2 in a model eye. Whole human blood was pumped through a 270 μm pipette to simulate a retinal vessel. Three different hemoglobin concentrations were used (\bullet = 13.5 g/dl, \circ = 10 g/dl, \square = 8.5 g/dl).

In addition to determining the oxygen saturation, we regress values of the hemoglobin concentration and diameter product, cd . Since the pipette diameter and hemoglobin concentrations of the samples are known, we are able to compare regressed and actual values of c . This is useful in verifying that our oximetry equation is properly modeling our experiment. Figure 6 shows the results of this comparison.

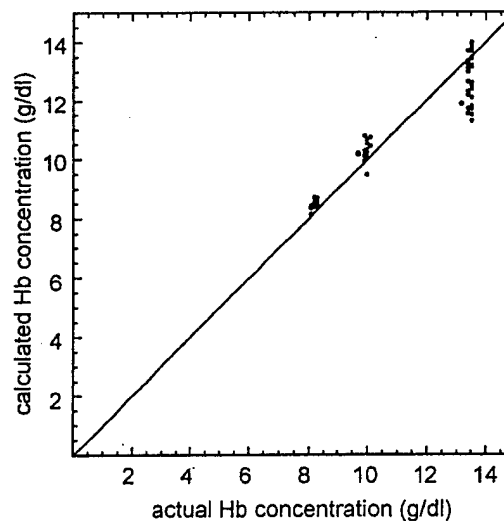


Figure 6. Calibration of the EOX-2 in a model eye. The regressed values of hemoglobin concentration compare well with the actual values of c .

Finally, it is also interesting to note the relationship between scattering losses, T_s , and hemoglobin concentration. We expect scattering losses to be a maximum near a hematocrit of 50%, or a hemoglobin concentration of ~15 g/dl. Additionally, scattering losses would be zero at hematocrits of 0% and 100% (concentrations of 0 g/dl and ~30 g/dl). As shown in Fig. 6, our data tends to support these expectations, however significantly more samples need to be generated before we draw significant conclusions from this data.

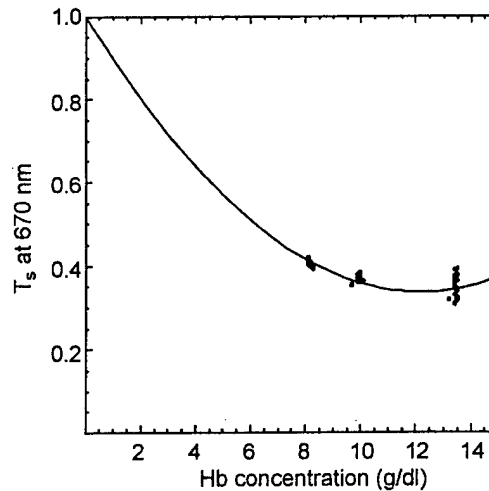


Figure 7. Calibration of the EOX-2. The calculated scattered transmittance is found to vary with hemoglobin concentration as expected.

4.2. Human Measurements

The model eye provides a well-controlled environment for calibrating the EOX-2. In this environment, we are able to test our instrumentation and our oximetry equations, and develop our understanding of the physics behind these measurements. Our next step is to apply this knowledge to animal and human subject. Here, we report our preliminary data from human eyes of three subjects. In each of the three subjects, the EOX-2 was used to simultaneously measure the oxygen saturation of a retinal artery and vein. The results of the three measurements are shown in Fig. 8.

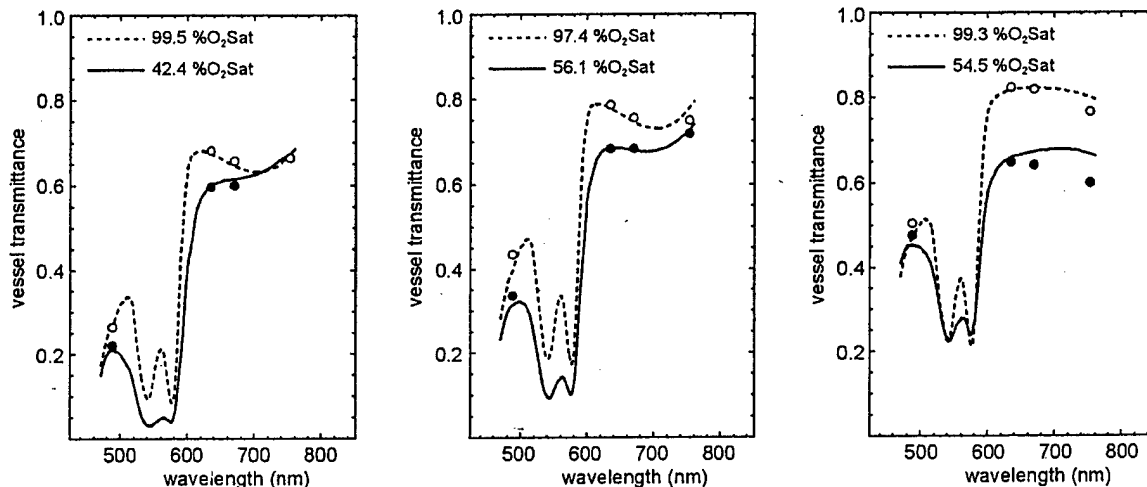


Figure 8. Measurements made with the EOX-2 on retinal arteries and veins of three human subjects. The solid lines and filled circles are venous measurements. The dashed lines and hollow circles are arterial measurements.

The values of $f(\lambda)$ and $\chi(\lambda)$ determined in the model eye experiment did not work in our human scans. In fact, no single set of values could be found that worked for all three subjects. Notice in Fig. 8 that the data set on the right looks significantly different than the other two. This subject had a very blonde fundus compared to the other two subjects, and we expect that variations in fundus reflectance dramatically affects our values of $f(\lambda)$ and $\chi(\lambda)$. Thankfully, the EOX-2 provides relative measurements of fundus reflectivity, and our current research efforts include identifying the relationships between these parameters. For now, however, we simply perform an individual calibration to each subject based on the arterial transmittance measurements and arterial saturations determined from pulse oximeter readings. Based on those calibrations, we measured the oxygen saturation in the largest veins near the optic disk to be between 42%O₂Sat and 56%O₂Sat in our three subjects. These measurements compare well with previously reported values.

5. DISCUSSION AND CONCLUSIONS

Although the model eye is particularly useful in helping us develop and test our instrumentation and our oximetry equations, it is not a perfect model. The two primary weaknesses of the model eye are that it does not model the scattering and reflective properties of the vessel wall, and that it does not model the spectral reflectance, R_p , of the ocular fundus. We intend to generate phantoms that more closely model the coloration of the human retina, but we have no plans to incorporate the vessel wall into the model.

Controlled hypoxia experiments in humans have been reported as a means of calibrating retinal vessel oximeters⁵. Retinal arterial saturation is compared to the known arterial saturation (measured by pulse oximetry or by analysis of drawn arterial samples) as the amount of oxygen supplied to the subject is reduced. Unfortunately, the lowest arterial saturation that can be safely generated is about 70%O₂Sat, which is significantly higher than expected normal venous oxygen saturation. Because venous saturation is more likely a clinically useful measurement, it is important to verify instrument calibration at low saturation levels. Because no technique yet exists that can be used as a reference measurement of retinal venous saturation, this low-saturation calibration will likely need to be performed in animals. We have performed numerous calibration experiments in swine, but we have identified several weaknesses in this model. Particularly, the optical quality of swine corneas and lenses is frequently very bad (depending on the species of swine), and the spectral reflectivity of the swine ocular fundus is very different than that of a human fundus. A pigment exists in the swine fundus that absorbs 635 nm so strongly that we are generally unable to make measurements at that wavelength with the EOX-2.

The difficulties associated with verifying the calibration of retinal saturation measurements in human subjects are significant, and our understanding of the physics comprising the measurement is still incomplete. Nevertheless, continued advancements to the field of retinal vessel oximetry since 1963 have brought the science and technology nearly to the point of a clinical viable technique. We expect that a technique for precisely and accurately measuring retinal vessel oxygen saturation will reach maturity in the next few years.

ACKNOWLEDGMENTS

We thank The Office of Naval Research and The U. S. Army Medical Research and Materials Command for their support of this work.

REFERENCES

1. Hickam J.B., Frayser R., Ross J.C., "A study of retinal venous blood oxygen saturation in human subjects by photographic means," *Circulation* 27, 375 (1963).
2. Van Assendelft, O.W., *Spectrophotometry of Haemoglobin Derivatives* (Charles C. Thomas, Springfield, IL, 1970).
3. Cohen A.J., Laing R.A., "Multiple scattering analysis of retinal blood oximetry," *IEEE Trans. Biomed. Eng.* 23(5), 391 (1976).

4. J. S. Tiedeman, S. E. Kirk, S. Srinivas, J. M. Beach, "Retinal oxygen consumption during hyperglycemia in patients with diabetes without retinopathy," *Ophthalmology* **105**(1), 31-36 (1998).
5. J. M. Beach, K. J. Schwenzer, S. Srinivas, J. S. Tiedeman, "Oximetry of retinal vessels by dual-wavelength imaging: calibration and influence of pigmentation," *J. Appl. Physiol.* **86**(2), 748-758 (1999).
6. Delori F.C., "Noninvasive technique for oximetry of blood in retinal vessels," *Appl. Optics* **27**(6), 1113 (1988).
7. M. H. Smith, K. R. Denninghoff, L. W. Hillman, R. A. Chipman, "Oxygen saturation measurements of blood in retinal vessels during blood loss," *J. Biomed. Optics* **3**(3), 296-303 (1998).
8. K. R. Denninghoff, M. H. Smith, R. A. Chipman, L. W. Hillman, P.M. Jester, F. Kuhn, D. Redden, L. W. Rue, "Retinal venous oxygen saturation correlates with blood volume," *Acad. Emerg. Med.* **5**(6), 577-582 (1998).
9. D. Schweitzer, L. Leistritz, M. Hammer, M. Scibor, U. Bartsch, J. Strobel, "Calibration-free measurement of the oxygen saturation in retinal vessels of men," in *Ophthalmic Technologies V*, Jean-Marie Parel, Qiushi Ren, Karen M. Joos, Editors, Proc. SPIE 2393, 210-218 (1995).
10. *Code of Federal Regulations*, Title 21, Food and Drugs, Part 1040.10, Performance Standards for Light-Emitting Products, laser products (U.S. Government Printing Office, 1998).
11. M. H. Smith, "Optimum wavelength selection for retinal vessel oximetry," *Appl. Optics* **38**(1), 258-267 (1999).
12. Delori F.C., Pflibsen K.P., "Spectral reflectance of the human ocular fundus," *Appl. Optics* **28**(6), 1061-1077 (1989).
13. A. Lompadó, M. H. Smith, K. R. Denninghoff, L. W. Hillman, "Multispectral confocal scanning laser ophthalmoscope for retinal vessel oximetry," in *Spectral imaging: Instrumentation, applications, and analysis*, G. H. Bearman, D. Cabib, R. M. Levenson, eds., *Proceedings of SPIE* Vol. 3920, (2000).
14. M. H. Smith, K. R. Denninghoff, A. Lompadó, L. W. Hillman, "Effect of multiple light paths on retinal vessel oximetry," *Appl. Opt.* (In press).
15. F. C. Delori, E. S. Gragoudas, R. C. Pruett, "Monochromatic ophthalmoscopy and fundus photography: The normal fundus," *Arch. Ophthalmol.* **95**, 861-868 (1977).
16. I. J. Hodgkinson, P.B. Greer, A. C. B. Molteno, "Point-spread function for light scattered in the human ocular fundus," *J. Opt. Soc. Am. A* **11**(2), 479-486 (1994).
17. N. M. Anderson, P. Sekelj, "Reflection and transmission of light by thin films of nonhaemolysed blood," *Phys. Med. Biol.* **12**(2), 185- 192 (1967).
18. S. Pahl has compiled data of hemoglobin extinction coefficients from several investigators. The data is available at <http://omlc.ogi.edu/spectra/hemoglobin/index.html>
19. J. J. Drewes, M. H. Smith, K. R. Denninghoff, L. W. Hillman, "An instrument for the measurement of retinal vessel oxygen saturation," in *Optical Diagnostics of Biological Fluids IV*, A. V. Priezzhev, M. V. Lomonosov, T. Asakura, eds. *Proc. SPIE* Vol. 3591, 114-120 (1999).

Multi-spectral confocal scanning laser ophthalmoscope for retinal vessel oximetry

Arthur Lompado*^a, Matthew H. Smith^a, Lloyd W. Hillman^a, Kurt R. Denninghoff^b

^aThe University of Alabama in Huntsville, Dept. of Physics, Huntsville, AL 35801

^bThe University of Alabama at Birmingham, Dept. of Emergency Medicine, Birmingham, AL 35226

ABSTRACT

Scanning laser microscopy is a widely used technique in ophthalmoscopy for providing high-resolution real time images of the retina. We describe a scanning laser ophthalmoscope that acquires retinal images at four wavelengths for the purpose of measuring the oxygen saturation of blood in retinal arteries and veins. Images at all four wavelengths are obtained across a single video frame using a temporal interlacing technique. An extraction procedure then permits analysis of four monochromatic images. A technique for calculating oxygen saturation from a multi-spectral image set is presented, along with preliminary measurements. The choice of wavelengths dramatically affects the oxygen saturation calculation accuracy and we present an optimized wavelength set and the calculated oxygen saturation results. The potential applications for this technology range from the diagnosis of various ophthalmic diseases to the detection of blood loss in trauma victims.

Keywords: Scanning laser ophthalmoscope, retina, oxygen saturation

1. INTRODUCTION

Real time digital imaging of the human ocular fundus is an important diagnostic tool for retinal disease state identification and monitoring (e.g., retinitis pigmentosa, retinal detachment, macular degeneration, diabetic retinopathy, etc.). Recently, scanning laser microscopy techniques have successfully been adapted to permit high resolution imaging of the retina for diagnostic methods such as reflectometry and optical sectioning^{1,2}. Incorporation of a confocal imaging arrangement to the optical system of such a device produces images that also exhibit high contrast and the resultant system is referred to as a confocal scanning laser ophthalmoscope (cslo)^{3,4}. Typically, imaging is performed at a single wavelength, resulting in an high quality intensity map of the retinal region under examination. However, this scanning technique may be adapted to include temporal multiplexing of a number of monochromatic light sources resulting in a multispectral measurement. The availability of the spectral properties of the target tissue permits expansion of the diagnostic capabilities of a cslo to spectrally dependent techniques. In particular, data reduction of the reflected spectral signature of blood in the retinal vessels may be used to determine the local oxygen saturation. This information is a useful indicator of retinal oxygen consumption for identification of localized disease⁵, and has been correlated to systemic irregularities⁶ including profuse occult bleeding^{7,8}. We report here the development of a multispectral cslo along with a data reduction technique for the determination of blood oxygen saturation (OS). The device, referred to as an eye oximeter (EOX), has been used to measure the OS of a blood sample in a controlled *in vitro* experiment employing a model eye containing a mock retinal vessel. Correlation of the measured OS to the known OS for a specific choice of illumination wavelengths and optical configuration of the EOX has been examined. Evaluation of the accuracy and potential of the EOX and its associated data reduction technique indicate that the system is sensitive to blood OS, although room for improved sensitivity exists.

2. BACKGROUND

2.1 Blood oxygen saturation

Homogenous, linear materials composed of two absorbers are known to attenuate an incident light beam via the Beer-Lambert law⁹,

$$I(\lambda) = I_0 10^{-[\epsilon_1(\lambda)c_1 + \epsilon_2(\lambda)c_2]} \quad (1)$$

* Correspondence: Email: LompadoA@email.uah.edu; WWW: <http://www.osig.uah.edu>;

Here, I_0 represents the incident irradiance, d is the interaction path length, c_n is the concentration and $\epsilon_n(\lambda)$ is the millimolar

absorbance coefficient of each absorber $n=1,2$. Knowing the absorbance coefficients for oxygenated and deoxygenated hemoglobin (i.e., the two primary absorbers in blood) and measuring the spectral transmittance of a blood sample permits calculation of the OS. The OS is defined as,

$$OS = \frac{c_{HbO_2}}{c_{HbO_2} + c_{Hb}} = \frac{c_{HbO_2}}{c_{Tot}} \quad (2)$$

Using $I/I_0 = T$, the transmittance, and $\text{Log}(1/T) = D$, the optical density, equations (1) and (2) may be combined and rewritten

$$D(\lambda) = [(1 - OS) \epsilon_{Hb}(\lambda) + OS \epsilon_{HbO_2}(\lambda)] d_{Tot} \quad (3)$$

Spectral measurements of $D(\lambda)$ permit solution of this equation for OS and the product dc_{Tot} via a least squares regression analysis.

The fact that blood is not a homogeneous absorber but instead attenuates an incident beam via both absorption and scattering means that Equation (1) is not completely valid. Many researchers have recognized this and offered a number of alternative developments, most of which were derived empirically^{10, 11, 12}. This is the approach taken in this research and derivation of a more appropriate model function for the EOX has been described⁴. The model function takes the form

$$T(\lambda) = S T_s^2(\lambda) 10^{-\chi c_{Tot} d [\epsilon_{Hb}(\lambda) + OS \{ \epsilon_{HbO_2}(\lambda) - \epsilon_{Hb}(\lambda) \}]} \quad (4)$$

where S is a scaling factor, $T_s(\lambda)$ is the spectral scattering transmittance for a single pass through the vessel, χ is a coefficient that considers the detection geometry of the EOX, c_{tot} is the blood hemoglobin concentration, and d is the vessel diameter. The sample OS is determined by measuring its spectral transmittance and fitting the measurements to the model function via a linear regression technique. Measurements at enough wavelengths allows regression of all the unknowns in the model function including the OS. The results of this procedure will be presented in Section 4.

3. MULTI SPECTRAL CONFOCAL LASER OPHTHALMOSCOPE

3.1 Confocal scanning laser ophthalmoscope

The cslo used for this study is similar in spirit to that reported in reference 3. This particular system does not run at the standard video rate of 30 Hz but instead is refreshed at 12.9 Hz. Due to the essentially static nature of this imaging application, the reduced refresh rate has proven adequate for retinal vessel oximetry studies and is hardly noticeable during operation. Figure 1 is a schematic of the optical layout of the system showing the illumination and detection paths. These are coincident and counterpropagating in the region between the beam splitter and the subject's retina. Also shown is the confocal filter arrangement which lies in a plane conjugate to the retinal surface. The illumination module (not explicitly shown) comprises four separate laser beams which are made coaxial through a set of dichroic combining mirrors. Three of the sources are diode laser modules emitting at 635 nm, 670 nm and 830 nm, while the fourth is an argon ion laser emitting at 488 nm. The laser beams are all linearly polarized and their electric fields are coarsely aligned and then passed through a Glan-Thompson prism for more precise alignment. The polychromatic beam is then incident on a two dimensional scanning mirror assembly that displaces it over a square area (≈ 3.5 mm side length) on the retina. The system scanning pupil is coincident with the subject's physiologic pupil to minimize vignetting of the illumination beam. A translating focusing lens placed in the common path of the incident and return laser beams accommodates any refractive error introduced by the subject.

Light reflected from the fundus traverses the incident path in the reverse direction up to the point of a separating beam splitter whereupon a portion is reflected into the detection path. This path contains the confocal filter (i.e., a pinhole) assembly and a relay lens to reimage the retinal surface at the avalanche photodiode detector. This confocal filter is efficient at removing optical noise (i.e., stray light) from the signal except that due to specular reflection from the optically smooth surfaces in the system. A second Glan-Thompson polarizer, oriented orthogonally to the first one, is used to eliminate this latter signal contribution. This polarizer has proven effective in minimizing the "glints" from the system surfaces and the subject's anterior cornea. Most importantly however, this arrangement has squelched the specular reflection from the apex of the retinal vessel surfaces which

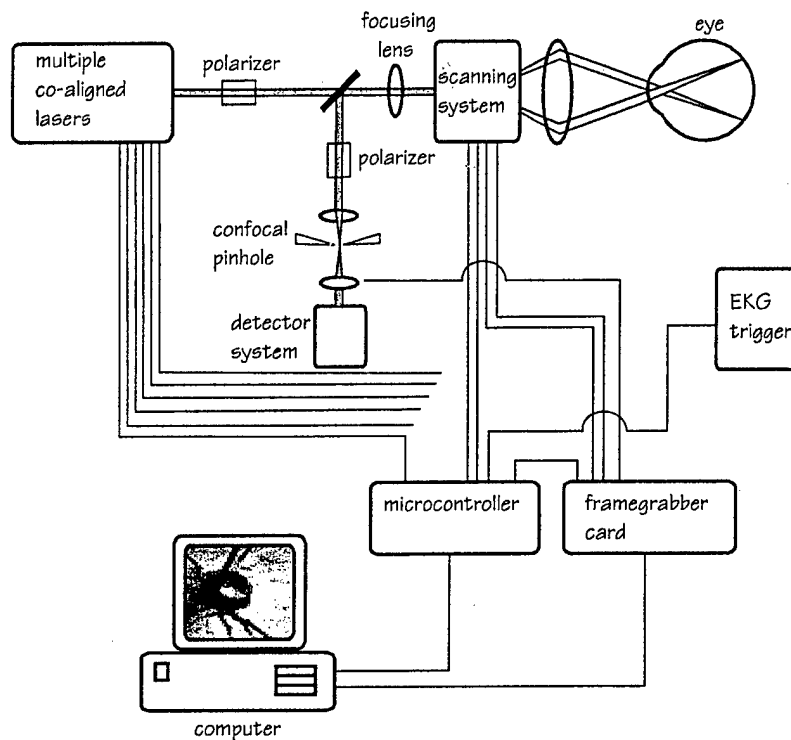


Figure 1. Optical and electronic schematic of EOX.

can falsely weigh the measured data as shown in Figure 2. Finally, blood oxygenation has been shown to be a function of the position within the cardiac cycle at which the measurement is performed. Therefore a triggering mechanism has been included that allows measurements to be performed at any time within the cardiac cycle by using the r-wave of an electrocardiogram as a reference point, and programming the desired delay time.

3.2 Interlaced imaging technique

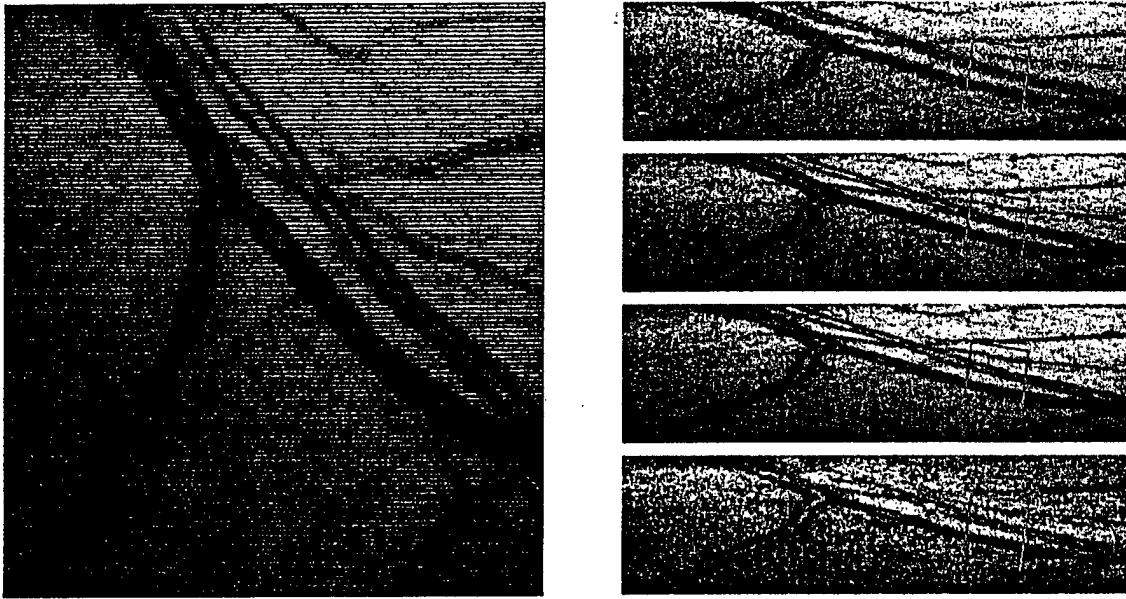


Figure 3. Interlaced raw image obtained from EOX and the four resulting monochromatic images. The boxes indicate the region to be analyzed for oxygen saturation.

A customized microcontroller also monitors the scanner timing synchronization signals and uses them to temporally multiplex the source lasers to create the interlaced image. The controller modulates the three diode lasers directly using a TTL signal and the argon ion laser via a TTL signal driving an acousto-optic modulator (AOM). The modulation depth of the three diode lasers is approximately 100% and the AOM has a modulation depth of >95%. The AOM leakage has been measured to be less than 10 nW at the subject's pupil and the reflected signal was undetectable.

During a multispectral frame acquisition, the lasers are modulated so that a single laser illuminates the retina during a given horizontal line scan. As the horizontal lines are accumulated, the lasers are sequenced and after the first four lines (i.e., wavelengths) are recorded, the cycle repeats until the entire 512 line frame is completed. The resultant image then contains four monochromatic subimages that are spatially interlaced. These may be extracted, albeit with reduced aspect ratios, as shown in Figure 3. This particular interlacing technique is advantageous because it minimizes the distance between subsequent monochromatic image measurements. It is a way of localizing the OS measurement on the vessel rather than performing four contiguous monochromatic measurements along the vessel. Any variation of the OS along the vessel would be difficult to



Figure 2. The retinal image on the left was acquired with the EOX without the use of crossed polarizers and displays severe reflections down the center of the vessels. The image on the right was obtained by illuminating with vertically polarized light and collecting only horizontally polarized light. Note that the vessel reflections are essentially eliminated.

accurately measure if the monochromatic data came from different vessel positions. Interlacing also minimizes the time lapse that would be experienced if complete monochromatic frames were acquired serially. A section of the separated images may then be selected for analysis as shown by the boxes in the monochromatic images of Figure 3

4. DATA ACQUISITION AND ANALYSIS

4.1 Data Acquisition

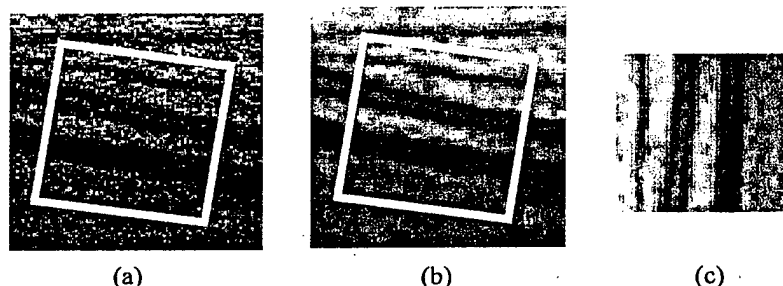


Figure 4. a) Subsection of retinal image showing the selected region for analysis in the white box. b) Filtered version of same. c) Selected region, reoriented

Operation of the EOX-A is quite simple. The framegrabber maps the mirror positions (i.e., the illuminated field positions) to the detector output at each position, accumulating a single 512x512 pixel image that is displayed on the control computer monitor. In the system targeting mode, imaging is performed using a single laser (830 nm), resulting in a pseudo-real time monochromatic image that is helpful in guiding the operator to a specific retinal feature. Retinal features of interest for eye oximetry include large retinal vessels on and around the optic disk, and artery-vein pairs that trace out similar paths. Once a feature is chosen, the operator acquires a single multispectral image for OS calculations. A margin of "background" tissue surrounding the vessel is included to allow calculation of the relative vessel transmittance. Once the monochromatic images are extracted, they are examined and filtered if they are exceptionally noisy. Filtering simplifies the OS calculations by making it easier to determine the principle points in the image used to calculate the vessel transmittance. This transmittance is determined by selecting a rectangular region of a monochromatic image that is aligned with the vessel. Figure 4 displays an section of a raw image, a filtered version of the same image, and a reoriented image of a region selected for transmittance calculations. The filtering technique in this case is a two-dimensional Savitsky-Golay slope preserving filter. It has been used because the slope of the measured irradiance is sometimes used in the vessel transmittance calculation. The measured irradiance across any horizontal line in Figure 4c can be plotted and used to determine the relative vessel transmittance.

Figure 5 represents how the principle points for the transmittance calculation may be obtained from a single irradiance line or vessel profile. The graph plots an example of a typical profile obtained from an image containing a single vertical vessel. The absorptive trough due to the presence of the vessel is obvious. A background irradiance level is determined from the value of the tissue surrounding the vessel (points A and D in the figure) and is considered the irradiance that would have been measured in the absence of a vessel. For vessels that do not exhibit any glints, the full depth of the vessel "trough" is used to determine the irradiance at the vessel center and the ratio of these last two values is stored as the vessel transmittance.

When the crossed polarizers are not used in the system, the vessel glints may be accommodated¹² by fitting a curve to the measured profile that bypasses the glints as shown in the figure. Principle points corresponding to the positions of maximum slope magnitude (points B and C) are used to select a region of the data to which a curve is fit. The minimum value of the fitted curve is then used in the transmittance calculation. It has been found empirically that a third order polynomial produces a good fit to the data and the resulting calculated transmittances produce acceptable OS values. Either of these procedures is performed

for as many horizontal lines as are available in the image, with more lines (i.e., data points) increasing the measurement signal to noise ratio. Once the transmittance values are obtained for each wavelength of the measurement, these values are substituted into the model function for the regression analysis used to determine the sample OS.

4.2 Data Analysis

Once the spectral transmittance values are measured, they comprise the data set to which the model function is fit. Also knowing the spectral absorbance coefficients permits regression of the unknown parameters in Eq. (4). The iterative linear regression technique requires seed values for the regressed variables which were obtained from the known optical configuration of the EOX and separate blood scattering measurements performed in our lab⁴. The regression is then performed allowing for the solution of OS, $T_s(\lambda)$, S and the dc_{Tot} product. Stability of the regressed parameters over a range of seed values has been verified.

A controlled OS measurement experiment was conducted using a model eye with a mock retinal vessel through which blood samples were flowed. The vessel was a 270 μm diameter micropipette encased in an index matched solution and placed in front of a diffusing white background used to simulate the fundus. The diffusing properties of the background material are meant to simulate the effect on the point spread function of a beam incident on a human retina, although the uniform reflectance and radiance of the material are known to only be approximations to the actual properties of a human fundus. Whole blood samples of varying OS were injected into the mock vessel and spectral transmittance measurements were made with the EOX. Figure 6 below shows a plot of the calculated (i.e., regressed) OS versus the actual OS as measured on a CO-oximeter. A line of unity is included for comparison, and the correlation coefficient (r^2) was calculated to be 0.99. This high value can be misleading as it applies to only five data points and the experiment was well controlled. Still, the results are encouraging and indicate that the system is sensitive to blood OS and could be calibrated and tested clinically.

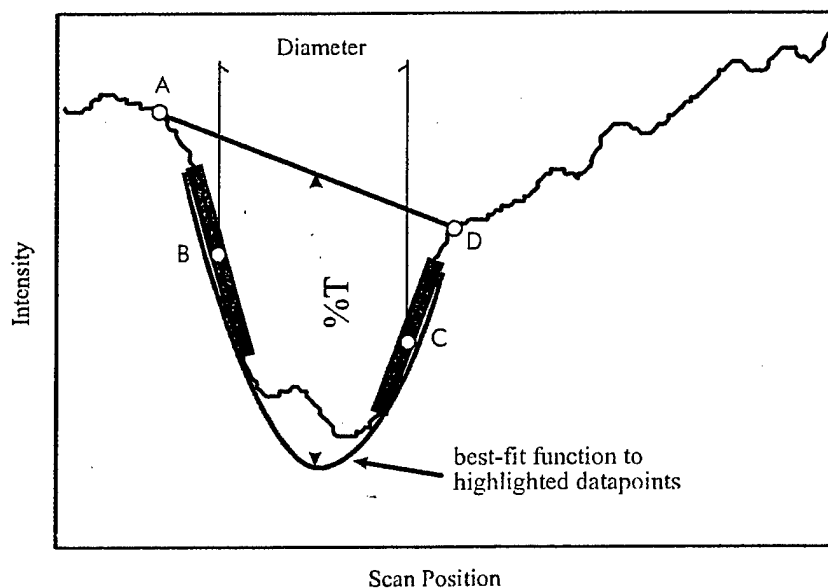


Figure 5. Typical vessel intensity profile showing principle points, curve fit to data and transmittance calculation method.

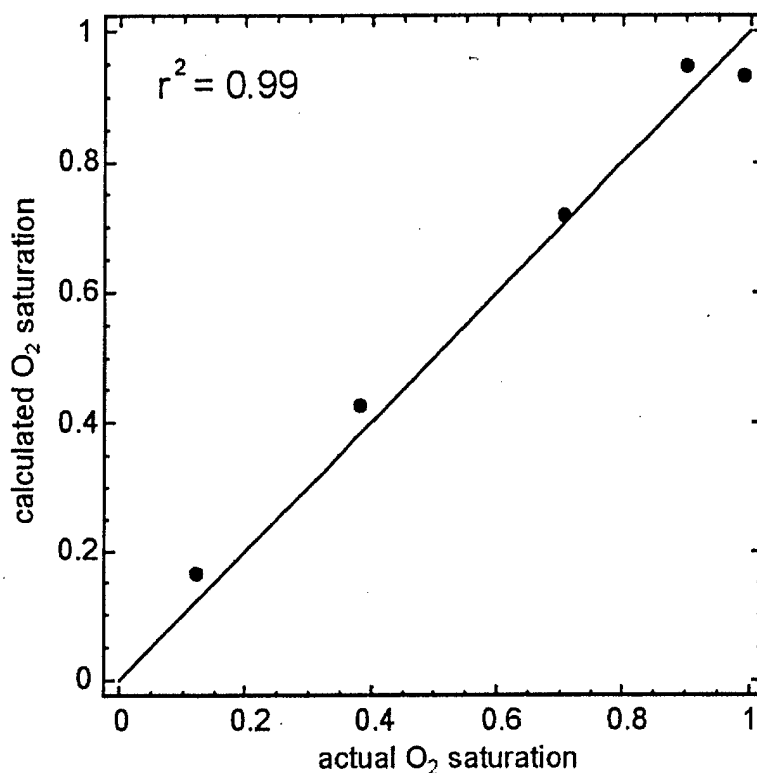


Figure 6. Comparison of calculated and known OS for *in vitro* model eye experiment.

4. DISCUSSION AND CONCLUSIONS

We have reported on a multi-spectral cslo adapted to perform retinal vessel oximetry measurements. A temporal interlacing scheme is used to obtain multiple monochromatic images across a single video frame. The spectral transmittance of a blood vessel is determined from these images, and used in a spectral linear regression technique to calculate the sample OS. Regression is performed on a model function that takes into account the geometry of the EOX optical system and the scattering effects of whole human blood. A controlled experiment using samples of know oxygenation indicated that the system is sensitive to oxygen. The system performance must however be examined under more rigorous clinical conditions to determine the potential.

5. ACKNOWLEDGEMENTS

We thank The U.S. Army Medical Research and Materiel Command for their support of this work.

4. REFERENCES

1. Elsner, A. E., Burns, S.A., Hughes, G.W., and Webb, R.H., "Reflectometry With a Scanning Laser Ophthalmoscope," *Applied Optics*, Vol. 31, No. 19, 1992, pp. 3697-3710.
2. Webb, R.H., Hughes, G.W., and Pomerantzeff, O., "Flying Spot TV Ophthalmoscope," *Applied Optics*, Vol. 19, 1980, pp. 2991-2997.

3. Webb, R.H., Hughes, G.W. and Delori, F.C., "Confocal Scanning Laser Ophthalmoscope," *Applied Optics*, Vol 26, 1987, pp. 1492-1499.
4. Lompado, A., "A Confocal Scanning Laser Ophthalmoscope for Retinal Vessel Oximetry," Ph.D. Dissertation, Physics Department, University of Alabama in Huntsville, 1999.
5. Hickam, J.B., Frayser, R., and Ross, J.C., "A Study of Retinal Venous Blood Oxygen Saturation in Human Subjects by Photographic Means," *Circulation*, Vol. 27, 1963, pp. 375-385.
6. De Vries, J.-P. P.M., Olthof, C.G., Visser, V., Kouw, P.M., and De Vries, P.M.J.M., "Continuous Measurement of Blood Volume Using Light Reflection: Method and Validation," *Medical and Biological Engineering and Computing*, Vol. 31, 1993, pp. 412-415.
7. Denninghoff, K.R., Smith, M.H., Chipman, R.A., Hillman, L.W., Jester, P.M., Hughs, C.E., Kuhn, F., and Rue, L.W., "Retinal Large Vessel Oxygen Saturations Correlate with Early Blood Loss and Hypoxia in Anesthetized Swine," *The Journal of Trauma: Injury, Infection and Critical Care*, Vol. 43, No. 1, 1997, pp. 29-34.
8. Denninghoff, K.R., Smith, M.H., Hillman, L.W., Redden, D., and Rue, L.W., "Retinal Venous Oxygen Saturation Correlates with Blood Volume," *Academic Emergency Medicine*, Vol. 5, No. 6, 1998, pp. 577-582.
9. van Assendelft, O.W., *Spectrophotometry of Hemoglobin Derivatives*, Assen, Roal Vangorcum, 1970.
10. Delori, F.C., "Noninvasive Technique for Oximetry of Blood in Retinal Vessels," *Applied Optics*, Vol. 27, No. 6, 1988, pp. 1113-1125.
11. Schweitzer, D., Leistritz L., Hammer, M., Scibor, M., Bartsch, U., and Strobel, J., "Calibration-Free Measurement of the Oxygen Saturation in Retinal Vessels of Men," in *Ophthalmic Technologies V*, J.-M. Parel, Q. Ren, K. M. Joos, Editors, Proc. SPIE 2393, 1995, pp. 210-218.
12. Smith, M.H., "Oximetry of Blood in Retinal Vessels," Ph.D. Dissertation, Physics Department, University of Alabama in Huntsville, 1996.

In-plane scatterometry of a small caliber blood column

Arthur Lompado^a, Matthew H. Smith^a, Lloyd W. Hillman^a, Kurt R. Denninghoff^b

^aThe University of Alabama in Huntsville, Dept. of Physics, Huntsville, AL 35801

^bThe University of Alabama at Birmingham, Dept. of Emergency Medicine, Birmingham, AL 35226

ABSTRACT

The scattering of He-Ne laser light incident on a flowing column of whole human blood has been measured and analyzed. An automated scatterometer whose sample chamber simulates a small caliber blood vessel was used to perform the measurements and is described. Angular scattered light distributions due to flowing blood columns for two independently varied parameters, blood oxygenation and hemoglobin concentration, are presented. It is found that the dependence of the scattering distribution on blood oxygenation is minimal while the dependence on hemoglobin concentration is strong. A nominally transparent sample of human plasma has also been investigated to quantify its scattering characteristics. The whole blood scattering results are compared to theoretical predictions obtained using a Monte Carlo simulation employing the Mie single particle phase function and macroscopic transport coefficients obtained from published literature. The best correlation was found when the largest published scattering coefficient was employed in the simulation. However, a strong correlation between the measured and predicted scattering distributions was only obtained when unphysically high values of the scattering coefficient were used in the simulation.

Keywords: scatterometry, blood, Monte Carlo simulation

1. INTRODUCTION

The proliferation of optical techniques in the fields of medicine and biomedicine has continued due to their unique match to many of the challenges encountered in modern day medicine. In particular, optical diagnostic methods for the human eye have burgeoned because of their typically non-invasive requirements and accurate results^{1,2}. Recently, lasers have been used to perform tasks ranging from simple illumination of the ocular structure for imaging and examination purposes³, to ablation and cauterization of both internal and surface structures⁴. The transparency of the anterior ocular media is advantageous in most procedures, but the highly scattering and absorptive properties of the ocular fundus have also been exploited to reveal information about systemic pathologies^{5,6}. In particular, the scattering and absorption of light by red blood cells (rbcs) within the vasculature of the fundus are phenomena that certain optical diagnostic techniques such as retinal vessel oximetry^{7,8} must quantify to assure accurate, beneficial outcomes. It is the purpose of this study to quantify the scattering of light by a column of whole blood in order to improve the accuracy of the data reduction method of such techniques. A secondary goal is to compare the measurements to theoretical predictions of the scattering characteristics of a small caliber blood vessel.

2. THEORY

The propagation of light through an inhomogeneous medium has been studied extensively and in most practical cases remains an extremely difficult system to model^{9,10,11}. Extinction of the incident energy by inhomogeneities in a turbid medium may be treated using different formalisms depending upon such variables as concentration, shape, size or velocity. The term extinction is understood to include the effect on the incident beam of both scattering and absorption, and inhomogeneities are also referred to as particles. All extinction calculations rely on certain physical attributes of the particles, or derived quantities thereof. These include the single particle extinction, scattering and absorption cross sections, σ_{ext} , σ_s , and σ_a , the related macroscopic scattering and absorption coefficients, μ_s and μ_a (also referred to as the transport coefficients), and the scattering phase function of the particle. The microscopic cross sections are used to describe the extinction due to a single particle, and the extinction behavior of an extended turbid medium is represented by the macroscopic transport coefficients and phase function. The relationship between the microscopic and bulk parameters is straightforward for singly scattering materials but is becomes nontrivial for highly scattering media. For turbid materials whose thickness-particle concentration product is small, single scattering prevails. Whole blood samples of thicknesses equivalent to small caliber vessel diameters (50-200 μm) exhibit

Correspondence: Email: LompadoA@email.uah.edu; WWW: <http://www.osig.uah.edu>

thickness-concentration products that are large and hence are multiply scattering. The macroscopic transport coefficients of

multiply scattering biological media are typically determined empirically and reported values tend to vary significantly¹².

Although whole blood is a multiply scattering medium, the single particle phase function is required to model an extended multiple scatterer via the Monte Carlo technique. Also required for the Monte Carlo method are the macroscopic transport coefficients. The single particle phase function is normalized such that

$$\int_{4\pi} p \, d\Omega = 1 \quad (1)$$

indicating that the probability of scattering into a 4π steradian sphere centered on the particle is one. The anisotropy of the scattered radiation, g , and the reduced scattering coefficient, $\bar{\mu}$, are descriptive characteristics related to the phase function via

$$g = \langle \cos\theta \rangle = \int_{4\pi} p(\theta) \cos\theta \, d\Omega \quad (2)$$

$$\bar{\mu} = \mu_s (1 - g) \quad (3)$$

Equation 2 indicates that the average cosine of the scattering angle ranges from preferentially forward, through the point of isotropic scattering, to preferentially rearward as g varies from 1 through 0 to -1 respectively. Biological tissues, including whole blood, tend to have g values of greater than 0.9, indicating that the scattering is preferentially forward.

For the geometrically simple case of a spherical scatterer, Mie theory predicts a phase function that describes the magnitude, directionality and polarization characteristics of the scattered radiation. For unpolarized incident light, the azimuthal component of the spherical particle phase function may be written as

$$p(\theta) = \frac{1}{k^2 r^2} (|S_1(\theta)|^2 + |S_2(\theta)|^2) \quad (4)$$

where $S_1(\theta)$ and $S_2(\theta)$ represent the complex amplitudes of the scattered parallel and perpendicular polarization components respectively. These functions depend on both the Ricatti-Bessel functions and the associated Legendre functions. Despite the fact that rbc's are not spherical, the Mie phase function has been compared to measured rbc single particle phase functions and has proven acceptable¹³.

Once the transport coefficients and phase function are known, a multiply scattering sample may be modeled using a Monte Carlo technique^{14,15}. The technique can accommodate arbitrary sample geometries at the expense of extended calculations. In this research, a modified Monte Carlo technique is employed to compare theoretical and measured scattering distributions and to determine the parameters which maximize the correlation between these two results. Our interest in this method stems from the fact that a retinal vessel blood flow model incorporates a high scatterer density yet the boundary requirements for a simple analytical technique are not met¹⁶.

3. CONSTRUCTION OF SCATTEROMETER

Quantifying the scattered flux from an assembly of particles in suspension requires a nephelometer or scatterometer. Whole human blood is a suspension of $\approx 45\%$ by volume rbc's and 1% white blood cells and platelets in a medium of essentially transparent plasma (91% water). The plasma is known to contain other scattering elements (e.g., proteins, electrolytes etc.), although these comprise only a small amount of the remaining volume and it will be shown that their contribution to the scattering distribution is negligible. An automated scatterometer was constructed containing a small caliber mock vessel and capable of measuring the scattering distribution of a sample over a range of $\pm 160^\circ$ from the axis of the incident beam. The system is confined to measurements in a single, horizontal plane.

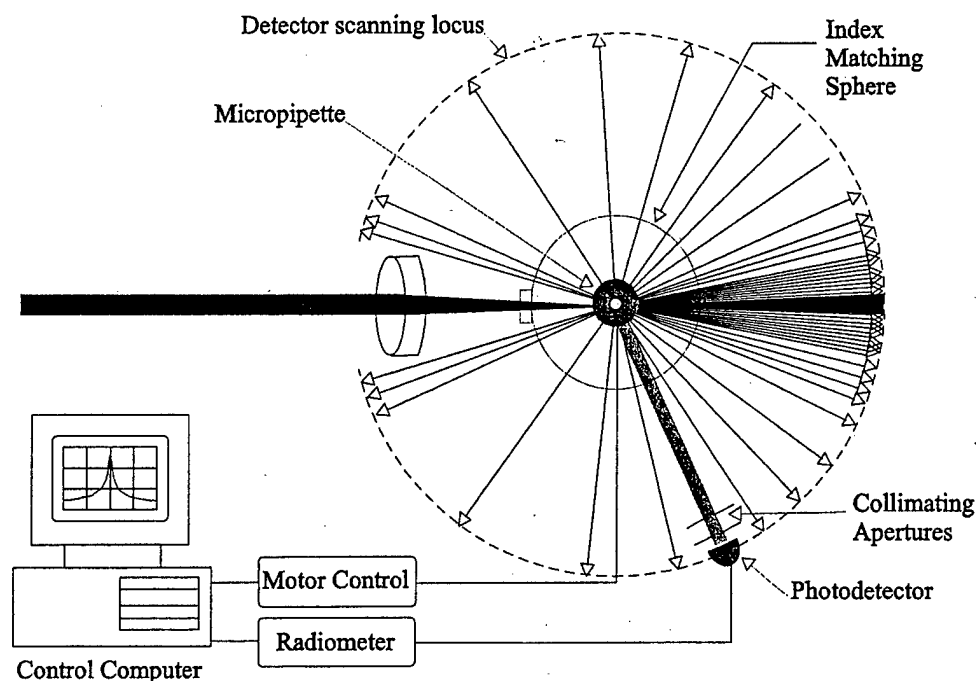


Figure 1. Overhead view of scatterometer.

An overhead view of the scatterometer system is illustrated in Figure 1. Light from a 5 mW HeNe laser ($\lambda = 632.8$ nm) is spatially filtered and then recollimated (not shown) with a $1/e^2$ beam diameter of 3.0 mm. This beam is incident from the left side of the figure and encounters a focusing lens with an effective focal length of 30 mm. The beam next passes through a flat window in the side of a spherical ampule, both made of Pyrex. The ampule has two Pyrex tubes emerging radially that intersect a full diameter of the sphere (29.6 mm) in the direction orthogonal to the figure. Rubber septum stoppers with centered feedthrough holes are set in the ends of the tubes to allow insertion of a Pyrex micropipette. The micropipette has an inner diameter of 270 μm that acts as a channel for the flowing blood. After a slight refraction from the flat window the beam comes to focus at the center of the blood column. The lines emerging radially from the pipette indicate the scattered light in the figure and their density is proportional to the scattered intensity for a typical blood sample. To limit the system's signature on the measured data, the sphere is filled with an index matching fluid.

Coaxial with the pipette axis is that of a stepper motor driven rotation stage. Secured to the stage and oriented radially to its axis is a boom arm, the distal end of which supports a silicon photodetector at a distance of 13.5 cm from the micropipette. The photodetector is preceded by two 0.5 mm diameter collimating circular apertures which provide angular resolution of less than 0.5° and a detection solid angle of 1.1×10^{-5} sr. The angular resolution of the stepper motor is specified as below 0.1° . Upon stepping the angular position of the stage, the photodetector scans a circular locus around the sample through a range of $\pm 160^\circ$ from the original beam direction. The system is automated by monitoring the rotating stage position and the photodetector output with a control computer. A computer program written in Visual BASIC allows the operator to choose the angular range and resolution for a scan. A provision is made in the software to measure and remove the dc background signal measured at each angular position of the detector. A scattering diagram is constructed from the measured scattered irradiance vs detector position once the background signal has been removed.

3.1 Human Blood Studies

Whole human blood (500 cc) was drawn from a healthy donor according to an Internal Review Board approved protocol. The blood was collected in a donor bag containing an anticoagulant (EDTA) to prevent clotting during the measurement. The whole blood was immediately packed in ice and samples were drawn and prepared as needed. The two independent variables in this

study were blood oxygenation and scatterer concentration. This latter variable, assuming that scattering is due primarily to rbc's, may also be referred to as the hemoglobin concentration which is a measure of the amount of hemoglobin per unit volume (in units of g/dl) in the sample. Modifying the hemoglobin concentration required simply centrifuging (4000 rpm for 15 min.) 120 cc of the whole blood to separate the rbc's from the plasma, and then reinfusing the packed rbc's into either the plasma or the remaining whole blood as required. Care was taken to avoid rupturing the rbc's during the separation and reinfusion processes. Similarly, the sample pH was maintained to prevent any osmolar induced volumetric changes to the rbc's which would manifest as a modification of the scattering distribution.

Setting the blood oxygenation required a more elaborate technique. A modified ventilator system was used to individually set the oxygen, nitrogen and carbon dioxide content of a gas mixture. The gas mixture passed over the blood sample in a laminar fashion as it flowed through a circuit. The laminar gas flow minimized the creation of any light scattering gas bubbles in the blood volume. A section of tubing used in the circuit was set in a warm water bath to keep the blood at body temperature. Finally, the blood passed through a humidifier to counteract any dessication caused by the gas mixture flow. The blood was allowed to flow through the circuit for as long as was required to obtain a certain oxygenation level, which was monitored using a CO-oximeter.

4. METHODS

4.1 Scatterometry

A prepared blood sample was placed in a 10 cc syringe that was mounted in a calibrated syringe pump. Some of the prepared blood was decanted and its hemoglobin concentration and oxygenation were measured using the CO-oximeter. The syringe was connected to the top of the micropipette via small diameter medical tubing. The average blood flow velocity in the retinal vessels of healthy males has been reported^{17, 18} and the automatic syringe pump maintained a flow velocity of 2.5 cm/s. After allowing some blood to flow through the system to assure all gas bubbles were passed out of the tubing, the scatterometer measurement was initiated while the blood flowed continuously. Irradiance measurements were made in 1° intervals over the full range of the device. Multiple readings (2-8) were taken at each position and the average irradiance was calculated and stored. A single scan across the entire plane required 25 minutes and the flowing blood prevented any settling of the rbc's during the measurement.

4.2 Monte Carlo Simulation

The Monte Carlo method has previously been employed to simulate the transport of radiation through a scattering biological medium and the particular technique used here has been described¹⁹. The technique relies on the probability density functions (pdfs) describing a photon's trajectory. It has been shown that, in a spherical coordinate system centered at the particle, the pdfs associated with the polar and the radial directions are uniform and exponentially decaying respectively, with the latter depending on the transport coefficients²¹. The azimuthal pdf for a spherized rbc is the Mie phase function which itself depends on the scatterer's size, relative refractive index and the polarization state of the incident illumination. The rbc's in the simulation are assumed spherical with a volume equivalent to that of an average rbc. The parameters required to generate the pdfs are either known, calculable or have been reported in the literature, and Table 1 summarizes the values used here.

The initial simulation assumed a scattering coefficient for whole blood of 239 mm⁻¹. The correlation between the measured distribution and that predicted by the simulation using this value of μ_s was marginal at best. Certain gross features of the measured data were not present in the simulated data, and the general shapes of the two curves were dissimilar. Therefore, a number of subsequent simulations were executed which assumed increased scattering coefficients in an effort to improve the correlation. In all cases, the absorption coefficient was maintained at a value of 1.3536×10^{-5} mm⁻¹.

The exiting photons were binned in 1° intervals in both the polar and azimuthal directions for comparison with the measured data. Since the actual measurement was confined to a single polar plane, the central three polar bins of the Monte Carlo data were extracted and used for comparison. This central 3° swath actually exceeded the measurement area but was chosen because the simulation did not vary substantially in the polar direction over this range. Use of the larger range permitted the statistics of the Monte Carlo simulation to be improved by including more photons per azimuthal bin, a technique that was advantageous in the lateral direction where the scattered intensity was minimal.

Table 1. Red blood cell parameters used in Mie phase function calculation.

Parameter (units)	Value	Reference
λ (μm)	0.6328	
V (μm^3)	82.4	20
r (μm)	2.7	
n_{rbc}	1.4025	21
n_{plasma}	1.348	22
κ_{rbc}	1.3536×10^{-5}	23
κ_{plasma}	0	

5. RESULTS

5.1 Scatterometry

Figure 2 is a scattering diagram displaying the normalized measured scatter function for three blood samples whose hemoglobin concentration was kept constant at ≈ 8.8 g/dl and whose oxygenation saturation varied from 6.2 % to 92.3 %. Normalization of each measurement is performed by dividing the intensity at each position by the integral of the data across the range, and the results are plotted on a logarithmic scale due to the large measured dynamic range. Figure 2 indicates that the oxygen saturation of the sample does not have a noticeable effect on the shape or normalized amplitude of the measured data. As well, all samples exhibit a strong central peak that is evident out to the range of $\pm 7^\circ$, corresponding to the coherently transmitted beam. This

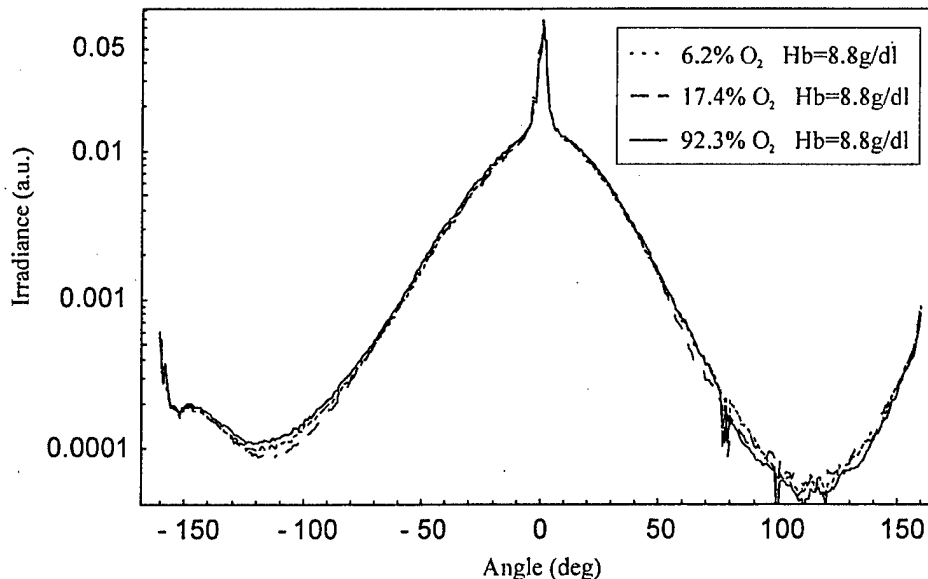


Figure 2. Scattering diagram of three blood samples with equivalent hemoglobin concentrations and varying oxygen saturations.

central peak extends over the angular range that would encompass the incident beam in the absence of a scattering sample.

Figure 3 shows the scattering diagrams for three samples whose oxygen saturation was maintained at ≈ 94.6 % while the hemoglobin concentration was varied from 3.9 g/dl to 13.9 g/dl. The plotted data trend as would be expected; the sample with

the highest scatterer concentration scatters more energy laterally and transmits less in the forward direction than that with the lowest concentration, with the third sample lying in between. The delineation between the central coherently scattered peak and the scattered energy becomes less obvious as the hemoglobin concentration is decreased.

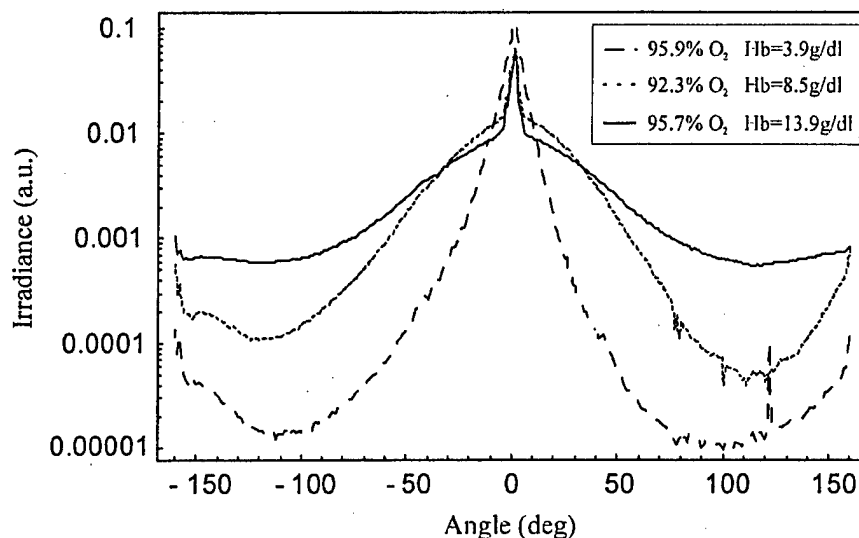


Figure 3. Scattering diagram of three blood samples with equivalent oxygen saturations and varying hemoglobin concentrations.

The weak dependence of scattering on blood oxygenation is not surprising since the parameters which are known to effect the scattering characteristics of a sample (scattering cross-section and coefficient, size parameter, and geometric shadow) are not modified as the oxygenation of the rbc's is changed. The absorption dependence on the fractional percentage of oxygenated and deoxygenated hemoglobin within the rbc's is the mechanism behind traditional transmission oximetry measurements.

It is known that the scattering of light by whole blood with normal hemoglobin concentrations (15.5 ± 2.2 g/dl for males, 13.7 ± 2.0 g/dl for females: avg ± 2 std dev)²⁴ and sample thicknesses equivalent to small caliber vessel diameters is a multiple scattering process due to the proximity of the rbc's. Even at the lowest hemoglobin concentrations examined here, the scatterer concentration, coupled with the sample thickness, exceeds the published limiting value for single scattering concentrations³⁰ by a factor of 30,000, indicating that these measurements were all performed safely in the regime of multiple scattering. Because scatterer concentration is known to effect the scattering distribution, deviations between measurements of samples with varying hemoglobin concentrations displayed in Figure 3 are expected. However, the obvious change in shape of the scattering distributions with scatterer concentration, as opposed to a simple scaling, was larger than expected. A similar effect has been previously reported although the results at normal hemoglobin concentrations appear to deviate from our findings²⁵.

Figure 4 is a graph of the scattering diagram measured for a sample of the whole plasma which was decanted from the centrifuged blood. Along with the plasma distribution is a system profile showing the absolute minimum measurable signal as a function of angular position (obtained with no sample in the system). It is seen that the plasma is essentially nonscattering, approaching the system profile in the angular range of $\pm 55^\circ$ and equivalent to the system noise beyond this range. Even though it is known that the plasma contains some scattering centers in the form of proteins, electrolytes and cellular components (the

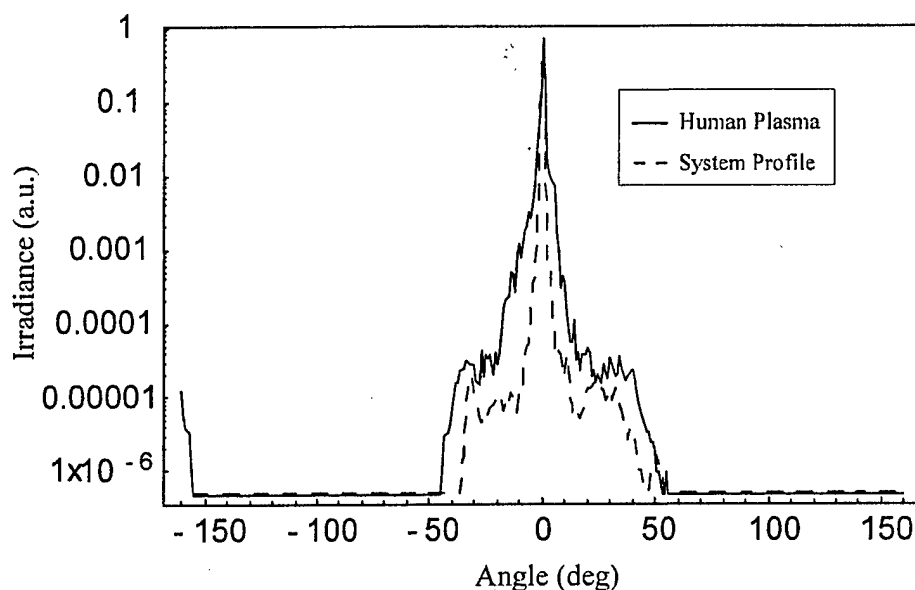


Figure 4. Scattering diagram of human plasma and system profile.

sample was unfiltered), the scattered energy due to these elements is negligible compared to that of the rbc's. The noise displayed in the data at the extreme of the negative angular direction is attributable to stray light reflection off the edge of the sphere window and is not a true scattering signal.

5.2. Monte Carlo Simulation

As an initial comparison, the Monte Carlo simulation was executed using the published scattering coefficient²⁵ $\mu_s = 239 \text{ mm}^{-1}$. The results of this comparison to whole blood measurements of samples with a hemoglobin concentration of 15.8 g/dl, along with those obtained for higher scattering coefficients, are displayed in Figure 5. The sample data in the figure have been normalized to the $\theta=7^\circ$ position to allow comparison of the incoherently scattered lateral intensity and to minimize the effect on the comparison of the central peak. Although the scattering coefficient was allowed to vary, the absorption coefficient and Mie phase

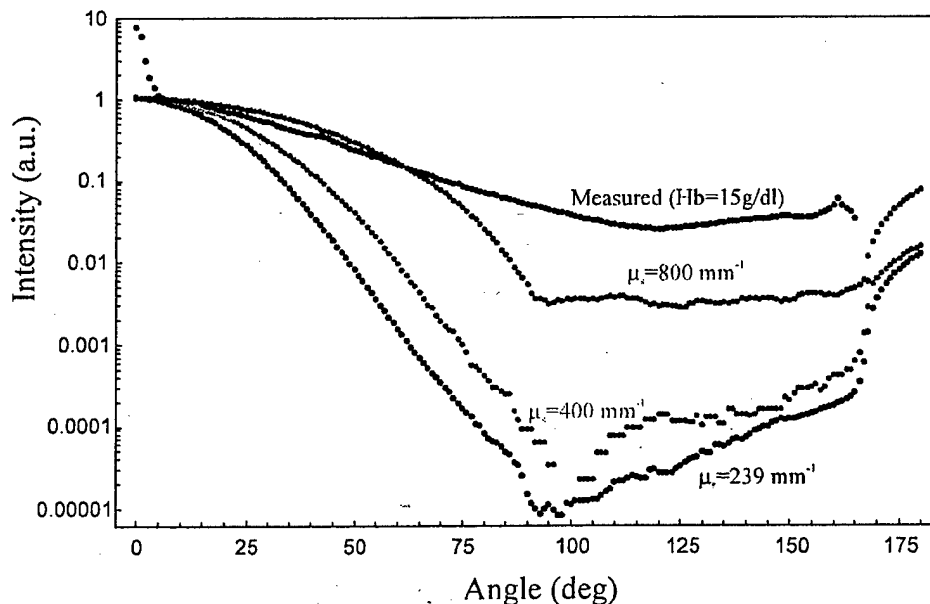


Figure 5. Comparison of measured scattering diagram for a whole blood sample to the predictions of the Monte Carlo simulation for three different scattering coefficients.

function remained constant across the simulations. Note that all of the simulation data have been filtered using a Savitsky-Golay slope preserving filter with a boxcar half width of 10 data points. This had the effect of reducing the noise in the $70^\circ < \theta < 170^\circ$ range while maintaining the overall shape of the curves. The noise is attributable to the poor lateral scattering efficiency of the blood column, exacerbated by the fact that the plotted data originates in the limited central 3° bin in the polar direction. Accumulating enough photons to smooth the prediction data to the level shown in the figure required between 1×10^6 and 3×10^6 photons be traced in each case. While this is obviously not optimal, truncating the simulation at this level allowed simulations to be performed in reasonable time periods (20-30 hrs per run).

Figure 5 displays large discrepancies between the measured scattering distribution and the predictions obtained for a number of different scattering coefficients in the simulation. Most prominent is the absence of a central peak in the simulation data. The central peak is the result of the coherent transmission of light directly through the sample. The failure of the simulation to predict this peak may be attributed to the fact that the phases of the incident and scattered waves are not monitored in the Monte Carlo technique.

Besides the central peak absence, the simulation predicts the scattered irradiance in the lateral direction to be substantially less than the measured scattered irradiance. The measured and predicted curves are seen to converge slightly as μ_s is increased, but never correlate well. The effect of an increase in μ_s to 800 mm^{-1} was examined to determine what theoretical μ_s value correlates well with the measured data. This corresponds to a scattering mean free path within the sample that approaches the known scatterer dimensions. Nonetheless, increasing μ_s to even higher (i.e., nonphysical) values still did not cause a strong correlation, indicating the need for a better simulation. Regardless of the cause of the discrepancy, the prediction of the central peak in the simulation data would necessarily remove a great deal of energy from the laterally scattered angular region, producing a higher correlation between measurement and theory.

The predicted minimum tends towards the direction orthogonal to propagation whereas the measured data troughs at $\approx 115^\circ$ from this direction and it is unclear whether a redistribution of irradiance due to a predicted central peak would correct this. The fidelity of the simulation in the retroreflected direction could not be precisely verified since the measurements truncated prior to this position. The increased backscatter displayed in the simulation data approximates the Gaussian shape of the input beam cross-sectional irradiance, an indication that it is comprised primarily of specularly reflected light at the interface between the pipette and the blood sample.

7. DISCUSSION

The scattering distribution of a column of whole blood has been examined for its dependence on the hemoglobin concentration and blood oxygen saturation. The measured dependencies trend as would be expected considering the physical modifications to the sample for each measurement. A Monte Carlo simulation of the scattering distribution from a model blood column has been executed and compared to the measured data. The correlation between measurement and the prediction is very low for published values of the scattering coefficient of whole human blood. This correlation can be improved if the scattering coefficient is allowed to increase, although reasonable agreement between theory and measurement is only achieved when its value becomes nonphysically high. This indicates that the simulation suffers shortcomings in its modeling methodology. The obvious lack of accommodation for residual coherent transmission which is present in the sample appears to be the reason for the discrepancy. A modeling technique that incorporates both the coherent and incoherent portions of the scattered light for a sample of this geometry is required to improve the correlation.

8. ACKNOWLEDGEMENTS

We acknowledge the U.S. Army Medical Research and Materials Command for their support of this work.

9. REFERENCES

1. Webb, R.H., "Manipulating Laser Light for Ophthalmology," *IEEE Engineering in Medicine and Biology Magazine*, December, 1985, pp 12-16.
2. Harris, A., Kagemann, L., and Cioffi, G.A., "Assessment of Human Ocular Dynamics," *Survey of Ophthalmology*, Vol. 42, No. 6, 1998, pp. 509-533.
3. Kobayashi, K., and Asakura, T., "Imaging Techniques and Applications of the Scanning Laser Ophthalmoscope," *Optical Engineering*, Vol. 34, No. 3, 1995, pp. 717-726.
4. Trempe, C.L., Mainster, M.A., Pomerantzeff, O., Avila, M.P., Jalkh, A.E., Weiter, J.J., McMeel, J.W., and Schepens, C.L., "Macular Photocoagulation. Optimal Wavelength Selection," *Ophthalmology*, Vol 89, 1982, pp. 721-729.
5. Denninghoff, K.R., Smith, M.H., Chipman, R.A., Hillman, L.W., Jester, P.M., Hughs, C.E., Kuhn, F., and Rue, L.W., "Retinal Large Vessel Oxygen Saturations Correlate with Early Blood Loss and Hypoxia in Anesthetized Swine," *The Journal of Trauma: Injury, Infection and Critical Care*, Vol. 43, No. 1, 1997, pp. 29-34.
6. Denninghoff, K.R., Smith, M.H., Hillman, L.W., Redden, D., and Rue, L.W., "Retinal Venous Oxygen Saturation Correlates with Blood Volume," *Academic Emergency Medicine*, Vol. 5, No. 6, 1998, pp. 577-582.
7. Delori, F.C., "Noninvasive Technique for Oximetry of Blood in Retinal Vessels," *Applied Optics*, Vol. 27, No. 6, 1988, pp. 1113-1125.
8. Smith, M.H., Denninghoff, K.R., Hillman, L.W., and Chipman, R.A., "Oxygen Saturation Measurements of Blood in Retinal Vessels During Blood Loss," *Journal of Biomedical Optics*, Vol. 3, No. 3, 1998a, pp. 296-303.
9. van de Hulst, H.C., *Light Scattering by Small Particles*, New York, Wiley, 1957.
10. Bohren, F.G. and Huffman, D.R., *Absorption and Scattering of Light by Small Particles*, New York, Wiley, 1983.
11. Chandrasekhar, S., *Radiative Transfer*, London, Oxford University Press, 1960.
12. Cheong, W.-F., Prahl, S.A., and Welch, A.J., "A Review of the Optical Properties of Biological Tissues," *IEEE Journal of Quantum Electronics*, Vol. 26, No. 12, 1990, pp. 2166-2185.
13. Steinke, J.M., and Shepherd, A.P., "Comparison of Mie Theory and the Light Scattering of Red Blood Cells," *Applied Optics*, Vol. 27, No. 19, 1988, pp. 4027-4033.
14. Wang, L., Jacques, S.L., and Zheng, L., "MCML - Monte Carlo Modeling of Light Transport in Multi-layered Tissues," *Computer Methods and Programs in Biomedicine*, Vol. 47, 1995, pp. 131-146.
15. Graaff, R., Koelink, M.H., de Mul, F.F.M., Zijlstra, W.G., Dassel, A.C.M., and Aarnoudse, J.G., "Condensed Monte Carlo Simulations for the Description of Light Transport," *Applied Optics*, Vol. 32, No. 4, 1993, pp. 426-434.
16. Anderson, N. M., and Sekelj, P., "Light Absorbing and Scattering Properties of Non-haemolysed Blood," *Phys. Med. Biol.*, Vol. 12, No.2, 1967, pp. 173-184.
17. Petrig, B.L., and Riva, C.E., "Near-IR Retinal Laser Doppler Velocimetry and Flowmetry: New Delivery and Detection Techniques," *Applied Optics*, Vol.30, No. 16, pp. 2073-2078.
18. Sullivan, P.M., Davies, G.E., Caldwell, G., Morris, A.C., and Kohner, E.M., "Retinal Blood Flow During Hyperglycemia - A Laser Doppler Velocimetry Study," *Investigative Ophthalmology and Visual Science*, Vol. 31, No. 10, 1990, pp. 2041-2045.
19. Smith, M.H., Lompado, A., "Three Dimensional Monte Carlo Simulation of Light Propagation Through a Blood Column," In preparation
20. Lee, V.S., and Tarassenko, L., "Absorption and Multiple Scattering by Suspensions of Aligned Red Blood Cells," *Journal of the Optical Society of America*, Vol. 8, No. 7, 1991, pp. 1135-1141.

21. Hammer, M., Schweitzer, D., Michel, B., Thamm, E., and Kolb, A., "Single Scattering by Red Blood Cells," *Applied Optics*, Vol. 37, No. 31, 1998, pp. 7410-7418.
22. Handbook of Chemistry and Physics, Weast, R.C. ed., The Cambridge Rubber Co (CRC), Cleveland, Ohio, 1970.
23. van Assendelft, O.W., *Spectrophotometry of Hemoglobin Derivatives*, Assen, Roal Vangorcum, 1970.
24. Williams, W.J., Beutler, E., Erslev, A.J., and Lichtman, M.A., *Hematology*, New York, McGraw-Hill, 1983.
25. Johnson, C.C., "Near Infrared Propagation in Blood," *Journal of the Association for the Advancement of Medical Instrumentation*, Vol. 4, No. 1, 1970, pp. 22-27.

An Instrument for the Measurement of Retinal Vessel Oxygen Saturation

Jonathan Drewes^{*a}, Matthew Smith^a, Kurt Denninghoff^b, Lloyd Hillman^a

^a Physics Department, The University of Alabama in Huntsville, Huntsville, AL 35899

^b Department of Emergency Medicine, The University of Alabama at Birmingham, Birmingham, AL 35226

ABSTRACT

Retinal vessel oxygen saturation has been suggested as a parameter for monitoring a wide range of conditions including occult blood loss and a variety of ophthalmic diseases. We have developed an Eye Oximeter (EOX), that noninvasively measures the oxygen saturation of the blood in individual large retinal vessels using scanning lasers. One-dimensional vessel extinction profiles are obtained at four wavelengths (629, 678, 821 and 899 nm), and the vessel transmittances computed. The oxygen saturation of blood within the vessel is then calculated from the transmittance data. We have performed an *in vitro* experiment on human blood which demonstrates the calibration of the EOX measurement and validates our oximetry equations. Retinal vessel oxygen saturation was measured in a human subject and found to be 65 %O₂Sat and 101 - 102 %O₂Sat in the veins and arteries on the optic disk. Irregularities in the background measured away from the optic disk resulted in a larger variance in the calculated saturation when compared to measurements made on the disk.

Keywords: retina, blood, oximetry, oxygen saturation, hemoglobin concentration, noninvasive, blood loss

1. INTRODUCTION

The arteries and veins of the human retina are not covered by thick layers of highly scattering tissue and can be directly imaged through the pupil of the eye. This optical accessibility has prompted several investigators to develop devices to measure the oxygen saturation of the blood within these vessels^{1,2,3,4,5,6}. These investigators hypothesized that retinal arterial and venous oxygen saturations may be useful parameters for diagnosis of conditions ranging from diabetic retinopathy to occult blood loss in a trauma setting. The accurate measurement of retinal oxygen saturation remains a significant challenge. We are unaware of any reliable and easy-to-use device in widespread clinical practice.

Our group previously reported on a two-wavelength Eye Oximeter (EOX) prototype⁵. We used this instrument in a series of animal studies to demonstrate the correlation between retinal venous oxygen saturation and early blood loss^{7,8}. However, the primary shortcoming of two-wavelength retinal oximetry is the inability to account for scattering caused by red blood cells. As a result, our early instrument could follow trends in oxygen saturation but could not provide calibrated measurements of saturation. In this paper, we present a second generation of the EOX. This device uses four diode lasers at wavelengths 629, 678, 821, and 899 nm which may allow for accurate, absolute measurements of oxygen saturation in retinal vessels.

* Correspondence: drewesj@email.uah.edu

2. INSTRUMENTATION

The EOX optical system is composed of four separately-functioning subsystems: the laser scanning system, the retinal illumination system, the retinal imaging system, and the laser detection system. The instrument is rugged and designed for use in an animal laboratory or clinical environment. The EOX is compact with a light-tight plastic cover.

The retinal illumination path (Figure 1) illuminates a circular portion of a patient's retina. This allows the operator to directly observe the patient's retinal vessels. White light is generated using an incandescent bulb (Welch Allyn WA-03000 ophthalmoscope bulb) and is linearly polarized by P2. The bulb illuminates a 3 mm diameter retinal area using lens L3 to image the filament onto the eye's pupil. This optical path is combined with the laser scanning path using a dichroic beamsplitter, DBS, that reflects the laser wavelengths greater than 620 nm and transmits the shorter wavelengths.

The retinal imaging path presents an image of the illuminated retinal area to the instrument operator. The EOX presents an upright retinal image to the operator, which allows a quick comparison with direct ophthalmoscopy. The fold mirror M1 corrects the image flip caused by reflection from the 50/50 beamsplitter, and a second lens L7 re-inverts the image. A prism redirects the optical path to the eyepiece which allows the EOX to be used on a prone (lying on the back) patient. The lens L7 is mounted to a translation stage to correct for the combined refractive errors of the patient and operator over a ± 7 diopter range.

In the laser scanning path, four laser beams are linearly scanned via a galvanometer scanner into the eye and across the retina. Two dichroic beamsplitters and one 50 % transmission neutral density filter combine and align the beams from four collimated, astigmatically corrected, TTL-modulated diode lasers. This produces a ~ 3 mm diameter beam. A protected aluminum mirror folds the colligned laser beams into the EOX head. The entire EOX laser module is detachable and uses dowel pins for precise re-alignment. This allows future versions of the EOX to have lasers coupled into the head via fiber optics. A broadband cube beamsplitter assures that the polarization orientations are all equal. Lenses L1 and L2 focus and re-collimate the beam. The refractive power of the emmetropic eye (focused at infinity) focuses the beams onto the retina. Translation of lens L1 corrects for refractive errors of the patient's eye over a ± 7 diopter range. The lens L2 images the scanner onto the eye's pupil. The diameter of the scanned beam at the eye's pupil is about 2 mm, sufficient to enter most constricted pupils. This design requires that the scan mirror move through an angle $\pm 5^\circ$, corresponding to a retinal scan length of 1400 μm . The laser output power of the EOX is about 130 μW during a measurement sequence. This power is approximately one-tenth of the Class I limit

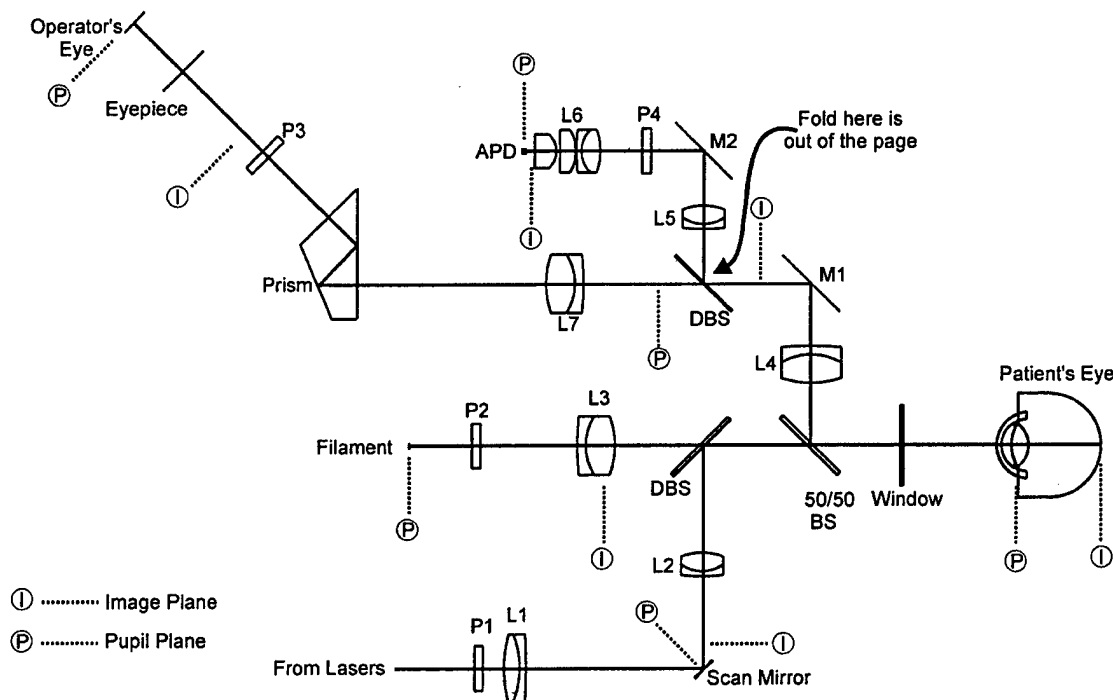


Figure 1 EOX optical layout showing the pupil and image planes.

for human eye exposure, given the modulation frequency, duty cycle, and scan time used¹⁰.

The laser light exiting the eye is collected by imaging the eye's pupil onto an avalanche photodiode (APD). The image at the APD remains stationary as the lasers are scanned. A dichroic beamsplitter, DBS, separates the white light in the retinal imaging path from the laser light for detection. The polarizer P4 in this path transmits the polarization state orthogonal to that of the lasers. This helps to attenuate the specular reflection of the lasers from the cornea and the vessel apex.

A Microstar Labs DAP3000/212a card controls the EOX. This card reads the APD signal with 12-bit A/D, modulates the laser output via TTL signals, and drives the galvanometer scanner with 12-bit D/A. The card uses an onboard 486-processor and 4 MB of RAM to perform measurements smoothly, without interrupt across the PC bus.

An operator observes the subject's retina through the eyepiece to target vessels for measurement. The patient follows a fixation target with the opposite eye until the vessel of interest is centered in the operator's eyepiece cross hairs. The operator focuses the instrument to correct for the refractive errors of the operator and the patient. Then the operator initiates the measurement sequence (lasting 68 ms), acquiring a vessel extinction profile. During one point of the scan, the four lasers fire sequentially for 24 μ s each (Figure 2). After this, a 24 μ s background signal is acquired. The detector is repeatedly sampled at regular intervals by the 12-bit A/D. The galvanometer scan mirror is driven by a linear voltage, creating a linear scan at the retina. The four lasers and background cycle 512 times during the scanner movement. Finally, we subtract the background signal from each laser sample and record the four acquired scans.

3. IN VITRO CALIBRATION

3.1 Experimental Procedure

The eye is a complex environment in which to perform spectroscopic measurements. We attempted to simplify this environment using a model eye in order to calibrate the EOX measurement. This was accomplished by eliminating characteristics of the human eye which are undesirable and difficult to control. Previous experiments on swine and human subjects have shown that there are many factors which can greatly influence the scan profile.

In the design of the model eye, the effective focal length and entrance pupil diameter are matched to that of the human eye. Within the artificial eye, a micropipet rests against a 4 mm thick slab of Spectralon® (Labsphere, Inc.). A tapered micropipet with an inner diameter that varies from 110 to 268 μ m along its length simulates the larger retinal vessels found near the optic disk. The interior of the artificial eye is filled with fluid that is index-matched to the micropipet. This eliminates reflection and refraction from the micropipet surface which affects the scan profiles. The orientation of the micropipet is nearly perpendicular

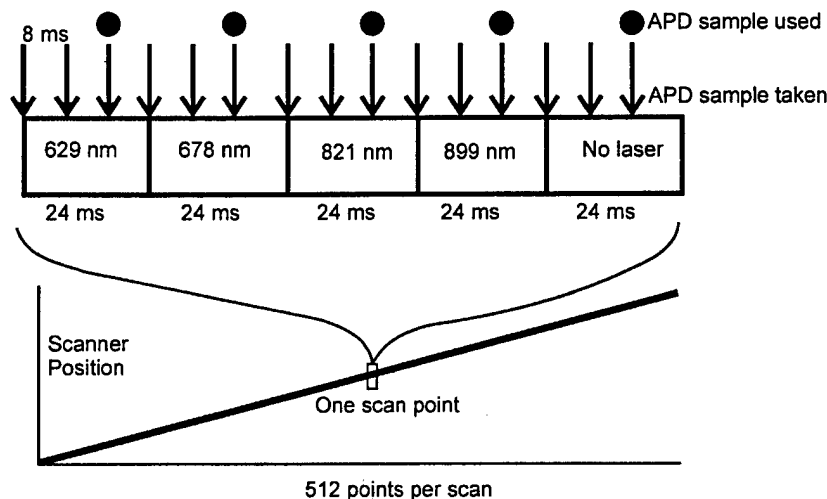


Figure 2 This block diagram illustrates the scan position, laser state, and detector sampling which occurs during one EOX measurement.

to the EOX scan for the measurements described here. With a syringe and connecting tube attached to one end of the pipet, blood is injected into the micropipet from outside of the artificial eye and exits the other end of the micropipet into a catch jar. For its diffuse reflectance properties, the Spectralon background material of the model eye was chosen so that only singly-passed light through the blood column is measured by the detector.

Five quantities of blood with different hemoglobin concentrations ranging from 5.0 to 27.2 g/100mL were prepared. For each quantity, blood was produced with saturations ranging from 6 to 87 %O₂Sat totaling 20 combinations of oxygen saturation and concentration. A CO-oximeter was used to measure the oxygen saturation and hemoglobin concentration. At a given diameter, 16 scans were acquired. For each blood sample injected into the model eye, between 5 and 13 different diameters were obtained. In all, 187 different combinations of s , c , and d were scanned.

3.2 Analysis and Results

The blood column extinction profiles are obtained at the four measuring wavelengths and the corresponding transmittances computed. The oxygen saturation is then calculated from the transmittance data. A linear wavelength-dependant scattering oximetry model is used to describe the transmittance of a vessel at a given wavelength

$$T^\lambda = T_s^{\lambda_0} \left[1 + m(\lambda - \lambda_0) \right] 10^{-cd \left[s\epsilon_{HbO_2}^\lambda + (1-s)\epsilon_{Hb}^\lambda \right]} \quad (1)$$

where c is the hemoglobin concentration, d is the diameter of the vessel, s is the oxygen saturation, the ϵ 's are the absorption coefficients of the hemoglobin and reduced hemoglobin, $T_s^{\lambda_0}$ is a constant describing the scattering transmittance at the shortest measuring wavelength λ_0 , and m is a constant that describes the linear wavelength dependance of the scattering transmittance. The model eye experiment was used to determine the value of m which calibrates the EOX measurement.

The oximetry model was applied to the data set to calculate s , cd , and $T_s^{\lambda_0}$. These three parameters are calculated for each of the 16 scans of a particular s , c , and d combination. Typical values of the scattering constant $T_s^{\lambda_0}$ are found to range between 0.70 to 0.95, with calculated cd products from 1000 to 8000 $\mu\text{m-g/dL}$. The 16 saturations are averaged to report a single measurement. To reduce measurement noise, the mean of the saturations was taken for similar values of the actual s and c parameters. This is justified since no dependance of the c nor d parameters on the calculated saturation was found to exist. In Figure 3 we report the mean calculated saturation against the known value with a line of unity indicated. The slope of the best fit line to this data is 0.90 with an intercept of 0.05 and an r -squared value of 0.91. Most of the data fell within one standard deviation of the expected error in saturation assuming a transmittance measurement error⁹ of 1 %. The value of the scattering slope factor that best calibrated the data set corresponds to a 3 % increase of the scattering transmittance over the EOX wavelengths. Further, the average residual between the measured transmittance and the model's prediction was 0.29 %.

4. HUMAN EYE MEASUREMENTS

The EOX is mounted to a slit lamp base to make measurements on human subjects. With the eye placed at the exit window of the EOX, the patient fixates on a light bulb positioned by the operator to target a retinal vessel. Focus adjustment is made which corrects for the combined refractive errors of the patient and operator. Adjustment of the laser focus is made by minimizing the observed width of the line scan on the patient's retina.

In this study, several locations of a subject's fundus were scanned on two occasions. Fundus photographs are used for reference during the EOX measurement to provide a record of the scan location. While this is not necessary to make the EOX measurement, the fundus photograph has proven to be a useful tool in understanding scan profile features. In this experiment, each scan site was chosen to allow the simultaneous measurement of both an artery and a vein. Vessels are scanned on the optic

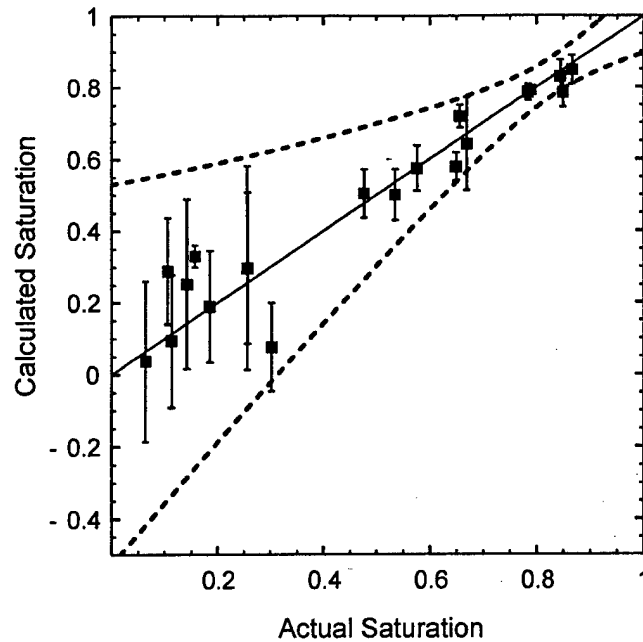


Figure 3 The calculated oxygen saturation from the model eye experiment was within the expected oxygen saturation error.

disk, near the disk, and up to 3 disk diameters away from the disk. There are 32 scans acquired at each site. Example scan profiles are presented in Figure 4.

The scans that are acquired off of the disk exhibit background features which can significantly influence the measured transmittance of a vessel. Often, these features are wavelength dependant and result in erroneous oxygen saturation measurement. As an example of a scan acquired off of the disk, Figure 4 shows a region to the left of the artery with a large intensity increase at 629 and 678 nm. This feature is not present at 821 and 899 nm. Measurement of the vessel transmittance, and in turn, the oxygen saturation, becomes difficult because of this background irregularity. There are other attributes of the scan profiles acquired off of the disk that introduce error into the transmittance measurement. Currently, we are investigating the cause of these attributes.

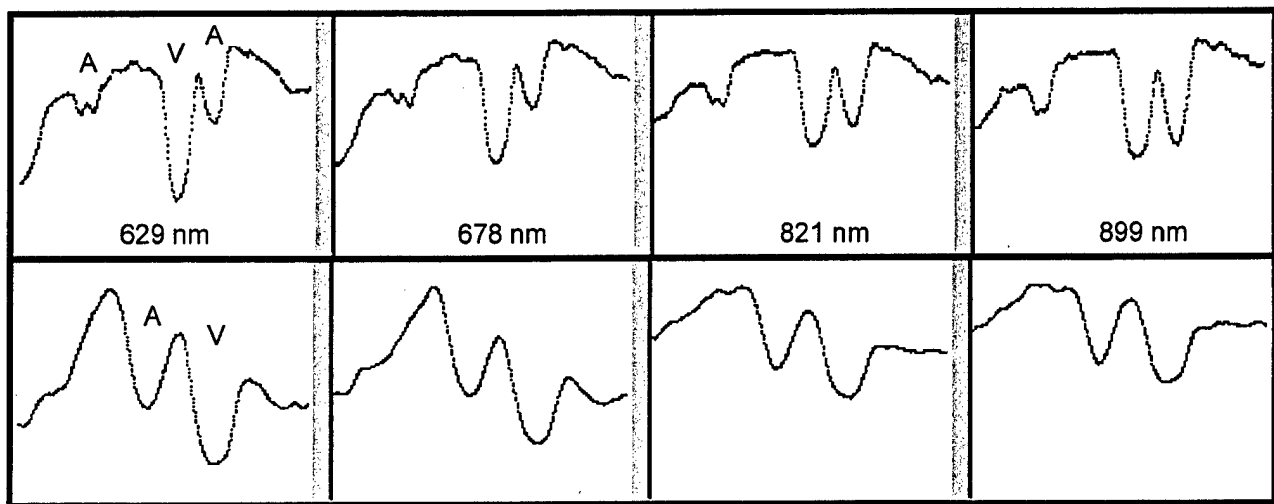


Figure 4 The top set of scans were taken on the optic disk; the bottom set of scans were acquired off of the disk.

Typically, the scans acquired on the disk are absent of background irregularities near the vessels. This lowers the error in the measured vessel transmittance. For this reason, we have more confidence in the oxygen saturation measurements made on the optic disk.

Using the *in vitro* calibration and Eqn. (1), s , cd , and $T_s^{\lambda_0}$ were calculated for each scan. Typical values calculated for the concentration-diameter parameter range from 2000 - 4500 $\mu\text{m-g/dL}$ and 0.80 - 0.97 for the scattering transmittance. Table 1 summarizes the calculated oxygen saturation, comparing its value at the two regions of the retina. As expected, the venous measurements have a larger standard deviation than the arteries. The oxygen saturation of the vessels on the disk was found to be 65 %O₂Sat and 101 - 102 %O₂Sat for veins and arteries, respectively. Retinal venous oxygen saturation has been reported in the literature to be 45 and 55 %O₂Sat^{3,4}. We expect arterial oxygen saturation to be near 100 %O₂Sat. Most notable in these results is the higher standard deviation of the calculated oxygen saturation for measurements made off of the disk. This is a result of the higher transmittance error, and thus the oxygen saturation error, caused by background irregularities near the vessel.

5. DISCUSSION

The design principles of the Eye Oximeter, an instrument which noninvasively measures the oxygen saturation of the blood within retinal vessels, have been discussed. We presented the EOX technique of scanning four lasers into the eye and across targeted vessels, generating one-dimensional intensity profiles. From the acquired scan profiles, the oxygen saturation of blood within these vessels is calculated. We use a linear wavelength dependent transmission model to account for scattering by the blood. Our oximetry equation was calibrated via an *in vitro* experiment which resulted in a 3 % increase in the scattering transmission over our wavelength range.

With the wavelengths used in the EOX, the expected error in calculated oxygen saturation has a minimum of $\pm 4\%$ at 83 %O₂Sat and increases to $\pm 52\%$ at 0 %O₂Sat. This calculation assumes a vessel diameter of 150 μm , a concentration of 15 g/dL, and a 1 % error in the transmittance. Calculated saturation error can be significantly reduced by carefully selecting wavelength combinations which are sensitive to oxygen saturation⁹. Other retinal oximeters which use different wavelength combinations are being implemented for future studies.

ACKNOWLEDGMENTS

This work was supported by grants from the United States Army Medical Research and Materials Command and The University of Alabama in Huntsville.

Table 1 Comparison of the measured oxygen saturation in locations on and off of the optic disk.

	Veins			Arteries		
	s (%O ₂ Sat)	s std. dev. (%O ₂ Sat)	number of scans	s (%O ₂ Sat)	s std. dev. (%O ₂ Sat)	number of scans
Experiment 1, off the disk	63	18	544	98	5	448
Experiment 1, on the disk	65	5	68	101	3	30
Experiment 2, on the disk	65	11	190	102	2	127

REFERENCES

1. J. B. Hickam, R. Frayser, J. C. Ross, "A study of retinal venous blood oxygen saturation in human subjects by photographic means," *Circulation* **27**, 375-385 (1963).
2. A. J. Cohen, R.A. Laing, "Multiple scattering analysis of retinal blood oximetry," *IEEE Trans. Biomed. Eng.* **23**(5), 391-400 (1976).
3. F. C. Delori, "Noninvasive technique for oximetry of blood in retinal vessels," *Appl. Optics* **27**(6), 1113-1125 (1988).
4. D. Schweitzer, L. Leistritz, M. Hammer, M. Scibor, U. Bartsch, J. Strobel, "Calibration-free measurement of the oxygen saturation in retinal vessels of men," in *Ophthalmic Technologies V*, Jean-Marie Parel, Qiushi Ren, Karen M. Joos, Editors, Proc. SPIE 2393, 210-218 (1995).
5. M. H. Smith, K. R. Denninghoff, L. W. Hillman, R. A. Chipman, "Technique for noninvasively monitoring blood loss via oxygen saturation measurements of blood in retinal vessels," *J. Biomed. Optics*, (in press).
6. J. S. Tiedeman, S. E. Kirk, S. Srinivas, J. M. Beach, "Retinal oxygen consumption during hyperglycemia in patients with diabetes without retinopathy," *Ophthalmology* **105**(1), 31-36 (1998).
7. K. R. Denninghoff, M. H. Smith, R. A. Chipman, L. W. Hillman, P.M. Jester, C.E. Hughes, F. Kuhn, L. W. Rue, "Retinal large vessel oxygen saturation correlates with early blood loss and hypoxia in anesthetized swine," *J. Trauma* **43**(1), 29-34 (1997).
8. K. R. Denninghoff, M. H. Smith, R. A. Chipman, L. W. Hillman, P.M. Jester, F. Kuhn, D. Redden, L. W. Rue, "Retinal venous oxygen saturation correlates with blood volume," *Acad. Emerg. Med.*, **5**(6), 577-582 (1998).
9. M. H. Smith, "Optimal wavelength combinations for retinal vessel oximetry," *Applied Optics*, **38**(1) (1999).
10. American National Standards Institute, *American National Standard for Safe Use of Lasers*, ANSI Z136.1-1993.

Effect of multiple light paths on retinal vessel oximetry

Revised Manuscript

Matthew H. Smith

Physics Department
The University of Alabama in Huntsville
Huntsville, AL 35899
phone: (256) 890-6417 ext. 318
fax: (256) 890-6077
email: SmithMH@email.uah.edu

Kurt R. Denninghoff

Department of Emergency Medicine
The University of Alabama at Birmingham
Birmingham, AL 35294

Arthur Lompado

Physics Department
The University of Alabama in Huntsville
Huntsville, AL 35899

Lloyd W. Hillman

Physics Department
The University of Alabama in Huntsville
Huntsville, AL 35899

Abstract

Techniques for noninvasively measuring the oxygen saturation of blood in retinal arteries and veins are reported in the literature, but none have been sufficiently accurate and reliable for clinical use. Addressing the need for increased accuracy, we present a series of oximetric equations that explicitly consider the effects of backscattering by red blood cells and lateral diffusion of light in the ocular fundus. The equations are derived for the specific geometry of a scanning-beam retinal vessel oximeter, however the results should also be applicable to photographic oximeters. We present *in vitro* and *in vivo* data that suggest the validity of these equations.

OCIS Codes

170.0170, 170.1470, 170.3660, 170.4460, 170.6510

1. Introduction

The arteries and veins of the retina are directly observable through the pupil of the eye. This optical accessibility of these vessels has prompted several investigations into noninvasive spectroscopic measurements of the oxygen saturation of the blood within the vessels^{1,2,3,4,5,6,7,8,9}. Each of the reported investigations into retinal vessel oximetry determines the oxygen saturation of blood within a retinal vessel via spectroscopic oximetry¹⁰. Proposed diagnostic applications of retinal vessel oxygen saturation measurements range from monitoring glaucoma and diabetic retinopathy to noninvasively indicating blood loss in trauma victims.

The first retinal oximetry experiments, reported by Hickam and Frayser in 1963, used two different wavelength combinations¹. Broadband (>100 nm FWHM) Wratten filters centered at 800 nm and 640 nm were used in a red/infrared instrument. A red/green instrument used interference filters (10 nm FWHM) centered at 640 nm and 510 nm. Both instruments were fundus cameras modified to take dual, quasi-monochromatic retinal photographs. Optical densities of the vessels were measured through manual analysis of the exposed film.

Cohen and Laing² reported a similar instrument in 1976. This instrument employed a blue/green combination, using interference filters (20 nm FWHM) centered at 470 nm and 515 nm. The Multiple Scattering Theory of Twersky¹¹ was used to explain their experimentally determined calibration curve.

In 1988, Delori³ reported a three-wavelength retinal vessel oximeter. This device scanned a slit of filtered light across the retina and automatically interpreted collected data via a computer algorithm. Three closely-spaced green wavelengths (558 nm, 569 nm and 586 nm) were chosen for this measurement so that the constant-scattering approximation of Pittman and Duling¹² could be applied.

Schweitzer *et. al.*⁴ demonstrated a retinal imaging spectrometer in 1995. This technique is unique in that it determines retinal vessel oxygen saturation via transmittance measurements made at 2 nm increments from 400 nm to 700 nm. An empirical model of the wavelength dependence of scattering losses by red blood cells is also presented.

A recent photographic retinal oximeter was described in 1998 by Tiedeman, Beach, *et. al.*⁷. This instrument illuminates the retina with filtered light (8 nm FWHM) at 569 nm and

600 nm, and acquires images on a high dynamic range CCD camera. These investigators have quantified the influence of retinal pigmentation on the calibration of their technique⁹.

Finally, Smith, Denninghoff, *et. al.*^{5,6} described in 1997 the first oximeter to focus lasers onto a subject's retina and scan the beams across a retinal vessel. Initial studies at two wavelengths (670 nm and 803 nm) showed significant variations in calibration between subjects. Recent *in vitro* studies¹³ at four wavelengths (729, 678, 821 and 899 nm) attained an excellent calibration in a model eye by identifying a scattering wavelength dependence of blood. It will be shown in this paper, however, that this wavelength-dependant scattering model does accurately describe measurements made *in vivo*.

Despite the scientific and engineering advancements made by each of these investigators, making highly accurate and reliable retinal saturation measurements remains an elusive goal. We are unaware of any devices that have been definitively shown to measure retinal oxygen saturation independent of vessel diameter, hemoglobin concentration, and fundus pigmentation.

One of the confounding aspects of whole-blood spectroscopic oximetry techniques is the scattering of light caused by the refractive index discontinuity between red blood cells and the plasma in which they are suspended^{14,15,16}. While most recent attempts at retinal vessel oximetry have employed some sort of scattering compensation, in this paper we broaden the analysis of these scattering effects.

We also describe another effect that complicates retinal vessel oximetry. This effect is the lateral diffusion of light in the layers of the ocular fundus that lie beneath the retinal vasculature. As a result of this diffusion, a fraction of the light detected by a retinal oximeter has undergone a single absorption pass through the blood vessel, and a portion of the light has

undergone a double pass. We refer to this mixture of single-pass and double-pass light as “multipass” transmission. Most previous retinal oximetry investigations mention this effect, but in this paper we provide a more detailed mathematical treatment.

By examining all of the light paths that comprise a retinal vessel oxygen saturation measurement, we derive an oximetry equation that accounts for both scattering and multipass effects. Unfortunately, it is difficult to calculate oxygen saturation using this equation due to the large number of unknown parameters. To overcome this difficulty, we present a number of approximations to the oximetry equation that allow the calculation of oxygen saturation under certain simplifying approximations. Finally, we present *in vivo* data acquired in swine and *in vitro* data acquired in a model eye that indicate the utility of these equations.

2. Light Paths in Retinal Vessel Oximetry

There are two optical techniques that have been used to spectroscopically determine the oxygen saturation of blood in retinal vessels. In the first method, an area of the retina is illuminated and retinal images are formed on film or on a CCD detector array. These retinal images are acquired at multiple wavelengths. In the second method, multiple monochromatic beams are scanned across a retinal vessel, and the light that reflects back out of the eye is collected at discrete points along the scan. In both methods, the reflected light from the center of the vessel is compared to the reflected light from the fundus on each side of the vessel to calculate the transmittance of the blood within the vessel. An oximetric equation is used to calculate oxygen saturation from the transmittance measurements made at multiple wavelengths.

The discussions that follow are derived for a scanning retinal vessel oximeter system; however, all of the results should be applicable to an imaging system.

Figure 1 illustrates the primary light paths in retinal vessel oximetry. A beam of light with flux Φ_0 is directed into the pupil of the eye and is focused onto a retinal vessel. A retinal vessel oximeter system then collects the fraction of light that is reflected back out of the pupil of the eye. There are several light paths that contribute to this collected power. First, some quantity Φ_{media} of the incident flux may directly backscatter from the lens or vitreous and be collected. Next, there is a specular reflection from the apex of the vessel, Φ_{glint} , that may exit the pupil and be collected. This reflection may originate from the inner limiting membrane¹⁷ or from the vessel wall, but any portion of this glint that is caused by backscattering from blood within the vessel is considered in a separate term, Φ_{bs} , below. As the incident beam propagates through the blood within the vessel, the flux of the beam is decreased via the Lambert-Beer Law due to absorption by hemoglobin and oxyhemoglobin within the red blood cells (RBCs). Additionally, light is scattered by the RBCs. Some quantity of this scattered light, Φ_s , is scattered into angles that cannot be collected by the instrument, causing an apparent *increase* in absorption. There is another quantity of light, Φ_{bs} , that is directly backscattered toward the instrument, resulting in an apparent *decrease* in absorption.

The beam that emerges from the other side of the vessel is enlarged due to scattering and attenuated due to absorption. The beam traverses the transparent rods and cones of the retina and finally reaches the scattering layers of the retinal pigment epithelium (RPE) and choroidal plexus that are $\sim 240 \mu\text{m}$ posterior to the vessel¹⁸. Strong melanin and hemoglobin absorption limits lateral diffusion and result in a tightly localized point spread function (PSF) on the RPE for

visible wavelengths shorter than 575 nm. Wavelengths much longer than 575 nm penetrate the choroid deeply, reflecting off of the sclera and passing back through the choroid. As a result, the laterally diffused PSF of these longer wavelengths is much larger than that of shorter wavelengths. Reasonable estimates for the width (twice the standard deviation) of the diffusion enlarged PSF in the nasal fundus (near the optic nerve head) have been reported to be $\sim 60 \mu\text{m}$ from 450 to 575 nm and $\sim 150 \mu\text{m}$ from 600 to 750 nm¹⁹. A fraction of the light, Φ_{dp} , within this diffused PSF will pass back through the vessel to be absorbed and scattered in double pass, and then exit the pupil of the eye. Additionally, a fraction, Φ_{sp} , will extend beyond the edge of the vessel and exit the pupil of the eye in single pass. Note that this geometry illustrated in Fig. 1 is specific to a scanning-beam oximeter. In a photographic oximeter geometry, the single pass component, Φ_{sp} , would be incident on the fundus lateral to vessel and reflect out of the eye through the vessel. The resulting equations derived in the next section, however, should remain the same.

Figure 2, drawn to scale, demonstrates the likely existence of both single-pass and double-pass components of collected light. A $100 \mu\text{m}$ retinal vessel positioned $240 \mu\text{m}$ anterior to the reflecting layers of the ocular fundus is considered. Two separate diffusion enlarged PSF's are considered, a $60 \mu\text{m}$ (twice the standard deviation) PSF typical of blue wavelengths and a $150 \mu\text{m}$ PSF typical of red and near infrared wavelengths. Finally, 10° cones of light are illustrated that indicate the acceptance angle of a $\sim 4 \text{ mm}$ diameter pupil located 22 mm away. Thus, only light in this solid angle can be collected by a retinal vessel oximeter. It is clear from this illustration that both single-pass and double-pass absorption need to be considered for typical retinal geometries. The relative magnitudes of these components depend on numerous factors

including the PSF size, the diameter of the pupil, the vessel diameter, and the specular / diffuse reflectance properties of the ocular fundus. The relative magnitudes of single-pass and double-pass transmission are also acutely dependant on the specific geometry of the oximeter apparatus. A Monte Carlo simulation of retinal vessel profiles performed by Hammer, *et. al.*²⁰ predicts that the single-pass, double-pass, and backscattered components contribute nearly equally for a 100 μm vessel. Single-pass light dominates for smaller (25 μm) vessels, and backscattered light dominates for larger (200 μm) vessels.

3. Oximetry Equations

3.1 The traditional oximetry equation

To date, all attempts at retinal vessel oximetry have employed some form of the equation

$$T_v(\lambda) = T_s(\lambda) \exp[-\varepsilon(\lambda) \chi c d], \quad (1)$$

where

$$\varepsilon(\lambda) = s \varepsilon_{HbO_2}(\lambda) + (1-s) \varepsilon_{Hb}(\lambda). \quad (2)$$

In this equation, $T_v(\lambda)$ is the measured transmittance of a retinal vessel at wavelength λ . This transmittance is calculated by dividing the collected flux from the center of a vessel, Φ_v , by the flux collected from the fundus on either side of the vessel, Φ_f . A typical technique for measuring T_v is illustrated in Fig. 3. The exponential term of Eq. (1) is simply the Lambert-Beer Law describing the absorption of light by the blood within the vessel, where s is the oxygen saturation, c is the hemoglobin concentration, and d is the diameter of the vessel (*i.e.*, the path length

through the vessel). The absorption coefficients $\varepsilon_{Hb}(\lambda)$ and $\varepsilon_{HbO_2}(\lambda)$ of hemoglobin and oxy-hemoglobin, respectively, are well known functions of wavelength^{10,21}. The scattering effects of RBCs are described by the transmittance factor $T_s(\lambda)$. This factor represents light that has been scattered into angles that are not collected by the retinal oximeter. These photons are “lost”, resulting in an apparent increase in the vessel absorption (*i.e.*, decreased transmittance). Some of the scattering factors that have been used include constants³, linear functions¹³, and empirical functions of wavelength⁴. A geometry-dependant correction factor, χ , can be included in the absorption term. By measuring $T_v(\lambda)$ at multiple wavelengths, values of s , $T_s(\lambda)$, and the χcd product can be directly calculated or determined by a least-squares regression.

The parameter χ in Eq. (1) warrants further consideration. If all of the light collected by a retinal oximeter traversed the blood vessel in double-pass, then χ would equal two. Similarly, if all of the collected light traversed the vessel in single-pass, then χ would equal one. It is tempting to assume that χ would simply take on a value between one and two for the case of multipass transmission and that this value would be absorbed into the χcd product. However, as shown in the next section, this assumption is not accurate.

3.2 The general multipass transmittance oximetry equation

We derive an oximetry equation based on the light paths described in Fig. 1. As illustrated in Fig. 3, the transmittance, T_v , of a retinal vessel is defined as the ratio

$$T_v = \frac{\Phi_v}{\Phi_f}, \quad (3)$$

where Φ_v is the measured flux from the center of a vessel, and Φ_f is the measured flux from the ocular fundus on either side of the vessel. The flux reflected from the fundus can be expressed simply as

$$\Phi_f = R_f \Phi_0, \quad (4)$$

where Φ_0 is the incident flux, and the reflectance of the fundus, R_f , can encompass numerous factors such as the transmittance of the ocular media, the spectral characteristics of the absorbing layers of the ocular fundus, and the diameter of the exit pupil of the eye. Note that Φ_f cannot be measured directly, and its value must be interpolated from reflectance measurements on either side of the vessel. In practice, the data used to determine Φ_f must be measured sufficiently far from the vessel that the diffusion enlarged PSF does not interact with the vessel causing a decreased background measurement.

To determine the flux collected from the center of a vessel, Φ_v , consider all of the light paths in Fig. 1 that can exit back out of the eye and be detected by the oximeter instrumentation. A summation of these light paths yields the expression

$$\Phi_v = \Phi_{sp} + \Phi_{dp} + \Phi_{bs}, \quad (5)$$

where Φ_{sp} is light that traversed the vessel in single-pass, Φ_{dp} traversed the vessel in double-pass, and Φ_{bs} is light that has been directly backscattered by the blood.

The single-pass and double-pass absorption components can be expressed via the Lambert-Beer Law, resulting in

$$\Phi_v = \alpha R_f \Phi_0 \exp(-\epsilon cd) + \beta R_f \Phi_0 \exp(-2\epsilon cd) + \Phi_{bs}. \quad (6)$$

The absorption coefficient ϵ is defined by Eq. (2), and the wavelength dependance of ϵ still exists but is no longer stated explicitly. The coefficients α and β are the fractions of light transmitted in single-pass and double-pass, respectively.

It is important to note that a series of approximations have been made in the derivations of Eq. (4) and Eq. (6). First, we have neglected Φ_{media} as a collected light path. A confocal optical system will prevent light backscattered from the lens and vitreous from reaching the detector. For photographic systems and non-confocal scanning systems, however, it is not clear that this backscattered light will be negligible. Future studies should address this effect. Additionally, we assume that Φ_{glint} will be prevented from affecting the measurement. Several techniques for eliminating the effects of the glint have been proposed; portions of the vessel lateral to the glint can be used for analysis^{3,9}, areas along the vessel that are free of glints can be used¹, or curve-fitting to the vessel profile can estimate the transmittance in the absence of the glint⁶. We have found that illuminating the eye with vertically polarized light and collecting only horizontally polarized light nearly eliminates the glint in scans acquired from a human eye. While the crossed polarizers result in significantly reduced signals, high quality scans that are free of glints (such as the scan in Fig. 3) can be easily obtained. Also note that any flux scattered out of the incident beam by the lens or vitreous and any light reflected out of the incident beam by the inner limiting membrane (ILM) or vessel wall should have been subtracted out of Φ_0 in Eq. (4) and Eq (6). We assume that these scattering and reflection losses are the same at the vessel and lateral to the vessel, and we choose to retain the term Φ_0 in order to reduce complexity and avoid confusion. Finally, note that the double-pass component of this expression is an approximation due to the elliptical cross section of retinal vessels.

The scattering properties of samples of whole blood have been studied extensively^{22, 23}, and several techniques^{24, 25, 26} have been used to predict these scattering properties. An important result of those studies is the relationship between the transmitted and reflected (*i.e.*, backscattered) portions of light incident on a sample of whole blood. Anderson and Sekelj²³ experimentally determined that the reflectance, R , of a blood sample is linearly related to the sample transmittance, T , resulting in the equation

$$R = a_1 + a_2 \exp(-\varepsilon cd) . \quad (7)$$

Here, a_1 and a_2 are critically dependant on the sample hematocrit (*i.e.*, volume fraction of RBCs in whole blood) and the geometries of the source, detector, and sample. However, neither a_1 nor a_2 depend on the oxygen saturation of the sample. The experimental data supporting Eq. (7) was acquired between 600 and 630 nm, and the reflectance, R , refers to the light reflected into the entire back hemisphere from a planar sample. This linear relationship between reflectance and transmittance is predicted by Twersky's Multiple Scattering Theory¹¹, and the relationship should remain valid at wavelengths outside the 600 to 630-nm range tested by Anderson. In addition, the parameters a_1 and a_2 account for the incomplete collection of the back hemisphere, as is the case in the eye. Because measurements were performed for planar slabs of blood, we are not certain that Eq. (7) is valid for light scattered by the cylindrical geometry of blood in a retinal vessel. However, we are unaware of any analytical models of light transport in blood that are capable of modeling this cylindrical geometry. Future efforts might explore a Monte Carlo simulation of photon transport through this cylindrical geometry, and verify those results through scattering measurements.

Using Eq. (7) as an expression for the backscattered reflectance, we rewrite Eq. (6) as

$$\Phi_v = \alpha R_f \Phi_0 \exp(-\varepsilon cd) + \beta R_f \Phi_0 \exp(-2\varepsilon cd) + a_1 \Phi_0 + a_2 \Phi_0 \exp(-\varepsilon cd) \quad (8)$$

Using Eqs. (2), (3) and (4), the transmittance of a retinal vessel can now be written as

$$T_v = \left(\alpha + \frac{a_2}{R_f} \right) \exp \left\{ - \left[s\varepsilon_{HbO_2} + (1-s)\varepsilon_{Hb} \right] cd \right\} + \beta \exp \left\{ -2 \left[s\varepsilon_{HbO_2} + (1-s)\varepsilon_{Hb} \right] cd \right\} + \frac{1}{R_f} \quad (9)$$

Equation (9) addresses the primary light paths that contribute to a retinal oxygen saturation measurement. Unfortunately, to calculate oxygen saturation, s , from Eq. (9) requires that values for seven variables (s , cd , α , β , R_f , a_1 , and a_2) be determined. It is important to note that the ocular fundus reflectivity R_f does *not* cancel out of this expression for vessel transmittance, explaining why some investigators have needed to include R_f in their retinal oximetry calculations. While values for R_f can be determined directly from retinal scans, it is unlikely that the remaining parameters could be determined from a least-squares regression to multi-wavelength transmittance measurements. Additionally, the parameters α , β , R_f , a_1 , and a_2 are expected to be functions of wavelength.

Because it is unlikely that Eq. (9) could be directly applied to measured transmittance data, it is useful to explore the expected magnitudes of the parameters of Eq. (9) in order to determine which terms, if any, can be neglected. The following sections present approximations to Eq. (9) that may prove more manageable for calculating oxygen saturation.

3.3 The negligible backscattering approximation

Equation (9) simplifies considerably if the effects of light directly backscattered by RBCs into the oximeter can be neglected. Backscattering can be neglected if $a_1/R_f \ll 1$ and $a_2/R_f \ll 1$. Measurements made on the optic disk (where fundus reflectivity is highest) or measurements made using green wavelengths (where backscattering is lowest due to high hemoglobin absorption) represent possible situations in which backscattering might be negligible. We have not experimentally verified these hypotheses, but present the equations as a starting point for future investigations.

In the absence of backscattering, Eq. (9) reduces to

$$T_v = \alpha \exp(-\varepsilon cd) + \beta \exp(-2\varepsilon cd). \quad (10)$$

In the cases of double-pass transmission ($\alpha = 0$) or single-pass transmission ($\beta = 0$), Eq. (10) reduces to the form of the traditional oximetry equation, Eq. (1). In general, however, this reduction is not possible. In theory, the four parameters α , β , s , and cd could be determined by measuring the vessel transmittance at four or more wavelengths. In practice, the nonlinear regression required to determine these four parameters proves difficult. However, a further level of simplification is often possible.

Taking the negative logarithm of Eq. (10) yields the expression,

$$D_v = -\ln[\alpha \exp(-\varepsilon cd) + \beta \exp(-2\varepsilon cd)]. \quad (11)$$

Equation (11) cannot be simplified further, but performing a series expansion about εcd yields

$$D_v = -\ln(\alpha + \beta) + \frac{\alpha + 2\beta}{\alpha + \beta} \epsilon c d - \frac{\alpha \beta}{2(\alpha + \beta)^2} (\epsilon c d)^2 + O[(\epsilon c d)^3]. \quad (12)$$

To determine how many orders of this expansion must be considered, the values of $\epsilon c d$, α , and β must be known. We assume a value for retinal diameter to be $d = 150 \mu\text{m}$, and a hemoglobin concentration of $c = 15 \text{ g/dl}$. Figure 4 shows the anticipated values of $\epsilon c d$ given the known values of ϵ for hemoglobin and oxyhemoglobin from 450 to 1000 nm (the safe wavelength range useful for retinal vessel oximetry).

We know that $0 \leq \alpha \leq 1$, $0 \leq \beta \leq 1$, and $\alpha + \beta \leq 1$. Measurements performed by our research group indicate that β is significantly smaller than α for our instrumentation, meaning that single pass transmission and backscattered light are the dominant collected light path²⁷. The Monte Carlo simulation by Hammer²⁰ predicts that the double-pass contribution is significantly smaller than the single-pass contribution for all typical retinal vessel diameters. Choosing a value of β to be 0.10, it can be shown that the second-order and higher terms of Eq. (12) still contribute as much as 10% to the D_v series for values $\epsilon c d > 2$ (wavelengths less than $\sim 595 \text{ nm}$). However, for $\epsilon c d < 0.5$ (wavelengths between ~ 625 and 1000 nm), these higher-order terms typically contribute less than 1% to the total summation. Therefore, for wavelengths longer than 625 nm, or for sufficiently small vessels (less than $50 \mu\text{m}$ diameter), we write Eq. (12) as

$$D_v = -\ln(\alpha + \beta) + \frac{\alpha + 2\beta}{\alpha + \beta} \epsilon c d. \quad (13)$$

The vessel transmittance can then be written as

$$T_v = (\alpha + \beta) \exp \left[-\varepsilon \left(\frac{\alpha + 2\beta}{\alpha + \beta} \right) cd \right]. \quad (14)$$

This expression has the same form as the traditional vessel oximetry equation, Eq. (1), where $T_s = \alpha + \beta$, and $\chi = (\alpha + 2\beta)/(\alpha + \beta)$. Appropriately, these terms have the limits $0 \leq T_s \leq 1$ and $1 \leq \chi \leq 2$.

The wavelength dependance of α and β are unknown, but it is reasonable to expect that they will be nearly constant over small wavelength ranges. Over larger spectral ranges, α and β likely must be expressed as functions of wavelength, requiring that T_s and χ be functions of wavelength. The traditional oximetry equation, Eq. (1), includes this wavelength dependance of T_s , however, the factor χ in Eq. (1) must also be a function of wavelength (except in the limiting cases $\alpha \rightarrow 0$ or $\beta \rightarrow 0$). To date, no reported attempts at retinal vessel oximetry have included this wavelength dependance of χ .

3.4 Negligible double-pass approximation

It is possible that the double-pass component of the signal collected by a retinal vessel oximeter is negligible (*i.e.*, $\beta \ll \alpha$). The Monte Carlo simulation by Hammer²⁰ predicts that the collect double-pass flux is the smallest component in retinal vessel oximetry, and that Φ_{dp} may be negligible for vessels larger than $\sim 160 \mu\text{m}$. If the double-pass component can be ignored, then the general oximetry equation, Eq. (9), can be written as

$$T_v = \left(\alpha + \frac{a_2}{R_f} \right) \exp(-\varepsilon cd) + \frac{a_1}{R_f}. \quad (15)$$

Equation (15) contains an additive term a_1/R_f that is not present in the traditional oximetry equation, Eq. (1). The existence of this term has not been reported previously, and we expect that including this term in retinal oximetric calculations could improve the accuracy of these measurements. The fundus reflectivity, R_f , remains as a term in Eq. (15), however measurements of R_f can be made directly by the oximeter instrumentation. If the wavelength dependencies of α , a_1 , and a_2 are assumed to be minimal (across sufficiently small wavelength ranges), then the five parameters (s , cd , α , a_1 , and a_2) might be determined from a regression to multi-wavelength transmittance measurements. More likely, the wavelength dependence of α , a_1 , and a_2 will need to be better understood so that broader wavelength ranges can be used.

It is interesting to explore a first-order expansion of Eq. (15) as was done in the previous section. In this case, T_v is found to be

$$T_v = \left(\alpha + \frac{a_1 + a_2}{R_f} \right) \exp \left(- \frac{a_2 + \alpha R_f}{a_1 + a_2 + \alpha R_f} \epsilon cd \right) \quad (16)$$

for small values of ϵcd . This expression has a form similar to the traditional oximetry equation, Eq. (1), where

$$T_s(\lambda) = \alpha + \frac{a_1 + a_2}{R_f} \quad (17)$$

and

$$\chi(\lambda) = \frac{a_2 + \alpha R_f}{a_1 + a_2 + \alpha R_f}. \quad (18)$$

Some observations can be made about the magnitudes of T_s and χ . For very low values of fundus reflectivity ($R_f \ll 1$) the scattering transmittance can become greater one ($T_s > 1$). In the case of a perfectly absorbing retinal background ($R_f = 0$), the typical vessel profile of Fig. 3 would instead show an *increase* in collected flux at the center of the vessel. More importantly, T_s will be dependant on wavelength because of the wavelength dependance of R_f .

Perhaps the most important observations regarding Eq. (16) relate to the parameter χ . It is shown that χ can be strongly dependant on wavelength (due to the wavelength dependance of R_f). This has the effect of a path length through the sample that varies with wavelength. Additionally, $\chi < 1$ for all possible values of α , R_f , a_1 , and a_2 , resulting in a reduced path length that could be detrimental to oxygen saturation sensitivity. Through a better understanding of the backscattering terms (a_1 and a_2), we expect to determine how small χ could become.

3.5 Summary

The equations in this paper were developed to explain the results from two different experiments performed by our group. These experiments are considered separately below. We have found that simplified versions Eqs. (14) or (16) work well in our experiments. Both of these equations can be simplified to the form

$$T_v(\lambda) = T_s(\lambda) \exp[-\chi(\lambda)cd\epsilon(\lambda)] . \quad (19)$$

Another equation that appears promising for experimental work is a simplified version of Eq. (15),

$$T_v(\lambda) = T_s(\lambda) \exp[-\epsilon(\lambda)cd] + g(\lambda) . \quad (20)$$

We have not yet successfully applied Eq. (20) to our experimental data.

4. Experimental Results

4.1 *In Vivo* Calibration of a Scanning Laser Oximeter

We have previously reported the successful *in vitro* calibration of a scanning laser retinal vessel oximeter¹³ called the Eye Oximeter (EOX). This instrument scans four laser beams (629, 678, 821, and 899 nm) into the eye and collects the returned flux as the beams are scanned across a retinal vessel. The *in vitro* calibration was performed in a model eye consisting of whole human blood pumped through a micropipette that was embedded in index-matched fluid. A plano-convex lens simulated the cornea and lens of the eye, and a 4 mm thick slab of Spectralon (Labsphere, Inc. North Sutton, NH) simulated the scattering layers of the ocular fundus. Spectralon provides extremely diffuse, high reflectance that is spectrally neutral across our wavelength range. Using the traditional oximetry equation, Eq (1), a good calibration was obtained by selecting a wavelength dependence for $T_s(\lambda)$ that increases linearly by 3% over the wavelength range 629 to 899 nm. This was performed by fitting the equation

$$T_v(\lambda) = T_s f(\lambda) \exp\left(-\chi c d \left[s \varepsilon_{Hb}(\lambda) + (1-s) \varepsilon_{HbO_2}(\lambda) \right]\right) \quad (21)$$

to the transmittance data, where the three unknowns are the oxygen saturation s , the product $\chi c d$, and a constant scattering transmittance T_s . The correction factor $f(\lambda)$ is a linear function that increases from 1.00 at 629 nm to 1.03 at 899 nm.

The next step in calibrating this instrument was to measure a retinal artery in an anesthetized swine during graded hypoxia. All animal protocols were approved by the

Institutional Animal Care and Use Committee of the University of Alabama at Birmingham and followed PHS Guidelines regarding the Care and Use of Laboratory Animals. The oxygen administered to the swine was decreased in a stepwise manner. At each oxygen level, arterial oxygen saturation from the femoral artery was measured with a CO-oximeter and a retinal artery was scanned with the EOX. Retinal measurements were acquired near the optic disc, and it is assumed that retinal and femoral arterial saturations are equal. Twelve saturation levels were measured, ranging from 36 %O₂Sat to 95 %O₂Sat.

Figure 5 shows the result of applying the model eye calibration, Eq. (19), to the swine measurements. The top graph displays the regressed values of oxygen saturation verses the known arterial saturations. While the correlation between actual saturation and calculated retinal saturation is quite strong ($r^2 = 0.958$), there is a systematic offset in the calculated saturations that results in low saturations being measured significantly too high. The bottom graph of Fig. 5 shows the results of the regression. The filled data points are the measured vessel transmittances for the 36 %O₂Sat measurement, and the hollow data points are for the 95 %O₂Sat measurement. The dashed line is the spectra calculated by Eq. (19) when the regressed values of s , χ_{cd} , and T_s are used. It is seen that Eq. (19) fits the transmittance data quite well, even though the regressed saturation values are incorrect.

The appearance of the scans acquired from the model eye and from the eye of the swine were extremely similar. The only significant difference between the scans was the reflectance of the ocular fundus, R_f . The Spectralon background used in the model eye is spectrally neutral, and highly reflective. In the swine, R_f was relatively high at 899 nm, where hemoglobin and melanin absorb weakly, but was approximately 10% as reflective at 629 nm due to higher hemoglobin and

melanin absorption. Unfortunately, at the time the measurements were made, it was believed that R_f did not affect our measurements. As such, we did not measure Φ_0 and cannot accurately quantify the reflectance of the swine fundus. Nevertheless, due to the obvious wavelength variation of R_f in the swine, we felt that selecting different values for the wavelength dependence of scattering, $f(\lambda)$, was justified.

An algorithm was developed to search for values of $f(\lambda)$ that yielded the optimum *in vivo* calibration using Eq. (19). Figure 6 displays the results of this calibration using the scattering factors $f(629) = 0.990$, $f(670) = 1.010$, $f(821) = 0.965$, and $f(899) = 1.000$. A piecewise cubic interpolating polynomial was applied to these values to facilitate plotting. As seen in the top graph of Fig. 6, a good calibration ($r^2 = 0.923$) was obtained, and no systematic offset was observed between the actual femoral artery saturation and the calculated retinal arterial saturation. The bottom graph of Fig. 6 demonstrates that although the regressed saturation values were correct, the model function, Eq. (19), does *not* provide a good fit to the transmittance data. As such, this calibration attempt is considered unsuccessful. Note that while only two saturation values are shown in the bottom graph of Fig. 6, these two curves are representative of the entire family of curves obtained by Eq. (19). No values of $f(\lambda)$ could be found that provided both correct saturation calculations and an acceptable fit to the transmittance data.

The inability of the wavelength-dependant scattering model of Eq. (1) and Eq. (19) to describe our *in vivo* measurements led to the development of the oximetry equations presented in this paper. Because changes in fundus reflectivity, R_f , appear to affect our measurement, we cannot justify the use of the negligible backscattering approximation. However, we have found that the first-order expansion of the negligible double-pass approximation of Eq. (16) offers some

improvement to our calibration. At present, we have made no attempt to quantify values for the wavelength dependant parameters α , a_1 , a_2 , and R_f of Eq. (16). Instead, we reduce these parameters into $\chi(\lambda)$ and $T_s(\lambda)$. As a final simplification, we assume that the wavelength dependance of $\chi(\lambda)$ is more significant than that of $T_s(\lambda)$, and therefore assume that $T_s(\lambda)$ is a constant. We fit the resulting equation

$$T_v(\lambda) = T_s \exp\left(-\chi(\lambda)cd\left[s\varepsilon_{HbO_2}(\lambda) + (1-s)\varepsilon_{Hb}(\lambda)\right]\right) \quad (22)$$

to our measured transmittance data, where s , cd , and T_s are the unknowns, and values of $\chi(\lambda)$ are selected to provide the optimum calibration.

Figure 7 contains the results of this calibration using the optimum χ values $\chi(629) = 0.65$, $\chi(670) = 0.7$, $\chi(821) = 0.85$, and $\chi(899) = 1.00$. Analysis of Fig. 7 reveals that Eq. (20) results in both accurate calculated arterial saturations ($r^2 = 0.944$) and an acceptable fit to the measured transmittance data. As such, allowing a wavelength dependant χ value while holding T_s constant has produced an acceptable calibration for this experiment. To the best of our knowledge, this is the first time such an equation has been applied to vessel oximetry.

It is interesting to note that the optimum values of χ were found to decrease as the reflectivity of the fundus decreased at shorter wavelengths (due to increased hemoglobin and melanin absorption)¹⁸. This behavior is predicted by Eq. (18). Note that the optimum values of $\chi(\lambda)$ can be scaled by an arbitrary constant, however the resulting cd product from a regression will scale inversely by the arbitrary constant, thus maintaining the same value of $\chi(\lambda)cd$. As such, the fact that these optimum values of $\chi(\lambda)$ are less than one does *not* necessarily imply the reduced path length predicted by the negligible double-pass approximation.

Finally, the data presented here was acquired from a single location on the retina of one swine. Studies with additional animals are ongoing, and preliminary results indicate that the use of Eq. (20) leads to an improved calibration compared to the use of the traditional oximetry equation, Eq. (1). However, we find that optimum values of $\chi(\lambda)$ tend to vary between subjects. We are working to quantify this variation, and attempting to find relationships between $\chi(\lambda)$ and the fundus reflectivity and vessel diameter.

4.2 *In Vitro* Calibration of a Confocal Scanning Laser Oximeter

We are currently developing a confocal scanning laser Eye Oximeter called the EOX-2²⁸. This instrument operates like a confocal scanning laser ophthalmoscope²⁹ and produces a live video image of a subject's retina acquired at 830 nm. To acquire a spectroscopic data set, the EOX-2 cycles through up to six lasers. In this study, the EOX-2 was equipped with three diode lasers (635, 670 and 830 nm) and a fiber-coupled Argon ion laser (488 nm). This wavelength combination was selected based on a previous study that predicts reduced errors in the calculated saturations⁸. These lasers are interlaced into a single video frame that is digitized at 10-bit resolution. The transmittance of the vessel is measured at each wavelength, and the oxygen saturation is calculated from these transmittances.

The confocal detection path of the EOX-2 significantly reduces the collection of light that is reflected or scattered from non-retinal planes such as the cornea and crystalline lens. In addition, the confocal arrangement should limit the collected light paths to the directly backscattered flux, Φ_{bs} , and double-pass transmitted flux, Φ_{dp} .

Using the model eye described in the previous section, we measured five blood samples ranging from 11 %O₂Sat to 100 %O₂Sat with the EOX-2. The hemoglobin concentration of the samples was 13.9 g/dl and a 270 μ m pipette (inner diameter) was used to simulate the retinal blood vessel.

Because it had worked well in previous model eye calibration experiments, we used the traditional oximetry equation, Eq. (19), to calculate s , χcd and T_s . The calibration procedure involved an iterative technique to determine optimum values for the wavelength dependant scattering factors $f(\lambda)$. We found that the values $f(488) = 1.000$, $f(635) = 0.919$, $f(670) = 0.892$, and $f(830) = 1.000$ resulted in an excellent calibration. The results of this study are shown in Fig. 8. The correlation between the actual oxygen saturation and the calculated saturation was extremely strong ($r^2 = 0.99$), however only five data points were present. Additionally, the model function fit the transmittance data well.

While this study demonstrates that accurate oxygen saturation values could be calculated *in vitro*, it is also interesting to examine the regressed values of χcd . Because the values $c = 13.9$ g/dl and $d = 270$ μ m were known, we could determine an absolute value of χ . We found that $\chi = 0.22$ for this data set. Although a value of $\chi < 1$ seems counterintuitive, this result was predicted by the negligible double-pass approximation. The reduced path length is a direct consequence of the backscattering of light by red blood cells. The factor a_1 in Eq. (7) shows that as ecd approaches infinity, the light backscattered by the blood column does *not* approach zero even though the transmitted flux does approach zero. This results in the apparent path length reduction that we experimentally measure.

5. Discussion and Conclusions

Our group has monitored changes in retinal vessel oxygen saturation^{6,5,30}, and recently we have demonstrated an accurate *in vitro* calibration¹³. Yet, after significant advancements in instrumentation, wavelength selection, and signal processing, we have not obtained consistently accurate calibrations in a swine model. The difficulties of *in vivo* calibration led to the development of the improved oximetry equations presented here. The complete retinal vessel oximetry equation, Eq. (9), contains too many terms to be useful in a measurement, however, more manageable expressions are obtained through some simplifying approximation. In this paper, we explore the negligible double-pass and negligible backscattering approximations. Further investigation is required in order to determine the validity of these approximations, however one of the resulting simplified expressions, Eq. (19), has been shown to provide a better model to *in vivo* data than the traditional oximetry equation, Eq. (1).

While Eqs. (19) and (20) both appear promising for retinal vessel oximetry, both equations contain wavelength dependant factors that are likely to be functions of fundus reflectivity, and are possibly functions of vessel diameter, retinal position (due to varying thickness of the retinal layers), and hemoglobin concentration. Monte Carlo simulations of light interaction with the retina²⁰ should provide a theoretical framework for determining the relationships between these parameters, however a large database of vessel saturation measurements acquired across a range of known oxygen saturations, hemoglobin concentration, retinal position, fundus pigmentations, and vessel diameters will eventually be required if we are to definitively show calibrated measurements from a retinal vessel oximeter.

This study emphasizes one of the tradeoffs that must be considered in the development of a retinal vessel oximeter. A recent study by Smith⁸ predicts that several discrete wavelengths ranging from 488 nm to 905 nm can be selected that offer the highest sensitivity to oxygen saturation across a range of vessel diameters. In order to use this large wavelength range, however, the wavelength dependence of the unknown parameters in Eqs. (19) and (20) will need to be well understood. The choice of three closely-spaced green wavelengths, as used by Delori³, minimizes the wavelength dependence of these unknown parameters, perhaps allowing constant values to be used. These wavelengths, however, also result in decreased sensitivity to oxygen saturation⁸. While it is not clear which approach will ultimately lead to well-calibrated retinal vessel oxygen saturation measurements, understanding the light paths that comprise the measurement will be critical to the success of the technique. We expect that the equations developed here will prove beneficial to future retinal vessel oximetry investigations, regardless of the wavelengths selected or instrumentation used for performing the measurements.

The authors thank J. E. Drewes and L. C. Heaton for their help in collecting and analyzing the data presented here. We gratefully acknowledge the financial support for this work by the U.S. Army Medical Research and Materials Command and by the Office of Naval Research.

FIGURE CAPTIONS

Figure 1 The primary light paths associated with a scanning-beam retinal vessel oximetry measurement; Φ_0 , incident light; Φ_{media} , scattered light from the lens and vitreous; Φ_{glint} , specular reflection from the inner limiting membrane (*ilm*) or vessel wall; Φ_s , light scattered away by red blood cells (RBCs) within the vessel; Φ_{bs} , light back-scattered to the detector by RBCs; Φ_{sp} , light collected that has traversed the vessel in single pass; Φ_{dp} , light collected that has traversed the vessel in double pass; Φ_{diff} , light diffused laterally in the choroid.

Figure 2 Laser light traverses a retinal blood vessel and diffuses laterally in the reflecting layers of the ocular fundus. The diameter of the diffusion enlarged PSF varies with wavelength, and two typical PSF diameters are illustrated. Only light that scatters into the indicated solid angle exits back out of the eye. The larger PSF demonstrates both single pass and double pass transmission through the vessel, while the smaller PSF demonstrates primarily single pass transmittance.

Figure 3 A typical vessel absorption profile is illustrated. The vessel transmittance, T_v , is calculated as Φ_v / Φ_f where Φ_v is the collected flux from the center of the vessel, and Φ_f is an estimate of the flux that would be collected from the ocular fundus in the absence of the retinal vessel (estimated here by a linear approximation).

- Figure 4** Values of ϵcd for a typical retinal vessel, where vessel diameter $d = 150 \mu\text{m}$, and the hemoglobin concentration $c = 15 \text{ g/dl}$. Absorption coefficient data from Ref. (21).
- Figure 5** Application of the model eye calibration equation to the *in vivo* swine data. The top graph compares the calculated retinal arteria saturation to the measured femoral artery oxygen saturation. The bottom graph displays the resulting best-fit spectra. The filled circles are measured vessel transmittances for a femoral artery saturation of 36 %O₂Sat, and the hollow circles are for 95 %O₂Sat.
- Figure 6** Application of the wavelength-dependant scattering equation, Eq. (21), to the *in vivo* swine data. The best-fit scattering factors $f(\lambda)$ were found to be $f(629) = 0.990$, $f(670) = 1.010$, $f(821) = 0.965$, and $f(899) = 1.000$.
- Figure 7** Application of the wavelength-dependant path length equation, Eq. (22), to the *in vivo* swine data. The best-fit path length factors $\chi(\lambda)$ were found to be $\chi(629) = 0.65$, $\chi(670) = 0.7$, $\chi(821) = 0.85$, and $\chi(899) = 1.00$.
- Figure 8** Calibration of the confocal scanning laser oximeter in a model eye. The top graph compares the calculated oxygen saturation to the actual saturation of the known whole blood samples. The bottom graph displays the resulting best-fit spectra. The filled circles are measured vessel transmittances for an oxygen saturation of 11 %O₂Sat, and the hollow circles are for 100 %O₂Sat.

References

1. J. B. Hickam, R. Frayser, J. C. Ross, "A study of retinal venous blood oxygen saturation in human subjects by photographic means," *Circulation* **27**, 375-385 (1963).
2. A. J. Cohen, R.A. Laing, "Multiple scattering analysis of retinal blood oximetry," *IEEE Trans. Biomed. Eng.* **23**(5), 391-400 (1976).
3. F. C. Delori, "Noninvasive technique for oximetry of blood in retinal vessels," *Appl. Optics* **27**(6), 1113-1125 (1988).
4. D. Schweitzer, L. Leistritz, M. Hammer, M. Scibor, U. Bartsch, J. Strobel, "Calibration-free measurement of the oxygen saturation in retinal vessels of men," in *Ophthalmic Technologies V*, Jean-Marie Parel, Qiushi Ren, Karen M. Joos, Editors, Proc. SPIE 2393, 210-218 (1995).
5. K. R. Denninghoff, M. H. Smith, R. A. Chipman, L. W. Hillman, P.M. Jester, C.E. Hughes, F. Kuhn, L. W. Rue, "Retinal large vessel oxygen saturation correlates with early blood loss and hypoxia in anesthetized swine," *J. Trauma* **43**(1), 29-34 (1997).
6. M. H. Smith, K. R. Denninghoff, L. W. Hillman, R. A. Chipman, "Oxygen saturation measurements of blood in retinal vessels during blood loss," *J. Biomed. Optics* **3**(3), 296-303 (1998).
7. J. S. Tiedeman, S. E. Kirk, S. Srinivas, J. M. Beach, "Retinal oxygen consumption during hyperglycemia in patients with diabetes without retinopathy," *Ophthalmology* **105**(1), 31-36 (1998).
8. M. H. Smith, "Optimum wavelength selection for retinal vessel oximetry," *Appl. Optics* **38**(1), 258-267 (1999).

9. J. M. Beach, K. J. Schwenzer, S. Srinivas, J. S. Tiedeman, "Oximetry of retinal vessels by dual-wavelength imaging: calibration and influence of pigmentation," *J. Appl. Physiol.* **86**(2), 748-758 (1999).
10. Van Assendelft, O. W., *Spectrophotometry of Haemoglobin Derivatives* (Charles C. Thomas, Springfield, IL, 1970).
11. V. Twersky, "Absorption and multiple scattering by biological suspensions," *J. Opt. Soc. Am.* **60**, 1084-1093 (1970).
12. Pittman R.N., Duling B.R., "A new method for the measurement of percent oxyhemoglobin," *J. Appl. Physiol.* **38**, 315-320 (1975).
13. J. J. Drewes, M. H. Smith, K. R. Denninghoff, L. W. Hillman, "An instrument for the measurement of retinal vessel oxygen saturation," in *Optical Diagnostics of Biological Fluids IV*, A. V. Priezzhev, M. V. Lomonosov, T. Asakura, eds. *Proc. SPIE* Vol. 3591, 114-120 (1999).
14. R. A. MacRae, J. A. McClure, P. Latimer, "Spectral transmission and scattering properties of red blood cells," *J. Opt. Soc. Am.* **51**(12), 1366-1372 (1961).
15. A. G. Borovoi, E. I. Naats, U. G. Oppel, "Scattering of light by a red blood cell," *J. Biomed. Opt.* **3**(3), 364-372 (1998).
16. M. Hammer, D. Schweitzer, B. Michel, E. Thamm, A. Kolb, "Single scattering by red blood cells," *Appl. Opt.* **37**(31), 7410-7418 (1998).
17. F. C. Delori, E. S. Gragoudas, R. C. Pruett, "Monochromatic ophthalmoscopy and fundus photography: The normal fundus," *Arch. Ophthalmol.* **95**, 861-868 (1977).
18. F. C. Delori, K. P. Pflibsen, "Spectral reflectance of the human ocular fundus," *Appl. Optics* **28**(6), 1061-1077 (1989).

19. I. J. Hodgkinson, P.B. Greer, A. C. B. Molteno, "Point-spread function for light scattered in the human ocular fundus," *J. Opt. Soc. Am. A* **11**(2), 479-486 (1994).
20. M. Hammer, S. Leistritz, L. Leistritz, D. Schweitzer, E. Thamm, K. H. Donnerhacke, "Monte Carlo simulation of retinal vessel profiles for the interpretation of *in vivo* oximetric measurements by imaging fundus reflectometry," *Proc. SPIE* Vol. 3192, 211-218 (1997).
21. S. Prahl has compiled data of hemoglobin extinction coefficients from several investigators. The data is available at <http://omlc.ogi.edu/spectra/hemoglobin/index.html>
22. N. M. Anderson, P. Sekelj, "Light-absorbing and scattering properties of nonhemolysed blood," *Phys. Med. Biol.* **12**(2), 173-184 (1967).
23. N. M. Anderson, P. Sekelj, "Reflection and transmission of light by thin films of nonhaemolysed blood," *Phys. Med. Biol.* **12**(2), 185- 192 (1967).
24. J. M. Steinke, A. P. Shepherd, "Diffusion model of the optical absorbance of whole blood," *J. Opt. Soc. Am. A* **5**(6), 813-822 (1988).
25. V. Twersky, "Absorption and multiple scattering by biological suspensions," *J. Opt. Soc. Am.* **60**, 1084-1093 (1970).
26. A. N. Yaroslavsky, I. V. Yaroslavski, T. Goldbach, H.-J. Schwarmaier, "Influence of the scattering phase function approximation on the optical properties of blood determined from the integrating sphere measurements," *J. Biomed. Opt.* **4**(1), 47-53 (1999).
27. J. J. Drewes, "Four wavelength retinal vessel oximetry," Ph.D. dissertation (University of Alabama in Huntsville, 1999).
28. A. Lompda, "A confocal scanning laser ophthalmoscope for retinal vessel oximetry," Ph.D. dissertation (University of Alabama in Huntsville, 1999).

29. R. H. Webb, G. W. Hughes, F. C. Delori, "Confocal Scanning Laser Ophthalmoscope," *Appl. Opt.*, **26**(8), 1492-1499 (1987).
30. K. R. Denninghoff, M. H. Smith, R. A. Chipman, L. W. Hillman, P.M. Jester, F. Kuhn, D. Redden, L. W. Rue, "Retinal venous oxygen saturation correlates with blood volume," *Acad. Emerg. Med.* **5**(6), 577-582 (1998).

Retinal Imaging Techniques in Diabetes

Word Count: 961

Kurt R. Denninghoff, M.D., University of Alabama at Birmingham; Matthew H. Smith, Ph.D. and Lloyd Hillman, Ph.D., University of Alabama in Huntsville.

Address for correspondence and reprints:

Kurt Denninghoff, MD

Assistant Professor

Department of Emergency Medicine

The University of Alabama at Birmingham

JTN 266, 619 South 19th Street

Birmingham, Alabama 35233-7013

(205) 975-7458 * FAX (205) 975-4662

kdenning@uabmc.edu

The ability to accurately and rapidly identify diabetic retinopathy will be a valuable tool for the care of the diabetic patient. Direct ophthalmoscopy is particularly unreliable early in the development of diabetic retinopathy when intervention is the most efficacious. Screening of diabetics for retinopathy is crucial since early detection and treatment is reported to prevent 70% of diabetes related blindness. There have been several studies published advocating the use of Doppler flowmetry, retinal photography, scanning laser ophthalmoscopy and retinal oximetry measurements as tools for identifying retinopathy prior to the onset of significant neovascularity. Drawbacks of these methods include the lack of compliance with yearly ophthalmologic exams by patients, failure of primary care physicians to use the devices to refer patients for evaluation, and failure of primary care physicians to identify the early onset of disease. As a result of these limitations, diabetic retinopathy in diabetics remains the leading cause of blindness during the productive period of life. The need for a method to identify diabetic retinopathy with a non invasive device which is fast, accurate and simple to use is apparent.

Several outcome studies have shown that laser coagulation therapy and screening programs for diabetic retinopathy are cost beneficial because they help

to prevent blindness. The basic principle of laser coagulation therapy in the care of patients with diabetic retinopathy is to ensure that the delivery of oxygen to the retina is sufficient to maintain aerobic metabolic functions and thereby prevent the growth of new vessels in response to tissue hypoxia. Unfortunately, patients often fail to receive therapy because they are not diagnosed prior to blinding. Consequently, a noninvasive, rapidly applicable technique that provides a reliable index of the balance between oxygen delivery and consumption during the evaluation and treatment of patients at risk for proliferative vascular diseases of the eye would be a valuable screening tool and treatment adjunct.

Denninghoff et. al.,^{1,2,3,4} Tiedeman et. al.,⁵ Beach et. al.,⁶ Schweitzer et. al.,⁷ Delori,⁸ Cohen⁹ and Laing,⁹ and Hickham et. al.,¹⁰ have published attempts at retinal vessel oximetry. These efforts demonstrate the potential of a device which can measure the oxygen saturation of the blood in the retinal vessels accurately. The potential benefit from using such a device to screen diabetics for retinopathy in the primary care physician's office is significant. However, a retinal oximeter must accurately measure the arterial and venous oxygen saturation, be easy to use, and be inexpensive if it is going to be used by a primary care physician.

Since the vessels on the retina are directly observable, the eye is a unique

portal for noninvasive optical measurements of the blood within them. It is the only place on the body where arteries and veins can be directly observed without thick intervening layers of skin or tissue. Furthermore, the retinal vasculature is a potential source of perfusion data. The eye is a preferred organ and maintains its perfusion through local auto-regulatory control. Our team of researchers at the University of Alabama at Birmingham (UAB) and the University of Alabama in Huntsville (UAH) are developing a device called an eye oximeter (EOX). This device can be used to screen and monitor diabetic retinopathy. Much like a scanning laser ophthalmoscope, the EOX scans low powered laser light into the eye and across the large blood vessels of the retina around the optic nerve head. The reflected and scattered light is collected, descanned and analyzed. In addition to determining oxygen saturation, the EOX yields data on vessel diameter and blood hematocrit. The operator views a video monitor and sees a highly detailed image of the retina. A complete scan of the eye takes 1/30th of a second. In a series of animal experiments we have demonstrated that retinal venous saturation measured with an EOX is a sensitive indicator of blood loss and hypoxia.^{1,2} We expect to be using a clinical device to study humans within the next two years.

Since the EOX can accurately measure the oxygen saturation of the blood in

the retinal vessels, we proposed that it can be used as a screening device for diabetic retinopathy. Furthermore, based upon our understanding of the pathology of diabetic retinopathy, the EOX will be a valuable tool for the assessment and evaluation of the treatment and intervention strategies. It has been posited that diabetic retinopathy develops because diabetes inhibits the eye's ability to auto-regulate its oxygen perfusion. Hence the failure to maintain adequate perfusion leads to a degeneration of the retinal tissues. The growth of proliferative vasculature is a pathologic reaction aimed at increasing oxygen delivery. The EOX can therefore detect the very early onset of diabetic retinopathy by measuring and characterizing the auto-regulatory state of the eye.

We are generating scientific data which suggests that retinal vessel oxygen saturations (both arterial and venous) may be used to identify retinal hypoxia prior to changes in retinal vascular architecture, to monitor the response to therapy, and to help optimize the balance between oxygen delivery and consumption in the retina. These studies will help identify the pathology of diabetic retinopathy and the physiologic mechanisms that precede and stimulate the onset of clinically observable changes. In particular, we seek to obtain a better understanding and control of laser retinal photocoagulation. The EOX will be used to study diabetics

Kurt Denninghoff, MD

across the spectrum of disease and during photocoagulation therapy. In addition to our work, Schweitzer and Tiedeman are both continuing to independently study retinal oximetry. The work we are doing in conjunction with these other investigators will likely lead to a clinically useful retinal oximeter in the next few years. We believe that this EOX will be used to evaluate the autoregulatory state of the retinal tissue and will be an adjunct for clinical screening and therapy for diabetic retinopathy.

References

1. Denninghoff KR, Smith MH, Hillman LW, ReddenD, Rue LW. Retinal venous oxygen saturation correlates with blood volume. *Acad Emer Med*. 1998; 5:577-582.
2. Denninghoff KR, Smith MH, Chipman RA, et al. Retinal large vessel oxygen saturations correlate with early blood loss and hypoxia in anesthetized swine. *J. Trauma-Injury Infection & Critical Care*. 1997; 43:29-34.
3. Smith MH, Denninghoff KR, Hillman LW, et al. Technique for noninvasive monitoring of blood loss via oxygen saturation measurements in the Eye. Invited paper in *Optical Diagnostics of Biological Fluids II*, Prezzhev AV, Asakura T eds., SPIE 2982, 1997.
4. Smith MH, Denninghoff KR, Hillman LW, Chipman RA. Oxygen saturation measurements of blood in retinal vessels during blood loss. *J of Biomedical Optics*. 1998; 3(3):296-303.
5. Tiedeman JS, Kirk SE, Srinvas S, Beach JM. Retinal oxygen consumption during hyperglycemia in patients with diabetes without retinopathy. *Ophthalmology*. 1998;105(1):31-36.

6. Beach JM, Schwenzer KJ, Srinivas S, Kim D, Tiedeman JS. Oximetry of retinal vessels by dual-wavelength imaging: calibration and influence of pigmentation. *J. Appl. Phys.* 1999; 86: 748-758.
7. Schweitzer D, Leistritz L, Hammer M, Scibor M, Bartsch U, Strobel J
“Calibration-free measurement of the oxygen saturation in the retinal vessels of men,” in *Ophthalmic Technologies V*, Jean-Marie Parel, Quishi Ren, Karen M. Joos, MD, Editors, Proc. SPIE 2393, 210-218 (1995).
8. Delori FC. Noninvasive technique for oximeter of blood in retinal vessels. *Appl Optics*. 1988; 27:1113-1125.
9. Cohen AJ, Laing RA. Multiple scattering analysis of retinal blood oximetry. *Biomed Eng.* 1976;23(5):391-400.
10. Hickman JB, Frayser R, Ross J. A study of retinal venous oxygen saturation in human subjects by photographic means. *Circ.* 1963; 27:275-385.

**The University of Alabama at Birmingham
School of Medicine Faculty**

PII Redacted

PERSONAL INFORMATION:

Name: Kurt Richard Denninghoff, MD
[REDACTED]

Foreign Language(s):
[REDACTED]
[REDACTED]
[REDACTED]

RANK/TITLE:

Assistant Professor, Tenure Earning
Department: Emergency Medicine
Business Address: The University of Alabama at Birmingham
266N Jefferson Tower
619 South 19th Street
Birmingham, AL 35233-7013
Phone: (205) 975-7458

HOSPITAL AND OTHER (NON ACADEMIC) APPOINTMENTS:

<u>Month/Year</u>	<u>Rank/Title</u>	<u>Institution</u>
12/92-present	Attending Physician	University Hospital, Birmingham, AL

EDUCATION:

Month/Year	Degree	Institution
05/87	MD	Vanderbilt University Nashville, TN
05/83	BE	Vanderbilt University Nashville, TN

LICENSURE:

12/97 Alabama #14765

BOARD CERTIFICATION:

02/94-02/04 Diplomate, American Board of Emergency Medicine

POSTDOCTORAL TRAINING:

Month/Year	Program	Institution
07/88-06/91	Residency - Emergency Medicine	Charity Hospital, New Orleans, LA
07/87-06/88	Internship - General Surgery	Charity Hospital, New Orleans, LA
05/85-08/86	NIH Medical Student Research Fellowship	Vanderbilt University (Lloyd King, M.D., Ph.D. Mentor)

ACADEMIC APPOINTMENTS:

Month/Year	Rank/Title	Institution
06/98-present	Acute Care Core Director	Injury Control Research Center, UAB
05/95-present	Research Director	Department of Emergency Medicine, UAB
04/95-present	Assistant Professor of Emergency Medicine	Dept. of Emergency Medicine, UAB
01/94-04/95	Instructor in Emergency Medicine	Dept. of Emergency Medicine, UAB
12/92-12/93	Clinical Instructor in Emergency Medicine	University Hospital (UAB) Birmingham, AL

HOSPITAL STAFF APPOINTMENTS:

Month/Year	Rank/Title	Institution
06/91-1992	Staff Position in Emergency Medicine	Humana Hospital, New Orleans, LA

AWARDS/HONORS:

12/99 Marquis Who's Who in Science and Engineering
09/91 Resident Research Competition, Southern Medical Association
05/83 Biomedical Engineering Award
05/83 Tau Beta Pi, Engineering Honorary Society
05/83 Eta Kappa Nu, Electrical Engineering Honorary Society

PROFESSIONAL SOCIETIES:

Founding Member, The American Academy of Emergency Medicine
Faculty, The American Academy of Emergency Medicine
Member, The Society for Academic Emergency Medicine
Faculty, American College of Emergency Physicians
Member, Alabama Chapter of the American College of Emergency Physicians
Faculty, Injury Control Research Center
Faculty, Vision Science Research Center

MEMBERSHIPS:

Member, Injury Control Research Center
Member, Vision Science Research Center

COUNCILS AND COMMITTEES:

1999-Present Member, University Hospital, Pharmacy and Therapeutics Committee

1998 Member, University of Alabama School of Medicine Search Committee for the Chair
Department of Emergency Medicine

- 9/96-present Member, University of Alabama Hospital Pastoral Care Committee
- 1/96-1/97 Member, University Hospital Disaster Preparedness Committee
- 9/96-present Chair, Department of Emergency Medicine Research Advisory Committee
- 3/96-present Member, Society for Academic Emergency Medicine Research Director's Task Force
- 3/95-present Member, University Hospital Psychiatric Emergency Services Committee
- 5/99-present Member, Society for Academic Emergency Medicine Injury Prevention Work Group
- 5/99-present Chair, Society for Academic Emergency Medicine Injury Prevention Work Group

UNIVERSITY ACTIVITIES:

Educational

- 1994-present Monthly Medical Student Lecture Series: "Orthopedic Emergencies"
- 1994-present Faculty Advisor for Medical Students During 4th Year Clerkship at UAB
- 1998 Medical Student Invited Lecture "The Eye Oximeter as a cost saving device in the care of the critically injured"
- 1994-1997 Founder and first Faculty Advisor for the Medical Student's Emergency Medicine Society at The University of Alabama at Birmingham School of Medicine
- 1994-1997 Monthly Medical Student Lecture Series: "Headache: Evaluation and Management in the Emergency Department"

Scholarly

Publications:

"Tympanic membrane thermometry in the care of out-of-hospital patients" S.J. Weiss, E.J. Hanhart, R. McBride, H. Johnson, K.R. Denninghoff, W.D. Johnson, *Ann. Of Emerg. Med.* 25(1), 41, January, (1995).

"Technique for noninvasive monitoring of blood loss via oxygen saturation measurements in the eye" M.H. Smith, K.R. Denninghoff, L.W. Hillman, C.E. Hughes, T.E. Minnich, and R.A. Chipman, Invited paper in *Optical Diagnostics of Biological Fluids II*, Proc. SPIE 2982, (1997).

"Retinal vessel oxygen saturation correlates with early blood loss and hypoxia in anesthetized swine"

K.R. Denninghoff, M.H. Smith, R.A. Chipman, L.W. Hillman, P.M. Jester, C.E. Hughes, F. Kuhn and L.W. Rue, *J. Trauma*, 43(1), 29, July, (1997).

"Retinal venous oxygen saturation correlates with the rate of blood loss in swine" K.R. Denninghoff, M.H. Smith, L.W. Hillman, D. Redden, L.W. Rue, *Academic Emergency Medicine*, 5(6), 577, June, (1998).

"Technique for noninvasive monitoring of blood loss via oxygen saturation measurements in the eye" M.H. Smith, K.R. Denninghoff, L.W. Hillman, R.A. Chipman, *Journal of Biomedical Optics*, 3(3), 296, July, (1998).

"Teaching students in an emergency walk in clinic does not delay care" K.R. Denninghoff, P.K. Moye, *Academic Medicine*, 73(12), 1311, December, (1998).

"An instrument for the measurement of retinal vessel oxygen saturation" J.D. Drewes, M.H. Smith, K.R. Denninghoff, L.W. Hillman, Invited paper in *Optical Diagnostics of Biological Fluids IV*, Proc. SPIE 3591 (1999).

"Handheld four-wavelength eye oximeter" C. Heaton, M.H. Smith, K.R. Denninghoff, L.W. Hillman, in *Ophthalmic Technologies X*, P. O. Rol, K.M. Joos, eds., *Proceedings of SPIE Vol. 3908*, January, (2000).

"Retinal vessel oximetry: Toward absolute calibration" M.H. Smith, K.R. Denninghoff, A Lompadó, L.W. Hillman, in *Ophthalmic Technologies X*, P. O. Rol, K. M. Joos, eds., *Proceedings of SPIE Vol. 3908*, January, (2000).

"In-plane scatterometry of small caliber blood column" A. Lompadó, M.H. Smith, K.R. Denninghoff, L.W. Hillman, in *Optical Diagnostics of Biological Fluids V*, A. V. Priezzhev, T. Asakura, eds., *Proceedings of SPIE Vol. 3923*, January, (2000).

"Multispectral confocal scanning laser ophthalmoscope for retinal vessel oximetry" A. Lompadó, M. H. Smith, K.R. Denninghoff, L W. Hillman, in *Spectral imaging: Instrumentation, applications, and analysis*, G. H. Bearman, D. Cabib, R. M. Levenson, eds., *Proceedings of SPIE Vo. 3920*, January, (2000).

"Enrollment of sudden cardiac death victims into a limited cardiac autopsy study in the emergency department: The effects of race." K.R. Denninghoff, *Journal of the National Medical Association* (In press).

"Effect of multiple light paths on retinal vessel oximetry" M.H. Smith, K.R. Denninghoff, J.E. Drewes, A. Lompadó, L.W. Hillman, *Applied Optics* (In press).

"Retinal Imaging Techniques in Diabetes" K.R. Denninghoff, M.H. Smith, L.W. Hillman, *Diabetes Technology and Therapeutics* (In press).

Manuscripts submitted but not yet accepted:

"An Optical Model of the Blood in the Large Retinal Vessels" K.R. Denninghoff, M.H. Smith. Submitted to *Journal of Biomedical Optics*, November, (1999).

Manuscripts in preparation:

"Three-Dimensional Monte Carlo Simulation of Light Propagation Through a Blood Column" M.H. Smith, A. Lompardo, K.R. Denninghoff, L.W. Hillman.

"Light Scattering by a Column of Whole Human Blood" A. Lompardo, M.H. Smith, K.R. Denninghoff, L.W. Hillman.

"Porcine retinal venous oxygen saturation correlates with cardiac output and blood volume during profound blood loss" K.R. Denninghoff, M.H. Smith, J.E. Drewes, L.W. Hillman.

"Retinal vessel diameter changes during blood loss and changes in inspired oxygen concentration" K.R. Denninghoff, M.H. Smith, S. Melton, L.W. Hillman.

"Four wavelength retinal vessel oximetry" M.H. Smith, K.R. Denninghoff, J.E. Drewes, L.W. Hillman.

"Two dimensional laser scanning retinal vessel oximetry" M.H. Smith, K.R. Denninghoff, A. Lompardo, L.W. Hillman.

"Scattering distribution of a cylindrical column of whole blood" A. Lompardo, M.H. Smith, K.R. Denninghoff, L.W. Hillman.

"The effects of hematocrit changes on retinal vessel oximetry" J.E. Drewes, M.H. Smith, K.R. Denninghoff, L.W. Hillman.

Published abstracts presented at national meetings:

"Retinal vessel diameter correlates with blood volume in a swine model" K.R. Denninghoff, *Acad. Emerg. Med.* Annual Meeting, Boston, MA, (1999)

"Eye Oximeter for Combat Casualty Care 1999-I" L.W. Hillman, K.R. Denninghoff, M.H. Smith, *Advanced Technology Applications to Combat Casualty Care*, Proc., Fort Walton Beach, FL (1999)

"Eye Oximeter for Combat Casualty Care 1999-II" K.R. Denninghoff, M.H. Smith, L.W. Hillman, *Advanced Technology Applications to Combat Casualty Care*, Proc., Fort Walton Beach, FL (1999)

"Noninvasive optical systems in systemic and ophthalmic diseases" K.R. Denninghoff, M.H. Smith, L.W. Hillman, *Optical Society America*, Annual Meeting, Santa Clara, CA, (1999)

"A scanning laser ophthalmoscope for retinal vessel oximetry" M.H. Smith, A. Lompado, K.R. Denninghoff, L.W. Hillman, *Optical Society America*, Annual Meeting, Santa Clara, CA (1999)

"Multiple light paths in retinal vessel oximetry" M.H. Smith, K.R. Denninghoff, A. Lompado, L.W. Hillman, *Optical Society of America*, Annual Meeting, Santa Clara, CA (1999)

"An eye oximeter for combat casualty care" K.R. Denninghoff, M.H. Smith, L.W. Hillman, *ATACCC98*, Proc., Fort Walton Beach, Florida (1998).

"Intelligent control systems for the LSTAT" W. Holdefer, K.R. Denninghoff, *ATACCC98*, Proc., Fort Walton Beach, Florida (1998).

"The effect of a diffusion-enlarged point spread function on retinal vessel oximetry" M.H. Smith, J.E. Drewes, L.W. Hillman, K.R. Denninghoff, *Optical Society of America*, Annual Meeting, Baltimore, MD (1998).

"Optomechanical design of an imaging eye oximeter for the measurement of retinal vessel oxygen saturation" J.E. Drewes, M.H. Smith, L.W. Hillman, K.R. Denninghoff, *Optical Society of America*, Baltimore, MD, Annual Meeting, (1998).

"Simulation and deconvolution of light scattering in the human eye" L.W. Hillman, M.H. Smith, A. Lompado, J.E. Drewes, K.R. Denninghoff, *Optical Society of America*, Annual Meeting, Baltimore, MD (1998)

"Retinal venous oxygen saturation correlates with blood volume changes in anesthetized swine" K.R. Denninghoff, M.H. Smith, R.A. Chipman, L.W. Hillman, P.M. Jester, F. Kuhn, L.W. Rue, D. Redden, *Acad. Emerg. Med.*, Proc., Washington, D. C. (1997).

"Teaching students in and emergency walk in clinic does not delay care" M.J. Bonnin, P.K. Moye, K.R. Denninghoff, *Acad. Emerg. Med.*, Proc., Washington, D.C. (1997).

"The use of an eye oximeter to monitor blood loss in a swine model" K.R. Denninghoff, M.H. Smith, D.R. Smith, and R.A. Chipman, *Acad. Emerg. Med.*, Proc., Denver, CO (1996).

"Oxygen saturation measurements of retinal arteries and veins during physiologic changes" M.H. Smith, R.A. Chipman, and K.R. Denninghoff, *Invest. Ophthalm. Vis. Sci.* 37(3) (ARVO Suppl.):840, Ft. Lauderdale, FL (1996).

"Rape: Findings on examination and outcomes in court" K.R. Denninghoff, Abstract, *Southern Medical Journal*, Proc., Atlanta, GA, September, (1991).

"Insulin receptors in intact human skin" K.R. Denninghoff, L. King, *J. Invest. Dermatology, Proc.*, New Orleans, LA, May, (1986).

Invited lectures at local and regional courses and meetings:

"An Eye Oximeter for Combat Casualty Care" K.R. Denninghoff, M.H. Smith, L.W. Hillman, S. Melton, *3rd Annual Issues in Trauma Care*, San Destin, FL (1999)

"Clinical device research: Patent To Patient Use" K.R. Denninghoff, *Alabama Clinical Research Practioners Symposium*. (1998)

Patents:

"Method and apparatus for accurately measuring the transmittance of blood within a retinal vessel" M.H. Smith, R.A. Chipman, L.W. Hillman, K.R. Denninghoff, T.E. Minnich, U.S. Patent Pending No. 08/803,065.

"Oximetric tonometer with intracranial pressure monitoring capability" K.R. Denninghoff, M.H. Smith, Provisional Patent No. 60/089,856, June 19, (1998)

"Technique for two-dimensional scanning spectroscopy of the ocular fundus" M.H. Smith, K.R. Denninghoff, Provisional Patent submitted March, (1999).

"Retinal 'autoregulatory state' as an indicator of perfusion status in systemic and ocular disease states" K.R. Denninghoff, M.H. Smith, T.E. Minnich, Provisional Patent submitted March, (1999).

Grants in Preparation:

Sponsor/Agency: NEI - NIH

Study: An Eye Oximeter for Diagnosis of Retinal Vascular Diseases

Grant: Total grant \$900,000

Role: Principle Investigator

Grants in Progress:

Sponsor/Agency: Office of Naval Research in Partnership with the United States Army Combat Casualty Research and Development Command

Study: An eye oximeter for non-invasive monitoring

Grant: Total grant award \$1,625,000 from 12/15/98 - 01/01/2002

Role: Principle Investigator for UAB sub-contract of \$865,000. 65% effort.

Sponsor/Agency: CDC

Study: Injury Control Research Center Grant
Grant: Total grant award \$5,000,000 from 07/01/99 - 06/30/2004
Role: Acute Care Core Director. 20% effort

Grants Completed:

Sponsor/Agency: AHA
Study: Sudden Cardiac Death in Blacks
Grant: Total grant award \$60,000 from 07/01/97 - 01/2000
Role: Co-Investigator. No % effort designated.

Sponsor/Agency: ViroPharma Incorporated
Study: "A Multicenter, Double Blind, Placebo Controlled Trial of Pleconaril in the Treatment of Enteroviral Meningitis in Adults"
Grant: Total grant award \$61,000 from 07/98 - 01/2000
Role: Principal Investigator. No % effort designated

Sponsor/Agency: United States Army Combat Casualty Research and Development Command
Study: An eye oximeter for combat casualty care
Grant: Total grant award \$923,000 from 12/97 to 12/99
Role: Principle Investigator. 35% effort.

Sponsor/Agency: UAH/Stranonen
Study: Retinal venous oxygen saturation changes during blood loss and hypoxia
Grant: Total grant award \$8,000 from 10/95 - 03/96
Role: Principle Investigator

Sponsor/Agency: UAB Research Foundation
Study: Retinal venous oxygen saturation changes during blood loss and hypoxia
Grant: Total grant award \$20,000 from 06/96 - 12/97
Role: Principle Investigator. 20% effort

Sponsor/Agency: Center for Social Medicine and Sexually Transmitted Diseases
Study: Victims of Partner Violence
Grant: Total grant award \$13,500 from 01/98 - 06/98
Role: Principle Investigator. 3% effort

Sponsor/Agency: NIH
Study: PEACH Study
Grant: Total grant award \$620,074 from 09/96 - 09/99
Role: Co-Investigator. 8% effort

Sponsor/Agency: CDC

Study: Injury Control Research Center Grant

Grant: Total grant award \$3,750,000 from 07/01/95 - 06/30/99

Role: Acute Care Core Director. 5% effort

MISCELLANEOUS:

Films, educational tapes, syllabi, software packages and courses developed, etc.

Matthew H. Smith

Curriculum Vita

home: 101 Dartmouth Drive
Madison, AL 35757
(256) 837-7273

office: Physics Department, OB-318
The University of Alabama in Huntsville
Huntsville, AL 35899
(256) 890-6417 ext. 393

Education:

- Ph.D. Physics (April 1996)
University of Alabama in Huntsville, Huntsville, AL
Dissertation title: "Oximetry of Blood in Retinal Vessels"
- M.S. Physics (May 1993)
University of Alabama in Huntsville, Huntsville, AL
Thesis Title: "Optical System Analysis of the Ground-Based Experimental Vector Magnetograph"
- B.S. Applied Optics (May 1991)
Rose-Hulman Institute of Technology, Terre Haute, IN

Professional Experience:

Assistant Research Professor, Physics Department, University of Alabama in Huntsville, 4/98 - present
Research Scientist, Physics Department, University of Alabama in Huntsville, 7/96 - 4/98
Graduate Research Assistant, The University of Alabama in Huntsville, 6/93-7/96
Optical Engineer Co-op, NASA Marshall Space Flight Center, 1/94 - 6/94, and 1/93 - 6/93
Optical Engineer Summer Intern, Omega Optical Inc., Brattleboro, VT, 6/90 - 8/90

Research Activities and Projects:

Develop techniques for imaging polarimetry and spectro-polarimetry
Application of multiple scattering theory and photon migration theory to retinal vessel oximetry
Optical and electronic design, assembly, and testing of prototype Eye Oximeter.
Use of an Eye Oximeter to measure blood loss in a swine model.
Optical design, assembly, and testing of a prototype white-light, confocal retinal microscope.
Bench testing and optical alignment of a solar telescope for measuring solar magnetic fields.

Professional Memberships and Affiliations:

I am a member of each of the following academic or profession organizations.

Faculty Member of the School of Graduate Studies, The University of Alabama in Huntsville
Scientific Staff of CAO - The Center for Applied Optics, The University of Alabama in Huntsville
SPIE - The International Society for Optical Engineering
OSA - Optical Society of America
HEOS - The Huntsville Electro-Optical Society

Refereed Publications:

This list includes papers that have been published (or are in press) in peer-reviewed journals.

- [6] P. Y. Gerligand, **M. H. Smith**, R. A. Chipman, "Polarimetric images of a cone," *Optics Express* **4**(10), 420-430 (1999).
- [5] **M. H. Smith**, "Optimum wavelength selection for retinal vessel oximetry," *Applied Optics* **38**(1), 258-267 (1999).
- [4] **M. H. Smith**, K. R. Denninghoff, L. W. Hillman, R. A. Chipman, "Oxygen saturation measurements of blood in retinal vessels during blood loss," *J. Biomed. Optics* **3**(3), 296-303 (1998).
- [3] K. R. Denninghoff, **M. H. Smith**, R. A. Chipman, L. W. Hillman, P.M. Jester, F. Kuhn, D. Redden, L. W. Rue, "Retinal venous oxygen saturation correlates with blood volume," *Acad. Emerg. Med.* **5**(6), 577-582 (1998).
- [2] K. R. Denninghoff, **M. H. Smith**, R. A. Chipman, L. W. Hillman, P.M. Jester, C.E. Hughes, F. Kuhn, L. W. Rue, "Retinal large vessel oxygen saturation correlates with early blood loss and hypoxia in anesthetized swine," *J. Trauma* **43**(1), 29-34 (1997).
- [1] E. A. West, **M. H. Smith**, "Polarization errors associated with birefringent waveplates," *Optical Engineering* **34**(6), 1574-1580 (1995).

Publications Currently in Review:

This list includes papers that have been submitted to refereed journals and are currently under review.

- [4] **M. H. Smith**, K. R. Denninghoff, J. E. Drewes, A. Lompado, L. W. Hillman, "Effect of multiple light paths on retinal vessel oximetry," *Applied Optics* (currently under review).
- [3] K.R. Denninghoff, **M.H. Smith**, Lloyd W. Hillman, Sherry Melton, "Retinal vein diameter changes during profound blood loss in swine," *Investigative Ophthalmology & Visual Science* (currently under review).
- [2] K.R. Denninghoff, **M.H. Smith**, "Retinal imaging techniques in diabetes," *Diabetes Technology & Therapeutics* (currently under review).
- [1] K.R. Denninghoff, **M.H. Smith**, "An optical model of the blood in large retinal vessels," *Journal of Biomedical Optics* (currently under review).

Conference Proceedings and Non-Refereed Publications:

This list includes abstracts and papers that have been published, but did not receive significant peer review.

- [27] L. W. Hillman, **M. H. Smith**, K. R. Hillman, "Eye Oximeter for Combat Casualty Care," *Proceedings of ATACCC '99* (1999).
 - [26] K. R. Denninghoff, **M. H. Smith**, L. W. Hillman, "Retinal Venous O₂ Sat Correlates with Blood Volume and Cardiac Output During Exsanguination and Reinfusion," *Proceedings of ATACCC '99* (1999).
 - [25] **M. H. Smith**, A. Lompado, K. R. Denninghoff, L. W. Hillman, "A scanning laser ophthalmoscope for retinal vessel oximetry," *Optical Soc. Am., Annual Meeting* (1999).
 - [24] **M. H. Smith**, K. R. Denninghoff, A. Lompado, L. W. Hillman, "Multiple light paths in Retinal Vessel Oximetry,"
-

Optical Soc. Am., Annual Meeting (1999).

- [23] **M. H. Smith**, J. D. Howe, J. B. Woodruff, M. A. Miller, G. R. Ax, T. E. Petty, E. A. Sornsin, "Multispectral infrared Stokes imaging polarimeter," in *Polarization: Measurement, Analysis, and Remote Sensing II*, D. H. Goldstein, D. B. Chenault, eds., *Proceedings of SPIE* Vol. 3754, 137-143 (1999).
 - [22] **M. H. Smith**, J. B. Woodruff, J. D. Howe, "Beam Wander Considerations in Imaging Polarimetry," in *Polarization: Measurement, Analysis, and Remote Sensing II*, D. H. Goldstein, D. B. Chenault, eds., *Proceedings of SPIE* Vol. 3754, 50-54 (1999).
 - [21] L. L. Deibler, **M. H. Smith**, "Infrared polarimetry using attenuated total reflection," in *Polarization: Measurement, Analysis, and Remote Sensing II*, D. H. Goldstein, D. B. Chenault, eds., *Proceedings of SPIE* Vol. 3754, 99-107 (1999).
 - [20] J. D. Drewes, **M. H. Smith**, D. R. Denninghoff, L. W. Hillman, "An Instrument for the Measurement of Retinal Vessel Oxygen Saturation," in *Optical Diagnostics of Biological Fluids IV*, Alexander V. Priezzhev, M. V. Lomonosov, Toshimitsu Asakura, eds., *Proceedings of SPIE* Vol. 3591, 114-120 (1999).
 - [19] K. R. Denninghoff, **M. H. Smith**, L. W. Hillman, "An Eye Oximeter for Combat Casualty Care," *Proceedings of ATACCC '98* (1998).
 - [18] **M. H. Smith**, J. E. Drewes, L. W. Hillman, K. R. Denninghoff, "The Effect of a Diffusion-Enlarged Point Spread Function on Retinal Vessel Oximetry," *Optical Soc. Am., Annual Meeting* (1998).
 - [17] J. E. Drewes, **M. H. Smith**, L. W. Hillman, K. R. Denninghoff, "Optomechanical Design of an Imaging Eye Oximeter for the Measurement of Retinal Vessel Oxygen Saturation," *Optical Soc. Am., Annual Meeting* (1998).
 - [16] L. W. Hillman, **M. H. Smith**, A. Lompado, J. E. Drewes, K. R. Denninghoff, "Simulation and Deconvolution of Light Scattering in the Human Eye," *Optical Soc. Am., Annual Meeting* (1998).
 - [15] A. Lompado, **M. H. Smith**, L. W. Hillman, K. R. Denninghoff, "Measurement of the Scattering Anisotropy of a Column of Whole Human Blood," *Optical Soc. Am., Annual Meeting* (1998).
 - [14] A. Lompdo, **M. H. Smith**, R. A. Chipman, "A real-time Stokes vector imaging polarimeter," *Optical Soc. Am., Annual Meeting* (1998).
 - [13] **M. H. Smith**, E. A. Sornsin, R. A. Chipman, T. J. Tayag, "Mueller matrix imaging of GaAs/AlGaAs self-imaging beamsplitting waveguides," in *Polarization Measurement, Analysis, and Remote Sensing*, Proc. SPIE 3121, (1997).
 - [12] P. Y. Gerligand, R. A. Chipman, E. A. Sornsin, **M. H. Smith**, "Polarization signatures of spherical and conical targets measured by Mueller matrix imaging polarimetry," in *Polarization Measurement, Analysis, and Remote Sensing*, Proc. SPIE 3121, (1997).
 - [11] K. R. Denninghoff, **M. H. Smith**, R. A. Chipman, L. W. Hillman, P.M. Jester, F. Kuhn, L. W. Rue, D. Redden, "Retinal venous oxygen saturation correlates with blood volume changes in anesthetized swine", *Soc.Academ.Emerg.Med.*, proc., (1997).
 - [10] **M. H. Smith**, K. R. Denninghoff, L. W. Hillman, C. E. Hughes, T. E. Minnich, R. A. Chipman, "Technique for noninvasive monitoring of blood los via oxygen saturation measurements in the eye," Invited Paper in *Optical Diagnostics of Biological Fluids and Advanced Techniques in Analytical Cytology*, Alexander V. Priezzhev, Toshimitsu Asakura, Robert C. Leif, eds., *Proceedings of SPIE* Vol. 2982, 46-52 (1997).
-

- [9] **M. H. Smith**, E. A. Sornsin, R.A. Chipman, "Polarization characterization of self-imaging GaAs/AlGaAs waveguide beamsplitters via Mueller matrix imaging polarimetry," in *Physics and Simulation of Optoelectronic Devices V*, M Osinski, W.W. Chow, eds., *Proc. SPIE* **2994**, 330-337 (1997).
- [8] **M. H. Smith**, "Oximetry of blood in retinal arteries and veins," Ph.D. Dissertation, The University of Alabama in Huntsville (1996).
- [7] **M. H. Smith**, R. A. Chipman, K. R. Denninghoff, "Oxygen saturation measurements of retinal arteries and veins during physiologic changes," *Invest. Ophthalm. Vis. Sci.* **37**(3) (ARVO Suppl.), 840 (1996).
- [6] K. R. Denninghoff, **M. H. Smith**, D. R. Smith, R. A. Chipman, "The use of an eye oximeter to monitor blood loss in a swine model," *Soc. Academ. Emerg. Med.*, proc. (May 1996).
- [5] **M. H. Smith**, D. A. Gregory, "Rectangular pixel-based fractal diffraction patterns," *Optical Pattern Recognition VI*, Friedrich O. Huck, Richard D. Juday, eds., *Proc. SPIE* **2488**, 344-349 (1995).
- [4] E. A. West, **M. H. Smith**, "Polarization characteristics of the MSFC experimental vector magnetograph," in *Polarization Analysis and Measurement II*, D.H. Goldstein and D.B. Chenault, Eds., *Proc. SPIE* **2265**, 272-281 (1994).
- [3] E. A. West, **M. H. Smith**, "Polarization errors associated with birefringent waveplates," in *Polarization Analysis and Measurement II*, D.H. Goldstein and D.B. Chenault, Eds., *Proc. SPIE* **2265**, 260-271 (1994).
- [2] L. W. Hillman, S. C. McClain, **M. H. Smith**, R. A. Chipman, "Eye oximeter for the noninvasive measurement of cardiac output," in *Vision Science and its Applications*, 1994 Technical Digest Series, Vol. 2 (Optical Society of America, Washington DC) pp. 151-154 (1994).
- [1] **M. H. Smith**, "Optical system analysis of the ground-based experimental vector magnetograph," Masters Thesis, The University of Alabama in Huntsville (1993).

Patents:

- [5] "Technique for Two-Dimensional Scanning Spectroscopy of the Ocular Fundus"
M. H. Smith, L. W. Hillman, K. R. Denninghoff
Patent Pending, submitted 9/99.
 - [4] "A Method of Determining Autoregulatory Status and Method for Using Same to Determine Perfusion Status in Systemic and Ocular Disease States,"
K. R. Denninghoff, **M. H. Smith**
Patent Pending, submitted 5/99.
 - [3] "Oximetric tonometer with intracranial pressure monitoring capability,"
K. R. Denninghoff, **M. H. Smith**
Provisional Patent #60-089,856 submitted 6/98.
Submitted as patent, serial number PCT/US99/13631
 - [2] "Method and apparatus for measuring blood oxygen saturation within a retinal vessel with light having several selected wavelengths."
M. H. Smith, R. A. Chipman, T. E. Minnich
U.S. Patent No. 5,776,060
-

- [1] "Method and apparatus for accurately measuring the transmittance of blood within a retinal vessel."
M. H. Smith, R. A. Chipman, L. W. Hillman, K. R. Denninghoff, T. E. Minnich
U.S. Patent Pending No. 08/803,065

Seminars, Colloquia, and Presentations:

This list includes the titles of talks that I have given. Also included are the hosting organizations, the locations, and the dates of the talks.

- [11] "Beam Wander Considerations in Imaging Polarimetry"
SPIE, Annual Meeting 1999
Denver, CO
July, 1999
- [10] "Multispectral Infrared Stokes Imaging Polarimeter"
SPIE, Annual Meeting 1999
Denver, CO
July, 1999
- [9] "The Eye Oximeter"
The Huntsville Electro-Optical Society
Huntsville, AL
October 23, 1998
- [8] "The Effect of a Diffusion-Enlarged Point Spread Function on Retinal Vessel Oximetry"
Optical Society of America, Annual Meeting 1998 (poster presentation)
Baltimore, MD
October, 1998
- [7] "Eye Oximetry"
Alabama Biomedical Optics Initiative, 4th Technical Interchange Forum
Huntsville, AL
April, 1998
- [6] "Technique for noninvasive monitoring of blood loss via saturation measurements in the eye"
BiOS '97
San Jose, CA
February, 1997
- [5] "Mueller matrix imaging of GaAs/AlGaAs self-imaging beamsplitting waveguides"
Photonics West '97
San Jose, CA
February, 1997
- [4] "Oxygen saturation measurements of retinal arteries and veins during physiologic changes"
Association for Research in Vision and Ophthalmology (poster presentation)
Fort Lauderdale, FL
April 28, 1996
-

- [3] **"In a Pig's Eye"**
 Physics Department Colloquium
 The University of Alabama in Huntsville
 Huntsville, AL
 January 30, 1996

- [2] **"An Eye Oximeter for Noninvasive Physiologic Monitoring"**
 Hyperbaric Medicine Division Colloquium
 Navy Medical Research & Development Command
 Bethesda, MD
 January 5, 1996

- [1] **"Eye oximeter for the noninvasive measurement of cardiac output"**
 Noninvasive Assessment of the Visual System (poster presentation)
 Sante Fe, NM
 February, 1994

Classes Taught:

This list describes the classes that I have taught. The following format is used:

<i>Class No.</i>	<i>Class Title Class Location</i>	<i>Date</i>	<i>Student Evaluation Score</i>
PH 113	Third Semester Undergraduate Physics The University of Alabama in Huntsville	Fall (1999-2000)	---
PH 305	Applied Physics The University of Alabama in Huntsville	Spring (1997-1998)	92.5
PH 113	Third Semester Undergraduate Physics The University of Alabama in Huntsville	Summer (1991-1992)	87.5
PH 114	First Semester Physics Laboratory The University of Alabama in Huntsville	Spring (1991-1992)	88.6
PH 114	First Semester Physics Laboratory The University of Alabama in Huntsville	Spring (1991-1992)	86.7
PH 114	First Semester Physics Laboratory The University of Alabama in Huntsville	Winter (1991-1992)	75.8
PH 114	First Semester Physics Laboratory The University of Alabama in Huntsville	Winter (1991-1992)	88.4
PH 114	First Semester Physics Laboratory The University of Alabama in Huntsville	Fall (1991-1992)	89.1

Proposals Submitted, Accepted, and Funded:

This list includes proposals that I have written in whole or in significant part. The following format has been used:

*No. Title, UAH account number
funding organization, date
investigators (principal investigator indicated as PI)
amount*

- [15] Liquid Crystal Retarder Characterization
QuesTech (for Night Vision Laboratories) , 9/1/97 - 9/30/98
Matt Smith PI
\$1,400
- [14] Infrared Retarder Alignment
QuesTech (for Night Vision Laboratories) , 9/1/99 - 9/30/99
Matt Smith PI
\$1,400
- [13] An Eye Oximeter for Noninvasive Physiologic Monitoring
Navy Medical Research and Development Command, 1/98 - 1/01
Lloyd Hillman PI, Matt Smith, Kurt Denninghoff (UAB)
\$1,000,000
- [12] Infrared Retarder Alignment
Nichols Research Corporation, 1/99 - 3/99
Matthew Smith PI
\$8,014
- [11] A Full-Color Scanning Laser Ophthalmoscope
Alabama Vision and Imaging Sciences Center, 5/98 - 5/99
Matt Smith PI, Glenn Hammack (UAB) Co-PI
\$15,000
- [10] Procurement of a Laser Confocal Retinal Scanning Head for Investigation of Multiplexed Multiple-wavelength
Retinal Scanning Applications
Alabama Vision and Imaging Sciences Center, 5/98 - 5/99
Glenn Hammack (UAB) PI, Matt Smith Co-PI
\$15,000
- [9] Development of an Infrared Stokes Imaging Polarimeter
QuesTech (for Night Vision Laboratories) , 6/1/97 - 12/30/98
Matt Smith PI
\$71,383
- [8] Beamsplitter Testing II, 5-34671
Eastman Kodak Co., 1/97 - 4/98
Matt Smith PI, Russell Chipman, Beth Sornsin
\$16,505
- [7] Use of an Eye Oximeter by Nurses - A Usability Study, 2-19107
UAH, 10/97 - 4/98
Matt Smith (PI), Billie Rozelle
\$24,000
-

- [6] An Eye Oximeter for Combat Casualty Care, 5-20054
U.S. Army Medical Research and Materials Command, 1/98 - 1/01
Kurt Denninghoff (UAB) PI, Lloyd Hillman Co-PI, Matt Smith Co-PI
\$1,540,920 (UAH's portion \$710,366)
- [5] Development of an Eye Oximeter, 5-34549
Vectranetics, 9/96 - 2/97
Russell Chipman PI, Matt Smith
\$28,813
- [4] Development of an Eye Oximeter, 5-34549
Vectranetics (add-on), 2/97 - 6/98
Russell Chipman PI, Matt Smith
\$23,895
- [3] Eye Oximeter, 2-12330
UAH, 7/96 - 12/96
Russell Chipman PI, Matt Smith (graduate research assistant)
\$15,975 + tuition
- [2] Eye Oximeter, 2-12330
UAH, 1/96 - 6/96
Russell Chipman PI, Matt Smith (graduate research assistant)
\$25,000 + tuition
- [1] Eye Oximeter, 2-12330
UAH, 12/94
Russell Chipman PI, Matt Smith (graduate research assistant)
\$20,000 + tuition

Proposals Submitted and Still Pending:

This list includes proposals that I have written in whole or in significant part. The following format has been used:

*No. Title
funding organization, date
investigators (principal investigator indicated as PI)
amount*

- [1] Sub-wavelength Structure Polarizing Beam Splitter Cubes
Alabama Research Institute, 7/99 - 7/00
Matthew Smith PI, Larry Pezzaniti (SY Technology)
\$50,000
-

Proposals Submitted and Rejected:

This list includes proposals that I have written in whole or in significant part. The following format has been used:

- | <i>No.</i> | <i>Title</i>
<i>funding organization, date</i>
<i>investigators (principal investigator indicated as PI)</i>
<i>amount</i> |
|------------|-------------------------------------------------------------------------------------------------------------------------------------------------------------------------------------------------------------------------------------------|
| [9] | Multi-Wavelength Confocal Retinal Tomography
part of an NSF EPSCOR , 1/99 - 1/01
Matthew Smith PI, Glenn Hammack (UAB)
\$73,053 |
| [8] | A Retinal Autoregulatory Index for the Detection of Glaucoma
Alabama Vision and Imaging Sciences Center , 5/98 - 5/99
Kurt Denninghoff (UAB) PI, Matt Smith Co-PI
\$15,000 |
| [7] | Noninvasive Monitoring of Blood Loss in Acute Trauma
National Institutes of Health R-01 with UAB, 2/96
Russell Chipman PI, Matt Smith Co-PI, Lloyd Hillman Co-PI
\$1,241,089 (UAH's portion \$659,465) |
| [6] | An Eye Oximeter for Noninvasive Monitoring: A new tool for cost-reduction...
Whitaker Foundation & NSF with UAB, 1/97
Lloyd Hillman PI, Matt Smith Co-PI, Russell Chipman Co-PI
\$777,560 (UAH's portion \$436,466) |
| [5] | Eye Oximeter for Noninvasive Cardiac Output Measurement
National Institutes of Health R-01 with UAB, 2/95
Russell Chipman PI, Lloyd Hillman, Matt Smith (graduate research assistant)
\$180,303 (UAH's portion \$143,095) |
| [4] | Eye Oximeter for Noninvasive Physiologic Monitoring
National Institutes of Health STTR , 12/95
Russell Chipman PI, Lloyd Hillman, Tom Minnich (Stranonen), Matt Smith (grad. research asst.)
\$100,000 |
| [3] | Eye Oximeter for Noninvasive Cardiac Output Measurement
National Institutes of Health R-01 , 2/94
Russell Chipman PI, Lloyd Hillman, Matt Smith (graduate research assistant)
\$280,000 |
| [2] | Eye Oximeter for Noninvasive Tissue Perfusion Monitoring
National Institutes of Health SBIR , 12/93
Tom Minnich (Stranonen) PI, Russell Chipman, Lloyd Hillman, Matt Smith (grad. research asst.)
\$75,000 |
| [1] | Eye Oximetry
National Institutes of Health AREA Grant , 4/93
Lloyd Hillman PI, Russell Chipman, Matt Smith (graduate research assistant)
\$75,000/year for 2 years (4/93). |
-

Students Supervised:

I have directly supervised the following student research assistants.

Elizabeth Tanner Undergraduate Research Assistant	7/99 - present
Raghunandan Manchenahalli Graduate Research Assistant	7/99 - present
Jacob Woodruff Graduate Research Assistant	8/98 - present
Lynn Deibler Graduate Research Assistant	5/98 - present
Chris Centamore Undergraduate Research Assistant	5/98 - 7/98
Chris Heaton Graduate Research Assistant Undergraduate Research Assistant	5/98 - present 2/98 - 5/98
Art Lompad Graduate Research Assistant	8/97 - present
Jonathan Drewes Graduate Research Assistant	1/97 - present
Sunil Devabahktuni Undergraduate Research Assistant	2/98 - 5/98
Jeff Hammock Undergraduate Research Assistant	9/96 - 5/97
Charles Hughes Graduate Research Assistant	6/96 - 1/97

Graduate Student Committees:

I have served on the Ph.D. or M.S. committee of each of the following students.

Chris Heaton M.S. Committee Chairman Practice Oriented Masters in Optics	
Jacob Woodruff M.S. Committee Chairman Practice Oriented Masters in Optics	
Panfilio Deguzman Ph.D. Committee Member Optical Science and Engineering	
Lynn Deibler Ph.D. Committee Chairman	Optical Science and Engineering

Jonathan Drewes
Ph.D. Committee Member Optical Science and Engineering

Art Lompadó
Ph.D. Committee Member Optical Science and Engineering

Other Public Service Activities:

For example, clinical practice, continuing education teaching, public policy guidance, public presentations, economic development activities, and studies for governments, other public institutions, companies.

Graduate Observer	Ph.D. defense for Atreya Srinivas, Materials Science May 1999
-------------------	------------------------------------------------------------------

Boy Scouts of America	Eagle Scout Sponsor for Charles Bider Feb 1999
-----------------------	---------------------------------------------------

VITAE

LLOYD WILLIAM HILLMAN

Associate Professor of Physics
University of Alabama in Huntsville

Mailing Address: Physics Dept., Optics Building 318
University of Alabama in Huntsville
Huntsville, Alabama 35899

Telephone: (256) 890-6417 ext. 318 or 319

Fax: (256) 890-6077 or 6873

E-Mail: HillmanL@UAH.edu

PROFESSIONAL POSITIONS:

1999 – Present	Chair, Department of Physics
1993 – Present	Associate Professor, Department of Physics (Tenured 1996) University of Alabama in Huntsville, Huntsville Alabama
1989 – 1993	Assistant Professor, Department of Physics University of Alabama in Huntsville, Huntsville Alabama
1986 – 1989	Assistant Professor, School of Electrical Engineering Cornell University, Ithaca, NY
1986	Research Associate, Kodak Research Laboratories, Rochester, NY
1984 – 1986	Research Scientist, Kodak Research Laboratories, Rochester, NY

EDUCATIONAL DEGREES:

1984 **Ph.D.** The Institute of Optics, University of Rochester, Rochester, New York
Dissertation: *Interaction of modulated optical field with saturable media and its application to laser instabilities*. Advisor – C.R. Stroud, Jr.

1976 **B.S.** Engineering Physics (With Distinction), University of Arizona, Tucson, Arizona

RESEARCH ACTIVITIES OUTLINE:

Biomedical Optics: eye oximetry, non-invasive optical diagnostic techniques, light scattering from tissues and cells, spectroscopic signatures of blood constituents.

Optical Systems and Integration: optical layout and design, opto-mechanical and physical constraints, system integration, opto-electronic interfacing, illumination systems, automotive lighting, systems optimization, radiometry, polarimetry and polarization ray tracing.

Quantum Optics: laser dynamics, optical resonance, quantum/classical correspondence.

ACADEMICS AMPLIFICATION

RESEARCH GRANTS AND CONTRACTS—PI/CO-PI

- "EOX for Noninvasive Physiologic Monitoring," UAH-5-20475, Office of Naval Research, N00014-99-1-0226, 14 Dec 1998—30 Sept 2001, \$1,000,000. (PI)
- "EOX for Combat Causality Care," UAH-5-20054, (Subcontract from University of Alabama at Birmingham) U.S. Army Medical Research and Materiel Command, 1 Dec 1997–20 Nov 2000, \$707,829 (PI).
- "Orbital Array of Wide Angle Lenses (OWL)," 5-20247, NASA/MSFC, 1 July 1998–31 Dec 1998, \$214,844 (of \$1,200,000), (CO-PI).
- "On-Site Development & Analysis of Progressive Lenses (Off-Campus)," UAH-5-20177, Innotech, Inc., May 1998–Sept 1998, \$22,199 (PI).
- "On-Site Development & Analysis of Progressive Lenses (On-Campus)," 5-20178, Innotech, Inc., May 1998–Sept 1998, \$13,429 (PI).
- "Spectropolarimetric Measurements," UAH-5-20109, ERIM, 3 March 1998–31 Aug 1998, \$27,624 (PI).
- "Wagner Lighting Retrofit," Wagner Lighting, Dec 1996 - May 1997, \$12,000 (PI).
- "Lighting for '97 Soft Touch and '98 Flush," Acustar, Jan 1995—March 1996, \$144,301 (PI).
- "Optical polymer components irradiance measurements," Allied Signal, 1 Mar 1994–30 June 1994, \$7,000 (PI).
- "Optical System Analysis for the Ground-Based EXUM," NASA Marshall Space Flight Center, 9 Aug 1992—9 July 1993, \$31,999 (CO-PI).
- "Analysis and Design of Illumination Systems for Meter & Gauge Clusters and Radio Products," Acustar Inc., April 1992-February 1993, \$155,728 (PI)
- "Polarization Analysis of the Polarization Input Stage" Eastman Kodak Company, 16 Nov 1991–26 May 1992, \$13,529 (CO-PI).
- "Polarization Ray Tracing and Testing of Birefringent Materials: Application to Design, Analysis, and Testing of MODIUS_T Depolarizer" Two Parts: Proposal #1, "Depolarization Design and Test Station," Proposal #2, "Polarization Raytracing Algorithms," 3 May 1991–3 Aug 1992, \$122,661 (with 4 Admendments) (CO-PI).
- "Surface Profilometry and BRDF measurements" Battelle Memorial Institute, June 1991–Aug 1991, \$2,400 (PI).
- "Aberration and error correction of trilateration distance measurements using multi-wavelength, laser-based instruments," Rocky Mountain Engineering and Equipment, Inc. June 1990–Dec 1990, \$16,000 (PI).

"Unrestricted Research Grant for PYI," Eastman Kodak Company, 1987–1992, \$50,000 (PI).

"Presidential Young Investigator Award: "Noise, Instabilities and Coherent Dynamics of Semiconductor Laser Diodes" National Science Foundation Dec 1987–Dec 1992, \$321,500 (PI).

PH.D. DEGREES AS ADVISOR/CHAIRMAN:

- (1) Stephen C. McClain, Ph.D. Physics, "Birefringent polarization ray tracing: theory and applications," (Cornell 1992).
- (2) Sungman Lee, Ph.D. Physics, UAH, "Highly coherent diode lasers: noise, frequency stabilization, and linewidth reduction," (UAH 1994).
- (3) Marius P. Schamschula, Ph.D. Physics, "Temporal behavior of a triple phase conjugate mirror in Barium Titanate," (UAH 1994).
- (4) Thomas A. Hough, Ph.D. Physics, "Design principles of nonimaging waveguide illumination systems," (UAH 1995).
- (5) Su-Keng Chiou, Ph.D. Physics, "Magnetic and optical properties of an anomalous Doppler-free absorption resonance of the Rubidium D2-line," (UAH 1995).
- (6) John Van Derlofske, Ph.D. Physics, "System modeling and material characterization for the design of nonimaging waveguide illumination systems" (UAH 1996).
- (7) Elizabeth Sornsin, Ph.D., Physics, "Mueller matrix polarimetry of PLZT electro-optics modulators," (UAH 1999)
- (8) Arthur Lompadò, Ph.D., Optical Science & Engineering, "A confocal scanning Laser ophthalmoscope for Retinal Vessel Oximetry," (UAH 1999).
- (9) Jonathan Drewes, Ph.D., Optical Science & Engineering, "Four Wavelength Retinal Vessel Oximetry," (UAH 1999)
- (10) David J. Lamb, Ph.D., Physics, "Design, Fabrication, and Testing of Fresnel Lenses for Astrophysics Applications," (UAH 1999).

MASTERS DEGREES AS ADVISOR/CHAIRMAN:

- (1) Stanely T. Lau, MS Electrical Engineering, "Single Mode Homogeneously Broadened Laser Instabilities", (Cornell 1990).
- (2) David Cohen, MS Electrical Engineering, "Phase Fluctuations and Damping in Two-Level Optical Resonance", (Cornell 1990).
- (3) Christopher J Walker, MS Physics, "Band Models for Laser Dynamics" (Cornell 1990).
- (4) Patrick T. Hoy, MS Physics, "Surface topography and the bidirectional reflectance distribution function: a correlation", (UAH 1992).

- (5) Matthew H. Smith, MS Physics, "Optical system analysis of the ground-based experimental vector magnetograph (EXVM)", (UAH 1993)
- (6) Andrew Nelson, MS Optical Science & Engineering, "Optical path generation with surface figure correction for precision diamond turning," (UAH 1999)

GRADUATE STUDENTS ADVISOR/CHAIRMAN (Current)

- (1) James Hadaway, Optical Science & Engineering, 5/92 - Present, Ph.D., "Design and Testing of Multifocal Lenses," Expected Date of Graduation - Dec 1999.
- (2) Shawn D. Pethel, Physics, 1/98 - Present, Ph.D., "Dynamics of Coupled Laser Arrays Diode," Expected Date of Graduation - May 2000.
- (3) Lynn Deibler, OSE, 1/98 - Present, Ph.D., "Application of Polarimetry in Biological Systems," Expected Date of Graduation - May 2000.
- (4) L. Chris Heaton, MS Physics, "Hand held Oximeter."

GRADUATE COMMITTEE SERVICE

Thomas Tumolilli, PhD Physics (1992).
 David Chenault, PhD Physics (1992).
 Jeff Cites, PhD Physics (1992).
 Larry Pezzaniti, PhD Physics (1993).
 Qiang Huang, PhD Physics (1993).
 Partick Reardon, PhD Physics (1993).
 James R. Meehan, MS Physics (1993)
 Janine Reardon, PhD Physics (1994).
 Jongmin Kim, PhD Physics (1994).
 John Jackson, MS Physics (1994)
 Jeong-Mee Kim, PhD Physics (1995).
 Shih-yau Lu, PhD Physics (1995).
 Mike Tocci, PhD (1995).
 Steven Kupiac, PhD Physics (1996).
 David Smith, PhD Physics (1996).
 Gerald A. Larson, PhD Physics (1997).
 Deana McMullin, PhD Physics (1998).
 Stephen Berry, MS Physics (1998).
 Sara Batson Fair PhD Mechanical Engineering (1998).
 Travis Taylor, PhD Optical Science & Engineering (1999).

HONORS SENIOR THESIS/ADVISOR:

- (1) Dorothy M Seitz, "Resolving a conflict between coherence theory and classical radiometry: Incoherent planar sources are Lambertian," Honors BS Optical Science (1994).

- (2) Tony B. Hargrove, "Controlling and Analyzing the output from an automated MTF analyzer for spectacle lenses," Honors BS Optical Science (1998).

TEACHING-CLASSES TAUGHT:

PH / OPT 341, "Geometrical Optics"
PH / OPT 342, "Physical Optics"
PH / EE 444, "Opto-Electronics"
PH 445, "Introduction to Lasers"
OPT 464 / PH 546, "Radiometry"
PH / OPT 441, "Optical Systems"
PH / OPT 442, "Interference and Diffraction"
PH / OSE / EE 541, "Geometrical Optics"
PH / OSE / EE 542, "Physical Optics"
PH / OSE / EE 601, "Linear Systems"
OSE 654, "Optical Testing"
PH 745, "Quantum Optics"

UNIVERSITY COMMITTEES:

Faculty Senate
University Curriculum Committee
SACS Self-Study Committee on Graduate Education
Center for Applied Optics Advisory Board
Summer Explorations in Science, Applied Mathematics and Engineering

DEPARTMENT COMMITTEES:

Optical Science & Engineering Program Committee
Optics Search Committee
Student Physical Society (SPS) Faculty Advisor

HONORS AND AWARDS:

Tau Beta Pi
1987 Presidential Young Investigator Award from the NSF
"Best Contributed Paper" Award at International Conference on Lasers 1994
U.S. Air Force Summer Faculty Fellow 1989
U.S. Army Summer Faculty Fellow 1991.

PROFESSIONAL SOCIETY MEMBERSHIPS:

Optical Society of America (OSA)
Institute of Electrical and Electronic Engineers (IEEE)
American Association of Physics Teachers (AAPT)
International Society of Engineers (SPIE)
Society of Automotive Engineers (SAE)
Huntsville Electro-Optics Society (HEOS)

PROFESSIONAL SERVICE:

Journal Article Reviewer: OSA, SPIE, American Physical Society.
Proposal Reviewer: NSF-SBIR.
Program Committee: International Conference on Lasers 1987-89.
Program Committee: SPIE International Symposium on Optical Science, Engineering,
and Instrumentation 1999.
Program Committee: OSA Annual Meeting 1999.

COMMUNITY SERVICE:

Manager/Coach Little League Baseball, Mayfair-John Hunt Park
Manager/Coach Youth Soccer, Mayfair-John Hunt Park
Scoutmaster, Troop 757
Activity Leader—"Merlin's Magic Marbles" Cub Scout Summer Day Camp
Alabama High School Athletic Association—Registered Wrestling Official
Wood Badge—Adult Scout Leadership Training.

PROFESSIONAL CONSULTING:

Eastman Kodak Company
Candela Lasers
Wagner—Cooper Automotive
Pentastar
Allied Signal Corporation
Mallory Controls
Aero Thermo Technologies
Dynetics
Adtram

PUBLICATIONS, PAPERS, PATENTS

REFEREED PUBLICATIONS:

- M. H. Smith, K. R. Denninghoff, J.E. Drewes, A. Lompado, L.W. Hillman, **"Effect of multiple light paths on retinal vessel oximetry,"** Submitted to Applied Optics.
- M. H. Smith, K. R. Denninghoff, L. W. Hillman, R.A. Chipman, **"Oxygen Saturation Measurements of Blood in Retinal Vessels During Blood Loss,"** *J. Biomed. Optics*, vol. 3 no. 3, pp. 296-303, July 1998.
- K. R. Denninghoff, M.H. Smith, L. W. Hillman, D. Redden, and L. W. Rue. **"Retinal Venous Oxygen Saturation Correlates with Blood Volume,"** *Academic Emergency Medicine* vol. 5 no. 6, June 1998.
- D.J. Lamb, L.W. Hillman, J.F. Van Derlofske, **"The use of aspheric surfaces in waveguide illumination systems for automotive displays,"** Paper #980874, *SAE International Congress and Exposition Proceedings, presented at the Society of Automotive Engineers International Congress and Exposition*, Detroit, MI, February, 1998.
- K.R. Denninghoff, M.H. Smith, R.A. Chipman, L. W. Hillman, P.M. Jester, C.E. Hughes, F. Kuhn, L.W. Rue. **"Retinal large vessel oxygen saturation correlates with early blood loss and hypoxia in anesthetized swine,"** *J. Trauma*, vol. 43 no. 1, pp. 29-34, 1997.
- Van Derlofske, J.F., Lamb, D.J., and Hillman, L.W., **"Computer Modeling of Illumination Systems for Automotive Displays,"** Paper #960525, *SAE International Congress and Exposition Proceedings, presented at the Society of Automotive Engineers International Congress and Exposition*, Detroit, MI, February, 1996.
- K.R. Denninghoff, M.H. Smith, D.R. Smith, L.W. Hillman, R.A. Chipman, **"The Use of an Eye Oximeter to Monitor Blood Loss in a Swine Model,"** *Soc. Academ. Emerg. Med.*, May 1996.
- T. A. Hough, J. F. Van Derlofske, and L. W. Hillman, **"Implementation of Radiometric Modeling and Measurement in the design of Waveguide Illumination Systems for Radio Control panels."** Paper #950964, *SAE International Congress and Exposition Proceedings, presented at the Society of Automotive Engineers International Congress and Exposition*, Detroit, MI, February, 1995.
- T. A. Hough, J. F. Van Derlofske, L.W. Hillman, **"Measuring and Modeling Intensity Distributions of Light Sources in Waveguide Illumination Systems,"** *Optical Engineering*, Vol. 34 No. 3, pp. 819-823 March 1995.
- J. F. Van Derlofske, T. A. Hough, and L. W. Hillman, **"Development of Design Tools for Modeling the Illumination of Automotive Displays and Instruments,"** Paper #940511, *SAE International Congress and Exposition Proceedings, presented at the Society of Automotive Engineers International Congress and Exposition*, Detroit, MI, February, 1994.

- T. A. Hough, J. Van Derlofske and L. W. Hillman, **"Management of light in thick optical waveguides fro dashboard illumination,"** Paper #940512, *SAE International Congress and Exposition Proceedings, presented at the Society of Automotive Engineers International Congress and Exposition*, Detroit, MI, February, 1994.
- S.C. McClain, L.W. Hillman and R.A. Chipman, **"Polarization Ray Tracing in anisotropic optically Active Media: I. Algorithms,"** *Journal of the Optical Society of America A*, vol 10, no. 11, 2371-2382 (Nov. 1993).
- S.C. McClain, L.W. Hillman and R.A. Chipman, **"Polarization Ray Tracing in Anisotropic Optically Active Media: II. Theory and Physics,"** *Journal of the Optical Society of America A*, vol. 10, no. 11, 2393-2393 (Nov. 1993).
- S.C. McClain, R.A. Chipman and L.W. Hillman, **"Aberrations of a horizontal-vertical depolarizer,"** *Applied Optics* 31, 2326-2331, 1992. (*Special Issue on Optical Design.*)
- K. Koch, B. G. Oliver, S. H. Chakmakjian, C. R. Stroud, Jr. and L. W. Hillman, **"Subharmonic Instabilities in Resonant Interactions with Bichromatic Fields,"** *Journal of the Optical Society of America-B*, 58-65, 1989.
- M. A. Kramer, R. W. Boyd, L. W. Hillman, and C. R. Stroud, Jr., **"Propagation of Modulated Optical Fields through Saturable-absorbing Media: A General Theory of Modulation Spectroscopy,"** *Journal of the Optical Society of America-B*, Vol 2, 1444-1455, 1985.
- L. W. Hillman, J. Krasinski, K. Koch, and C. R. Stroud, Jr., **"Dynamics of Homogeneously Broadened Lasers: Higher-order Bichromatic States of Operation,"** *Journal of the Optical Society of America-B*, 211-217, 1985. (Invited Paper)
- L. W. Hillman, J. Krasinski, R. W. Boyd, and C. R. Stroud, Jr., **"Observation of Higher-order Dynamical States of a Homogeneously Broadened Laser,"** *Physical Review Letters*, 1605-1608, 1984.
- M. Malcuit, R. W. Boyd, L. W. Hillman, J. Krasinski, and C. R. Stroud, Jr., **"Saturation and Inverse-saturation Absorption Line Shapes in Alexandrite,"** *Journal of the Optical Society of America-B*, 73-75, 1984.
- L. W. Hillman, J. Krasinski, John A. Yeazell, and C. R. Stroud, Jr., **"Intracavity Power Measurement by Rayleigh Scattering"** *Applied Optics*, 3474, 1983.
- L. W. Hillman, R. W. Boyd, J. Krasinski, and C. R. Stroud, Jr., **"Observation of a Spectral Hole Due to Population Oscillations in a Homogeneously Broadened Absorption Line,"** *Optics Communications*, 416-419, 1983.
- L. W. Hillman, R. W. Boyd and C. R. Stroud, Jr., **"Natural Modes for the Analysis of Optical Bistability and Laser Instability,"** *Optics Letters*, 426-428, 1982.

U.S. PATENTS:

M. H. Smith, L. W. Hillman, K. R. Denninghoff, **"Technique for Two-Dimensional Scanning Spectroscopy of the Ocular Fundus,"** Patent Pending, submitted 9/99.

Matthew H. Smith, Russell A. Chipman, Thomas E. Minnich, Lloyd Hillman, and Kurt R. Denninghoff, **"Method and apparatus for accurately measuring the transmittance of blood within a retinal vessel,"** U.S. Patent Number 5,935,076, August 1999.

Lloyd W. Hillman, **"Design of Reflector"** U.S. Design Patent Number 346,562 May 1994.

Lloyd W. Hillman, **"Specific Intensity Distribution Light Reflector"** U.S. Patent Number 5,251,115, Oct 1993.

PROCEEDINGS AND OTHER PUBLICATIONS:

J. D. Drewes, M. H. Smith, D. R. Denninghoff, L. W. Hillman, **"An Instrument for the Measurement of Retinal Vessel Oxygen Saturation,"** in *Optical Diagnostics of Biological Fluids IV*, Alexander V. Priezzhev, M. V. Lomonosov, Toshimitsu Asakura, eds., *Proceedings of SPIE* Vol. 3591, 114-120 (1999).

K. R. Denninghoff, M. H. Smith, L. W. Hillman, **"An Eye Oximeter for Combat Casualty Care,"** *Proceedings of ATACCC '98* (1998).

M.H. Smith, K.R. Denninghoff, L.W. Hillman, C.E. Hughes, T.E. Minnich, R.A. Chipman, **"Technique for Noninvasive Monitoring of Blood Loss Via Oxygen Saturation Measurements in the Eye,"** *Invited paper in Optical Diagnostics of Biologic Fluids II*, A.V. Priezzhev, T. Asakura, eds., *Proceedings of the SPIE* 2982, 1997.

K.R. Denninghoff, M.H. Smith, R.A. Chipman, L. W. Hillman, P.M. Jester, C.E. Hughes, F. Kuhn, L.W. Rue. **"Retinal large vessel oxygen saturation correlates with early blood loss and hypoxia in anesthetized swine,"** *Soc. Academ. Emerg. Med.*, proc., 1997.

D. A. Lamb, R.A. Chipman, L.W. Hillman, Y. Takahashi, and J. O. Dimmock, **"Computer Modeling of Optical Systems Containing Fresnel Lenses,"** *Giant Cosmic Ray Air Showers from $\geq 10^{20}$ eV Particles from Space*, Greenbelt, MD, November 1997, pp. 434- 43.

T.M. Leslie, E. Burleson, J. Dimmock, D.J. Lamb, L.W. Hillman, Y. Takahashi, M.D. Watson, **"Polymer Selection Criteria for the Orbiting Wide Angle Light-collector (OWL) Project Lens Materials"** American Institute of Physics, *"Workshop on Observing Giant Cosmic Ray Air Showers from $\geq 10^{20}$ eV Particles from Space"*, Greenbelt, MD, November 1997, pp.511-515.

D.J. Lamb, R.A. Chipman, L.W. Hillman, Y. Takahashi, J. Dimmock, **"Focal Plane Reduction of Large Aperture Optical Systems"** American Institute of Physics, *"Workshop on Observing Giant Cosmic Ray Air Showers from $\geq 10^{20}$ eV Particles from Space"*, Greenbelt, MD, November 1997, pp.439-445.

- D.J. Lamb, R.A. Chipman, L.W. Hillman, Y. Takahashi, J. Dimmock, **"Wide Angle Refractive Optics for Astrophysics Applications"** American Institute of Physics, *"Workshop on Observing Giant Cosmic Ray Air Showers from $\geq 10^{20}$ eV Particles from Space"*, Greenbelt, MD, November 1997, pp.428-433.
- D.J. Lamb, R.A. Chipman, L. W. Hillman, Y. Takahashi, J. Dimmock, **"Principles of Wide Angle, Large Aperture Optical Systems"** American Institute of Physics, *"Workshop on Observing Giant Cosmic Ray Air Showers from $\geq 10^{20}$ eV Particles from Space"*, Greenbelt, MD, November 1997, pp.304-311.
- D.J. Lamb, R.A. Chipman, L. W. Hillman, Y. Takahashi, J. Dimmock, **"Computer Modeling of Optical Systems Containing Fresnel Lenses,"** American Institute of Physics, *"Workshop on Observing Giant Cosmic Ray Air Showers from $\geq 10^{20}$ eV Particles from Space"*, Greenbelt, MD, November 1997, pp.434-438.
- L.W. Hillman, S.C. McClain, M.H. Smith, R.A. Chipman, **"Eye oximeter for the noninvasive measurement of cardiac output,"** in *Vision Science and its Application*, 1994 Technical Digest Series, Vol. 2 (Optical Society of America, Washington DC) pp. 151-154 (1994).
- F. J. Duarte and L. W. Hillman, Eds. **Dye Laser Principles: With Applications.** Author of Chapter I, **"Introduction,"** 1-16, and Chapter II, **"Laser Dynamics."** *Academic Press*, Inc. April 1990.
- L. W. Hillman and D. Cohen **"Phase Fluctuations and Damping in Two-level Optical Resonance,"** Published in *Coherence and Quantum Optics VI*, L. Mandel and E. Wolf, Eds., *Plenum Press* 1990.
- L. W. Hillman and S. C. McClain. **"Understanding Squeezed States and Their Detection Using the Schrodinger Picture,"** Published in *Coherence and Quantum Optics VI*, L. Mandel and E. Wolf, Eds., *Plenum Press* 1989.
- L. W. Hillman, S.C. McClain and M. Anderson. **"Second harmonic Generation in Optical Fibers,"** Final report submitted to Universal Energy Systems under the U.S. Air Force Summer Faculty Fellowship Program, October 1989.
- L. W. Hillman. **"Coherence Effects in Film Granularity Measurements,"** Kodak Technical Report 1988.
- L. W. Hillman. **"Coherent Dynamics of Lasers: A Source of Instabilities and Noise,"** in proceedings of the International Conference on Lasers '87, F. J. Duarte, ed., STS Press, McLean, Virginia, pp. 4-11, 1988.
- S. Chakmakjian, L. W. Hillman, K. Koch and C. R. Stroud, Jr., in *Optical Bistability III*, H. M. Gibbs, P. Mandel, N. Peyghambarian, and S. D. Smith, eds., **"Multimode Instabilities of Homogeneously Broadened Lasers,"** *Springer-Verlag*, New York, 345-347, 1986.
- L. W. Hillman and K. Koch, in *Optical Instabilities*, R. W. Boyd, M. G. Raymer, and L. M. Narducci, eds. **"Multimode Instabilities in Homogeneous Broadened Lasers"** *Cambridge University Press*, 256-258, 1985.

L. W. Hillman, R. W. Boyd, J. Krasinski, and C. R. Stroud, Jr., in *Optical Bistability II*, M. Bowden, H. M. Gibbs, and S. L. McCall. **"Intrinsic Instabilities in Homogeneously Broadened Lasers"** *Plenum Publishing Corp.*, New York, 305-310, 1983.

CONFERENCE PRESENTATIONS (not in print):

L.W. Hillman, M.H. Smith, K.R. Denninghoff, **"Eye oximeter for combat casualty care,"** ATACCC '99, Ft. Walton Beach, Florida, October 18-22, 1999.

K.R. Denninghoff, M.H. Smith, L.W. Hillman, **"Retinal Venous O₂ Sat Correlates with Blood Volume and Cardiac Output During Exsanguination/Reinfusion,"** ATACCC '99, Ft. Walton Beach, Florida, October 18-22, 1999.

M. H. Smith, A. Lompado, K. R. Denninghoff, L.W. Hillman, **"A scanning laser ophthalmoscope for retinal vessel oximetry,"** TuNN2, *Optical Soc. Am., Annual Meeting*, Santa Clara, California, Sept 26-30, 1999.

K. R. Denninghoff, M. H. Smith, L.W. Hillman, **"Noninvasive optical systems in systemic and ophthalmic diseases,"** TuNN4, *Optical Soc. Am., Annual Meeting*, Santa Clara, California, Sept 26-30, 1999. (Invited Paper)

D. J. Lamb, L.W. Hillman, **"Analytic and computer modeled analysis of facet vignetting in Fresnel lenses,"** TuTT2, *Optical Soc. Am., Annual Meeting*, Santa Clara, California, Sept 26-30, 1999.

M. H. Smith, K. R. Denninghoff, J.E. Drewes, L. W. Hillman, **"Multiple light paths in Retinal Vessel Oximetry,"** TuXX79, *Optical Soc. Am., Annual Meeting*, Santa Clara, California, Sept 26-30, 1999.

M. H. Smith, A. Lompado, L. W. Hillman, K. R. Denninghoff, **"A scanning laser ophthalmoscope for retinal vessel oximetry,"** *Optical Soc. Am., Annual Meeting*, Santa Clara, California, September 26-30, 1999.

L.W. Hillman, D.J. Lamb, **"Efficiency of fused and unfused glass fiber bundles for automotive distributed lighting systems,"** presented at the 1999 SAE Congress and Exposition, Detroit, MI, February 23-26, 1999.

M. H. Smith, J.E. Drewes, L. W. Hillman, K. R. Denninghoff, **"The effect of diffusion-enlarged paint spread function on retinal vessel oximetry,"** *Optical Soc. Am., Annual Meeting*, Baltimore, Maryland, October 4-10, 1998.

J.E. Drewes, M.H. Smith, L.W. Hillman, K.R. Denninghoff, **"Optomechanical design of an imaging eye oximeter for the measurement of retinal vessel oxygen saturation"** *Optical Soc. Am., Annual Meeting*, Baltimore, Maryland, October 4-10, 1998.

A. Lompado, M.H. Smith, L.W. Hillman, K.R. Denninghoff, **"Measurement of the scattering anisotropy of a column of whole human blood,"** *Optical Soc. of Am., Annual Meeting*, Baltimore, Maryland, October 4-10, 1998.

- L. W. Hillman, M.H. Smith, A. Lompado, J.E. Drewes, K. R. Denninghoff, "**Simulation and deconvolution of light scattering in the human eye**" Optics In Biology And Medicine Division General Poster Session, *Optical Soc. of Am., Annual Meeting*, Baltimore, Maryland, October 4-10, 1998.
- F. Sealy, H. Comfort, L.W. Hillman, A.G.Emslie, "**Undergraduate Physics Program at UAH**", AAPT Conference on Revitalization of Undergraduate Physics, Washington, D.C., October 2-4, 1998.
- D. J. Lamb, L.W. Hillman, J. F. Van Derlofske, "**The Use of Aspheric Surfaces in Waveguide Illumination Systems for Automotive Displays**," presented at the 1998 SAE Congress and Exposition, Detroit, MI, February 23-26 1998.
- D.J. Lamb, R.A. Chipman, L.W. Hillman, Y. Takahashi, "**Design of a Large Aperture, Wide Field Air Shower Detector with Use of Fresnel Lenses**," presented at the Optical Society of America's Annual Meeting, Long Beach, CA, October, 1997.
- D.J. Lamb, L.W. Hillman, "**Input and Output Waveguide Structures for Fiber Optic Illumination Systems**," International Congress of the Society of Automotive Engineers, Technical Paper No. 970255, Detroit, MI, Feb. 1997.
- D. J. Lamb J.F. Van Derlofske, L.W. Hillman, "**Optimization Techniques for the Design of Thick Waveguide Illumination Systems**," Paper MMM6 Optical Society of America Annual Meeting, Rochester, NY, Oct 1996.
- J.F. Van Derlofske, D.J. Lamb, L.W. Hillman, "**The Use of Stereolithography for Design and Optimization of Thick Waveguide Illumination Systems**," Paper MCCC4 Optical Society of America Annual Meeting, Rochester, NY, Oct. 1996.
- S. Lee and L. W. Hillman, "**Measurement of Relaxation Oscillation Frequency and its Dependence on Gain and Longitudinal Modes in GaAlAs Laser**" presented at the 1994 International Conference on Lasers Quebec, Canada, 1994.
- S. Lee and L. W. Hillman, "**Observation of a New Doppler-Free Resonance in the Saturated, Zeeman-Shifted 85Rb-D2-Line**," presented at the 1994 International Conference on Lasers Quebec, Canada 1994.
- L. W. Hillman, T. A. Hough, J. F. Van Derlofske, "**Solving Illumination Problems of Meter and Gauge Clusters for the Automotive Industry**," International Conference on Lasers '92, Houston, TX, December 1992. (Invited Plenary Talk.)
- L.W. Hillman, "**Taming, Tuning, and Tweaking Dye Laser Dynamics**," 24th Annual Mardi Gras Symposium in Theoretical Chemistry, New Orleans, February 1991. (Invited Plenary Speaker.)
- L.W. Hillman and S. Lee, "**Frequency Stabilization of Diode Lasers**," International Conference of Lasers '91, WD3, San Diego, California, December 1991.
- L.W. Hillman, "**Nonlinear Lasers Instabilities**," presented at International Conference of Lasers '90, MA3, San Diego, California, December 1990. (Invited Plenary Speaker.)

- L. W. Hillman, **"Physics of Tunable Semiconductor Lasers,"** International Conference of Lasers '90, MH4, San Diego, California, December 1990.
- S. McClain and L. W. Hillman, **"Understanding Squeezed States and their Detection Using the Schrödinger Picture,"** Sixth Rochester Conference on Coherence and Quantum Optics, Rochester, New York, June 1989.
- D. Cohen and L. W. Hillman, **"Phase Fluctuation and Damping in Two-level Optical Resonance,"** presented at Sixth Rochester Conference on Coherence and Quantum Optics, Rochester, New York, June 1989.
- S. McClain and L. W. Hillman, **"Time Dynamics of Squeezed States,"** presented at International Conference of Lasers '88, MH3, Lake Tahoe, Nevada, December 1988.
- L. W. Hillman, **"Coherent Dynamics of Lasers: A Source of Instabilities and Noise,"** presented at International Conference of Lasers '87, Lake Tahoe, Nevada, December 1987. (Invited Plenary Speaker.)
- L. W. Hillman, **"Coherent Optical Interactions in Semiconductor Lasers,"** presented at the Annual Meeting of the Optical Society of America, WO10, Rochester, NY, October 1987. [Abstract in JOSA-A, P74 (1987).]
- L. W. Hillman, **"Resonance Fluorescence with Modulated Excitation,"** presented at the Annual Meeting of the Optical Society of America, WF8, Rochester NY, October 1987. [Abstract in JOSA-A, P65 (1987).]
- K. Koch, B. J. Oliver, L. W. Hillman, and C. R. Stroud, Jr., **"Subharmonic Instabilities in Resonant Interactions with Bichromatic Fields,"** presented at the Annual Meeting of the Optical Society of America, WF7 Rochester, NY, October 1987. [Abstract in JOSA-A, P65 (1987).]
- K. Koch, S. H. Chakmakjian, L. W. Hillman, C. R. Stroud, Jr., **"Broadband Atomic Response to Incommensurate Modulation Frequencies,"** presented at the Annual Meeting of the Optical Society of America, WF6, Rochester, NY, October 1987. [Abstract in JOSA-A, P65, (1987).]
- S. H. Chakmakjian, K. Koch, L. W. Hillman, and C. R. Stroud, Jr., **"Incoherent Pump Effects in AM Spectroscopy,"** presented at the Annual Meeting of the Optical Society of America, MD6, Rochester, NY, October 1987. [Abstract in JOSA-A, P9 (1987).]
- L. W. Hillman, **"Coherent Dynamics of Semiconductor Laser Diodes"** presented at International Workshop on Instabilities, Dynamics, and Chaos in Nonlinear Optical Systems, Il Ciorro, Lucca Italy, July 1987. (Invited Paper.)
- K. Koch, S. H. Chakmakjian, L. W. Hillman, and C. R. Stroud, Jr., **"Effects of Detuning on Laser Instabilities,"** presented at the Annual Meeting of the Optical Society of America, FT3, Seattle, WA, October 1986. [Abstract in JOSA-A, P120 (1986).]
- L. W. Hillman, **"Noise in Polarization-sensitive Optical Systems,"** presented at the Workshop on Magneto-Optic Recording, Saratoga Springs, NY, June 1986.

- C. R. Stroud, Jr., K. Koch, S. H. Chakmakjian, and L. W. Hillman, **"Multimode Instabilities in CW Dye Lasers,"** presented at the SPIE Symposium on Optical Chaos, Quebec City, Quebec, June 1986.
- S. H. Chakmakjian, L. W. Hillman, K. Koch, and C. R. Stroud, Jr., **"Multimode Instabilities of Homogeneously Broadened Lasers,"** presented at the Third Topical Meeting on Bistability, MD18, Tucson AZ, December 1985.
- L. W. Hillman, K. Koch and C. R. Stroud, Jr., **"Multimode Instabilities in Homogeneous Broadened Lasers,"** presented at the Annual Meeting of the Optical Society of America, TuW1, Washington, D.C., October 1985. [Abstract in JOSA-A, P24 (1985).]
- L. W. Hillman and K. Koch, **"The Source of Multimode Instabilities in Homogeneously Broadened Lasers,"** presented at the International Meeting on Instabilities and Dynamics of Lasers and Nonlinear Optical Systems, ThA3, Rochester, NY, June 1985. (Invited Paper.)
- L. W. Hillman and C. R. Stroud, Jr., **"Instabilities in Homogeneously Broadened Lasers,"** presented at the Annual Meeting of the Optical Society of America, FM3, San Diego, CA, October 1984. [Abstract in JOSA-A, 1321 (1984).] (Invited Paper.)
- L. W. Hillman, J. Y. Yuan, K. Koch, J. Krasinski, and C. R. Stroud, Jr., **"Behavior of Homogeneously Broadened Lasers Operating Far Above Threshold,"** presented at the Thirteenth International Quantum Electronics Conference, MEE5, Anaheim, CA, June 1984. [Abstract in JOSA-B, 440 (1984).]
- L. W. Hillman, J. Krasinski, R. W. Boyd, and C. R. Stroud, Jr., **"Giant Mode Splitting and Hysteresis in a Continuous-Wave High-Q-Cavity Dye Laser,"** presented at the Annual Meeting of the Optical Society of America, ThP3, New Orleans, LA, October 1983. [Abstract in JOSA, 1960 (1983).]
- R. W. Boyd, L. W. Hillman, M. A. Kramer, J. Krasinski, M. Malcuit, and C. R. Stroud, Jr., **"Probe-beam Absorption Line Shapes in Homogeneously Broadened Media,"** presented at the Annual Meeting of the Optical Society of America, WT3, New Orleans, LA, October 1983. [Abstract in JOSA, 1929 (1983).]
- L. W. Hillman, R. W. Boyd, J. Krasinski, and C. R. Stroud, Jr., **"Intrinsic Instabilities in Homogeneously Broadened Lasers,"** presented at the Second Topical Meeting on Optical Bistability, ThB12, Rochester, NY, June 1983.
- R. W. Boyd, L. W. Hillman, J. Krasinski, and C. R. Stroud, Jr., **"Spectral Hole Burning in a Homogeneously Broadened Transition,"** presented at the Annual Meeting of the Optical Society of America, Post Deadline, Tucson, AZ, October 1982. [Abstract in JOSA, 1748 (1982).]
- J. S. Wilczynski, M. A. Wesley and L. W. Hillman, **"Astronomical Application of the Synthetic Aperture Telescope (SAT),"** presented at the Annual Meeting of the Optical Society of America, ThE3, Rochester, NY, October 1979. [Abstract in JOSA, 1455 (1979).]

L. W. Hillman and C. R. Stroud, Jr., "**Optical Bistable Switching Using Frequency Modulation,**" presented at the Annual Meeting of the Optical Society of America, TuR3, Rochester, NY, October 1979. [Abstract in JOSA, 1421 (1979).]

ARTHUR LOMPADO

2508 Alabama Street • Huntsville, AL 35801 • 256-539-0287 (H) • 256-890-6276 x314 (W)

SUMMARY: Experience and credentials in optical science and engineering with strengths in biomedical optics and polarimetry.

EDUCATION:

1999	Ph.D.	Optical Science and Engineering University of Alabama in Huntsville, Huntsville, AL Dissertation: "A Two-Dimensional Confocal Scanning Laser Ophthalmoscope for Retinal Vessel Oximetry"
1988	B.S.	Optics University of Rochester, Rochester, NY

COMPETENCIES:

- Thorough understanding of fundamental and applied optics.
- Excellent problem solving abilities as well as good organizational and time management skills.
- Working knowledge of popular optical thin film design codes (CAM5, Film Star, FILM*CALC, Code V) and optical system design codes (Zemax, Code V, OPTEC-I, OptiCAD, Beam3).
- Strong mathematical modeling and simulation capabilities using Mathematica and MathCAD.
- Substantial optical laboratory experience with typical and novel laboratory equipment including computer interfacing for system automation.

COMPUTER LITERACY:

- Fluent programming skills in BASIC, Visual BASIC, and "C/C++".
- Familiarity with FORTRAN, Pascal.
- Extensive experience with PC's (IBM and Macintosh platforms) and workstations running under VAX/VMS, UNIX and Solaris operating systems.

EXPERIENCE:
05/99 - Present

Senior Research Associate, University of Alabama in Huntsville
Conduct biomedical optics research and teach introductory physics. Major responsibilities:

- Perform both theoretical and experimental research in the field of Retinal Vessel Oximetry. This includes studies regarding the propagation of light through turbid media such as human tissue.
- Investigate the scattering of light by whole human blood and its effect on the perceived transmittance of blood samples.
- Perform live animal (swine) and human studies of retinal oxygen saturation as well as preliminary *in vitro* studies using a unique model human eye.
- Design and construct a novel polar scatterometer to perform light scattering measurements on columns of whole human blood (i.e., simulated blood vessels).
- Teach introductory Physics course (Physics I with Calculus) in mechanics.
- Provide guidance to graduate students working on biomedical optics and polarimetry projects.
- Coherently present, both orally and through written reports, program status to contracting agencies funding the research
- Write proposals for project funding of biomedical optics projects.

02/95 – 05/99

Graduate Research Assistant, University of Alabama in Huntsville

Conducted polarimetric and biomedical optics research. Major responsibilities:

- Designed and constructed a Stokes Vector Imaging Polarimeter for use in remote sensing and metrology applications.
- Designed, constructed and developed a novel scanning laser ophthalmoscope for imaging the internal ocular structure. Device also determines subject's blood oxygenation level spectroscopically from retina-reflected light.
- Presented undergraduate and graduate level lectures in Geometrical Optics, Physical Optics, Radiometry, and Linear Systems/Fourier Optics.
- Contributed to various proposals and reports to scientific funding agencies such as the NSF and the U.S. Army.

08/94-01/95

Graduate Teaching Assistant, University of Alabama in Huntsville

Provided tutoring in freshman level Mechanics and Electricity and Magnetism courses and laboratories.

- Taught Advanced Placement (AP) Physics at Johnson High School (Huntsville, AL) as part of a cooperative teaching program between the University and local high schools.

11/90 – 08/94

Optical Scientist, Surgical Laser Technologies, Oaks, PA

Engaged in contact laser-tissue interaction research to evaluate the overall effect of absorptive tissue heating in conjunction with conductive heating on tissue vaporization rates.

- Helped design artificial sapphire laser scalpels of various geometric configurations for surgical procedures.
- Contributed to the engineering and development of Nd:YAG based medical laser systems for use as coagulation and vaporization tools in the surgical community.
- Tested fiber optic delivery systems used to conduct laser energy from the laser source to the sterile operating arena..
- Contributed substantially as technical consultant in patent-related litigation resulting in a favorable judgment.

08/88 - 11/90

Staff Scientist, Spire Corporation, Bedford, MA

Responsible for all stages of several optics-related research and development contracts from proposal to fruition in surface scatterometry, thin film design and deposition techniques, spectrophotometry, optical baffle materials development, and system evaluation for stray light control and rejection.

- Designed, fabricated, qualified operation, and ultimately automated optical scattering and thin film metrology systems and presented results.

01/88 - 06/88

Independent Researcher, Laboratory for Laser Energetics, Rochester, NY

- Designed and implemented method to determine optical constants of an inhomogeneous thin film using data acquired *in-situ*.
- Automated a coating deposition chamber to monitor film transmission data in real time and inform operator of variation in the film's refractive index and extinction coefficient as a function of film thickness.

PRESENTATIONS:

A. Lompado, M.H. Smith, K.R. Denninghoff, and L.W. Hillman, "Measurement of the Scattering Anisotropy of a Column of Whole Human Blood", paper presented at the 82nd annual meeting of OSA, Baltimore, MD. (October 1998).

LOMPADO, A.

A. Lompado, M.H. Smith, R.A. Chipman, and L.W. Hillman, "A Real Time Stokes Vector Imaging Polarimeter", paper presented at the 82nd annual meeting of OSA, Baltimore, MD. (October 1998).

L.W. Hillman, K.R. Denninghoff, M.H. Smith, A. Lompado, and J.J. Drewes, "Simulation and Deconvolution of Light Scattering in the Human Eye", poster presented at the 82nd annual meeting of OSA, Baltimore, MD. (October 1998).

M.H. Smith, A. Lompado, L.W. Hillman, and K.R. Denninghoff, "A Scanning Laser Ophthalmoscope for Retinal Vessel Oximetry", paper presented at the 83rd annual meeting of OSA, San Jose, CA. (October 1999).

M.H. Smith, K.R. Denninghoff, A. Lompado, and L.W. Hillman, "Multiple Light Paths in Retinal Vessel Oximetry", poster presented at the 83rd annual meeting of OSA, San Jose, CA. (October 1999).

PATENTS:

Light energy emitting probe with inclusions distributed within and throughout probe's tip portion, T.A. Fuller, A. Lompado, M.A. DeStefano, #5,520,681; May 28, 1996.

Light energy emitting probe with light-affecting inclusions distributed throughout, T.A. Fuller, A. Lompado, M.A. DeStefano, #5,807,390; September 15, 1998.

HONORS:

Rochester National Scholarship
New York State Regents Scholarship

AFFILIATIONS:

Optical Society of America (OSA) - member
Society of Photo Instrumentation Engineers (SPIE) - member

PERSONAL DATA:

Citizenship: United States
Security clearance - DOD "secret" level

REFERENCES:

Available upon request

PUBLICATIONS:

M.H. Smith, K.R. Denninghoff, A. Lompado, J.J. Drewes, and L.W. Hillman, "Effect of Multiple Light Paths on Retinal Vessel Oximetry," submitted for publication in *Applied Optics*, 1999.

A. Lompado, E.A. Sornsin and R.A. Chipman, "HN22 Sheet Polarizer, an Inexpensive Infrared Retarder," *Appl. Opt.*, **36**, pp. 5396-5402, 1997.

J. Goela, M.A. Pickering, R.L. Taylor, B.W. Murray and A. Lompado, "Properties of chemical-vapor-deposited silicon carbide for optics applications in severe environments," *Appl. Opt.*, **30**, pp. 3166-3175, 1991.

J. Goela, R.L. Taylor, B.W. Murray and A. Lompado, "Chemical Vapor Deposition of Silicon and Silicon Carbide Optical Substrates for Severe Environments, " in Optical Systems Resistant to Severe Environments, S. Musikant (ed.), *Proc. SPIE 1330*, pp. 25-28, 1991.

A. Lompado, B.W. Murray, J. S. Wollam and J. F. Meroth, "Characterization of Optical Baffle Materials, " in Scatter From Optical Components, J.C. Stover (ed.), *Proc. SPIE 1165*, pp. 212-216, 1989.

B.W. Murray, A. Lompado, and J. K. Hirvonen, "Durable Solar Reflective Surfaces in Beryllium, " in Space Optical Materials and Space Qualification of Optics, R.R. Hale (ed.), *Proc. SPIE 1118*, pp. 73-87, 1989.

OPTICAL SCANNING SPECTROSCOPIC APPARATUS AND ASSOCIATED METHOD

FIELD OF THE INVENTION

The present invention relates generally to an optical imaging apparatus and associated methods and, more particularly, to an optical scanning spectroscopic apparatus and associated methods for generating images of the posterior portion of a
5 subject's eye.

BACKGROUND OF THE INVENTION

By examining the posterior portions of a subject's eye, such as the retinal vessels and the choroidal vessels, a significant amount of data can be collected for various diagnostic and analytical applications. For example, the blood oxygen
10 saturation or blood oxygen content of the blood in the retinal vessels is determinative of the arteriovenous oxygen difference as described by U.S. Patent No. 5,308,919 to Thomas E. Minnich, U.S. Patent No. 5,776,060 to Matthew H. Smith, et. al., and U.S. Patent No. 5,935,076 to Matthew H. Smith, et. al. Based upon the arteriovenous oxygen difference, the cardiac output of the subject can be determined in order to
15 assist in post-operative monitoring and the management of critically ill patients. By monitoring the blood oxygen saturation, the loss of blood can also be detected and the rate and quantity of blood loss over time can be estimated as described by U.S. Patent No. 5,119,814 to Thomas E. Minnich.

In addition to blood oxygen saturation, the concentration of cytochrome
20 oxidase a3 can be measured in order to monitor retinal tissue perfusion. Further, by observing the magnitude of the choroidal reflectance pulsation across the cardiac cycle, such as with a pulse oximeter, the choroidal oxygenation can also be monitored. See J.P. de Kock, L. Tarrassenko, C.J. Glynn, A.R. Hill, "Reflectance Pulse Oximetry Measurements from the Retinal Fundus," IEEE Transactions on
25 Biomedical Engineering, vol. 40, no. 8, 817-23 (1993). In addition to the foregoing

examples, a number of other anatomic features and physiological parameters, such as the degree of melanin pigmentation of the fundus, can be determined by examining the posterior portion of a subject's eye, as described by F.C. Delori, K.P. Phlipsen, "Spectral reflectance of the human ocular fundus," Applied Optics, vol. 28, no. 6,
5 1061-77 (1989).

In order to examine the posterior portion of a subject's eye, several non-invasive techniques have been developed. In this regard, the traditional technique for examining the posterior portions of a subject's eye is fundus photography. Fundus photography illuminates a subject's eye with a flash of white light. Fundus
10 photography then detects the light returning from the subject's eye, such as a result of the reflection of a portion of the light from the retinal and choroidal vessels, as well as the reflection and scattering of portions of the light from other features of the posterior portion of the subject's eye. Since the subject's eye is initially illuminated with white light, fundus photography typically spectrally separates the light that
15 returns from the subject's eye in order to separately evaluate the signals that return from the subject's eye at different wavelengths of interest.

Because traditional fundus photography involves illuminating the subject's eye with a flash of white light, care must generally be taken to ensure that the subject's eye is not exposed to excessively high levels of light that could harm the subject's eye.
20 As such, the intensity of the flash of white light must generally be maintained below some relatively low threshold, such as below about _____, in order to protect the subject's eye. Since the flash of white light must generally be maintained below some threshold, the resulting serial to noise ratio of the signals returning from the posterior portion of the subject's eye is also relatively low in comparison to the higher signal to
25 noise ratios that would be obtained if the flash of white light could have a greater intensity. As a result of the relatively low signal to noise ratio, at least some of the signals returning from the posterior portions of the subject's eye generally are lost in the noise, and the overall validity or credibility of the signals returning from the posterior portions of the subject's eye is subject to more questions.

30 Even though the flash of white light that illuminates a subject's eye in traditional fundus photography is somewhat limited in order to protect the subject's eye, the flash of white light is still generally sufficiently intense to prevent serial measurements from being obtained. In this regard, the flash of white light is still

sufficiently intense to cause the pupil of the subject's eye to constrict and, in some instances, to cause the metabolism of the subject's eye to be altered. In order to monitor the posterior portions of the subject's eye under consistent conditions, traditional fundus photography must therefore wait until the subject's pupil is no longer constricted prior to collecting another image of the posterior portions of the subject's eye. While it may take different lengths of time for the pupils of different subjects to return to normal, traditional fundus photography must typically wait at least _____ prior to obtaining another image of the posterior portions of the subject's eye, thereby disadvantageously delaying the entire examination process.

More recently, scanning laser ophthalmoscopes have addressed at least some of the shortcomings of traditional fundus photography. For a general description of scanning laser ophthalmoscopes, see Noninvasive Diagnostic Techniques in Ophthalmology, Barry R. Masters, editor, Chapter 22, Scanning Laser Ophthalmoscope, by Robert H. Webb, Springer-Verlag, New York (1990). Scanning laser ophthalmoscopes generally include a plurality of laser sources, each of which emits a laser signal of a different wavelength. A scanning laser ophthalmoscope scans the laser signals emitted by each of the laser sources in a predetermined pattern across posterior portions of a subject's eye to thereby define a frame having a number of scan lines. A scanning laser ophthalmoscope also typically includes dichroic beam splitters for separating the signals that return from the posterior portions of the subject's eye based upon the wavelength of the return signals. As such, the return signals attributable to the laser signals emitted by each of the laser sources are effectively separated and can therefore be individually analyzed.

Conventional scanning laser ophthalmoscopes include three laser sources. Since a scanning laser ophthalmoscope generally simultaneously illuminates a subject's eye with the laser signals emitted by each of the laser sources, a conventional scanning laser ophthalmoscope may also have the potential to expose the subject's eye to excessive amounts of light. As such, the intensity of the laser signals emitted by each of the laser sources is generally maintained at a relatively low level, such as below about _____, such that the cumulative intensity of the laser signals remains safe for the subject's eye. As such, the signal-to-noise ratio of the signals returning from the posterior portions of the subject's eye is therefore correspondingly reduced relative to the signal-to-noise ratio of the return signals that would be

possible if the intensity of the laser signals emitted by each of the laser sources were not reduced in order to protect the subject's eye. At least some of the signals returning from the posterior portion of the subject's eye will therefore be lost in the noise and the overall validity of the return signals will be somewhat more questionable due to the lower signal-to-noise ratio.

In addition, it has been proposed that a scanning laser ophthalmoscope should sequentially scan the posterior portions of a subject's eye with the laser signals emitted by the plurality of laser sources. See U.S. Patent No. 5,815,242 to Douglas C. Anderson, et al. that describes a scanning laser ophthalmoscope having first, second and third laser sources. In operation, the scanning laser ophthalmoscope initially scans the posterior portions of the eye with the laser signals emitted by the first laser so as to create a first data frame based upon the return signals. Thereafter, the scanning laser ophthalmoscope scans the posterior portions of the eye with laser signals emitted by the second laser source in order to create a second data frame. Finally, the scanning laser ophthalmoscope scans the posterior portions of the eye with the laser signals emitted by the third laser source in order to create a third data frame. While sequentially scanning the posterior portions of the eye with the laser signals emitted by the different laser sources permits the laser sources to emit laser signals having a greater intensity, the overall examination process takes longer since separate data frames must be constructed for the laser signals emitted by each of the laser sources. In addition, since the posterior portions of the eye are scanned with the laser signals emitted by each of the different laser sources at different intervals of time, the test conditions may change between the times at which the eye is exposed to laser signals from different ones of the laser sources. For example, the subject may move slightly, thereby altering the area of the peripheral portion of the eye that is illuminated and therefore examined. Alternatively, the subject's pupil may constrict as a result of the laser illumination. Since the test conditions can change between the time at which the laser signals emitted by one of the laser sources are scanned across the posterior portions of the eye and the time at which the laser signals emitted by another one of the laser sources are scanned across the posterior portions of the eye, the consistency and correlation between the data frames attributable to the laser signals emitted by each of the laser sources are limited.

Accordingly, while several techniques have been developed for examining the posterior portions of a subject's eye, each of these techniques is somewhat limited. As such, an improved method and apparatus for examining the posterior portion of an eye is therefore desired which does not expose a subject's eye to excessive illumination.

5 In addition, it would be desirable to examine the posterior portions of a subject's eye during specific predetermined portions of the subject's cardiac cycle since a number of the features that are being examined are at least somewhat dependent upon the phase of the cardiac cycle. Traditional fundus photography and scanning laser
10 ophthalmoscopes have not generally considered the phase of the cardiac cycle of the subject, but have, instead, obtained images or other data related to the posterior portions of the subject's eye without regard to the phase of the cardiac cycle of the subject. As such, the variations in those features of the posterior portion of the subject's eye that are dependent upon the phase of the cardiac cycle of the subject have typically not been taken into account.

15

SUMMARY OF THE INVENTION

An improved optical scanning spectroscopic method and apparatus is therefore provided according to the present invention. The optical scanning spectroscopic method and apparatus of the present invention alternately scans the posterior portion
20 of an eye with laser signals emitted by different ones of a plurality of lasers such that a data frame can be constructed that includes interlaced portions formed from signals returning from the posterior portion of the eye in response to illumination by laser signals emitted by different ones of the plurality of lasers. As such, the same data frame includes data attributable to the reflection of laser signals from each of the
25 plurality of lasers even though the subject's eye is not subjected to simultaneous illumination by each of the lasers, thereby protecting the subject's eye. According to one further aspect of the present invention, the optical scanning spectroscopic method and apparatus can illuminate the posterior portion of the subject's eye in response to a trigger at a predetermined point in the cardiac cycle of the subject such that the
30 resulting data frame relates to at least a predetermined portion of the cardiac cycle of the subject, thereby permitting a detailed analysis of one or more phases of the cardiac cycle of the subject.

The optical scanning spectroscopic apparatus includes a plurality of lasers for emitting laser signals having different respective wavelengths. For example, the optical scanning spectroscopic apparatus can include first, second, third and fourth lasers for emitting laser signals having first, second, third and fourth wavelengths, respectively. The optical scanning spectroscopic apparatus also includes a scanner for repeatedly scanning the laser signals emitted by the plurality of lasers across the posterior portion of a subject's eye. The optical scanning spectroscopic apparatus can also include a detector for detecting signals returning from the posterior portion of the eye in response to illumination by the laser signals. As such, a data frame having a number of interlaced portions can be formed from the returning signals. In this regard, the optical scanning spectroscopic apparatus also includes a controller for alternately activating different ones of the plurality of lasers while the scanner scans the laser signals across the posterior portion of the eye. As such, the adjacent interlaced portions of the resulting data frame are formed from signals returning from the posterior portion of the eye in response to illumination by laser signals emitted by different ones of the plurality of lasers.

For example, in the embodiment in which the optical scanning spectroscopic apparatus includes first, second, third and fourth lasers, the controller alternately activates the first, second, third and fourth lasers while the scanner scans the laser signals across the posterior portion of the eye. In particular, the controller alternately activates the first, second, third and fourth lasers such that a different laser is activated while the laser signals are scanned along different scan lines of the same frame. For example, the controller may activate the first laser while the scanner scans the laser signals emitted by the first laser across the first scan line. The controller may then activate the second laser while the scanner scans the laser signals emitted by the second laser along the second scan line. The controller then activates the third laser while the scanner scans the laser signals emitted by the third laser along the third scan line, before finally activating the fourth laser while the scanner scans the laser signals emitted by the fourth laser along the fourth scan line. The controller can then repeat this process by alternately activating the first, second, third and fourth lasers while the scanner scans the respective laser signals along the different scan lines until each of the scan lines of the same frame has been completed.

The optical scanning spectroscopic apparatus can also include means, such as a computer, for deinterlacing the data frame to form a plurality of images. In this regard, each image is generated in response to illumination of the posterior portion of the eye by laser signals emitted by different ones of the plurality of lasers. For
5 example, in the embodiment in which the controller alternately activates the plurality of lasers such that only a single laser is activated at any one time, the plurality of resulting images are monochromatic. In the embodiment in which the optical scanning spectroscopic apparatus includes first, second, third and fourth lasers, for example, the four resulting monochromatic images will have been separately
10 generated in response to illumination in the posterior portion of the eye by laser signals emitted by the first, second, third and fourth lasers, respectively.

The optical scanning spectroscopic apparatus can also include other components. For example, the optical scanning spectroscopic apparatus can include a target laser for illuminating the posterior portion of the eye in order to generate a
15 corresponding image. Once the target laser illuminates a predetermined area of the posterior portion of the eye, the controller preferably deactivates target laser and activates the plurality of lasers to form the data frame. In order to appropriately filter the signals returning from the posterior portion of the eye, the optical scanning spectroscopic apparatus can also include an orthogonal polarizer. Since the plurality
20 of lasers of this embodiment emit linearly polarized laser signals, the orthogonal polarizer will block the linearly polarized laser signals, such as the return signals reflected from the surface of the retinal vessels that maintain the same polarization, while passing the orthogonally polarized signals, such as the return signals reflected by the blood within the retinal vessels, to the detector. In addition, the optical
25 scanning spectroscopic apparatus can include at least one of a confocal filter and an anti-confocal filter positioned upstream of the detector for further selecting or filtering the signals to be delivered to the detector.

According to one aspect of the present invention, the optical scanning spectroscopic method and apparatus can also include a triggering mechanism for
30 providing a trigger signal indicative of a predetermined point in a cardiac cycle of the subject. For example, the triggering mechanism can provide a trigger signal in response to an r-wave of an electrocardiogram (EKG) of the subject. The controller of this embodiment can therefore activate the one or more of the lasers in response to

the trigger signal such that the posterior portion of the eye is illuminated during at least a predetermined portion of the cardiac cycle of the subject. The controller can activate the laser immediately upon receiving the trigger signal or the optical scanning spectroscopic apparatus can include a timer for delaying activation of the laser by at least a predetermined time following receipt of the trigger signal. In either instance, a data frame can be captured based upon the return signals relating to at least the predetermined portion of the cardiac cycle of the subject. As such, the optical scanning spectroscopic method and apparatus of this aspect of the invention can collect data that is specific to one or more phases of the cardiac cycle of the subject which may be particularly important for certain diagnostic or analytical applications.

The optical scanning spectroscopic method and apparatus of the present invention therefore illuminates the posterior portion of an eye with the laser signals emitted by a plurality of lasers having different respective wavelengths. However, by alternately illuminating the posterior portion of the eye with different ones of the plurality of lasers, the eye is not simultaneously subjected to illumination from each of the lasers, thereby protecting the eye from exposure to excessive illumination. As such, the intensity of the laser signals emitted by the lasers need not be reduced in order to protect the eye. Instead, the lasers can be operated at greater intensity levels than the lasers of conventional scanning laser ophthalmoscopes that simultaneously illuminate the eye with the laser signals emitted by a plurality of lasers. As such, the signal-to-noise ratio of the signals returning from the posterior portion of the eye and detected according to the present invention is greater than the signal-to-noise ratio of the return signals detected by conventional scanning laser ophthalmoscopes as a result of the increased intensity of the laser signals emitted by the lasers. Thus, fewer signals returning from the posterior portion of the eye will be lost in the noise and the validity of the detected signals will be more reliable. By alternately illuminating the posterior portion of the eye with laser signals emitted by different ones of the lasers, the resulting data frame includes interlaced portions formed from signals returning from the posterior portion of the eye in response to illumination by laser signals emitted by different ones of plurality of lasers. The optical scanning spectroscopic method and apparatus of the present invention are therefore capable of alternately scanning the posterior portion of the eye with the laser signals emitted by different lasers in a rapid fashion such that the measurement conditions, such as the position of

the subject and the constriction of the subject's pupil, do not change appreciably between the times at which the subject's eye is illuminated by different lasers. As such, the resulting images generated in response to illumination of the posterior portion of the eye by laser signals emitted by different ones of the lasers should be more consistent and more easily correlated than sequential data frames generated by the illumination of the subject's eye with the different lasers.

BRIEF DESCRIPTION OF THE DRAWINGS

Fig. 1 is a block diagram illustrating an optical scanning spectroscopic apparatus according to one advantageous embodiment of the present invention.

Fig. 2 is a schematic representation of a portion of a data frame generated according to the optical scanning spectroscopic method and apparatus of one embodiment of the present invention that indicates the source of the laser signals that generated the respective scan line.

Fig. 3 is a data frame having a number of interlaced portions that was obtained by the optical scanning spectroscopic method and apparatus of one embodiment of the present invention.

Figs. 4A-4D are the monochromatic images formed by deinterlacing the interlaced portions of the data frame of Fig. 3 wherein each monochromatic image is generated in response to the illumination of the posterior portion of the eye by laser signals emitted by a different laser of the optical scanning spectroscopic apparatus of the present invention.

Fig. 5 is a flow chart illustrating the operations performed by the optical scanning spectroscopic method and apparatus according to one advantageous embodiment of the present invention.

DETAILED DESCRIPTION OF THE INVENTION

The present invention now will be described more fully hereinafter with reference to the accompanying drawings, in which preferred embodiments of the invention are shown. This invention may, however, be embodied in many different forms and should not be construed as limited to the embodiments set forth herein; rather, these embodiments are provided so that this disclosure will be thorough and

complete, and will fully convey the scope of the invention to those skilled in the art. Like numbers refer to like elements throughout.

Referring now to Fig. 1, an optical scanning spectroscopic apparatus **10** according to one embodiment of the present invention is depicted. The optical scanning spectroscopic apparatus includes a plurality of lasers **12** for emitting laser signals having different respective wavelengths. While the optical scanning spectroscopic apparatus can include any number of lasers, such as three lasers or five lasers, the optical scanning spectroscopic apparatus of one advantageous embodiment includes first, second, third and fourth lasers for emitting laser signals having first, second, third and fourth wavelengths, respectively.

According to the present invention, the plurality of lasers **12** can be selected so as to have any combination of wavelengths. Most commonly, however, the lasers are selected so as to emit laser signals having wavelengths that are appropriate for the particular application. For example, in order to monitor the blood oxygen saturation or blood oxygen content of the blood in retinal vessels, the optical scanning spectroscopic apparatus **10** preferably includes first, second, third and fourth lasers that emit laser signals having wavelengths of 488 nm, 635 nm, 670 nm and 830 nm, respectively. In order to measure other anatomic features or physiological parameters, however, the optical scanning spectroscopic apparatus can include a plurality of lasers that emit laser signals having different wavelengths, if so desired. The lasers **12** can also be physically embodied in different manners without departing from the spirit and scope of the present invention. Typically, however, the lasers are diode lasers.

As shown in Fig. 1, the optical scanning spectroscopic apparatus **10** also includes one or more beam combiners **14**, such as one or more dichroic beam combiners, for combining the laser signals emitted by the plurality of lasers to form a composite beam having each of the different respective wavelengths. The combined beam is then directed so as to illuminate the posterior portion **16a** of a subject's eye **16**. Depending upon the application, different areas of the posterior portion of the subject's eye can be illuminated. For example, an optical scanning spectroscopic apparatus designed to measure the blood oxygen content of the retinal vessels would illuminate the retina including the retinal vessels disposed along the rear surface of the eye. Alternatively, in order to monitor choroidal oxygenation, the composite

beam can be directed to illuminate the choroid including the choroidal vessels. While the composite beam can be directed in a number of different fashions, the optical scanning spectroscopic apparatus of the illustrated embodiment includes a lens **18** for focusing the composite beam upon the desired area of the posterior portion of the subject's eye and for compensating for _____.

The optical scanning spectroscopic apparatus **10** is designed to repeatedly scan the laser signals emitted by the plurality of lasers **12** across the posterior portion **16a** of the eye **16**. As such, the optical scanning spectroscopic apparatus also includes a scanner **20**. While the optical scanning spectroscopic apparatus can include a variety of scanners, the scanner of one advantageous embodiment is a two-axis scanner having a VSH-8kHz video scan head that is provided by General Scanning, Inc. In more detail, the two-axis scanner includes one galvanometer scanner and one resonant scanner. Preferably, the scanner raster scans the laser signals in a predetermined pattern across the posterior portion of the eye to thereby define a frame having a plurality of scan lines. For example, one conventional scanner scans the laser signals in a predetermined pattern consisting of 512 scan lines arranged in a generally square pattern within a relatively short time, such as 77 msec.

According to the present invention, the optical scanning spectroscopic apparatus **10** also preferably includes a detector **22**, such as a photodetector, for detecting signals returning from the posterior portion **16a** of the eye **16** in response to illumination by the laser signals. In this regard, the detector typically measures the intensity of the light reflected from the posterior portion of the eye, including the light scattered and reflected by the retinal and choroidal vessels. As a result of the scanning of the laser signals in a predetermined pattern of scan lines across the posterior portion of the eye, the return signals are also arranged in the predetermined pattern. In one advantageous embodiment, the detector, such as an avalanche photodiode, detects the return signals on a pixel by pixel basis. The detector then transfers the pixel to a means, such as a frame grabber card **24**, for constructing a data frame from the pixels provided by the detector. While a variety of frame grabber cards can be utilized, one conventional frame grabber card is _____.

The data frame constructed by the frame grabber card can be shaped and sized in different manners. However, the shape and size of the data frame typically corresponds to the shape and size of the predetermined pattern established by the

scanner 20. In this regard, the data frame constructed by the frame grabber card typically has the same number of lines as the number of scan lines. In one embodiment, for example, the data frame includes 512 lines, each of which is formed of 512 pixels, to thereby form a data frame that is sized to be 512 pixels x 512 pixels.

5 In order to insure that the framegrabber card constructs a data frame that corresponds to the predetermined pattern established by the scanner, the scanner typically provides control signals to the framegrabber card that consist of a vertical sync signal that indicates that a new frame is about to begin, a horizontal sync signal that indicates that a new line is about to begin and a pixel clock that indicates that a new pixel is
10 being generated.

As depicted in Fig. 1, the optical scanning spectroscopic apparatus 10 preferably includes a controller 26 for alternately activating different ones of the plurality of lasers 12 while the scanner 20 scans the laser signals across the posterior portion 16a of the eye 16. In one example in which the optical scanning
15 spectroscopic apparatus includes first, second, third and fourth lasers, the controller alternately activates the first, second, third and fourth lasers such that a different one of the lasers is activated while the laser signals are scanned along different scan lines of the same frame. For example, the controller can initially activate the first laser while the scanner scans the laser signals emitted by the first laser along a first scan
20 line across the posterior portion of the eye. The controller then deactivates the first laser and activates the second laser while the scanner scans the laser signals emitted by the second laser along the second scan line across the posterior portion of the eye. Thereafter, the controller deactivates the second laser and activates the third laser while the scanner scans the laser signals emitted by the third laser along a third scan
25 line across the posterior portion of the eye. Finally, the controller deactivates the third laser and activates the fourth laser while the scanner scans the laser signals emitted by the fourth laser along a fourth scan line across the posterior portion of the eye. Thereafter, the controller alternately activates the first, second, third and fourth lasers as the scanner scans the laser signals across the fifth, sixth, seventh and eighth scan
30 lines, respectively, across the posterior portion of the eye. See Fig. 2. The controller then repeats this alternate activation of the first, second, third and fourth lasers until each of the scan lines of the frame has been completed. Although the optical scanning

spectroscopic apparatus of the above example includes four lasers, the optical scanning spectroscopy apparatus can include more or fewer lasers, if so desired.

While the controller **26** of the foregoing example alternately activates a single laser **12** while the scanner **20** scans the laser signals emitted by the laser along a scan line across the posterior portion **16a** of the eye **16**, the controller can concurrently
5 activate two or more lasers while the scanner scans the laser signals emitted by the activated lasers along a scan line across the posterior portion of the eye. According to the present invention, however, the controller activates different ones or different combinations of the lasers while the scanner is scanning the laser signals across the
10 posterior portion of the eye during the generation of a single data frame. In addition, while the controller of the above example activates different lasers for each scan line, the controller can activate different lasers at other intervals during the generation of a single data frame, such as by activating a different laser to generate each pixel of a data frame. However, the controller of the optical scanning spectroscopic apparatus
15 **10** of the present invention need only activate a different laser or a different combination of lasers at some point while the scanner is scanning the laser signals in a predetermined pattern across the posterior portion of the eye such that different portions of the same data frame are based upon signals returning from the posterior portion of the eye in response to illumination by laser signals emitted by different
20 lasers.

Since different ones of the plurality of lasers **12** are alternately activated by the controller **26** while the scanner **20** scans the laser signals across the posterior portion **16a** of the eye **16**, the data frame constructed by the detector **22** based upon the signals returning from the posterior portion of the eye includes a plurality of
25 interlaced portions, adjacent ones of which are formed from return signals in response to illumination by laser signals emitted by different ones or different combinations of the lasers. As shown in Fig. 2, for example, the data frame constructed as a result of the alternate activation of the first, second, third and fourth lasers for each scan line is depicted. As shown, the first, fifth and ninth lines of the data frame are attributable to
30 return signals generated in response to illumination by the first laser. Likewise, the second, sixth and tenth lines of the data frame are attributable to return signals generated in response to the illumination by the second laser. Further, the third, seventh, and eleventh lines of the data frame are attributable to return signals

generated by the illumination by the third laser, while the fourth, eighth and twelfth lines of the data frame are attributable to return signals generated by the illumination by the fourth laser. As such, each line of the data frame of this embodiment is an interlaced portion. However, the interlaced portions can be larger, such as two or
5 more lines, or smaller, such as one or more pixels, depending upon the manner in which the controller alternately activates different ones of the plurality of lasers as described above.

As depicted in Fig. 1, the optical scanning spectroscopic apparatus **10** also generally includes means, such as a computer **28**, a processor or the like, for de-
10 interlacing the data frame to form a plurality of images. In this regard, each resulting image will have been generated in response to the illumination of the posterior portion **16a** of the eye **16** by laser signals emitted by different ones of the plurality of lasers **12**. In the above example in which the optical scanning spectroscopic apparatus includes first, second, third and fourth lasers that alternately illuminate the posterior
15 portion of the eye, the resulting data frame can be de-interlaced to form first, second, third and fourth images generated in response to the illumination of posterior portion of the eye by laser signals emitted by the first, second, third and fourth lasers, respectively. By way of example, a data frame having a number of interlaced portions is depicted in Fig. 3. In addition, the resulting images that are constructed upon de-
20 interlacing the data frame of Fig. 3 are depicted in Figs. 4A-4D which are attributable to the illumination of posterior portions of the eye by the first, second, third and fourth lasers, respectively. As such, in instances in which the controller alternately activates the plurality of lasers such that only a single laser is activated at any one time, such as described above in conjunction with the embodiment that includes first,
25 second, third and fourth lasers, the means for de-interlacing the data frame forms a plurality of monochromatic images, each being attributable to laser signals having a single wavelength.

By interlacing portions attributable to illumination by different ones of the lasers **12**, the speed and responsiveness of one optical scanning spectroscopic method
30 and apparatus **10** is equivalent to that of conventional scanning laser ophthalmoscopes that simultaneously illuminate the eye with signals generated by each of a plurality of lasers. As a result of dividing the data frame into a plurality of interlaced portions, however, the resolution of the image created upon de-interlacing the portions will be

less than the resolution of the images captured by conventional scanning laser ophthalmoscope. However, the resolution of the images created upon de-interlacing the portions of the data frame should still be sufficient for most, if not all, applications.

5 Although not necessary for the practice of the present invention, the optical scanning spectroscopic apparatus **10** can also include a target laser **30**, such as an infrared laser, for illuminating the posterior portions **16a** of the eye **16** with relatively low levels of infrared signals. By detecting the signals returning from the posterior portions of the eye in response to illumination by the target laser, the detector **22** in
10 conjunction with the frame grabber card **24**, can obtain a video image of the posterior portion of the eye. Among other things, this video image can be displayed upon a display for visual analysis by the system operator and/or provided to the computer for automated analysis. Upon detecting a desired feature or area, such as the retinal vessels and/or the choroidal vessels that appear as dark lines emanating from the optic
15 nerve, the relative positions of the subject and the optical scanning spectroscopic apparatus **10** are fixed. The controller **26** can then deactivate the target laser and activate one or more of the primary lasers **12** for illuminating the desired area of the posterior portion of the eye and for collecting data relating thereto. As such, the target laser provides a mechanism by which the desired area of the posterior portion
20 of the eye can be specifically located prior to collecting data.

 In addition, the optical scanning spectroscopic apparatus **10** can include various types of filters in order to appropriately condition the return signals presented to the detector **22**. In this regard, the optical scanning spectroscopic apparatus can include an orthogonal polarizer **32** positioned upstream of the detector. Since the
25 plurality of lasers **12** emit linearly polarized laser signals, the orthogonal polarizer will filter out or block the return signals that have the same linear polarization since most of these return signals have reflected from the outer surface of the retinal vessels and do not include information relating to the oxygenation of the blood or the like. As such, the polarized signals are preferably never presented to the detector and do not
30 skew or otherwise disadvantageously alter the data frame constructed by the detector and the frame grabber card **24**. However, the orthogonal polarizer will permit the orthogonally polarized return signals that are primarily attributable to the laser signals

that have been scattered and that include information relating to the blood oxygen saturation or the like.

5 The optical scanning spectroscopic apparatus **10** can include other types of filters **34**, such as a confocal filter or an anti-confocal filter, positioned upstream of the detector **22**. As known to those skilled in the art, a confocal filter and an anti-
confocal filter are designed to permit return signals that have been reflected and/or scattered from different depths within the posterior portion **16a** of the eye **16** to be presented to the detector. In this regard, a confocal filter generally defines a pin hole such that return signals that are reflected or scattered from the surface of the posterior
10 portion of the eye pass through the pin hole and are presented to the detector, while all other return signals that have been scattered from deeper regions are filtered out. Conversely, an anti-confocal filter, such as a glass plate having a silver dot thereupon, filters out the return signals attributable to the laser signals that are reflected or scattered by the surface of the posterior portion of the eye and, instead, permits the
15 return signals that have been reflected or scattered from regions below or behind the surface of the posterior portion of the eye to be detected.

The optical scanning spectroscopic method and apparatus **10** of the present invention can be activated during any portion of the cardiac cycle of a subject. In some applications, however, the optical scanning spectroscopic method and apparatus
20 is preferably controlled so as to monitor the posterior portion **16a** of the eye **16** and obtain data relating thereto during one or more predetermined portions of the cardiac cycle of the subject. As such, the optical scanning spectroscopic apparatus of this embodiment can also include a triggering mechanism **35** for providing a trigger signal indicative of a predetermined point in a cardiac cycle of the subject. While various
25 types of triggering mechanisms can be employed, the triggering mechanism of one advantageous embodiment provides a trigger signal in response to an r-wave of an electrocardiogram (EKG) of the subject. As known to those skilled in the art, the r-wave indicates _____. As such, the triggering mechanism can be an EKG machine that generates an EKG and provides a number of outputs, including the r-
30 wave.

Upon receiving the trigger signal, the controller **26** can immediately activate one or more of the lasers **12** in order to illuminate the subject's eye **16** and to begin collecting data. Alternatively, the controller can be adapted to activate one or more of

the lasers at some predetermined time following the receipt of the trigger signal. In this regard, the optical scanning spectroscopic apparatus **10** can also include a timer **36** that is responsive to the triggering mechanism **34**. While the timer can be a separate component, the timer can also form a portion of the controller, if so desired.

5 Upon receipt of the trigger signal, the timer is activated. Once the timer has determined that a predetermined time has elapsed since receipt of the trigger signal, the timer will issue a signal notifying the controller. The controller can then activate the lasers in order to illuminate the subject's eye to begin collecting data.

In most instances, the plurality of lasers **12** are scanned across the posterior portion **16a** of the eye **16** as described above. In this regard, the scanner **20**, such as the two-axis scanner provided by General Scanning, Inc., periodically issues vertical sync signals indicative of the commencement of another frame and horizontal sync signals indicative of the commencement of another line. As such, upon receipt of a signal from the timer **36** representing that a predetermined time has elapsed since the receipt of the trigger signal, the controller **26** awaits receipt of the next vertical sync signal from the scanner. Upon receipt of the next vertical sync signal, the controller then monitors the horizontal sync signal issued by the scanner. Upon receipt of the first horizontal sync signal following the vertical sync signal, the controller activates at least one of the lasers in order to illuminate the posterior portion of the eye. The controller also issues a signal to the timer that stops the timer such that the value of the timer is representative of the actual delay time from receipt of the trigger signal to activation of the lasers. The controller can then alternately activate each of the lasers as each subsequent line is scanned, as described above.

10
15
20

According to this embodiment of the present invention, the optical scanning spectroscopic apparatus **10** can obtain images of the posterior portion **16a** of the eye **16** during predetermined portions of the cardiac cycle of the subject. As such, more detailed or specific information relating to the performance of the subject during predetermined phases of the cardiac cycle can be obtained for diagnostic and/or analytical purposes.

25

While the method of operation has been described heretofore in conjunction with the various components of the optical scanning spectroscopic apparatus **10**, the method of one advantageous embodiment is described hereinbelow for purposes of clarity and with reference to Fig. 5. As will be apparent, the subsequently described

30

method includes an embodiment of the optical scanning spectroscopic apparatus that includes a target laser **30** and a triggering mechanism **35**. However, the optical scanning spectroscopic apparatus need not include a target laser or a triggering mechanism.

5 By way of illustration, the method of one advantageous embodiment initially illuminates the posterior portion **16a** of a subject's eye **16** with a target laser **30**, such as an infrared laser, to obtain a real-time image of the posterior portion of the eye. See block **40**. The operator then repositions the optical scanning spectroscopic apparatus **10** and/or the subject until the desired area of the posterior portion of the
10 eye is in view. See block **42**. In this embodiment in which a predetermined portion of the cardiac cycle of the subject is to be analyzed, the operator also sets the timer **36** to a predetermined delay time indicative of the delay to be inserted after receipt of the trigger signal prior to illuminating the posterior portion of the eye with the primary lasers **12** and obtaining data. See block **44**. Once the desired area of the posterior
15 portion of the eye is identified, the operator deactivates the targeting laser and presses a key or otherwise indicates that the posterior portion of the eye should be scanned following receipt of the next trigger signal. See block **46**. Upon receipt of a trigger signal, such as in response to the next r-wave of the subject's EKG, the controller **26** activates the timer to provide the predetermined delay time. See blocks **48** and **50**.
20 Once the timer indicates that the predetermined delay time has elapsed, the controller monitors the scanner **20** to identify the next vertical sync signal indicative of the commencement of the next frame. See blocks **52** and **54**. Upon receipt of a vertical sync signal, the controller continues to monitor the scanner to identify the next horizontal sync signal indicative of the commencement of the first line of the new
25 frame. See block **56**. Upon receiving the next horizontal sync signal, the controller stops the timer such that the value of the timer is the actual delay time. See block **58**.

 The controller **26** then activates a first one of the lasers **12** that is scanned across the first line of the new frame. Upon completion of the first line, the first laser is deactivated and a second laser is activated so as to be scanned across the second
30 line of the new frame. Thereafter, the second laser is deactivated and a third laser is scanned across the third line of the new frame. Finally, the third laser is deactivated and a fourth laser is scanned across the fourth line of the new frame. The controller then repeats this process of alternately activating the first, second, third and fourth

lasers until the scanner **20** has scanned all of the lines of the frame. See block **60**. During the scanning process, the detector **22** also detects signals returning from the posterior portion **16a** of the eye **16** and communicates the detected return signals to the frame grabber card **24**, to form a data frame having a number of interlaced portions or lines that are representative of return signals that were generated in response to illumination by the first, second, third and fourth lasers. See blocks **62** and **64**. Once the entire frame has been completed, the lasers are all deactivated and the target laser **30** can again be activated to obtain real time video. See block **66**. Thereafter, the data frame can be stored, viewed and/or otherwise analyzed. For example, the interlaced portions or lines can be de-interlaced such that separate images are formed for those return signals generated in response to illumination by the first, second, third and fourth lasers. See block **68**.

In addition, by recording the actual delay time, the predetermined portion of the cardiac cycle of the subject can be identified in order to assist in the diagnostic and/or analysis process. Since the frames are generally acquired at regular intervals as defined by the operation of the scanner **20**, such as about 15 frames per second, the actual delay time will typically be somewhat larger than the predetermined delay time set by the operator since the controller **26** must await commencement of the next frame following expiration of the preset delay time prior to activating the lasers **12** and beginning to gather additional data. By identifying the actual delay time, however, the optical scanning spectroscopic method and apparatus **10** of this embodiment of the present invention can still precisely identify the portion of the cardiac cycle of the subject that is occurring while the data is being collected.

The optical scanning spectroscopic method and apparatus **10** of the present invention therefore illuminates the posterior portion **16a** of an eye **16** with the laser signals emitted by a plurality of lasers **12** having different respective wavelengths. However, by alternately illuminating the posterior portion of the eye with different ones of the plurality of lasers, the eye is not simultaneously subjected to illumination from each of the lasers, thereby protecting the eye from exposure to excessive illumination. As such, the intensity of the laser signals emitted by the lasers need not be reduced in order to protect the eye. Instead, the lasers can be operated at greater intensity levels than the lasers of conventional scanning laser ophthalmoscopes that simultaneously illuminate the eye with the laser signals emitted by a plurality of

lasers. As such, the signal-to-noise ratio of the signals returning from the posterior portion of the eye and detected according to the present invention is greater than the signal-to-noise ratio of the return signals detected by conventional scanning laser ophthalmoscopes as a result of the increased intensity of the laser signals emitted by the lasers. Thus, fewer signals returning from the posterior portion of the eye will be lost in the noise and the validity of the detected signals will be more reliable. By alternately illuminating the posterior portion of the eye with laser signals emitted by different ones of the lasers, the resulting data frame includes interlaced portions formed from signals returning from the posterior portion of the eye in response to illumination by laser signals emitted by different ones of plurality of lasers. The optical scanning spectroscopic method and apparatus of the present invention is therefore capable of alternately scanning the posterior portion of the eye with the laser signals emitted by different lasers in a rapid fashion such that the measurement conditions, such as the position of the subject and the constriction of the subject's pupil, do not change appreciably between the times at which the subject's eye is illuminated by different lasers. As such, the resulting images generated in response to illumination of the posterior portion of the eye by laser signals emitted by different ones of the lasers should be more consistent and more easily correlated than sequential data frames generated by illumination of the subject's eye with the different lasers.

Many modifications and other embodiments of the invention will come to mind to one skilled in the art to which this invention pertains having the benefit of the teachings presented in the foregoing descriptions and the associated drawings. Therefore, it is to be understood that the invention is not to be limited to the specific embodiments disclosed and that modifications and other embodiments are intended to be included within the scope of the appended claims. Although specific terms are employed herein, they are used in a generic and descriptive sense only and not for purposes of limitation.

THAT WHICH IS CLAIMED:

1. An optical scanning spectroscopic apparatus comprising:
 - a plurality of lasers for emitting laser signals having different respective wavelengths;
 - a scanner for repeatedly scanning the laser signals emitted by said plurality of
 - 5 lasers across a posterior portion of an eye;
 - a detector for detecting signals returning from the posterior portion of the eye in response to illumination by the laser signals to thereby form a data frame comprising a plurality of interlaced portions; and
 - a controller for alternately activating different ones of said plurality of lasers
 - 10 while said scanner scans the laser signals across the posterior portion of the eye such that adjacent interlaced portions of the data frame are formed from signals returning from the posterior portion of the eye in response to illumination by laser signals emitted by different ones of said plurality of lasers.
2. An optical scanning spectroscopic apparatus according to Claim 1
- 15 further comprising means for deinterlacing the data frame to form a plurality of images, wherein each image is generated in response to illumination of the posterior portion of the eye by laser signals emitted by different ones of said plurality of lasers.
3. An optical scanning spectroscopic apparatus according to Claim 2
- 20 wherein said controller alternately activates said plurality of lasers such that a single laser is activated at any one time, and wherein said means for deinterlacing the data frame forms a plurality of monochromatic images.
4. An optical scanning spectroscopic apparatus according to Claim 1
- 25 further comprising a triggering mechanism for providing a trigger signal indicative of a predetermined point in a cardiac cycle of a subject, wherein said controller activates at least one of said plurality of lasers in response to the trigger signal such that the posterior portion of the subject's eye is illuminated during at least a predetermined portion of the cardiac cycle of the subject.

5. An optical scanning spectroscopic apparatus according to Claim 4 wherein said triggering mechanism provides a trigger signal in response to an r-wave of an electrocardiogram (EKG) of the subject.

6. An optical scanning spectroscopic apparatus according to Claim 4 further comprising a timer, responsive to said triggering mechanism, for delaying activation of at least one of said plurality of lasers by at least a predetermined time following receipt of the trigger signal.

7. An optical scanning spectroscopic apparatus according to Claim 1 further comprising a target laser for illuminating the posterior portion of the eye in order to generate a corresponding image, wherein said controller deactivates said target laser and activates said plurality of lasers once said target laser illuminates a predetermined area of the posterior portion of the eye.

8. An optical scanning spectroscopic apparatus according to Claim 1 wherein said plurality of lasers emit linearly polarized laser signals, and wherein the optical scanning spectroscopic apparatus further comprises an orthogonal polarizer positioned upstream of said detector for only passing to said detector those signals returning from the posterior portion of the eye that are orthogonally polarized.

9. An optical scanning spectroscopic apparatus according to Claim 1 further comprising at least one of a confocal filter and an anti-confocal filter positioned upstream of said detector.

10. An optical scanning spectroscopic apparatus comprising:
first, second, third and fourth lasers for emitting laser signals having first, second, third and fourth wavelengths, respectively;
a scanner for repeatedly scanning the laser signals emitted by said first, second, third and fourth lasers in a predetermined pattern across a posterior portion of an eye to thereby define a frame comprising a plurality of scan lines; and
a controller for alternately activating said first, second, third and fourth lasers while said scanner scans the laser signals across the posterior portion of the eye, said

controller alternately activating said first, second, third and fourth lasers such that a different laser is activated while the laser signals are scanned along different scan lines of the same frame.

11. An optical scanning spectroscopic apparatus according to Claim 10
5 further comprising a detector for detecting signals returning from the posterior portion of the eye in response to illumination by the laser signals to thereby form a data frame comprising a plurality of interlaced portions.

12. An optical scanning spectroscopic apparatus according to Claim 11
10 further comprising means for deinterlacing the data frame to form a plurality of monochromatic images, wherein each monochromatic image is generated in response to illumination of the posterior portion of the eye by laser signals emitted by a different laser.

13. An optical scanning spectroscopic apparatus according to Claim 10
15 further comprising a triggering mechanism for providing a trigger signal indicative of a predetermined point in a cardiac cycle of a subject, wherein said controller activates at least one of said first, second, third and fourth lasers in response to the trigger signal such that the posterior portion of the subject's eye is illuminated during at least a predetermined portion of the cardiac cycle of the subject.

14. An optical scanning spectroscopic apparatus according to Claim 13
20 wherein said triggering mechanism provides a trigger signal in response to an r-wave of an electrocardiogram (EKG) of the subject.

15. An optical scanning spectroscopic apparatus according to Claim 13
further comprising a timer, responsive to said triggering mechanism, for delaying activation of at least one of said first, second, third and fourth lasers by at least a
25 predetermined time following receipt of the trigger signal.

16. An optical scanning spectroscopic apparatus according to Claim 10
further comprising a target laser for illuminating the posterior portion of the eye in

order to generate a corresponding image, wherein said controller deactivates said target laser and activates at least one of said first, second, third and fourth lasers once said target laser illuminates a predetermined area of the posterior portion of the eye.

5 17. A method for optically scanning a posterior portion of an eye, the method comprising:

 alternately scanning laser signals having different wavelengths across the posterior portion of the eye;

 detecting signals returning from the posterior portion of the eye in response to illumination by the laser signals; and

10 forming a data frame comprising a plurality of interlaced portions,

 wherein laser signals having different wavelengths are alternately scanned across the posterior portion of the eye such that adjacent interlaced portions of the data frame are formed from signals returning from the posterior portion of the eye in response to illumination by laser signals having different wavelengths.

15 18. A method according to Claim 17 further comprising deinterlacing the data frame to form a plurality of images, wherein each image is generated in response to illumination of the posterior portion of the eye by laser signals having different wavelengths.

20 19. A method according to Claim 17 further comprising providing a trigger signal indicative of a predetermined point in a cardiac cycle of a subject, wherein scanning the laser signals is initiated in response to the trigger signal such that the posterior portion of the subject's eye is illuminated during at least a predetermined portion of the cardiac cycle of the subject.

25 20. A method according to Claim 19 wherein receiving the trigger signal comprises receiving the trigger signal in response to an r-wave of an electrocardiogram (EKG) of the subject.

21. A method according to Claim 19 further comprising delaying illumination of the posterior portion of the eye by at least a predetermined time following receipt of the trigger signal.

22. A method according to Claim 17 further comprising:

5 illuminating the posterior portion of the eye with laser signals emitted by a target laser in order to generate a corresponding image;

identifying a predetermined area of the posterior portion of the eye within the corresponding image; and

10 deactivating the target laser and commencing the alternate scanning of laser signals having different wavelengths across the posterior portion of the eye following identification of the predetermined area of the posterior portion of the eye.

OPTICAL SCANNING SPECTROSCOPIC APPARATUS AND ASSOCIATED METHOD

ABSTRACT OF THE DISCLOSURE

An improved optical scanning spectroscopic method and apparatus is provided that alternately scans the posterior portion of an eye with laser signals emitted by different ones of a plurality of lasers such that a data frame can be
5 constructed that includes interlaced portions formed from signals returning from the posterior portion of the eye in response to illumination by laser signals emitted by different ones of the plurality of lasers. As such, the same data frame includes data attributable to the reflection of laser signals from each of the plurality of lasers even though the subject's eye is not subjected to simultaneous illumination by each of the
10 lasers, thereby protecting the subject's eye. According to one further aspect of the invention, the optical scanning spectroscopic method and apparatus can illuminate the posterior portion of the subject's eye in response to a trigger at a predetermined point in the cardiac cycle of the subject such that the resulting data frame relates to at least a predetermined portion of the cardiac cycle of the subject, thereby permitting a
15 detailed analysis of one or more phases of the cardiac cycle of the subject.

CLT01/4384016v2

5-21-99 Via U
Campus Mail

LAW OFFICES
**GIFFORD, KRASS, GROH, SPRINKLE,
ANDERSON & CITKOWSKI, P.C.**
PATENT, TRADEMARK AND COPYRIGHT PRACTICE
280 N. OLD WOODWARD AVENUE, SUITE 400
BIRMINGHAM, MICHIGAN 48009-5394

ERNEST I. GIFFORD
ALLEN M. KRASS
IRVIN L. GROH (1,2)
DOUGLAS W. SPRINKLE
THOMAS E. ANDERSON (3)
RONALD W. CITKOWSKI
JUDITH M. RILEY
JULIE A. GREENBERG
DOUGLAS J. MCEVOY
ELLEN S. COGEN (3)
JOHN G. POSA
DAVID R. KURLANDSKY
DOUGLAS L. WATHEN
AVERY N. GOLDSTEIN, PH.D.
MARK D. SCHNEIDER

OF COUNSEL
ROBERTA J. MORRIS, PH.D. (4)
CHARLES F. SCHROEDER (5)

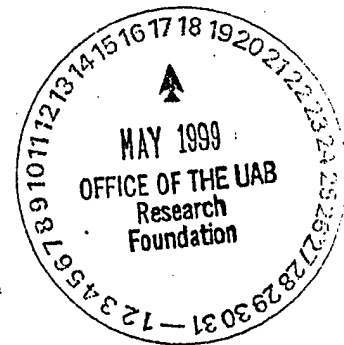
(248) 647-6000
FACSIMILE (248) 647-5210
info@patlaw.com

May 11, 1999
Our File: UAB-15318/22

ALFRED L. PATMORE, JR.
(1929-1997)
ANN ARBOR OFFICE
101 NORTH MAIN, SUITE 885
ANN ARBOR, MICHIGAN 48104-1476
(734) 913-9300
FACSIMILE (734) 913-6007
FLORIDA OFFICE
101 WEST VENICE AVE., SUITE 28
VENICE, FLORIDA 34285
(941) 488-4245
FACSIMILE (941) 484-5258
ALSO ADMITTED IN:
(1) WISCONSIN
(2) OHIO
(3) FLORIDA
(4) NEW YORK
ONLY ADMITTED IN:
(5) OHIO & ILLINOIS

Mr. David L. Day
The UAB Research Foundation
The University of Alabama at Birmingham
1120 G Administration Building
701 20th Street South
Birmingham, AL 35294-0111

RE: U.S. Provisional Application No. 60/132,023
"A Method of Determining Autoregulatory Status
and Method for Using Same to Determine Perfusion
Status in Systemic and Ocular Disease States"
Inventor: Kurt R. Denninghoff



Dear David:

The U.S. Patent and Trademark Office has acknowledged receipt of the subject provisional patent application. The application has been assigned Serial No. 60/132,023 with a filing date of April 30, 1999. Also enclosed is an Assignment for signature by Dr. Denninghoff. Upon receipt of the executed Assignment, we will file same with the U.S. Patent and Trademark Office.

It is important to remember that the provisional application serves only to establish a filing date for the invention described in the application. Provisional applications are not examined by the U.S. Patent & Trademark Office and are automatically abandoned one year after filing. To maintain the priority date obtained by this filing, a formal patent application must be filed by April 30, 2000.

In the meantime, your invention has a patent pending status and if you produce products covered by this invention they should be marked "Patent Pending."

If you have any questions regarding this matter, please contact me at your convenience.

Very truly yours,

Ellen S. Cogen
Ellen S. Cogen

ESC/st: enclosures
cc: Kurt R. Denninghoff (w/application only)

**A METHOD OF DETERMINING AUTOREGULATORY STATUS
AND METHOD FOR USING SAME TO DETERMINE PERFUSION
STATUS IN SYSTEMIC AND OCULAR DISEASE STATES**

Technical Field

5 The present invention relates to a method of determining the autoregulatory status of a subject. More specifically, the present invention relates to a method for measuring the autoregulatory status of a subject by noninvasively monitoring blood vessel changes in the retina.

Background of the Invention

10 Local autoregulation is the physiologic phenomenon where the vascular bed attempts to match supply of substrate (primarily oxygen and glucose) and the removal of metabolic waste (primarily carbon dioxide and lactic acid) to the metabolic demand of the tissues by changing the resistance to flow therethrough. Resistance to flow is controlled by changes in blood vessel wall tension which
15 changes the diameter of the blood vessels. When supply is generous, the blood vessels constrict decreasing flow. Conversely, when supply is limited, the blood vessels dilate increasing flow. Some of the substances which are known to change the autoregulatory state of tissues include oxygen, glucose, carbon dioxide and lactic acid.

20 Blood supply to the tissues is regulated by chemical signals transported throughout the body by the blood, by local metabolic demand, and by the autonomic nervous system which has nerve endings traveling with the blood vessels. Circulating substances generally regulate the balance of flow to the major

organ systems of the body. An example of this is when a subject is bleeding and circulating catecholamines are released which shunt blood flow from the peripheral tissues to the central organs such as the brain and heart.

5 The retina is an embryologic extension of the brain and, as such, it is a centrally perfused organ and would not be expected to restrict flow in response to circulating substances released to maintain flow to the central circulation. The autonomic nerve endings which travel with the blood vessels in the body stop at the lamina cribosa prior to entering the retina. This allows the retinal circulation to respond to circulating chemical regulators and to local metabolic demand
10 without interference from the autonomic nervous system. Accordingly, this characteristic makes the retina an ideal location for studying and assessing autoregulatory states by analyzing changes in the retinal blood vessel diameter and/or oxyhemoglobin saturation.

The analysis of retinal blood vessels to diagnose autoregulatory
15 function/dysfunction can be useful in diagnosing and treating various diseases which have an autoregulatory dysfunction as a component of the disease. Examples of such diseases include diabetes, hypertension and glaucoma.

Glaucoma accounts for between 9% and 12% of all cases of blindness in the United States. Between two and three million people aged forty and older have
20 glaucoma, and between 89,000 and 120,000 are blind from it. Glaucoma was originally believed to be a problem of elevated intraocular pressure (IOP) causing damage to the optic nerve. It is now clear that glaucoma clinically is a

heterogenous collection of disorders with a similar clinical course and presentation. There are many treatment modalities for glaucoma, yet all are designed to do only one thing -- lower IOP. Without treatment there is a relentless course of progressive visual loss. Unfortunately, many people have continued progression
5 even when treatment is believed to have stabilized IOP in the normal range. This finding coupled with the fact that approximately one-third of glaucoma patients have normal IOP or Normal Tension Glaucoma (NTG) has led to exploration of other etiologies, such as vascular causes. A vascular role was initially suggested because of the association of glaucoma with systemic vascular diseases such as
10 hypertension, migraine, diabetes and peripheral vascular disease. In addition, the presence of disk hemorrhages and retinal vein occlusions early in the glaucomatous disease process supports the vascular theory.

Although research on the vascular theories of glaucoma have focused on autoregulation, many of the parameters related to the blood vessel size, shape and
15 blood flow hemodynamics have been difficult to quantify. Color Doppler Imaging (CDI) has been used to measure the peak blood flow velocity in the ocular blood vessels. These studies have demonstrated that blood velocity is decreased in the ophthalmic artery, posterior ciliary artery and central retinal artery of glaucoma patients.

20 Quantification of the vascular aspects of glaucoma has been difficult due to our limited knowledge of blood flow hemodynamics and autoregulatory mechanisms in the eye. Because there is no autonomic innervation of the retinal

circulation distal to the lamina cribosa, autoregulatory mechanisms in the retina are controlled locally. Several studies have concluded that autoregulation in normal patients is similar to the autoregulation in ocular hypertensive patients, but autoregulation in glaucoma patients is insufficient.

Accordingly, it would be both advantageous and desirable to have a rapid, noninvasive method for measuring the retinal autoregulatory status of a subject in order to obtain information regarding the subject's condition which will be useful in the diagnosis and treatment of conditions having an autoregulatory component including glaucoma.

10 Brief Description of the Drawings

The following detailed description is best understood with reference to the following drawings in which:

Figure 1 is a graph illustrating changes in the autoregulatory state of the retinal during bleeding and resuscitation.

15 Detailed Description of the Invention

The present invention provides a method of determining or monitoring the autoregulatory status of a subject, including humans and animals, by obtaining a measurement of a selected parameter of retinal blood vessels in a non-stimulated subject. As defined herein, "non-stimulated" refers to a subject in a normal or static condition who has not received any particular stimulus or substrate and/or inducing treatment. The subject can then be administered a preselected stimulus or substrate such as oxygen, glucose, carbon dioxide, lactic acid, or other

circulating substances such as epinephrine. After the administration of the preselected stimulus or substrate, a measurement of the selected parameter of the retinal blood vessels of the subject is taken in order to determine the response of the subject to the administration of the selected stimulus or substrate. The changes
5 in the autoregulatory state of the vascular bed can be determined by comparing the ratio of the measurement for the selected parameter in the retinal blood vessels of the non-stimulated subject to the measurement of the selected parameter for the retinal blood vessels following the administration of the selected stimulus or substrate in order to identify imbalances between the supply and consumption of
10 the stimulus or substrate.

Normal autoregulatory function is defined herein as a balance between the stimulus or substrate supply and its consumption as determined by measurement techniques including retinal analysis.

The preselected parameters can include measuring the oxygen saturation
15 of the retinal blood vessels, measuring the diameter of the retinal blood vessels, a combination of both and/or other parameters. Measurement of the selected parameters can be accomplished by utilizing a laser eye oximeter (EOX) which is directly aimed into the eye, much like an ophthalmoscope, and which will take readings (pictures) of the retina. The EOX is preferably an r-wave triggered laser
20 scanning device which measures the blood vessel diameters near the optic disk of the retina and can accurately measure the oxygen saturation in the retinal artery and vein by measuring the saturations in the artery/vein pair near the optic disk.

Suitable EOX devices include those disclosed in United States Patent Nos. 5,119,814 and 5,308,919 to Minnich.

The measurements of the selected parameters can be used to calculate a ratio which is indicative of the balance or imbalance of the autoregulatory function
5 of the subject or individual.

Changes in the autoregulatory state of a vascular bed can be monitored by monitoring the changes in the vessel diameter and the balance between substrate supply and consumption. The autoregulatory status can be calculated based on the data obtained from the retinal blood vessels.

10 *Vessel Diameter Changes*

Measuring the vessel diameter (D) changes when a subject is breathing oxygen (D_{O_2}) and when they are on room air (D_a) yields a ratio which is related to the autoregulatory responsiveness of those tissues. This expressed by the equation:

$$AS \propto D_a / D_{O_2}$$

15 *The Ratio of Oxygen Consumption to Delivery*

Effective autoregulation of blood supply balances the supply of oxygen with tissue oxygen demand. Thus, when oxygen delivery changes, vascular tone also changes maintaining the oxygen supply to the tissue.

The autoregulatory state can be quantified by measuring the change in
20 substrate (oxygen) delivery to the tissue and substrate (oxygen) consumption. Oxygen consumption is equal to the blood flow volume (V) times the arteriovenous

oxygen difference. The oxygen content of arterial blood (C_aO_2) is defined by the equation:

$$C_aO_2 = [Hb](1.34)(S_aO_2/100) + (P_aO_2)(0.003)$$

wherein $[Hb]$ is the hemoglobin concentration in grams per deciliter of blood, S_aO_2 is the percent oxygen saturation of hemoglobin in the arterial blood, and P_aO_2 is the partial pressure of oxygen in the arterial plasma. Thus the arteriovenous oxygen difference ($\Delta_{av}O_2$) is defined by the equation:

$$\Delta_{av}O_2 = [Hb](1.34)((S_aO_2 - S_vO_2)/100) + (P_aO_2 - P_vO_2)(0.003)$$

wherein S_vO_2 is the percent oxygen saturation of hemoglobin in the venous blood and P_vO_2 is the partial pressure of oxygen in the venous plasma. Oxygen consumption and oxygen delivery can be estimated by assuming that the plasma contribution to oxygen delivery is negligible under isobaric conditions. The equation is:

$$\begin{aligned} \text{Oxygen consumption} &\approx V(\Delta_{av}O_2) \approx V([Hb](1.34)(S_aO_2 - S_vO_2)/100) \\ \text{Oxygen delivery} &\approx V(C_aO_2) \approx V([Hb](1.34)(S_aO_2/100)) \end{aligned}$$

The ratio of oxygen consumption to oxygen delivery is a measure of the autoregulatory state (AS) of the tissue and can be estimated using the equation:

$$AS \approx V([Hb](1.34)((S_aO_2 - S_vO_2)/100))/V([Hb](1.34)(S_aO_2/100))$$

Dividing out common terms gives the equation:

$$AS \approx (S_aO_2 - S_vO_2)/S_aO_2$$

A typical test to determine the autoregulatory status of an individual can include, for example, taking a measurement of the oxygen saturation of the retinal blood vessels with the EOX while the subject is breathing room air. The subject

will then be scanned utilizing the EOX device while breathing supplemental oxygen (e.g., 15 liters/ minute via non-rebreather mask). The measurements obtained by the EOX scan are analyzed to generate a ratio of the non-stimulated to stimulated oxygen saturation levels to determine whether a balance or imbalance exists and, thus, when an autoregulatory imbalance exists.

This method can be adapted for the diagnosis and/or monitoring of subjects with glaucoma using the EOX to measure retinal arterial and venous oxygen saturation during normoxia (un-stimulated) and hyperoxia (stimulated) conditions. An imbalance in the levels of stimulus/substrate delivery and consumption are utilized to ascertain autoregulatory function and/or dysfunction. In addition to glaucoma diagnosis and monitoring, the present method can also be utilized to diagnose and/or monitor other diseases with a component of autoregulatory dysfunction including diabetes and hypertension.

Measurements of retinal vessel parameters can also be used to monitor a patient or subject for blood loss during resuscitation from blood loss, during transfusions, during surgery or during the treatment of anemia or traumatic injury.

The ratio of retinal venous oxygen saturation to retinal venous diameter can be utilized for this purpose.

Because the present methods provide for quick, non-invasive, and accurate measurements of the autoregulatory status of a subject, they provide a new and valuable clinical tool for the diagnosis, treatment, and/or monitoring of diseases or conditions associated with autoregulatory dysfunction.

The EOX has been used to monitor the changes in retinal venous oxygen saturation and retinal venous diameter during the removal of forty percent of the blood and the subsequent reinfusion of blood in six swine. The results of this study are shown in Figure 1 and demonstrate that the retinal venous oxygen saturation
5 decreased during blood removal and returned to near normal levels rapidly after reinfusion of blood was initiated and that the retinal vessel diameter increased during blood removal and generally decreased during reinfusion of blood. The retinal venous oxygen saturation divided by the retinal venous diameter demonstrated the highest correlation with blood volume ($r = 0.9$), emphasizing the
10 importance of the autoregulatory state as defined herein.

In view of the teaching presented herein, other modifications and variations of the present invention will readily be apparent to those of skill in the art. The discussion and description are illustrative of some embodiments of the present invention, but are not meant to be limitations on the practice thereof. It is the
15 following claims, including all equivalents, which define the scope of the invention.

Any patents or publications mentioned in the specification are indicative of the levels of those skilled in the art to which the invention pertains. These patents and publications are herein incorporated by reference to the same extent as if each individual publication was specifically and individually indicated to be incorporated
20 by reference.

Claims

1 1. A method of determining the autoregulatory status of a subject, said
2 method comprising the steps of:
3 obtaining a measurement of a selected parameter of the retinal blood
4 vessels in a non-stimulated subject;
5 administering to the subject a preselected stimulus;
6 obtaining a measurement of the selected parameter of the retinal blood
7 vessels of the subject in response to the administration of the selected stimulus; and
8 determining the ratio of the measurement for the selected parameter in the
9 non-stimulated retinal blood vessels to the measurement of the selected parameter
10 for the retinal blood vessels following the administration of the selected stimulus
11 whereby the ratio provides an indicator of the autoregulatory function or status of
12 the subject.

1 2. A method according to claim 1, wherein said obtaining steps further
2 comprise measuring the selected parameter with a laser scanning device.

1 3. A method according to claim 1, wherein the selected parameter
2 comprises oxygen saturation of the retinal blood vessels.

1 4. A method according to claim 1, wherein the selected parameter
2 comprises retinal blood vessel diameter.

1 5. A method according to claim 1, wherein the preselected parameter
2 includes both oxygen saturation and blood vessel diameter in retinal blood vessels.

1 6. A method according to claim 1, wherein the preselected stimulus
2 is 100% oxygen.

1 7. A method according to claim 1, wherein the preselected stimulus
2 is selected from the group consisting of glucose, lactic acid, and carbon dioxide.

1 8. A method according to claim 1, wherein said determining step
2 further comprises calculating the autoregulatory state using the equation:

3
$$\text{autoregulatory state} \approx (S_aO_2 - S_vO_2)/S_aO_2,$$

4 wherein S_aO_2 is the percent oxygen saturation of hemoglobin in arterial blood and
5 S_vO_2 is the percent oxygen saturation in venous blood.

1 9. A method of diagnosing and monitoring glaucoma in a subject by
2 assessing autoregulatory function, said method comprising the steps of:

3 measuring the venous oxygen saturation level of retinal blood vessels of a
4 subject under normoxic conditions;

5 measuring the venous oxygen saturation level of the retinal blood vessels
6 of the subject under hyperoxic conditions; and

7 determining the ratio of the normoxic venous oxygen saturation level to the
8 hyperoxic venous oxygen saturation level, whereby the ratio provides an indicator
9 of the autoregulatory function or status of the subject which can be used to
10 diagnose and/or monitor the subject for glaucoma.

1 10. A method according to claim 9 further including the step of
2 administering oxygen to the subject to induce the hyperoxic condition.

1 11. A method according to claim 9, wherein said determining step
2 further comprises calculating the autoregulatory state using the equation:

3 autoregulatory state $\approx (S_aO_2 - S_vO_2)/S_aO_2$,

4 wherein S_aO_2 is the percent oxygen saturation of hemoglobin in arterial blood and
5 S_vO_2 is the percent oxygen saturation in venous blood.

1 12. A method of monitoring blood loss in a subject, said method
2 comprising the steps of:

3 measuring of retinal venous oxygen saturation;

4 measuring retinal venous diameter; and

5 calculating the ratio of the measurement of retinal venous oxygen saturation
6 to retinal venous diameter whereby the ratio provides an indicator of the amount
7 of blood loss in the subject.

Abstract

A method of determining the autoregulatory status of a subject by obtaining a measurement of a selected parameter of the retinal blood vessels in a non-stimulated subject, administering to the subject a preselected stimulus, obtaining
5 a measurement of the selected parameter of the retinal blood vessels of the subject in response to the administration of the selected stimulus, and determining the ratio of the measurement for the selected parameter in the non-stimulated retinal blood vessels to the measurement of the selected parameter for the retinal blood vessels following the administration of its selected stimulus whereby the ratio provides an
10 indicator of the autoregulatory function or status of the subject.

Changes in the Autoregulatory State of the Retinal Circulation During Bleeding and Resuscitation

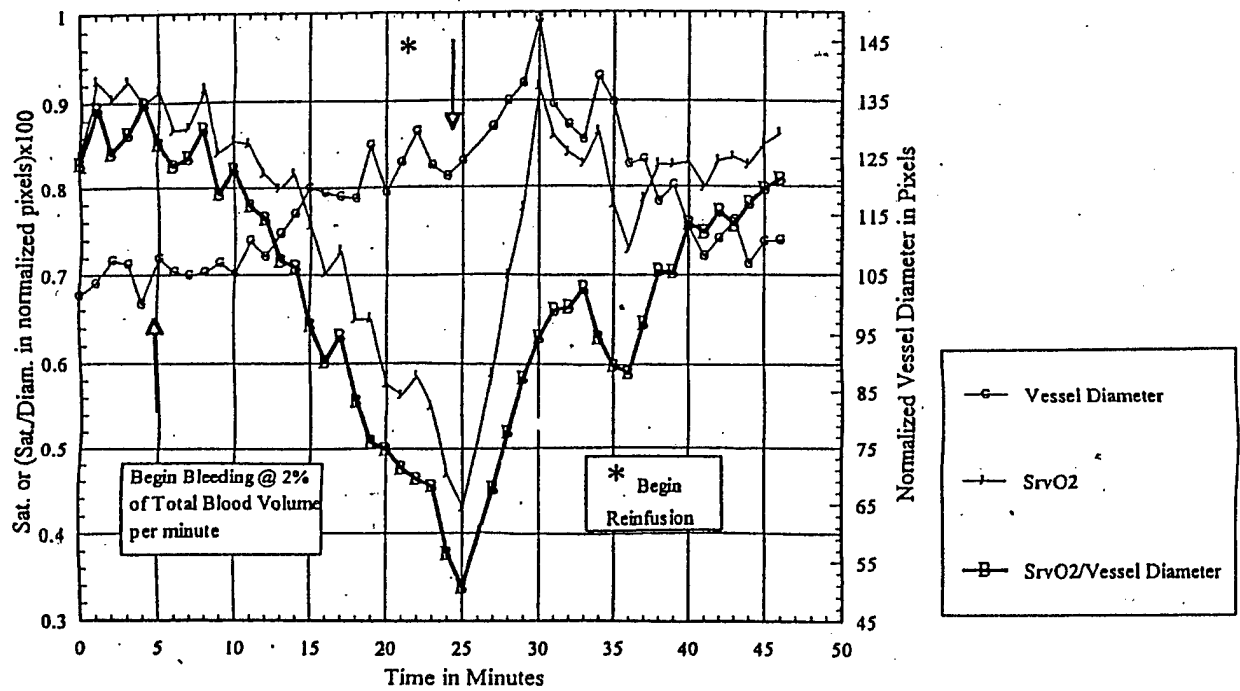


FIGURE 1

Bibliography of all publications/abstracts associated with this grant:

"An instrument for the measurement of retinal vessel oxygen saturation" J.D. Drewes, M.H. Smith, K.R. Denninghoff, L.W. Hillman, Invited paper in *Optical Diagnostics of Biological Fluids IV*, Proc. SPIE 3591 (1999).

"Handheld four-wavelength eye oximeter" C. Heaton, M.H. Smith, K.R. Denninghoff, L.W. Hillman, in Ophthalmic Technologies X, P. O. Rol, K.M. Joos, eds., *Proceedings of SPIE Vol. 3908*, January, (2000).

"Retinal vessel oximetry: Toward absolute calibration" M.H. Smith, K.R. Denninghoff, A. Lompado, L.W. Hillman, in Ophthalmic Technologies X, P. O. Rol, K. M. Joos, eds., *Proceedings of SPIE Vol. 3908*, January, (2000).

"In-plane scatterometry of small caliber blood column" A. Lompado, M.H. Smith, K.R. Denninghoff, L.W. Hillman, in Optical Diagnostics of Biological Fluids V, A. V. Priezhev, T. Asakura, eds., *Proceedings of SPIE Vol. 3923*, January, (2000).

"Multispectral confocal scanning laser ophthalmoscope for retinal vessel oximetry" A. Lompado, M. H. Smith, K.R. Denninghoff, L W. Hillman, in Spectral imaging: Instrumentation, applications, and analysis, G. H. Bearman, D. Cabib, R. M. Levenson, eds., *Proceedings of SPIE Vo. 3920*, January, (2000).

"Effect of multiple light paths on retinal vessel oximetry" M.H. Smith, K.R. Denninghoff, J.E. Drewes, A. Lompado, L.W. Hillman, *Applied Optics* (In press).

"Retinal Imaging Techniques in Diabetes" K.R. Denninghoff, M.H. Smith, L.W. Hillman, *Diabetes Technology and Therapeutics* (In press).

"An Optical Model of the Blood in the Large Retinal Vessels" K.R. Denninghoff, M.H. Smith. Submitted to *Journal of Biomedical Optics*, November, (1999).

"Retinal vessel diameter correlates with blood volume in a swine model" K.R. Denninghoff, *Acad. Emerg. Med.* Annual Meeting, Boston, MA, (1999)

"Eye Oximeter for Combat Casualty Care 1999-I" L.W. Hillman, K.R. Denninghoff, M.H. Smith, *Advanced Technology Applications to Combat Casualty Care*, Proc., Fort Walton Beach, FL (1999)

"Eye Oximeter for Combat Casualty Care 1999-II" K.R. Denninghoff, M.H. Smith, L.W. Hillman, *Advanced Technology Applications to Combat Casualty Care*, Proc., Fort Walton Beach, FL (1999)

"Noninvasive optical systems in systemic and ophthalmic diseases" K.R. Denninghoff, M.H. Smith, L.W. Hillman, *Optical Society America*, Annual Meeting, Santa Clara, CA, (1999)

"A scanning laser ophthalmoscope for retinal vessel oximetry" M.H. Smith, A. Lompado, K.R. Denninghoff, L.W. Hillman, *Optical Society America*, Annual Meeting, Santa Clara, CA (1999)

"Multiple light paths in retinal vessel oximetry" M.H. Smith, K.R. Denninghoff, A. Lompado, L.W. Hillman, *Optical Society of America*, Annual Meeting, Santa Clara, CA (1999)

"An eye oximeter for combat casualty care" K.R. Denninghoff, M.H. Smith, L.W. Hillman, *ATACCC98*, Proc., Fort Walton Beach, Florida (1998).

"The effect of a diffusion-enlarged point spread function on retinal vessel oximetry" M.H. Smith, J.E. Drewes, L.W. Hillman, K.R. Denninghoff, *Optical Society of America*, Annual Meeting, Baltimore, MD (1998).

UAB personnel paid from this research effort:

Kurt Denninghoff, MD
Penny Jester, RN
Diana Hablitz, RN
Sandi Partain, RN
Henry Slappy, RN
Anthony Browning, RN
Joan Hargrove

UAH personnel paid from this research effort:

Matthew Smith, PhD
Lloyd Hillman, PhD
Arthur Lompado, PhD
Jonathon Drewes, PhD
Chris Heaton
Jake Woodruff
Carolyn Schneider